Functional Au and Ag Nanoparticles in Polymer Composites

And

Molecular Assemblies

A dissertation submitted to
Indian Institute of Technology Guwahati
for the degree of Doctorate of Philosophy
in Chemistry

By

A. Murugadoss

Roll NO: 05612211

Department of Chemistry
Indian Institute of Technology Guwahati

Guwahati 781039, INDIA
September 2008

TH-777_05612211

Dedicated to my beloved Parents

and Sisters

..... Muruga

TH-777_05612211

INDIAN INSTITUTE OF TECHNOLOGY GUWAHATI

Department of Chemistry

STATEMENT

I hereby declare that the matter embodied in this thesis is the result of investigations carried out by me in the Department of Chemistry, Indian Institute of Technology Guwahati, and India under the supervision of Prof. Arun Chattopadhyay, Professor of Chemistry.

In keeping with the general practice of reporting observations, due acknowledgements have been made wherever the work described is based on the findings of other investigations.

I. I. T. Guwahati A. Murugadoss

September, 2008

TH-777_05612211



TH-777_05612211

Prof. Arun Chattopadhyay
Professor of Chemistry
INDIAN INSTITUTE OF TECHNOLOGY GUWAHATI
Department of Chemistry
E-mail: arun@iitg.ernet.in
Tel. 91 361 26902304
Fax. 91 361 2690762

CERTIFICATE

This is to certify that Mr. A. Murugadoss has been working under my supervision since August 2004. I am forwarding his thesis, entitled, "**Functional Au and Ag Nanoparticles in Polymer Composites and Molecular Assemblies**" being submitted for the degree of Doctorate of Philosophy of this Institute. I certify that he has fulfilled all the requirements according to the rules of this Institute, and that the investigations embodied in this thesis have not been submitted elsewhere for a degree.

I. I. T. Guwahati
September- 2008

Prof. Arun Chattopadhyay
Supervisor

TH-777_05612211

INDIAN INSTITUTE OF TECHNOLOGY GUWAHATI

Department of Chemistry

COURSE CERTIFICATE

This is to certify that Mr. A. Murugadoss has satisfactorily completed all the courses required for the Ph. D. degree programme. These courses include:

CH 621	New Reagents for Organic Synthesis
CH 605	Applied Crystallography
CH 630	A Fundamental Approach to Physical Chemistry
CH 611	Bioinorganic Chemistry
NT 710	Nanobioscience

Mr. A. Murugadoss has successfully completed his Ph. D. qualifying examination in February, 2006.

Prof. Abu Taleb Khan
Head
Department of Chemistry
I. I. T. Guwahati

Dr. Anil Kumar Saikia
Secretary
Departmental Post Graduate Committee
Department of Chemistry

TH-777_05612211

I. I. T. Guwahati

INDIAN INSTITUTE OF TECHNOLOGY GUWAHATI

Department of Chemistry

Ph. D. Grade Card

Name: A. Murugadoss

Roll No: 05612211

Department: Chemistry

Semester: July-November, 2005

Course	Course name	Credit	Grade
CH 621	New Reagents for Organic Synthesis	6	AA
CH 605	Applied Crystallography	6	BC
CH 630	A Fundamental Approach to Physical Chemistry	6	AA
CH 611	Bioinorganic Chemistry	6	BB
NT 710	Nanobiosciences	6	AB

TH-777_05612211

Cumulative Performance Index (C.P.I.): 8.80

I. I. T. Guwahati
September- 2008

Assistant Registrar
Academic Section

TH-777_05612211

Acknowledgement

The results of the works reported in the thesis are based on interdependence rather than independence, which reflect where I have been escorted and supported by many people and that gives me a pleasant opportunity to express my gratitude to all of them. First and foremost, with a deepest sense of gratitude, I wish to express my sincere thanks to my supervisor, Prof. Arun Chattopadhyay who has been an excellent supervisor, and taught me how one can start understanding a problem in the simplest possible way. I am so fortunate to utter that his enthusiasm and integral view on research and his efforts in producing high quality work, which have made a deep impression on me. He gave me freedom to pursue my own interests. His trust, scientific thinking, valuable suggestions, discussions and constant support have inspired me to take right decisions at crucial moments and I find myself privileged to have worked under his kind guidance.

I would like to acknowledge my sincere gratitude to Dr. Anumita Paul for her constant inspiration, help and valuable suggestions during my Ph. D. tenure. My sincere thanks are due to all my doctoral committee members for their constant inspiration and valuable suggestions. I am grateful to Dr. S. S. Ghosh, Dr. A. Ramesh and Dr. P. K. Iyer for their insightful advices. I am thankful to my Institute, Indian Institute of Technology Guwahati for providing us with the infrastructure and facilities for research. My sincere thanks are due to all other faculty members in the Department of Chemistry for their help and encouragement and the non-teaching staffs of the Department for their technical support. I would like to take this opportunity to thank staff members of Department of Biotechnology, Centre for Nanotechnology and Department of Physics. The special thanks go to Sidhananda Sarma for constant help and providing me with support to use their instruments for my research work.

I am highly indepted to Dr, Mamoranjan Kar, who gives me constant inspiration and encouragement whenever I felt frustrated during my research time. I am so grateful to express my sincere thanks for his constant support, help and valuable scientific hints. I wish

TH-777_05612211

to thank Dr. Aslam Khan and Dr. Papori Goswami for their contribution in shaping my thesis.

I wish to thank Mr. Indrajit Talukdar, who has been always ready to help in recording TEM for our samples, which was a boost to my enthusiasm. My sincere thanks to Mr. Chandan Borgohain and Mr. K. Senapathy of Central Instruments facility, IIT-Guwahati for their help in all the characterizations (SEM, NMR, and LCMS) required during my research work.

I am grateful to Mr. S. Chakrabarty, IACS, Kolkata and Dr. Renu Pasricha, NCL, Pune for helping in TEM measurements of my samples for my research work.

My heartfelt thanks to Mr. Anto Pradeep. He is my friend, with whom I am mostly used to discuss my research work and some times that discussion may be strong arguments and that gives me a clear understanding of my research what I am doing and that will be the boost to finish my research project early.

I would never forget to thank my lab members Biswa bhayya, Gitanjali sister, Sonit, Jashmini, Subojit Das, Partho and Saducharan for timely help and support. I am very fortunate to have invaluable help from Dr. Biswa Rajan Panda, who has also taught me how to perform reaction and to maintain laboratory. I also take this opportunity to thank my seniors and colleagues for lending their hands of support whenever needed.

I would like to thank Dr. P. Gopinath, Mr. Atul Kumar Singh and Mr. Kiran, who had helped me to use the ultracentrifugation for my research work.

I would like to express my appreciation to my other friends in the campus, Krishna, Pallab Sanpui, Ramakrishnan, Saravana anna, Arumugam, Shivasankar, Senthil and my 2005 Ph.D batch mates for the wonderful time I had with them.

The financial support from Council of Scientific and Industrial Research (CSIR), New Delhi in the form of an SRF is duly acknowledged. I also thank Indian Institute of Technology, Guwahati for the initial financial support.

Finally, my Ph. D endeavor could not be completed without the endless love and blessing from my family. I wish to express my sincere gratitude to my parents, especially to my mother, without whom I could not have completed even my B. Sc first year. She is the main soul and inspiration for each and every step that I achieve in my life and she taught me

TH-777_05612211

the value of hard work and rendered enormous support to me during the whole tenure of my research work. I also wish to thank my sisters, grandparents, uncles and aunts for their unwavering faith in my capabilities, which has always encouraged me to go ahead.

TH-777_05612211

Section A

TH-777_05612211

Section B

- Stabilizing Agent Specific Synthesis of Multi- branched and Spherical Au Nanoparticles by Reduction of $AuCl^-_4$ by Fe^{2+} ions. A. Murugadoss, Arun Chattopadhyay. ***J. Nanosci and***

TH-777_05612211

Section C

- A “Green” Chitosan-Silver Nanoparticle Composite as a Heterogeneous as well as Micro-heterogeneous Catalyst. A. Murugadoss, Arun Chattopadhyay. **Nanotechnology** 2008, 19, 015603.

- ‘Green’ Chitosan bound Silver Nanoparticles for Selective C-C bond Formation via in situ Iodination of Phenols. A. Murugadoss, Papori Goswami and Arun Chattopadhyay (**Communicated**).

- Stabilizer Specific Interaction of Gold Nanoparticles with a Thermosensitive Polymer Hydrogel. A. Murugadoss, Aslam Khan, Arun Chattopadhyay (**Communicated**).

TH-777_05612211

Section D

- Acetanilide Mediated Reversible Assembly and Disassembly of Au Nanoparticles. A. Murugadoss, M. Kar, Arun Chattopadhyay, **J. Colloid Interface Sci.** 2008, 324, 230.

- Surface Area Controlled Differential Catalytic Activities of One Dimensional Chain-Like Arrays of Gold Nanoparticles. A. Murugadoss, Arun Chattopadhyay. **J. Phys. Chem. C** 2008. 112, 11265.

- Acetanilide as a Precursor for Shape and Size Selective Polyaniline-Au Nanoparticle Composite. A. Murugadoss, Arun Chattopadhyay. **(Under preparation)**.

- Concentration Dependence and Specificity in the Amino acid induced Assembly of Gold Nanoparticles. A. Murugadoss, Arun Chattopadhyay. (**Under preparation**), 2008.

- Ascorbic acid as a Mediator and Template for Assembling Metallic Nanoparticles. A. Murugadoss, R. Pasricha, Arun Chattopadhyay. J**. Colloid Interface Sci**. 2007, 311, 303.

- Silver Fused Conducting Fiber Formation of Au@Ag Core-shell Nanoparticles Mediated by Ascorbic Acid. A. Murugadoss, R. Pasricha, Arun Chattopadhyay. **(Communicated)**. 2008.

TH-777_05612211

TH-777_05612211

CHAPTER 1

INTRODUCTION

TH-777_05612211

CHAPTER 2

STABILIZING AGENT SPECIFIC SYNTHESIS OF MULTI-BRANCHED AND SPHERICAL Au NANOPARTICLES BY REDUCTION OF $AuCl_4^-$ BY Fe^{2+} IONS

TH-777_05612211

CHAPTER 3

A "GREEN" CHITOSAN-SILVER NANOPARTICLE COMPOSITES AS A HETEROGENEOUS AS WELL AS MICRO-HETEROGENEOUS CATALYST

TH-777_05612211

CHAPTER 4

'GREEN' CHITOSAN BOUND SILVER NANOPARTICLES FOR SELECTIVE C-C BOND FORMATION VIA IN SITU IODINATION OF PHENOLS

TH-777_05612211

CHAPTER 5

STABILIZER SPECIFIC INTERACTION OF GOLD NANOPARTICLES WITH A THERMOSENSITIVE POLYMER HYDROGEL

TH-777_05612211

CHAPTER 6

ACETANILIDE MEDIATED REVERSIBLE ASSEMBLY AND DISASSEMBLY OF Au NANOPARTICLES AND ITS APPLICATION IN CATALYSIS

TH-777_05612211

CHAPTER 7

ACETANILIDE AS A PRECURSOR FOR SHAPE AND SIZE SELECTIVE POLYANILINE-Au NANOPARTICLE COMPOSITES

TH-777_05612211

CHAPTER 8

CONCENTRATION DEPENDENCE AND SPECIFICITY IN THE AMINO ACID INDUCED ASSEMBLY OF GOLD NANOPARTICLES

TH-777_05612211

CHAPTER 9

ASCORBIC ACID AS A MEDIATOR AND TEMPLATE FOR ASSEMBLING METALLIC NANOPARTICLES

TH-777_05612211

Contents

A. Statement I
B. Certificate II
C. Course Certificate III
D. Ph. D. Grade Card IV
E. Acknowledgement V
F. Abstract VII
G. Contents XVIII

SECTION A

Chapter 1 – Introduction

1.1.1 Nanomaterials and their future 1
1.1.2 Synthesis of shape selective Nanomaterials 1
1.1.3 Functional Nanoparticles and Polymer-Nanoparticles Composite 3
1.1.4 Assembly of Nanoparticles Using Molecular Level Interactions 7
1.1.5 Works described in the thesis 9
1.1.6 References 14

SECTION B

Chapter 2

2.1 Stabilizing Agent Specific Synthesis of Multi-branched and Spherical Au Nanoparticles by Reduction of $AuCl^-_4$ by Fe^{2+} Ions

2.1.1 Introduction 23
2.1.2 Experimental Section 24
2.1.3 Results and Discussion 25
2.1.5 Conclusion 32

TH-777_05612211

2.1.4 References 32

TH-777_05612211

SECTION C

Chapter 3

3.1 A "Green" Chitosan-Silver Nanoparticle Composite as a Heterogeneous as well as Micro-heterogeneous Catalyst

3.1.1 Introduction 34

3.1.2 Experimental Section 36

3.1.3 Results and discussion 38

3.1.4 Conclusion 55

3.1.5 Appendix-I 55

3.1.6 References 58

Chapter 4

4.1 'Green' Chitosan bound Silver Nanoparticles for Selective C-C bond Formation via in situ Iodination of Phenols

4.1.1 Introduction 60

4.1.2 Experimental section 61

4.1.3 Results and discussion 62

4.1.4 Conclusion 70

4.1.5 Appendix-I 71

4.1.6 Appendix-II 73

4.1.7 References 81

Chapter 5

5.1 Stabilizer Specific Interaction of Gold Nanoparticles with a Thermosensitive Polymer Hydrogel

5.1.1 Introduction 84

5.1.2 Experimental section 86

5.1.3 Results and discussion 89

TH-777_05612211

5.1.4 Conclusion 111
5.1.5 Appendix-I 112
5.1.6 Appendix-II 113
5.1.7 References 115

SECTION D

Chapter 6

6.1 Acetanilide Mediated Reversible Assembly and Disassembly of Au Nanoparticles
6.1.1 Introduction 119
6.1.2 Experimental Section 120
6.1.3 Results and discussion 122
6.1.4 Conclusion 133
6.1.5 References 133
6.2 Surface Area Controlled Differential Catalytic Activities of One Dimensional Chain-Like Arrays of Gold Nanoparticles
6.2.1 Introduction 135
6.2.2 Experimental section 136
6.2.3 Results and discussion 138
6.2.4 Conclusion 152
6.2.5 Appendix-I 154
6.2.6 Appendix-II 156
6.2.7 Appendix-III 159
6.2.8 References 161

Chapter 7

7.1 Acetanilide as a Precursor for Shape and Size Selective Polyaniline-Au Nanoparticle Composites

TH-777_05612211

7.1.1 Introduction 163
7.1.2 Experimental Section 165
7.1.3 Results and discussion 167
7.1.4 Conclusion 175
7.1.5 References 176

Chapter 8

8.1 Concentration Dependence and Specificity in the Amino acid Induced Assembly of Gold Nanoparticles

8.1.1 Introduction 179
8.1.2 Experimental section 181
8.1.3 Results and discussion 184
8.1.4 Conclusion 198
8.1.5 Appendix-I 199
8.1.6 Appendix-II 200
8.1.7 Appendix-II 201
8.1.8 Appendix-II 202
8.1.9 Appendix-II 203
8.1.10 References 204

Chapter 9

9.1 Ascorbic Acid as a Mediator and Template for Assembling Metallic Nanoparticles

9.1.1 Introduction 207
9.1.2 Experimental Section 209
9.1.3 Results and discussion 211
9.1.4 Conclusion 223
9.1.5 Appendix-I 224
9.1.6 References 226

TH-777_05612211

9.2 Silver Fused Conducting Fiber Formation of Au@Ag Core-shell Nanoparticles Mediated by Ascorbic Acid

9.2.1 Introduction 228

9.2.2 Experimental section 228

9.2.3 Results and discussion 231

9.2.4 Conclusion 242

9.2.5 References 242

List of Publications 244

TH-777_05612211

Abstract

My Ph. D. thesis consists of three broad areas, which are focused on the synthesis, characterization and application of nanomaterials.

The thesis is divided into four sections, with each section divided into appropriate chapter(s).

Section A

Chapter 1

1.1. Introduction

This chapter contains an overview of studies related to synthesis of shape selective nanomaterials. It also contains a brief review of synthesis of multi-branched Au nanoparticles (NPs) and their potential application in future nanoscience and technology. Additionally, it also briefly outlined the importance of the functional nanomaterials and that can be subsequently used for the generation of polymer-metal NPs composites, which is having the high pontential impact for fabrication of nanodevice based application. Further, this section also has briefly summarized the molecularly controlled assembly of nanoparticles and their emphasis of controlling the properties of nanomaterials. Moreover, the brief summary of the work reported in thesis also has been discussed.

Section B

In this section, we describe a simple method of preparation of shape selective Au NPs by using Fe^{2+} as the reducing agent in the presence of various stabilizing agents.

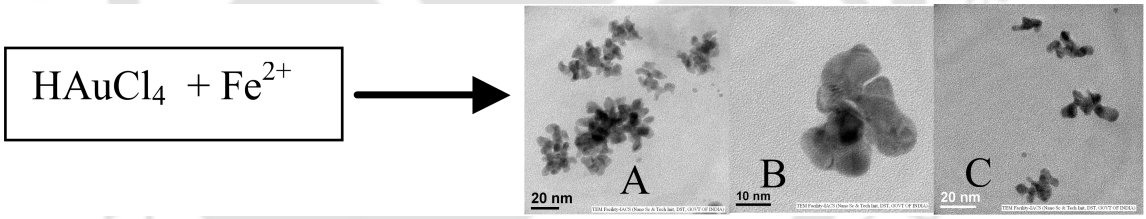
TH-777_05612211

Abstract

Chapter 2

2.1. Stabilizing Agent Specific Synthesis of Multi- branched and Spherical Au Nanoparticles by Reduction of $AuCl_4^-$ by Fe^{2+} ions.

Here, we report on the development of a new method of synthesis of Au nanoparticles (NPs) of muti-branched and spherical shapes. $HAuCl_4$ when reduced by Fe^{2+} ions in aqueous solution, in the presence of sodium dodecyl sulfate (SDS), produced multi-branched Au NPs including a shape that could be termed as a "nanofan". On the other hand spherical particles were produced in the presence of Na_2S and SDS or starch (instead of SDS). UV-vis, X-ray diffraction, transmission electron microscopic (TEM) studies revealed the difference in optical properties and shapes under various conditions. The essential conclusion is that stabilizing agent and other reagents have special roles in controlling the shape of the NPs produced.



Section C

In this section, we discuss the development of a novel method for the generation of green chitosan-silver nanoparticles composite (Chi-Ag NPs), which is subsequently used in efficient catalysis for the reduction of 4-nitrophenol into 4-aminophenol. The composite could also be used for the selective C-C bond formation of phenolic coupling reactions. Further, the interaction of the thermoresponsive polymer hydrogel with different stabilizing agent capped Au NPs has also been reported in this section. This section has been divided

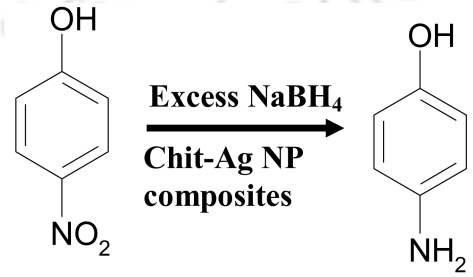
TH-777_05612211

into three chapters with each chapter containing introduction, experimental section, results and discussion and conclusion.

Chapter 3

3.1. A "Green" Chitosan-Silver Nanoparticle Composite as a Heterogeneous as well as Micro-heterogeneous Catalyst

In this chapter, we report on the catalytic activity of a newly synthesized metal nanoparticle-polymer composite consisting of Ag nanoparticle (NP) and environmentally friendly ("green") chitosan. The polymer (chitosan) not only acted as the reducing agent for the metal ions, but also stabilized the product NPs by anchoring them. The majority of the NPs produced in this way had sizes less than 5 nm. The catalytic activity of the composite was investigated photometrically by monitoring the reduction of 4-nitrophenol (4NP) in the presence of excess $NaBH_4$ in water, under both heterogeneous and micro-heterogeneous conditions. The reaction was first order with respect to the concentration of 4NP. We also observed that the apparent rate constant, k_{app}, for the reaction was linearly dependent on the amount of Ag NPs present in the composite. Moreover, the turn over frequency (TOF) of the catalyst was found to be $1.5 \pm 0.3 \times 10^{-3}$ s^{-1}, when the reaction was carried out under heterogeneous conditions. The Ag NPs in the composite retained their catalytic activities even after using them for 10 cycles. Our observations also suggest that the catalytic efficiency under micro-heterogeneous condition is much higher than the heterogeneous condition.



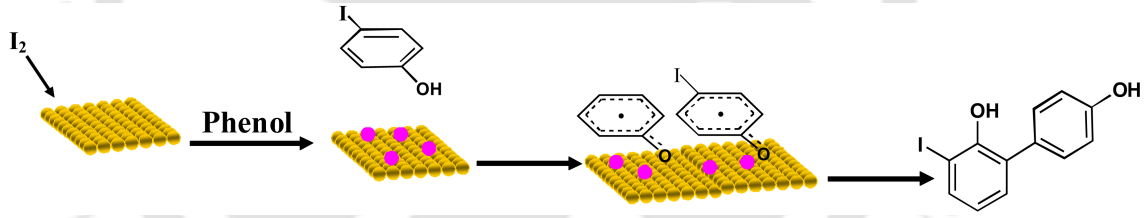
TH-777_05612211

Abstract

Chapter 4

4.1. A "Green" Chitosan-Silver Nanoparticle Composite as a Heterogeneous as well as Micro-heterogeneous Catalyst

Herein we report on the use of chitosan-Ag NP composite as an efficient catalyst in selective C-C coupling of phenolic compounds in the presence of molecular iodine. This is the first report on the C-C coupling with Ag NPs as the catalyst. The reactions were carried out with phenol and a few of its derivatives as well as naphthols. The results indicate that the reaction proceeded via the formation of p-iodophenol followed by *o-p* coupling leading to the products. The reactions were complete in 3 h with high yields. When the para position of phenol was blocked by a substituent then iodination at the ortho position could only be observed and the formation of coupled products did not occur. In the case of naphthols *o-o* coupling could only be observed. Based on the results a mechanism is proposed for the coupling reaction occurring at the surface of Ag NP.



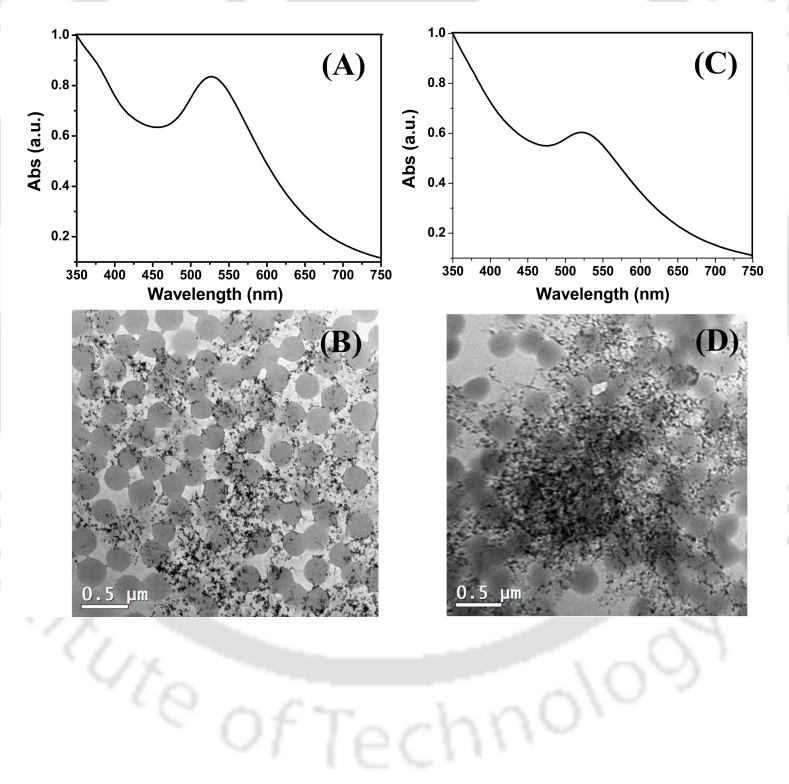
Chapter 5

5.1. Stabilizer Specific Interaction of Gold Nanoparticles with a Thermosensitive Polymer Hydrogel

In this chapter, we discuss the experimental results on temperature dependent studies of interactions between a novel biocompatible thermosensitive polymer hydrogel and different stabilizing agent capped gold nanoparticles (Au NPs). Stabilizing agents such as thioglycolic acid, tryptophan and phenylalanine have been used as capping agents for Au NPs. The poly-N-isopropyl acrylamide-co-acrylic acid (pNIPAm-AAc) was synthesized by radical polymerization of a selected mixture of N-isopropyl acrylamide (NIPAm),

TH-777_05612211

methylene-bis-acrylamide and acrylic acid (AAc). The capped Au NPs were mixed with a solution of pNIPAm-co-polymer hydrogel. The temperature dependent properties of the mixture were studied by UV-vis spectroscopy, dynamic light scattering based particle size analysis and transmission electron microscopy (TEM). The observations indicated change in the lower critical solution temperature (LCST) depending on the nature of the stabilizer, with hydrophobic ones lowering the value while hydrophilic stabilizers increasing the same. Also, the optical absorption due to Au NPs, when stabilized with hydrophobic groups, reduced significantly at above LCST along with significant blue shift of wavelength maximum.



Section D

The final section of this thesis deals with the molecularly controlled assembly of gold nanopartilces (Au NPs) into one dimensional chain-like array of superstructures. Moreover, this section also discusses the assemblies of the NPs and their associated optical and catalytic properties. The length and nature of the assembly could be controlled by controlling

TH-777_05612211

Abstract

the nature of the molecules that are involved in the assembly formation. Further, the molecules involved in the assembly formation can subsequently be used for the different shape and size selective polymer-metal NPs composite formation. Finally, that the ordinary compound like vitamin C could also be used for assembling metallic NPs in the form long linear or network of fibers is also discussed in this section. This section has been divided into four chapters: chapter 6 and chapter 9 consist of two sub-chapters with each describing introduction, experimental section, results and discussion and conclusion.

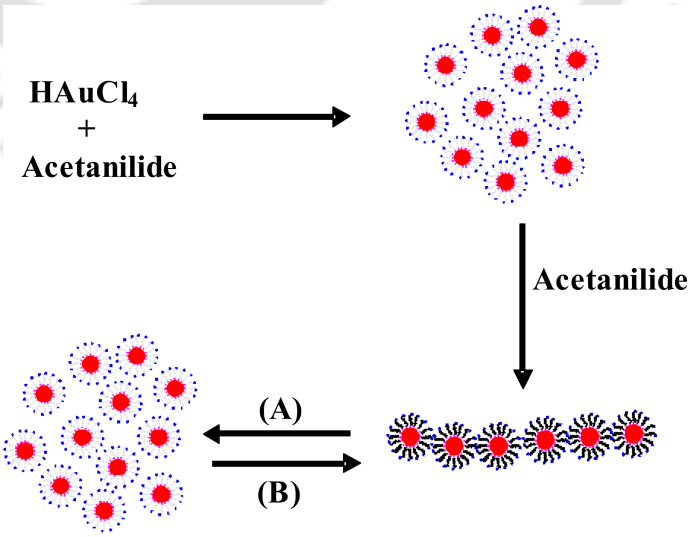
TH-777_05612211

Abstract

Chapter 6

6.1. Acetanilide Mediated Reversible Assembly and Disassembly of Au Nanoparticles

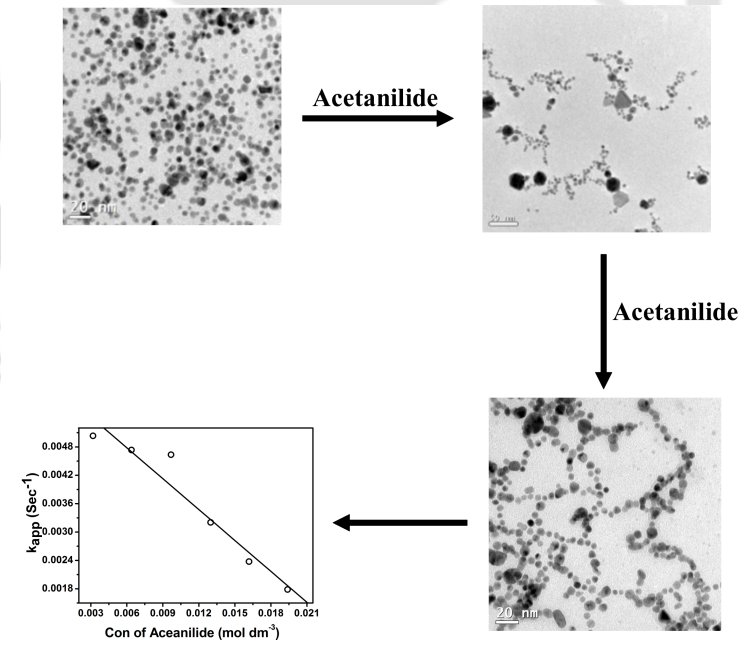
In this chapter, we report the generation of Au nanoparticles (NPs) by sparingly soluble acetanilide in water, leading to the formation of linear chain-like superstructures of self-assembled Au NPs, in the presence of excess acetanilide. This could be achieved in two different ways. In the first method, acetanilide was added, with increasing concentration, into aqueous $HAuCl_4$ to produce Au NPs as well as for the formation of assembly, which varied according to the concentration of acetanilide. The other route involved formation of spherical Au NPs at the lowest concentration of acetanilide, which was followed by the formation of assembly of various lengths upon further addition of variable amount of acetanilide. The assemblies were stable in aqueous solution for days with characteristic UV-vis absorption spectra consisting of two peaks. While the wavelength of the first peak remained the same, the position of the second peak changed to longer wavelength with increasing acetanilide concentration. Interestingly, the linear chain-like arrays could be broken into individual particles by first dilution of the solution concentration followed by treatment with ultrasonic waves. The individual Au NPs again formed linear chain-like arrays upon addition of excess acetanilide.



TH-777_05612211

6.2. Surface Area Controlled Differential Catalytic Activities of One Dimensional Chain-Like Arrays of Gold Nanoparticles

In this chapter, we report on the formation of linear assemblies of citrate stabilised spherical gold nanoparticles (GNPs) in the presence of acetanlide in aqueous medium. The length of the assembly was dependent on the concentration of acetanilide. At higher concentrations branching of the assembly occurred instead of increase in the length of assembly. Interestingly, the catalytic properties of the assemblies were dependent on the concentration of the acetanilide. This means the effective surface areas of the metal nanoparticles in the assembly were much dependent on the length of the assembly, which could be controlled by the concentration of acetanilide. The results indicate a linear dependence of the effective surface area on the concentration of acetanilide. Also, the observations suggest that the presence of $NaBH_4$ in the reaction medium led to the fusion of GNPs into fibrous form thus reducing the effective surface area for catalysis.

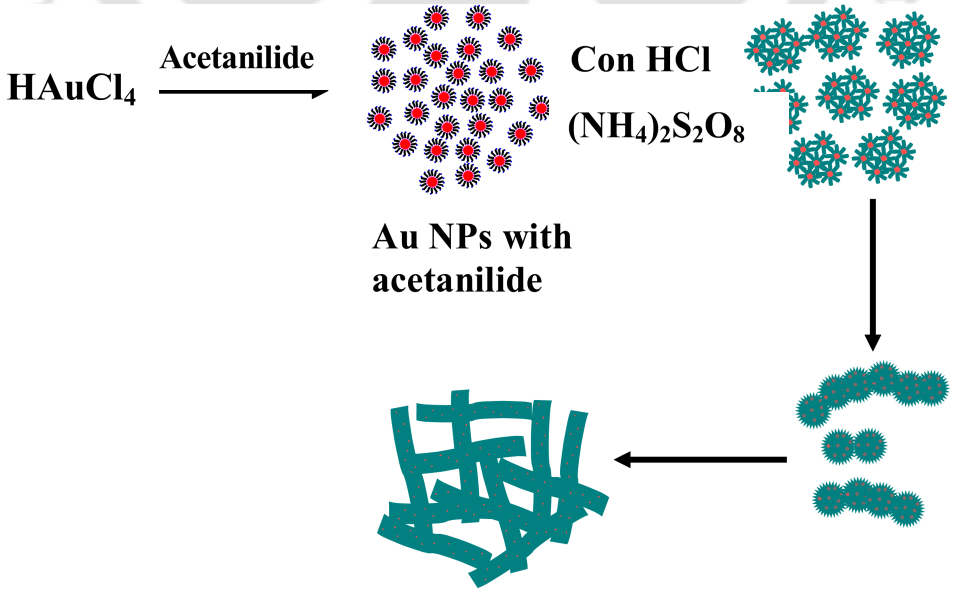


TH-777_05612211

Chapter 7

7.1. Acetanilide as a Precursor for Shape and Size Selective Polyaniline-Au Nanoparticle Composite Synthesis

Here in we report the development of a method for the generation of water-dispersible and stable polyaniline-Au NP nanocomposite with size and shape selectivity. Sparingly soluble acetanilide has been used to first generate Au nanoparticles (NPs) by reduction of $HAuCl_4$, followed by polymerization leading to the formation of the composite. The size and shape of the composites could by tuned by controlling the concentration of acetanilide. At the lowest concentrations of acetanilide, nano-raspberry-like particles of PANI – Au NP composites were formed. At higher concentrations these spherical structures were joined by polymer to form continuous fibers. Moreover, this method offers composites that are water soluble and stable for months without precipitating and thus overcome the fundamental challenges of insolubility and intractability associated with polyaniline and their composites. This work may pave various ways for systematic development of three-dimensional water-soluble metal NP-polymer composites with tunable electrical, optical and chemical properties.



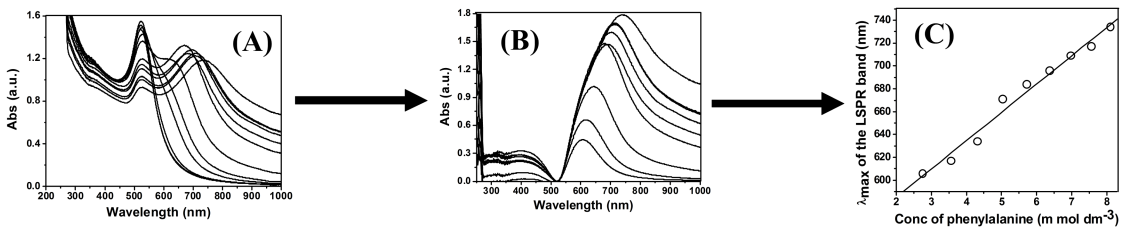
TH-777_05612211

Abstract

Chapter 8

8.1. Concentration Dependence and Specificity in the Amino acid Induced Assembly of Gold Nanoparticles

We have recently found that several amino acids could assemble citrate-stabilized spherical Au NPs into 1-D chain-like superstructures. The nature of the assembly formation and associated optical properties were found to be dependent on the concentration of amino acid as well as the nature of the side chain group present in the amino acid. The changes were highly specific to the amino acid present in the medium. For example, when lysine or tryptophan was used micromolar quantities of the acid was enough to induce a large scale organization. On the other hand, when phenylanine and glutamine were used milli molar quantities of amino acids were required to achieve significant changes in the absorption spectra. Thus the assembly formation could not only be useful for identification of amino acids but also may be used to estimate their solution concentrations. In addition, 1D chain of necklace-like Au NPs converted into nanofibers when excess hydrophilic amino acid was used. On other hand, at higher concentration of hydrophobic amino acids, the necklace-like Au NPs did not get transformed into nanofibers. Our observations suggest that the nature of the side chains present in the amino acids with their functional groups may play an important role for controlling the interparticles interaction and their subsequent fusions in the amino acid assembled Au NPs chain.



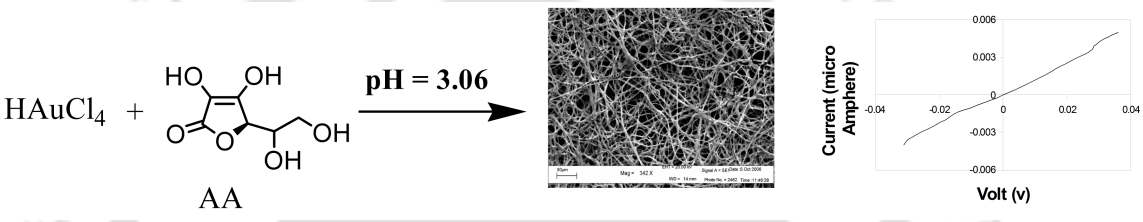
TH-777_05612211

Abstract

Chapter 9

9.1. Ascorbic Acid as a Mediator and Template for Assembling Metallic Nanoparticles

In this chapter, we discuss the use of vitamin C (L-Ascorbic acid; AA) for the generation of Au NPs as well as their organization in the form of one-dimensional nanowire like structures consisting of Au NPs and polymerization product of AA. The fibrous degradation product of AA also has been used as a template for deposition of metal NPs such as Au, Pt and Ag. These fibers appear in the form of a fiber bundle with branched structures having overall dimensions on the order of several millimeters.



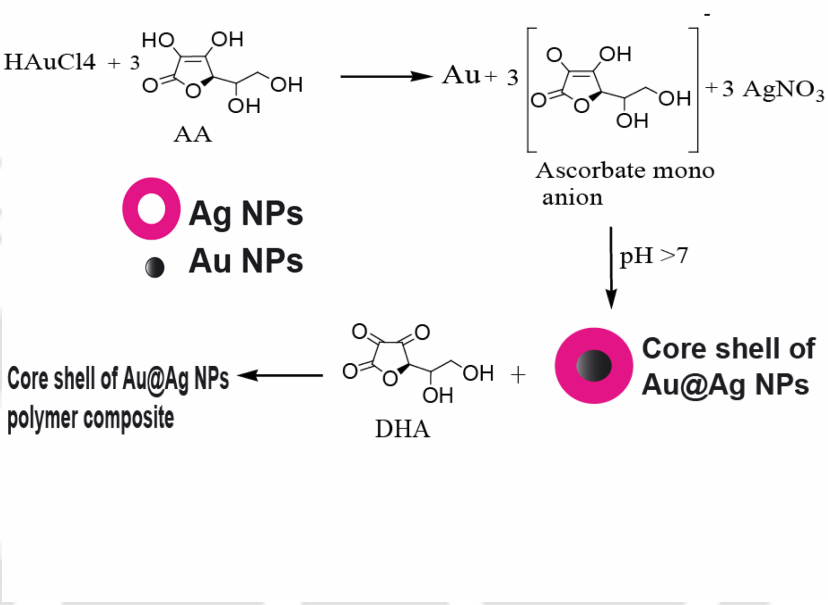
They have typical widths of 1 – 4 μm with length of each segment of fiber bundle on the order of 40 μm. The composite fiber bundle has been found to be electrically conducting with surface resistivity on the order of 2.16 X 10^3 ohm cm. That the backbone of the composite fiber has organic moiety provides additional chemical and mechanical flexibility. The present work is expected to provide a new and interesting way of generating and organizing metallic NPs into three-dimensional functional networks useful for nanotechnology based devices.

9.2. Silver Fused Conducting Fiber Formation of Au@Ag Core-shell Nanoparticles Mediated by Ascorbic Acid

In continuation of the method reported in chapter 9.1, we have found that core-shell of Au@Ag NPs also could assemble into a one-dimensional fiber-like structure in the presence of ascorbic acid (AA). AA acted as both reducing agent for the metal salts as well as mediator for the formation of fibers. The process of fiber formation involved three steps – reduction of $HAuCl_4$ to Au NPs by AA; subsequent formation of Au@Ag core-shell NPs

TH-777_05612211

after addition of $AgNO_3$ and spontaneous formation of fibers from the mixtures in water. It took typically about 30 days to form complete fibers that are of lengths of several hundred micrometers to millimeters, although nanofibers started forming from the first day of solution preparation.



The width of each of these fibers was typically about 1-4 µm with length of each segment of fiber bundle on the order of 40 µm. Formation of fibers was also observed in absence of $AgNO_3$. These fibers consisted of Au NPs and polymer of AA degradation products and were not electrically conducting. Also, low concentrations of $AgNO_3$ produced fibers with low electrical conductivity. However, it was observed that increase in the amount of $AgNO_3$ led to the formation of fibers that were electrically conducting with conductivity values in the range of metallic conductivity. Spectroscopic and electron microscopic investigations were carried out to establish the formation of fibers. The present method of generating core-shell NPs and their subsequent self organization in the presence of increasing amount of Ag introduces a new approach towards systematic development of three-dimensional structures with nanoscale components.

TH-777_05612211

Abstract

TH-777_05612211

1.1 Introduction

1.1.1 Nanomaterials and their future

'Nano' is one of the most exciting topics in science and technology, which would be considered as key in the modern technology of 21st century. This is due to newer size and shape dependent properties of materials that arise when at least one of its dimensions fall within 1-100 nm. Realization of these new physical and chemical properties of nanomaterials would lead to enormous applications in the field of chemical industries[1], medicine[2], photonics, and optoelectronics[3]. Nanomaterials can be generated in the form of metals nanoparticles (especially Au, Ag, Pt and Pd), semiconductors (Gr. II-IV metal oxides or metal sulfides) with special optical properties, magnetic materials, polymer materials, composites and ceramics, with a number of unusual properties that are either absent in their bulk materials counterparts. The unusual properties may originate from quantization due to reduced dimensions of matter[4] and increased surface to volume ratio[5]. There could also be properties that come from directed assembly of nanoparticles (NPs). In order to harness the properties of nanomaterial for potential applications in the form of device collaborative efforts of chemists, physists, biologists, computer scientists and engineers are required so that the term 'Nanotechnology' could be appropriately made into reality.

1.1.2 Synthesis of shape selective nanomaterials

Recent developments in the nanoscale science and technology have witnessed rapid growth in the number of synthetic methods for obtaining metal, semiconductor and other NPs in the form of specific sizes and shapes - from spherical, prismatic to tetrapodes[6]. These progresses have primarily been guided by the application potential of size and shape dependent optical, chemical and biochemical properties of nanomaterials. Several synthetic methods are available for their preparation and they may roughly be divided into two groups

TH-777_05612211

such as physical and chemical methods. Physical methods generally involve mechanical grinding, mechanical alloying, spray coating, and use of light, laser, and electron and ion beams[7]. Chemical methods include precipitation and redox reactions, thermal decomposition of organometallic compounds, electrochemical and sonnochemical methods[8]. In terms of ease of synthesis, sample handling and purification, and cost chemical methods are convenient than their physical counterparts. In this respect, the most widely used and convenient method is the 'wet chemical' process which is based on redox and precipitation reactions in solution.[9] The method essentially involves mixing various precursors under controlled conditions such as reagent and additive concentrations, solvent polarity, temperature and pH of the medium to obtain well-dispersed nanomaterials with desired structural features. For example, Lin and coworkers synthesized spherical Au NPs, which have been turned into penta-twinned, decahedron, truncated tetrahedron, cubes, octahedron and finally hexagonal nanosheets by introducing a small amount $AuCl_4^-$ salt into N, N-dimethy formamide solution containing poly (vinyl pyrrolidone), in conjunction with varying temperatures.[10] Murphy, Yang and coworkers subsequently developed the process for producing Au nanorods with different aspect ratio by adjusting the concentration of silver ion in solution containing cetyl trimethyl ammonium bromide (CTAB) as a stabilizer[11]. Chen et al reported the synthesis with high yield of nanocages by galvanic replacement reaction of silver templated $HAuCl_4$ in aqueous solution[12]. Although, various synthetic methods are available for the production of different shaped nanomaterials, the biochemical and biological methods of synthesis of well defined nanomaterials are powerful in their ability of controlled growth as well as appeal as environmental friendly methods. Sastry and coworkers have done significant work on the production of different shaped nanomaterials by biochemical and biological approaches[13].

At present there is a considerable interest for producing branched NPs of inorganic nanomaterials to achieve their specific optical, chemical, electronic and other properties for

TH-777_05612211

important applications[14]. In addition, these mono or multi-branched particles would be of particular importance in building hierarchical structures where each part of the NP may be used for the specific purposes. Multi-branched NPs have been synthesized by Carroll and coworkers where they have reported silver plate seeded synthesis of gold monopods, bipods, tripods and tetrapods using CTAB as the capping agent[15]. Multi-pods of metallic NPs were presented by Sau et al, where seeds of gold NPs were grown by reducing gold salts in the presence of CTAB[16]. Kuo et al subsequently developed the synthesis of small multi-branched gold NPs using multi step seeded growth approach with sodium dodecyl sulphate (SDS) as the surfactants[17]. Most recently, Barker et al synthesized multi-branched urchin like gold NPs by using water soluble thiol terminated molecules[18]. Our laboratory developed the production of multi-branched gold NPs by reduction of $AuCl_4^-$ by Fe^{2+} ions in the presence of SDS as the capping agent, where the growth would be centered at multiple places rather than a single one[19]. This is important not only in the understanding of growth mechanism but also technically useful with respect to their spectroscopic and catalytic properties and also using them for further selective growth of different structures using individual branched sites.

1.1.3 Functional Nanoparticles and Polymer-Nanoparticles Composite

Exploiting optical, electronic and catalytic properties of NPs for the development of ultrasensitive detection and imaging methods for biomedical sensors[20], catalysis for chemical reaction[21] and optoelectronic devices[22] is becoming increasingly important. For these kinds of applications, attaching specific molecular functionality on the surface of the NPs has attracted maximum attention. In addition, introducing the multiple functionalities to NPs would be of great value as it provides more flexibility and opportunity for multiplexing in bioanalytical application. It also provides new tools for precise control in the bottom-up assembly of nanoarchitectures[23]. In this regard, there are numerous reports that are available in the literature for the application of functionalized NPs. For example, functionalized

TH-777_05612211

magnetic NPs are used as magneto-switch devices for sensing of glucose and lactose.[24] DNA functionalized gold NPs are used in a bimolecular detection assay.[25] In addition, many bimolecularly functionalized gold NPs are used as building blocks of nanosuperstructures, detection of proteins and specific recognition of enzymes.[26] Another important nanomaterial is the semiconductor quantum dot, which produces a new class of fluorescent probes upon conjugating with biomolecules that have affinity for binding with selected biological structures.[27] On the other hand, water soluble hydroxylated quantum dots have been developed for labeling of oligonucleotides used as the probe for applications in fluorescent *in situ* hybridization assay in sperm cells.[28] Recently, quantum dot labeled RNA has been used in microarray assays for miRNA expression.[29] This is followed by successful use of streptavidin conjugated quantum dots for detection of human metaphase chromosomes with biotinylated oligonucleotide.[30] Additionally, functionalized carbon nanotubes (CNTs) portend many applications in nanobiotechnology. The use of chemically functionalized CNTs has been much emphasized to achieve specificity in binding to biological structures and as to how an electrolyte facilitates the control of the electrical properties of CNTs.[31]

Despite numerous methods that are available for the syntheses of molecular functionalized nanomaterials, the most widely used are the solution based ones that exploit chemical reduction of metal salts in the presence of surfactant molecules that wrap around the NPs surface leading to the formation of monolayers, which not only protect the NPs from agglomeration but also determine the nature of the interaction with their environment, hence controlling their solubility in different media and assembly into complex superstructures. On the other hand, functionality of the molecules on the NP surface is the key factor defining almost every application of the nanomaterials.[32] Recently, it has been realized that molecule-surface interactions are mainly dependent on the crystallographic orientation of the surface facets that will be particularly weak at the vertices of the NP polyhedron.[33] In

TH-777_05612211

addition, covalent and strong noncovalent interactions between molecules attached to the NPs have been used to engineer various nanostructures, including mono and multilayers and nanocomposites with electrically conducting polymer and oligomers. In this regard, creation of functionality on the surfaces of NPs is desirable, for the construction of superstructures and controlled growth of nanocomposites of metal and polymer materials.[34]

Creating functionality on the surface of NP is desirable for the purpose of the particles handling and construction of functional architecture and subsequently that can combine the mechanical flexibility, optical properties of conducting polymer. High electrical conductivity and magnetic properties of surface modified metal NPs have inspired the development of several techniques for the controlled growth of nanocomposites of metal and polymeric materials.[35] These nanocomposite materials can act as substrates for catalysis and help in the detection of biologically active species.[36] In addition, these metal and polymer nanocomposites have a variety of application potential, such as electrodes for fuel cells, support for heterogeneous and homogeneous catalysis in selected chemical reaction and optical and optoelectronics devices, chemical and electrochemical sensors and actuators.[37]

Among the composite materials, polyaniline-gold NP (PANI-Au NP) composites have attracted extraordinary attention due to their ease of synthesis, environmental stability, tunable conductivity and unique doping/dedoping chemistry.[38] In addition, there is vast number of recent works in the literature related to the composites of PANI with Ag NPs, Cu NPs or semiconductor NPs.[39] A significant scientific attention has been paid to the discovery of newer methods of generation of nanoscale shape and size selective 1-dimensional nanofibers, nanotubes and raspberry like spherical structures, flowers, stars and plates of PANI and their composites especially with gold NPs.[40] It is also known that PANI nanofibers decorated with Au NPs exhibit non-volatile memory devises.[41] Metal NP supported PANI can also be used as potential candidates for catalysis of some organic reaction and subsequently that PANI can also act as a colorimetric sensor due to its acid-base redox reaction.[42] There are a vast number of techniques which have been developed to

TH-777_05612211

achieve PANI-Au NP composites. Sarma et al reported for the first time a one-spot synthesis of PANI-Au NP composite by using hydrogen peroxide as reducing as well as oxidizing agent.[43] This has been followed by their report on water soluble colloidal dispersion of PANI or PANI-Au NPs composites from monomer of aniline vapor, which can overcome their poor processability.[44] Kaner group have been developed a different technique to achieve water dispersible PANI or PANI-Au NP composite with different size and shape selectivity.[45] Further, the attachment between the metal NPs and conducting polymer of nanocomposite materials may play crucial role in electronics devices, because the charge transfer at the contact between the metal NPs and polymer plays an important role in many areas of technology. In this regard, the 'grafting from' approach is an effective means of enhancing the attachment between polymer and filler of metal NPs matrices.[46]

Further, tailored sensoric, electronic, optical, photoelectrochemical and bioelectroanalytical properties can be designed by organized molecular or biomolecular NP hybrid configuration on surfaces.[47] The surface modifier of the nanomaterials may then be used to couple unique electronic, photonics and catalytic properties of quantum sized nanomaterials with molecular or macromolecular functionalities to yield hybrid system of a new feature. In this regard, there is an considerable interest in rapidly expanding field of nanobiotechnology in integrating hard and soft structures into complex functional nanosystem that have stimuli responsive properties.[48] On the other hand stimuli responsive materials such as hydrogels are important for futuristic nanoscale drugs, which can change their properties such as size, shape and solubility in solvent in response to changes in stimuli such as temperature, pH and other chemical or biological species, make the hydrogel ideal for drug delivery and controlled release of bioactive molecules.[49] One of the important hydrogels is poly-N-isopropyl acrylamide (pNIPAm) with a lower critical solution transition temperature (LCST) at 32^{o}C and the same can be changed up to 60^{o}C by various degree of co-polymerization with monomer of acrylic acid (AAc), which offer a robust architecture that can response very well to environmental changes such as temperature, pH, ionic strength

TH-777_05612211

and solvents.[50] On the other hand, chemically or biologically functionalized NPs could be encapsulated to hydrogels that are held by electrostatic (due to carboxylic acid group on the backbone of the hydrogel) or van der Waals forces and the functionalized NPs could thus be released in response to a stimulus and subsequently that can be applied to the delivery system in the emerging field of biomedical sciences.[51] In addition, pNIPAm hydrogels grafted with thiol functionalized metallic NPs can also alter the physical properties of the hydrogel as well as metal NPs. Zhu et al showed that hydrogel with hydrophobically conjugated thiol attached gold NPs have enhanced the phase switching behavior of the thermosensitive hydrogels.[52] However, understanding the functioning of both kinds of hybrids is important for the development of potential thermosensitive applications in sensors, photonics, electronic devices and site specific drug delivery.[53] Kumacheva and co-workers reported photothermally triggered reversible deswelling of hydrogels loaded with gold nanorods by absorbing near IR-light, which can be used promising application for drug delivery and photodynamic therapy.[54]

One of most important goals in the fast growing field of nanotechnology is to develop more environmentally friendly and sustainable methods for the synthesis of nanomaterials. The primary challenges in this regard are maximization of usages of environmentally friendly materials and integration of the principle of 'green chemistry' as far as chemistry is involved in the generation of nanscale based products. Such approaches will also be advantageous for the generation of metal NP based polymer composite into biologically relevant systems.[55] In recent years, biodegradable polymer based metal NP composites have gained maximum attention due to their potential application for the design of drug delivery system, support for homogeneous or heterogeneous catalysis for important chemical reactions, antibacterial activities, biosensors and interconnects for the hierarchical assembly of nanoscale component into macroscale systems.[56] One of important biodegradable polymers is chitosan, which is the second most abundant natural polymer after cellulose. Chitosan (β-(1, 4) 2-amino-2-*D*-glucose) is a cationic biopolymer obtained by

TH-777_05612211

alkaline N-deacetylation of chitin, which is the main component of the shells of the crabs. Chitosan has many potential applications in the field of biotechnology, pharmaceutical, wastewater treatment, cosmetic coatings and food sciences.[57] Another advantage of chitosan is that the backbone of the polymer has significant content of primary amine and hydroxyl functional groups making the polymer to have high affinity towards the metal ions. Several groups have taken the opportunity to reduce the metal salts physisorbed onto chitosan to corresponding NPs and shown their catalytic activity by reducing chromate (using Pd), phenol (Pd) and aromatic nitro compounds (Ni, Cu, Cr, Zn).[58] Most recently, our laboratory developed a novel green method of synthesis of chitosan-silver NP composite and the composite has a significant catalytic activity for the reduction of 4-nitro phenol into 4-amino phenol and also higher antibacterial activity compared to the individual components of either chitosan or silver NPs.[59] In addition, some of the chitosan-metal NP composites have been used for the catalysis of carbon-carbon bond formation involving Suzuki, Heck and Sonogashiva type of reactions.[60] Further, if chitosan can also be made in the form of beads, fibers, membranes then the application potential of the chitosan based metal NP polymer composite could become even more versatile.

1.1.4 Assembly of Nanoparticles Using Molecular Level Interactions

In the next generation, the frontiers of nanoscience and technology would depend primarily on organization of one, two and three dimensional nanostructures into hierarchical higher order functional structures.[61] However, such organization of particles would necessarily involve the principles of chemistry, physics and biology in order to have the meaningful application. The ability to assemble the NPs with controllable sizes and shapes is important because of the many frontier applications, such as sensors, catalysis, medical diagnostics, information storages and quantum computation; require controlled arrays of nanoarchitectures and component minaturation.[62] Further, self assembly or assisted assembly of anisotropic nanomaterials into linear chain-like array of superstructures has currently attracted great attention due to their collective properties that are arise from

TH-777_05612211

coupling of optical and electronic properties individual NPs.[63] Alternatively, these properties of assembled materials can be used to make the potential devices such as fabrication of plasmonics waveguides, surface plasmon based biosensors and single electron transistor.[64] In the literature, there are many different techniques that are available for the assembling of NPs into different geometrics such as solvent evaporation hydrophobic NPs, molecular cross linking in colloidal aggregates, template directed assembly using biomacrolecules such as DNA, protein, antigen-antibody, peptide and biodegradable synthetic polymer.[65] Among them template directed self assembling of NPs attracted interest in nanoscience and technology. Despite, numerous methods that are available for the generation of 2D and 3D assembly of NPs, which are commonly in the form of squares, hexagonal arrangement or stacks, their assembly into 1-D arrays, are limited because of the difficulty that arises owing to their ways of preparation. There are some reports are available in the literatures for the preparation of 1-D linear chain-like arrays involving methods such as physical confinement in ion beam etched tracks glass, porous anodic alumina or using linear supramolecular or macromolecular templates of DNA, oligonuleotides, protein, peptides, tobacco mosaic virus rods and carbon nanotubes.[66] However, these methods are either expensive or require multiple steps; moreover materials used as templates may influence the photonics and electronics properties of 1-D NP assembly. Furthermore, 1-D NPs assembly can also produced by spontaneously self assembling isotropic NPs with intrinsic magnetic and electric dipoles. However, in this way the assembly of face centered cubic (fcc) crystalline metallic NPs (especially gold and silver NPs) into 1-D chain-like array is very difficult because it does not have any intrinsic electric dipoles which is the origin of electronic dipole-dipole interaction.[67] To overcome this difficulty, the NPs surface charge should be in heterogeneity and that can be achieved either in non uniform spatial distribution of capping ligand on different crystallographic faces or nanospace separation in mixed ligand stabilization layer which could be responsible for the driving force for the assembly of NPs into 1-D linear superstructures.[68]

TH-777_05612211

The central themes of the part of the introduction presented above hover around newer methods of syntheses of NPs, their organization into superstructures and their composites with polymer. Each of the above topics has implicit in it a potential for commercial applications, in addition to fundamental understanding of the process involved. They guide the objective of the present thesis in developing newer synthetic methods for the syntheses of NPs and their systematic assembly into hierarchical higher order structures and syntheses and application of their polymer composites. Thus while only synthesis of NP has been stressed minimum in the thesis the ulterior aim of organization and composite formation followed by their use have been stressed in more detail. For example, molecularly controlled assembled NPs would not only reveal a great deal about the nature of molecular interaction between the NPs and assembling molecules but also offer newer materials with tunable properties that could have real applications. This is especially true with respect to use of molecular interactions as the driving force of organization. Availability of methods of organization based on molecular interactions would allow the full use of chemistry in building materials made of NPs. Especially, the use of 'soft' interaction may offer the possibilities of molecular level control over reversible assembly and disassembly of NPs in solution, which remain much to be explored. Further, understanding of the interparticle interactions involving NPs, which is essential for controlling catalytic, electrical and optical properties of the assembled GNPs, can be expected to aid in the development of robust superstructures. Moreover, the formation of arrays of GNPs by using molecular interaction could prove to be much superior over the hard and soft template based methods, as the molecules involved in the organization may influence the properties of the assembled structures. Additionally, the molecular assembly approach could turn out to be a convenient way of generating well-defined composite nanowires and nanofibres that would pave the further advancement in nanoscience and technology. Keeping the above points in view the brief introduction about the chapters presented in the thesis is given below.

TH-777_05612211

1.1.5 Works described in the thesis

The work described in the thesis is to address the development of novel and simple methods of syntheses of shape selective NPs and polymer metal NPs composites and molecularly controlled organization of NPs and their subsequent use in applications based on their physical, chemical and biological properties.

Chapter 2 reports the simple method of synthesis of Au NPs using an inorganic ion, Fe^{2+}, for reducing $HAuCl_4$. Single or multiple branched Au NPs were formed when the reaction was carried out in the presence of sodium dodecyl sulfate (SDS). In some cases specific shapes of the particle took the forms such as the one which could be termed as a "nanofan". On the other hand when the same reaction was carried in the presence of SDS and Na_2S, spherical NPs of less than 10 nm diameters were formed. In addition, the reaction when carried out in the presence of starch (instead of SDS) resulted in the production of spherical Au NPs of primarily small sizes. Overall, the observations suggest that the combination of factors that involve reagents and other reaction conditions such as the stabilizing agent that finally contributes towards the shape in the formation of NPs. Also, the role of Fe^{2+} ions towards the shape formation cannot be ruled out. This is important in order to understand the growth mechanism of higher order structure, which can be potentially useful with respect to their spectroscopic and catalytic properties.

Chapter 3 introduces a green and mild approach to one-step synthesis of Ag NP-chitosan composite, by using chitosan as the reducing agent, at $95^{o}C$ and in the presence of aqueous sodium hydroxide. The NPs generated in the present method were of uniform and narrow particle sizes; with typical sizes less than 5.0 nm. The composite was tested for heterogeneous catalysis with Ag NPs being the active catalyst and chitosan as the support. The catalytic efficiency for the reduction of 4NP to 4AP for the composite was high with a TOF value of $1.58 \pm 0.3 \times 10^{-3}$ s^{-1}. The small particle size and thus high number of surface atoms makes the composite a rather appealing material for catalysis and other application.

TH-777_05612211

Further, the additional advantage of being able to use the catalyst under micro-heterogeneous conditions makes its usefulness rather appealing. For example, while catalyst concentrations needed under heterogeneous condition was on the order of several g/L, the same reaction could be achieved in similar times using catalyst concentrations of mg/L. The synthetic method, which we have developed in the present study, might be useful for further development of green NP synthesis in other situations. Since chitosan is biocompatible, the composite can be useful for biological applications such as antimicrobial agents. Recently, our group reported that (not incorporated in the thesis) the antibacterial activity against *E. coli* was significantly enhanced by the loading of chitosan-Ag NPs composite compared to those of either chitosan or Ag NPs. Since, chitosan can be made in the form of beads, fibers, membranes the application potential of the composite could become even more versatile.

Chapter 4 reports the application of the composite reported in Chapter 3, using Ag NPs present in the composite as an efficient catalyst, in selective C-C coupling of phenolic compounds, in the presence of molecular iodine. The reactions were carried out with phenol and a few of its derivatives as well as naphthols. The results show that the reaction proceeded via formation of p-iodophenol followed by *o-p* coupling leading to the product. When the para position of phenol was blocked by a substituent then only iodination at the ortho position could be observed without the formation of coupled products. In the case of naphthols *o-o* coupling could only be observed. Based on the results a mechanism is proposed for the coupling reaction occurring at the surface of Ag NPs. Iodine atoms present on the surface of Ag NP catalyst plays the key role in the formation of selective coupling via the *p*-iodophenol intermediate. Also, the formation of sandwich-type geometry between phenoxyl radical and p-iodophenoxyl radical provides the key step in *o-p* coupling with high yield. The present approach may open new vistas in synthetic organic chemistry; especially Ag NP catalyzed C-C coupling reactions beyond the reported examples.

Chapter 5 reports the results of investigations related to the changes in the LCST (lower critical solution temperature) of a thermosensitive polymer hydrogel, in the presence of different stabilizing agent capped gold nanoparticles (GNPs), by using surface plasmon

TH-777_05612211

resonance (SPR) as a probe. Different stabilizing agent such as thioglycolic acid, tryptophan and phenylalanine were attached to GNP surface by strong covalent bonding. The resulting capped GNPs were then mixed with pNIPAm-co-polymer hydrogel. The pNIPAm- AAc consists of a known bioadhesive and biocompatible thermoresponsive copolymer derived by radical polymerization of selected mixture of N-isopropyl acrylamide (NIPAm), methylene-bis-acrylamide and acrylic acid (AAc). Depending on the nature of the capping molecules their volume phase transition temperature varied from 34^{o}C to 40^{o}C. The optical absorption due to Au NPs reduced significantly when stabilized with hydrophobic groups and with significant blue shift of wavelength maximum. Thus the surface plasmon resonance absorption of Au NPs could be used as a probe for the studies of interaction between the stabilizer of NPs and the polymer hydrogel. The more biocompatible nature of these composites hydrogel polymer will create a number of applications as optical, electronic and biomedical functional materials.

Chapter 6 reports the generation of assembly of 1-dimensional chain-like array of Au nanoparticles (NPs) by sparingly soluble acetanilide in water. This was achieved in two different ways. In the first method, acetanilide was added, with increasing concentration, into aqueous $HAuCl_4$ to produce Au NPs as well as for the formation of assembly, which varied according to the concentration of acetanilide. The second method involved formation of spherical Au NPs at the lowest concentration of acetanilide, which was followed by the formation of assembly of various lengths upon further addition of variable amount of a acetanilide. We found that the linear chain-like arrays could be broken into individual particles by first dilution of the solution concentration followed by treatment with ultrasonic waves. The individual Au NPs again formed linear chain-like arrays upon addition of excess acetanilide. In addition, the role of acetanilide for the formation of linear chain-like array of Au NPs is also discussed in this chapter. However, the present methods yielded the GNPs with broad size distribution, which could not be used effectively for surface area controlled catalytic activity studies. In order to study the surface area controlled catalytic activity of 1-D assembly of Au NPs, we have developed a method for the formation of linear assemblies of

TH-777_05612211

citrate stabilized spherical gold nanoparticles (GNPs) in the presence of acetanilide in aqueous medium. The length of the assembly was dependent on the concentration of acetanilide. At higher concentrations branching of the assembly occurred instead of increase in the length of assembly. The catalytic properties of the assemblies were dependent on the concentration of the acetanilide. This means the effective surface areas of the metal nanoparticles in the assembly were much dependent on the length of the assembly, which could be controlled by the concentration of acetanilide. The results indicated a linear dependence of the effective surface area on the concentration of acetanilide. Also, the observations suggest that the presence of $NaBH_4$ in the reaction medium led to the fusion of GNPs into fibrous form thus reducing the effective surface area for catalysis.

Chapter 7 consists of description of the generation of water-dispersible and stable polyaniline-Au NP nanocomposite with size and shape selectivity. Sparingly soluble acetanilide has been used to first generate Au nanoparticles (NPs) by reduction of $HAuCl_4$, followed by polymerization leading to the formation of the composite. The size and shape of the composites could by tuned by controlling the concentration of acetanilide. At the lowest concentrations of acetanilide nano-raspberry-like particles of PANI-Au NP composites were formed. At higher concentrations these spherical structures were joined by polymer to form continuous fibers. Acetanilide has unique advantages over aniline because of its environmental and solvent stability and is amenable to functionalization using well-established synthetic schemes. The knowledge obtained from this work may pave various ways of systematic development of three-dimensional water-soluble metal NP-polymer composites with tunable electrical, optical and chemical properties.

Chapter 8 reports the results on the investigation of the effect of amino acids on the assembly formation of citrate-stabilized spherical Au NPs into 1-D chain-like superstructures. The nature of the assembly formation and associated optical properties were found to be dependent on the concentration of amino acid as well as the nature of the side chain group present in the amino acid. The changes were highly specific to the amino acid

TH-777_05612211

present in the medium. For example, when lysine or tryptophan was used micromolar quantities of the acid was enough to induce a large scale organization. On the other hand, when phenylanine and glutamine were used milli molar quantities of amino acids were required to achieve significant changes in the absorption spectra. Thus the assembly formation could not only be useful for identification of amino acids but also may be used to estimate their solution concentrations. In addition, 1D chain of necklace-like Au NPs converted into nanofibers when excess hydrophilic amino acid was used. On other hand, at higher concentration of hydrophobic amino acids, the necklace-like Au NPs did not get transformed into nanofibers. Our observations suggest that the nature of the side chains present in the amino acids with their functional groups may play an important role for controlling the interparticles interaction and their subsequent fusions in the amino acid assembled Au NPs chain.

Chapter 9 reports the results on the use of an ordinary compound like vitamin C being used not only as a reducing agent but also in the organization of the generated NPs into one-dimensional wire-like structures. The spontaneous fiber formation and formation of Au NPs by ascorbic acid (AA) have been coupled to generate fibers made up of composite of Au NPs and the polymer from the degradation product of AA. The fiber appeared in the form of a fiber bundle with branched structures having overall dimensions on the order of several millimeters. They have typical widths of 1-4 μm with length of each segment of fiber bundle on the order 40 μm. These fibers can also be decorated with previously synthesized metallic NPs and the electrical conductivity with the characteristic of a metal can be achieved in the fibers. We have also developed a new strategy for the generation and fibrous assembly of core shell (Au/Ag) metal NPs using the same vitamin. These assembled wires have different optical properties and electrical conductivities depending on the level of presence of metal NPs. These structures have electrical properties ranging from insulator to metallic conductor and thus can be useful for versatile usages.

TH-777_05612211

1.1.6 References

1. (a) Mayer, G. J.; Searson, P. C. *The Electrochemical Society Interface 23* (Witner ***1993***). (b) Matthew, R. W. *J. Phys. Chem.* **1987**, *91*, 238. (c) Hulteen, J. C.; Martin, C. R. *J. Mater. Chem.* **1997**, *7*, **1075**. (d) Lakshmi, B. B.; Patrissi, C. J.; Martine, C. R. *Chem. Mater*. 1997, *9*, 2544. (d) Turkevich, J.; Kim, G. Science **1970**, 169, 873.

2. (a) Lavine, M.; Vinson, V.; Coontz, R. *Science* **2005**, *310*, 1131. (b) Voura, E. B.; Jaiswal, J. K.; Mattoussi, H.; Simon, S. M. *Nat. Medicine* **2004**, *10*, 993. (c) Wu, X. Y.; Liu, H. J.; Liu, J. Q.; Haley, K. N.; Treadway, J. A.; Larson, J. P.; Ge, N. F.; Peale, F.; Bruchez, M. P. *Nat. Biotechnology* **2003**, *21*, 41.

3. (a) Alivisatos, A. P. *Science* **1996**, *271*, 933. (b) Link, S.; Mohamed, M. B.; El-Sayed, M. A. *J. Phys. Chem. B* **1999**, *103*, 303. (c) Link, S.; El-Sayed, M. A. *J. Phys. Chem. B* **1999**, *103*, 8410. (d) Brioude, A.; Jiang, X. C.; Pileni, M. P. *J. Phys. Chem. B* **2005**, *109*, 13138.

4. (a) Murray, C. B.; Kagan, C. R.; Bawendi, M. G. *Science* **1995**, *270*, 1335. (b) Lee, P. A. Ramakrishnan, T. V. *Rev. Mod. Phys*. **1985**, *57*, 287. (c) El-Sayed, M. A. *Acc. Chem. Res.* **2001**, *34*, 257. (d) Henglein, A. *Top. Curr. Chem*. **1998**, *143,* 113.

5. (a) Corma, A.; Garcia, H. *Chem. Soc. Rev*. **2008**, *37*, 2096. (b) Schmid, G.; Baumle, M.; Geerkens, M.; Helm, I.; Osemann, C.; Sawitowski, T. *Chem. Soc. Rev*. **1999**, *28*, 179.

6. (a) Sanedrin, R. G.; Georganopoulou, D. G.; Park, S.; Mirkin, C. A. *Adv. Mater*. **2005**, *17*, 1027.(b) Jin, R. C.; Cao, Y. W.; Mirkin, C. A.; Kelly, K. L.; Schatz, G. C.; Zheng, J. G. *Science* **2001**, *294*, 1901. (c) Murphy, C. J.; San, T. K.; Gole, A. M.; Orendorff, C. J.; Gao, J. X.; Gou, L.; Hunyadi, S. E.; Li, T. *J. Phys. Chem. B* **2005**, *109*, 13857. (d) Hao, E.; Bailey, R. C.; Schatz, G. C.; Hupp, J. T.; Li, S. Y. *Nano Lett*. **2004**, *4*, 327. (e) Hao, E.; Schatz, G. C.; Hupp, J. T. *J. Fluoresc.* **2004**, *14*, 331. (f) Jana, N. R.; Gearheart, L.; Murphy, C. J. *J. Phys. Chem. B* **2001**, *105,* 4065.

7. (a) Mayer, A. B. R. *Polymer. Adv. Technol*. **2001,** *12,* 96. (b) Dowling, A. P. Nano Today **2004**, 20. (c) Yu, D.; Tretyakov, A.; Lukashin, V. *Russ. Chem. Rev.* **2004**, *73*, 899. (d) Toshima, N.; Yonezawa, T. *New. J. Chem*. **1998**, *22*, 1179.

TH-777_05612211

8. (a) Aiken, J. D.; Finke, R. G. *J. Mol. Cata. A* **1999**, *145*, 1. (b) Bonnemann, H.; Richards, R. M. *Eur. J. Inorg. Chem*. **2001**, 2455. (c) Liz-Marzan, L. M. *Mater. Today* **2004**, 7, 26. (d) Gedanken, A. *Ultrasonics Sonochem*. **2004**, *11*, 47.

9. (a) Horn, D.; Rieger, J. *Angew. Chem. Int. Ed.* **2001**, *40*, 4330. (b) Park, J.; Privman, E. V.; Matijevic, E. *J. Phys. Chem. B* **2001**, *105,* 11630. (c) Goia, D. V. *J. Mater. Chem.* **2004**, *14*, 451. (e) Suber, L.; Sondi, I.; Matijevic, E. *J. Colloid Interface Sci*. **2005**, *288*, 489.

10. Chen, Y.; Gu, X.; Nie, C-G.; Jiang, Z-J. ; Xie, Y. Z. ; Lin, C. J. *Chemm. Commun*. **2005**, 4181.

11. (a) Jana, N. R. ; Gearheart, L. ; Murphy, C. J. *Chem . Commun.* **2001**, 617. (b) N. R.; Gearheart, L.; Murphy, C. J. *Adv. Mater*. **2001**, *13*, 1389. (c) Kim, F.; Song, J. H.; Yang, P. *J. Am. Chem. Soc.* **2002**, *124,* 14316.

12. Chen, J.; Wiley, B.; Li, Z. Y.; Campbell, D.; Saeki, F.; Hu, C.; Au, L.; Lee, J.; Li, X.; Xia, Y. *Adv. Mater.* **2005**, *17,* 2255.

13. (a) Parikh, R. Y.; Singh, S.; Prasad, B. L. V.; Patole, M. S.; Sastry, M.; Shouche, Y. S. *Chem. Bio. Chem.* **2008**, *9*, 1415. (b) Singh, S.; Bhatta, U. M.; Satyam, P. V.; Dhawan, A.; Sastry, M.; Prasad, B. L. V. *J. Mater. Chem.* **2008**, *18*, 2601. (c) Singh, A.; Hede, S.; Sastry, M.; *Small* **2007**, *3*, 466. (d) Bansal, V.; Poddar, P.; Ahmad, A.; Sastry, M.; *J. Am. Chem. Soc.* **2006**, *128,* 1958. (e) Senapati, S.; Ahmad, A.; Khan, M. I.; Sastry, M.; Kumar, R. *Small* **2005**, *1*, 517. (f) Shankar, S. S.; Rai A.; Ankamwar B.; Singh A.; Ahmad, A.; Sastry, M. *Nat. Mater.* **2004**, *3*, 482.

14. (a) Narayanan, R.; El-Sayed, M. A. *J. Phys. Chem. B* **2005**, *109*, 12663. (b) Cui, Y.; Banin, U.; Bjork, M. T.; Alivisatos, A. P. *Nano Lett.* **2005**, *5,* 1519. (c) Millstone, J. E.; Park, S.; Shuford, K. L.; Qin, L. D.; Schatz, G. C.; Mirkin, C. A. *J. Am. Chem. Soc.* **2005**, *127*, 5312.

15. Chen, S. H.; Wang, Z. L.; Ballato, J.; Foulger, S. H.; Carroll, D. L. *J. Am. Chem. Soc.* **2003**, *125*, 16186.

16. Sau, T. K.; Murphy, C. J. *J. Am. Chem. Soc.* **2004**, *126*, 8648.

17. Kuo, C.-H.; Huang, M. H. *Langmuir* **2005**, *21,* 2012.

TH-777_05612211

18. Barker, O. M.; Wunsch, B. H.; Stellacci, F. *Chem. Mater*. **2006**, *18,* 3297.

19. Murugadoss, A.; Chattopadhyay, A. *J. Nanosci. Nanotechnol.* **2007**, *7,* 1730.

20. (a) Salem, A. K.; Searson, P. C.; Leong, K. W. *Nat. Mater.* **2003**, *2*, 668. (b) Loo, C.; Lowery, A.; Halas, N.; West, J.; Drezek, R. *Nano Lett*. **2005**, *5*, 709. (c) Gloudenis, M.; Foss, C. A. *J. Phys. Chem. B* **2002**, *106*, 9484.

21. (a) Ornelas, C.; Ruiz, J.; Salmon, L.; Astruc, D. *Adv. Synth. Catal*. **2008**, *350*, 837. (b) Marubayashi, K.; Takizawa, S.; Kawakusu, T.; Arai, T.; Sasai, H. *Nano Lett*. **2003**, *5*, 4409.

22. (a) Zubarev, E. R.; Xu, J.; Sayyad, A.; Gibson, J. D. *J. Am. Chem. Soc*. **2006**, *128*, 4958.

23. (a) Katz, E.; Willner, I. *Angew. Chem. Int. Ed*. **2004**, *43*, 6042. (b) Storhoff, J. J.; Mirkin, C. A. *Chem. Rev*. **1999**, *99*, 1849. (c) Wang, Z.; Levy, R.; Fernig, D. G.; Brust, M. *Biconjugate Chem*. **2005**, *16*, 497.

24. (a) Katz, E.; Weizmann, Y.; Willner, I. *J. AM. Chem. Soc*. **2005**, *127*, 9191. (b) Katz, E.; Willner, I. *Chem. Commun*. **2005**, 4089.

25. (a) MacBeath, G. *Nat. Genet.* **2002**, *32*, 526. (b) Rosi, N. L.; Mirkin, C. A. *Chem. Rev*. **2005**, *105*, 1547. (c) Butron, A. S.; Mirkin, C. A.; Stoeva, S. I.; Lee, J.-S. *Nanoscape*, **2007**, *4*, 3.

26. (a) Niazov, T.; Pavlov, V.; Xiao, Y.; Gill, R.; Willner, I. *Nano Lett*. **2004**, *4*, 1683. (b) Nimeyer, M.; Ceyhan, B.; Hazarika, P. *Angew. Chem. Int. Ed*. **2003**, *42*, 5766. (c) Sastry, M.; Rao, M.; Ganesh, K. N. *Acc. Chem. Res*. **2002**, *35*, 847.

27. (a) Wang, M.; Dykstra, T. E.; Lou, X.; Salvador, M. R.; Scholes, G. D.; Winnik, M. A. *Angew. Chem, Int. Ed*. **2006**, *45*, 2221. (b) Waller, H. *Angew. Chem. Int. Ed*. **1993**, *32*, 41. (c) Michalet, X.; Pinaud, F. F.; Bentolila, L. A.; Tsay, J. M.; Doose, S.; Li, J. J.; Sundaresan, G.; Wu, A. M.; Gambhir, S. S.; Weisss, S. *Science* **2005**, *307*, 538. (d) Zu, L.; Zhu, M. Q.; Hurst, J. K.; Li, A. D. Q. *J. Am. Chem. Soc*. **2005**, *127*, 8968. (d) Alexson, D.; Chen, H.; cho, M.; Dutta, M.; Li, Y.; Shi, P.; Raichura, A.; Ramadurai, D.; Parikh, S.; Stroscio, M. A.; Vasudev, M. *J. Phys. Condens. Mater*. **200**5, *17*, R637.

TH-777_05612211

28. Pathak, S.; Choi, S. K.; Arnheim, N.; Thompson, M. E. *J. Am. Chem. Soc*. **2001**, *123*, 4103.

29. Liang, R. Q.; Li, W.; Li, Y.; Tan, C. Y.; Li, J. X.; Jin, Y. X.; Ruan, K. C. *Nucleic Acids Res*. **2005**, *33*, e17.

30. (a) Xiao, Y.; Barker, P. E. *Nucleic Acids Res*. **2004**, *32*, e28. (b) Chan, P. M.; Yuen, T.; Ruf, F.; Gonzalez-Maeso, J.; Sealfon, S. C. *Nucleic Acids Res*. **2005**, *33*, e161.

31. (a) Sethuraman, A.; Stroscio, M. A.; Dutta, M. *Potential Application of Carbon Nanotube in Bioengineering Biological Nanostructures and Applications of Nanostructures in Biology: Electrical, Mechanical and Optical* (Bioengineering Vol 5) ed Stroscio, M. A.; Dutta, M. (New York: Kiuwer-Academic): **2004**. (b) Chen, R.; Zhang, Y.; Wang, D.; Dai, H. *J. Am. Chem. Soc*. **2001**, *123*, 3838. (c) Kurger, M.; Buitelaar, M. R.; Nussbaumer, T.; Schonenberger, C.; Forro, L. *Appl. Phys. Lett*. **2001**, *78*, 1291. (c) Torrones, M.; Torrones, H.; Banhart, F.; Charlier, J,-C.; Ajayan, P. M. *Science* **2000**, *288*, 1226.

32 (a) Hu, Y.; Uzun, O.; Stellacci, F. *J. Phys. Chem. C* **2008**, *112*, 6279. (b) Verma, A.; Nakade, H.; Simard, J. M.; Rotello, V. M. *J. Am. Chem. Soc*. **2004**, *126*, 10806. (c) Templeton, A. C.; Wuelfing, M. P.; Murray, R. W. *Acc. Chem. Res*. **2000**, *33*, 27. (d) Stellacci, F.; Bauer, C. A.; Meyer-friedrichsen, T.; Wenseleers, W.; Alain, V.; Kubler, S. M.; Pond, S. J. K.; Zhang, Y. D.; Marder, S. R. Perry, J. W. *Adv. Mater*. **2002**, *14*, 194. (e) Devries, G. A.; Brunnbaur, M.; Hu, Y. ; Jackson, A. M. ; Long, B. ; Neltner, T. ; Uzun, O. ; Wunch, B. H. ; Stallacci, F. *Science* **2007**, *315*, 358.

33. (a) Perepichka, D. F.; Rosei, F. *Angew. Chem. Int. Ed*. **2007,** *46*, 6006. (b) Love, J. C.; Estroff, L. A.; Kriebel, J. K.; Nyzzo, R. G.; Whitesides, G. M. *Chem. Rev*. **2005**, *105*, 1103. (c) Ulman, A. *Chem. Rev*. **1996**, *96*, 1533. (d) Hostellar, M. J.; Templeton, A. C.; Murray, R. W. *Langmuir* **1999**, *15*, 3782.

34. (a) Daniel, M,-C.; Astruc, D. *Chem. Rev*. **2004**, *104*, 293. (b) Sih, B. C.; Wolf, M. O.; *Chem. Commun* **2005**, 3375.

TH-777_05612211

35. (a) Lahav, M.; Weiss, E. A.; Xu, Q.; Whitesides, G. M. *Nano Lett*. **2006**, *6*, 2166. (b) Cepak, V. M.; Hulteen, J. C.; Che, G.; Jirage, K. B.; Lakshmi, B. B.; Fisher, E. R.; Martin, C. R. *J. Mater. Res*. **1998**, *13*, 3070. (c) Park, S.; Lim, J,-H.; Chung, S,-W.; Mirkin, C. *Science* **2004**, *303*, 348. (e) Lov, J. C.; Urbach, A. R.; Prentiss, M. G.; Whitesides, G. M. *J. Am. Chem. Soc*. **2003**, *125*, 12696.

36. (a) Wang, J.; Dai, J.; Yarlangadde, T. *Langmuir* **2005**, *21*, 9. (b) Astruc, D.; Lu, F.; Aranzaes, J. R. *Angew. Chem. Int. Ed*. **2005**, *44*, 7852. (c) Payne, F. G.; Raghavan, S. R. *Soft Mattter* **2007**, *3*, 1. (c) Liu, J.; Tian, S.; Knoll, W. *Langmuir* **2005**, *21*, 5596.

37. (a) Bashyam, R.; Zelenay, P. *Nature* **2006**, *443*, 63. (b) Kamat, P. V. *J. Phys. Chem. B* **2002**, *106*, 7729. (c) Novak, P.; Mueller, K.; Santhanam, K. S. V.; Has, O. *Chem Rev*. **1997**, *97*, 207. (d) Holdcroft, S. *Adv. Mater*. **2001**, *13*, 1753. (e) Virji, S.; Huang, J.; Kaner, R. B.; Weiller, B. H. *Nano Lett*. **2004**, *4*, 591. (f) Herrikhuyzen, J. V.; George, S. J.; Vos, M. R. J.; Sommerdijk, N. A. J. M.; Ajayaghosh, A.; Meskers, S. C. J.; Schenning, A. P. H. J. *Angew, Chem. Int. Ed.* **2007**, *46*, 1825.

38. (a) Gangeopadhyay, R.; De, A. *Chem. Mater*. **2000**, *12*, 608. (b) Jin, Z. ; Su, Y. ; Duan, Y. *Sens. Actuators, B* **2001**, 72, 75. (c) Chiang, J. C.; MacDiarmid, A. G. *Synth. Met.* **1986**, *13*, 193. (d) Xia, Y. N.; Wiesinger, J. M.; MacDiarmid, A. G.; Epstein, A. *J. Chem. Mater*. **1995**, *7*, 443.

39. (a) Mazur, M.; Krysinski, P. *Electrochim. Acta* **2001**, *46*, 3963. (b) Liao, C.; Gu, M. *Thin Solid Films* 2002, *408*, 37. (c) Chen, Y.; Kang, E. T.; Neoh, K. G. *Appl. Surf. Sci*. **2002**, *185*, 267. (d) Inou, M. B.; Nebesny, K. W.; Fernando, Q.; Castillo-Ortega, M.; Inoue, M. *Synth. Met*. **1990**, *38*, 205.

40. (a) Sanjanlal, P. R.; Sreeprasad, T. S.; Nai, S.; Pradeep, T. *Langmuir* **2008**, *24*, 4607. (b) Shiigi, H.; Yamamoto, Y.; Yoshi, N.; Nakao, H.; Nagaoka, T. *Chem. Commun*. **2006**, 4288. (c) Li, D.; Kaner, R. B. *J. Am. Chem. Soc*. **2006**, *128*, 968. (d) Huang, J.; Kaner, R. B. *Nat. Mater*. **2004**, *3*, 783. (e) Zhang, X.; Manohar, S. K. *Chem. Commun*. **2004,** 2360.

TH-777_05612211

41. Tseng, R. J.; Huang, J. X.; Ouyang, J. Y.; Kaner, R. B. Yang, Y. *Nano Lett*. **2005**, *5*, 1077.

42. (a) Majumdar, G.; Goswami M.; Sarma T. K.; Paul, A. Chattopadhyay, A. *Langmuir* **2005**, *21*, 1663. (b) Gallon, B. J.; Kojima, R. W.; Kaner, R. B.; Diaconescu, P. L. *Angew. Chem. Int. Ed*. **2007**, *46*, 1.

43. Sarma, T. K.; Chowdhury, D.; Paul, A.; Chattopadhyay, A. *Chem. Commun.* **2002**, 1048.

44. Sarma, T.; K.; Chattopadhyay, A. *J. Phys. Chem. A* **2004,** *108*, 7837.

45. Li, D.; Kaner, R. B. *Chem. Commun*. **2005**, 3286.

46. (a) Pillalamarri, S. K.; Blum, F. D.; Bertino, M. F. *Chem. Commun*. **2005**, 4584. (b) Advincula, R. C. *J. Dispersion Sci. Technol*. **2003**, *24*, 343. (c) Li, J.; Zhu, L.; Luo, W.; Liu, Y.; Tang, H. *J. Phys. Chem. C* **2007**, *111*, 8383.

47. (a) Willner, I.; Willner, B. *Pure. Appl. Chem*. **2002**, *74*, 1773. (b) Shipway, A. N.; Willner, I. *Chem. Commun*. **2001**, 2035. (c) Patolsky, F.; Weizmann, Y.; Lioubashevski, O.; Willner, I. *Angew. Chem. Int. Ed*. **2002**, *41*, 2323.

48. (a) Zhu, M.-Q.; Wang, L.-Q.; Exarhos, G. J.; Li, A. D. Q. *J. Am. Chem. Soc*. **2004**, *126*, 2656. (b) Redl, F. X.; Cho, K. S.; Murray, C. B.; O'Brien, S. *Nature* **2003**, *423*, 968. (c) Gao, J. M.; Watanabe, S.; Kool, E. T. *J. Am. Chem. Soc*. **2004**, *126*, 12748.

49. (a) Snowden, M. J.; Chowdhry, B. Z.; Vincent, B.; Morris, G. E. *J. Chem. Soc., Faraday Trans.* **1996,** *92*, 5013. (b) Kim, J. H.; Lee. T. R. *Chem. Mater.* **2004,** *16*, 3647. (c) Jones, C, D.; Lyon, L. A. *Langmuir* 2003, *19*, 4544. (d) Wang, J.; Gan, D.; Lyon, L. A.; El-Sayed, M. A. *J. Am. Chem. Soc.* **2001**, *123*, 11284.

50. (a) Berndt, I.; Pedersen, J. S.; Richtering, W. *J. Am. Chem. Soc.* **2005**, *127*, 9372. (b) Meyer, S.; Richtering, W. *Macromolecules* **2005**, *38*, 1517. (c) Berndt, I.; Richtering, W. *Macromolecules* **2003**, *36*, 8780. (d) Zhou, J.; Wang, G.; Hu, J.; Lu, X.; Li, J. *Chem. Commun.* **2006,** 4820. (e) Malik, R. R.; Solis, F. J.; Vernon, B. L. *J. Appl. Polym. Sci*. **2004**, *94*, 210.

TH-777_05612211

51. (a) Kim, J. H.; Lee, R. *Drug. Dev. Res*. **2006**, *67*, 61-69. (b) Holtz, J. H.; Asher, S. A. *Nature* **1997**, *389*, 829. (c) Zhao, X.; Ding, X.; Deng, Z.; Zheng, Z.; Peng, Y.; Tiang, C.; Long, X. *New. J. Chem*. **2006**, *30*, 915.

52. Zhu, M.-Q.; Wang, L-,Q.; Exarhos, G. J.; Li, A. D. Q. *J. Am. Chem. Soc*. **2004**, *126*, 2656.

53. (a) Hyk, W.; Ciszkowska, M. *J. Electrochemical Soc*. **2000**, *147*, 2268. (b) Suzuki, D.; Kawaguchi, H. *Langmuir* **2005**, *21*, 8175.

54. Das, M.; Sanson, N.; Fava, D.; Kumacheva, E. *Langmuir* **2007**, *23*, 196.

55. (a) Raveedran, P.; Wallen, S. L. *J. Am. Chem. Soc*. **2003**, *125*, 13940. (b) Raveedran, P.; Wallen, S. L. J. *Green Chem*. **2006**, *8*, 34.

56. (a) Kim, Y.; Johnson, R. C.; Hupp, J. T. *Nano Lett*. **2001**, *1*, 165. (b) Du, W.-L.; Xu, Y.-L.; Xu, Z. R. ; Fan, C. L. *Nanotechnology* **2008**, *19*, 085707. (c) Chang, J. S.; Kong, Z. L. ; Hwang, D. F. ; Chang, L. B. *Chem. Mater*. **2006**, *18*, 702. (d) Gronnow, M. J.; Luque, R.; Macquarie, D. J.; Clark, J. H. *Green Chem*. **2005**, *7*, 552. (e) Doi, S.; Clark, J. H. ; Macquarrie, D. J. ; Milkowski, K. *Chem. Commun*. **2002**, 2632.

57. (a) Kobayashi, S.; Toshitsugu, K.; Shin-Ichiro, S. *J .Am. Chem. Soc*. **1996**, *118*, 13113. (b) Shin, Y.; Yoo, D. I.; Jang, J. *J. Appl. Polym. Sci*. **1999**, *74*, 2911. (c) Shigehiro, H.; Yasuo, K.; Shuntaro, K.; Testsuo, T.; Hisaya, T.; Kakuko, M.; Takeshi, Y. *Biochem. Syst. Ecol*. **1991**, *19*, 379. (d) Domare, A.; Roberts, G. A. F. *Advances in chitin science*; Andre, J., Ed.; National Taiwan Ocean University Keelung, Taiwan, **1998**. (e) Dhanikula, A. B.; Panchangnula, R. *The AAPS journal*. **2004**, *6*, 1. (f) Payne, F. G.; Raghavan, S. R. *Soft matter*. **2007**, *3*, 1. (g) Roy, K.; Mao, H. Q.; Huang, S. K.; Leong, K. W. *Nat. Med*. **1999**, *5*, 387.

58. (a) Hardy, J. J. E.; Hubert, S.; Macquarrie, D. J.; Wilson, A. J. *Green Chem*. **2004**, *6*, 53. (b) Vincent, T.; Guibal, E. *Int. Eng. Res. Chem*. **2002**, *41*, 5158. (c) Han, H. S.; Jiang, S. N.; Huang, M.; Jiang, J. *J. Polym. Adv. Technol*. **1996**, *7*, 704.

59. (a) Murugadoss, A.; Chattopadhyay, A. *Nanotechnology* **2008**, *19*, 015603. (b) Sanpui, P.; Murugadoss, A.; Durga Prasad, P. V.; Ghosh. S. S.; Chattopadhyay. A. *Int. J. Food. Micro*. **2008**, *124*, 142.

TH-777_05612211

60. Calo. V.; Nacci, A.; Monopoli, A.; Fornaro, A.; Sabbatini, L.; Cioffi, N.; Ditaranto, N. *Organometallics* **2004**, *23*, 5154.

61. (a) Chen, J.; Wiley, B. J.; Xia, Y. *Langmuir* **2007**, *23*, 4120. (b) Zhang, J.; Liu, Y.; Ke, Y.; Yan, H. *Nano Lett*. **2006**, *6*, 248. (c) Shevchenko, E. V.; Talapin, D. V.; Kotov, N. A.; O'Brien, S.; Murray, C. B. *Nature* **2006**, *439*, 55.

62. (a) Elghanian, R.; Storhoff, J. J.; Mucic, R. C.; Letsinger, R. L.; Mirkin, C. A. *Science* **1997**, *277*, 1078. (b) Murugadoss, A.; Chattopadhyay, A. *J. Phys. Chem. C* **2008**, *112*, 11265. (c) Imre, A.; Csaba, G.; Ji, L.; Orlov, A.; Bernstein, G. H.; Porod, W. *Science* **2006**, *311*, 205. (d) Cowburn, R. P.; Welland, M. E. *Science* **2000**, *287*, 1466. (e) Grzelczak, M.; Perez-Juste, J.; Mulvaney, P.; Liz-Marzan, L. M. *Chem. Soc. Rev*. **2008**, *37*, 1783.

63. (a) Pramod, P.; Joseph, S. T. S.; Thomas, K. G. *J. Am. Chem. Soc*. **2007**, *129*, 6712. (b) Sudeep, P. K.; Thomas, K. G. *J. Am. Chem. Soc*. **2005**, *127*, 6516. (c) Zhong, Kou, X.; Yang, Z.; Shi, Q.; Stucky, G. D.; Sun, L.; Wang, J.; Yan, C. *Chem. Commun*. **2007**, 1816.

64. (a) Maier, S. A.; Kik, P. G.; Atwater, H. A.; Meltzer, S.; Harel, E.; Koel, B. E.; Requicha, A. A. *Nat. Mater*. **2003**, *2*, 229. (b) Tang, Z. Y.; Kotov, A. N. *Adv. Mater*. **2005**, *17*, 951. (c) Kang, Y.; Erickson, K. J.; Taton, T. A. *J. Am. Chem. Soc*. **2005**, *127*, 13800.

65. (a) Shenton, W.; Davis, S. A.; Man, S. *Adv. Mater*. **1999**, *11*, 449. (b) Polavarapu, L.; Xu, Q. H. *Nanotechnology* **2008**, *19*, 075601. (c) Connolly, S.; Fitzmaurice, D. *Adv. Mater*. **1999**, *11*, 1202. (d) Mirkin, C. A. *Inorg. Chem*. **2000**, *39*, 2258. (e) Kinge, S. S.; Crego-Calama-Crego, M.; Reinhoudt, D. N. *Langmuir* **2007**, *23*, 8772. (f) Maltzahn, G. V.; Harris, T. J.; Park, J. H.; Min, D. H.; Schmidt, A. J.; Sailor, M. J.; Bhatia, S. N. *J. Am. Chem Soc*. **2007**, *129*, 6064.

66. (a) Harris, T. J.; Maltzahn, G. V.; Derfus, A. M.; Ruoslahti, E.; Bhatia, S. N. *Angew. Chem. Int. Ed*. **2006**, *45*, 3161. (b) Braun, E.; Eichen, Y.; Sivan, U.; Ben-Yoseph, G. *Nature* **1998**, *391*, 775. (c) Dujardin, E.; Peet, C.; Stubbs, G.;

TH-777_05612211

Culver, J. N.; Mann, S. *Nano Lett*. **2004**, *4*, 2437. (d) Ugarta, D.; Chatelain, A.; De Heer, W. A. *Science* **1996**, *274*, 1897.

67. (a) Hang, Y. Z.; Zeng, H. C.; *J. Phys. Chem. B* **2006**, *110*, 16812. (b) Wang, J. C.; Neogi, P.; Forciniti, D. *J. Chem. Phys*. **2006**, *125*, 194717-1.

68. (a) Lin, S.; Li, M.; Dujardin, E.; Girard, C.; Mann, S. *Adv. Mater*. **2005**, *17*, 2553. (b) Sardar, R.; Shumaker-parry, J. S. *Nano Lett*. **2008**, *8*, 731.

TH-777_05612211

2.1 Stabilizing Agent Specific Synthesis of Multi- branched and Spherical Au Nanoparticles by Reduction of $AuCl_4^-$ by Fe^{2+} Ions

2.1.1 Introduction

In recent times, progresses in the nanoscale science and technology have witnessed rapid growth in the number of synthetic methods for obtaining metal, semiconductor and other nanoparticles (NPs) in the form of specific sizes, shapes (such as spherical, triangular, hexagonal, rod, and helical) and also assemblies of some of these particles into structures of higher dimensions[1-3]. These developments have primarily been guided by the possibilities of applications of these materials with their shape and size dependent physical, chemical and biochemical properties. However, the future frontiers of nano-technology would rely on the ability to assemble or grow one, two and three dimensional structures using nanoscale particles as the building block. The realization of this goal would be possible if the building blocks of various sizes and shapes at different length scales, in addition to spherical ones, are made available for the construction of hierarchical higher order structures. Chemical, biochemical and biological methods of synthesis of well-defined NPs are powerful in their ability of controlled growth using properties at the molecular level. The results are the development of a significant number of methods for the production of shape and size selective Au and other metallic or semiconductor NPs, and also their assemblies into higher order structures[4-7].

It is being increasingly realized that branched NPs of inorganic materials are also important in achieving specific optical, chemical and other properties for practical applications. In addition, these mono or multi – branched particles would be particularly important in building hierarchical structures with parts of the NPs used for specific purposes. There have also been a few recent reports on the synthesis of Au NPs in the form of bipod, tripod, tetrapod and pentapod branched structures using seed mediated growth as one of the

TH-777_05612211

synthetic methods[8-10]. However, none of the methods reported have found evidence of formation of multiply branched NPs, where the growth is centered around multiple places rather than a single one. This is important not only in the understanding of growth mechanism of higher order structures but also useful technologically where their spectroscopic and catalytic properties could be used, and also for further sectional growth of different structures using individual branched sites.

In this chapter, a new method of synthesis of Au NPs using an inorganic ion, Fe^{2+}, for reducing $HAuCl_4$ is being reported. It was observed that single or multiple branched Au NPs were formed when the reaction was carried out in the presence of sodium dodecyl sulfate (SDS). In some instances shapes of the particle took the forms such as the one which could be called as a "nanofan". On the other hand when the same reaction was carried in the presence of SDS and Na_2S, spherical NPs of less than 10 nm diameters were formed. However, the reaction when carried out in the presence of starch (instead of SDS) resulted in the production of spherical Au NPs of primarily small sizes. The NPs formed were characterized by UV-visible spectroscopy, X-ray diffraction (XRD) and transmission electron microscopic (TEM) measurements. The observations suggest that the stabilizing agent plays an important role in controlling the shape of the NPs. However, this may not be the only reason as spherical Au NPs were produced in the presence of Na_2S.

2.1.2 Experimental Section

The synthesis of the NPs was carried out using three different reaction conditions. The details are given below.

Method 1

To a 10.0 mL aqueous solution of 8.3 mM sodium dodecyl sulfate (SDS), 50 μL of $HAuCl_4$ solution (diluted from 17% $HAuCl_4$ in HCl - Aldrich) was added so that the final

TH-777_05612211

concentration of $HAuCl_4$ was 8.4 x 10^{-5} M. To that a freshly prepared 25 µL of ferrous ammonium sulfate (FAS) was then added with the final concentration being 1.25 x 10^{-4} M. This immediately resulted into a purple coloured solution. The solution was used for subsequent analysis. The pH of the final solution was measured to be 3.35.

Method 2

To a 10.0 mL SDS (8.3 mM) solution, 0.058 mM (final concentration) Na_2S and 0.125 mM (final concentration), FAS (ferrous ammonium sulfate) were added. The resulting solution was clear light yellow and the pH of the solution was measured to be 6.49. To this solution 0.086 mM (final concentration) of HAuCl4 was added. The solution immediately turned dark brown. After about 5 min the solution turned purple in color. The pH of the final solution was 3.17.

Method 3

To a 10.0 mL aqueous solution of 0.15% starch, 100 µL of $HAuCl_4$ solution was added so that the final concentration of $HAuCl_4$ was 1.7 x 10^{-4} M. To that a freshly prepared 50 µL of FAS was then added with the final concentration being 2.5 x 10^{-4} M. That immediately resulted into a purple colored solution. The pH of the final solution was measured to be 2.98.

2.1.3 Result and Discussion

When $HAuCl_4$ was treated with FAS strong purple coloration of the solution was observed indicating the formation of Au NPs. The formation could be justified by redox potential in favor of the reduction of the Au^{3+} ions (equations 1-3)[11].

$$3\,Fe^{2+} = 3Fe^{3+} + 3e^- \qquad E^0/ -0.771\ V \qquad (1)$$

TH-777_05612211

$$AuCl_4^- + 3e^- = Au \qquad E^0/ 1.002\ V \qquad (2)$$

$$3\ Fe^{2+} + AuCl_4^- = 3Fe^{3+} + Au \qquad E^0/ 0.231V \qquad (3)$$

However, FAS was used because of its inherent stability compared to that of $FeSO_4$. It was observed that FAS worked equally well in the reduction of $HAuCl_4$. In all the cases, strong visible absorption in the range of 532 to 580 nm region characteristic of that of Au NPs was observed. However, there was observable difference in the position and nature of the peaks. For example, the peak appeared at 542 nm when the reduction was carried out in the presence of SDS and also the peak was generally broad (Figure 2.1.1A). On the other hand, when the reaction was carried out in the presence of Na_2S and other reagents as above, a relatively stronger peak occurred at 535 nm (Figure 2.1.1B). Further, the peak was broader and appeared at 565 nm when starch was used as the stabilizing agent instead of SDS (Figure 2.1.1C).

TH-777_05612211

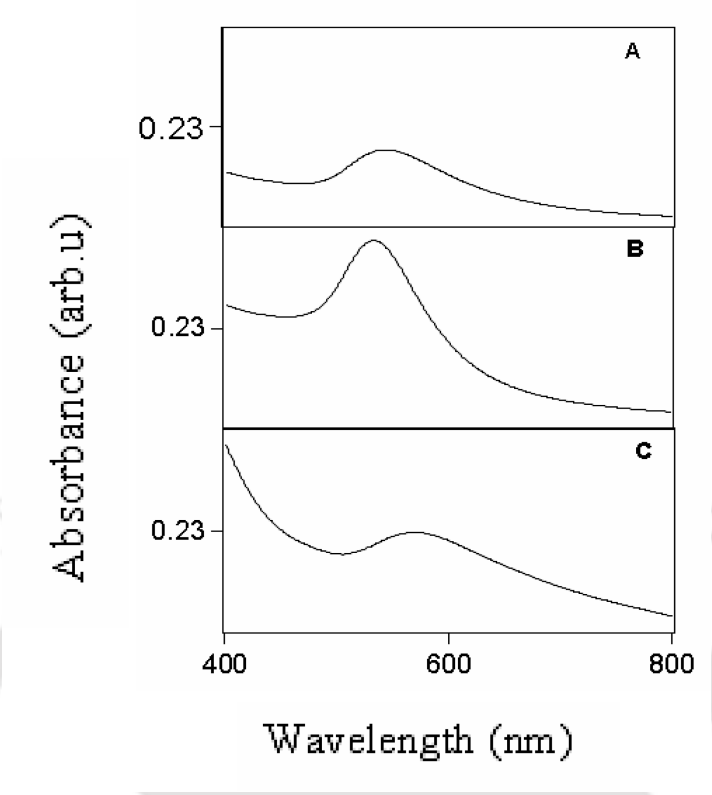


Figure 2.1.1. *UV-Visible spectra of Au NPs prepared using Method 1 (A), Method 2 (B) and Method 3 (C).*

The results of XRD measurements of evaporated films of drops of freshly prepared solutions are shown in Figures 2.1.2A, 2B and 2C for solutions obtained from Method 1 (in the presence of SDS), Method 2 (in the presence of SDS plus Na_2S) and Method 3 (in the presence of starch) respectively. The XRD of the film obtained from solution in Method 1 contains a single peak occurring at 38.4^o, due to the (111) lattice plane of Au. In addition, there is one more peak occurring at 40.3^o possibly due to the product formed from oxidation of FAS[12-13]. The XRD of films obtained from solution generated Method 2 consists of two peaks at 38.4^o, 44.5^o and 77.5^o (not shown here) due to (111), (200) and (311) planes respectively of Au, whereas the other two occurring at 42.2^o and 51.7^o are due to possible formation of iron sulfides[12, 14]. The reaction carried out in the presence of starch (Method 3) produced Au particles with growth in the (111) and (200) and (220) planes due to which

TH-777_05612211

the peaks occurred at 38.4^{o}, 44.5^{o} and 64.5^{o} respectively. It may be mentioned here that the number of peaks due to Au NPs generated using Method 1 varied from sample to sample and sometimes two peaks could be observed, the additional one being due to (200) plane of Au indicating the possible growth of different planes.

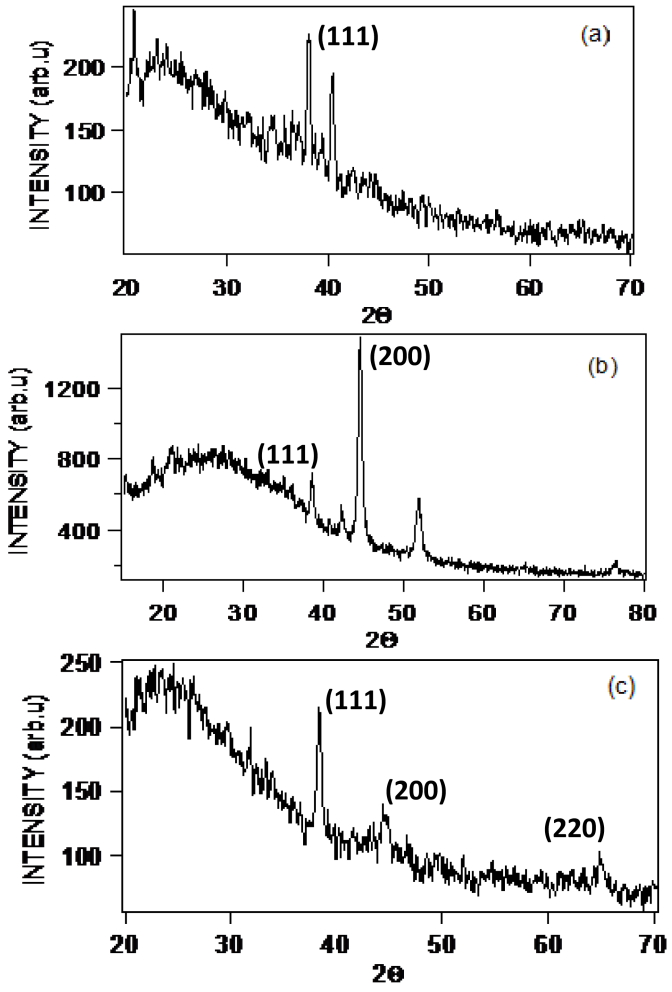


Figure 2.1.2. *X-ray diffraction patterns of the nanoparticles generated under various conditions as in (A) Method 1; (B) Method 2 and (C) Method 3. The lattice planes of Au are identified.*

Further analysis of the samples were pursued by TEM of individual samples recorded after evaporating a drop of liquid on a carbon-coated copper grid and the experiments were performed at 200 KV in a JEOL TEM. Figure 2.1.3A shows the TEM of a sample obtained

TH-777_05612211

from Method 1. As is clear from the figure the particles formed are multi-branched with no simple pattern of growth. The diameters of the branched particles are on the order of 20 nm, while the lengths are different for different particles occurring in the range of 10-50 nm length scale.

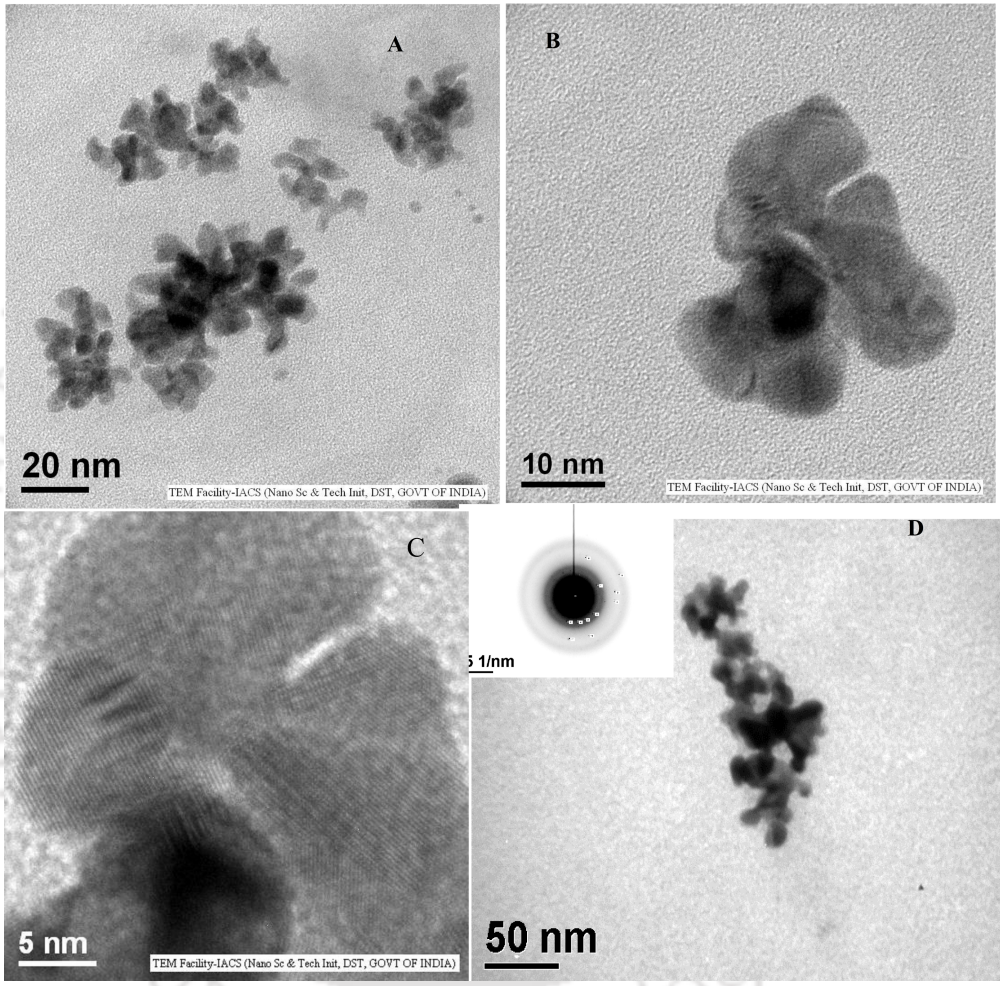


Figure 2.1.3. *TEM micrographs of the samples prepared using Method 1 (A and B). (C) Shown is the expanded picture of (B) indicating the presence of lattice fringes in the lighter area. (D) TEM micrograph of another sample prepared using the same method and corresponding SAD (inset).*

However, the width of a sharp edge of a branch-head could be as low as 2 nm. It is also interesting to note that the growth seems to have occurred with multiple nucleation points giving rise to branched wings and the TEM of the nucleation points appear to be darker than

TH-777_05612211

the wings, indicating more (three-dimensional) growth at those points than at the wings. This can be more easily seen in Figure 2.1.3B, where the growth appeared to have occurred in the form of a "fan" with two major "blades" and each blade also has branched structure.

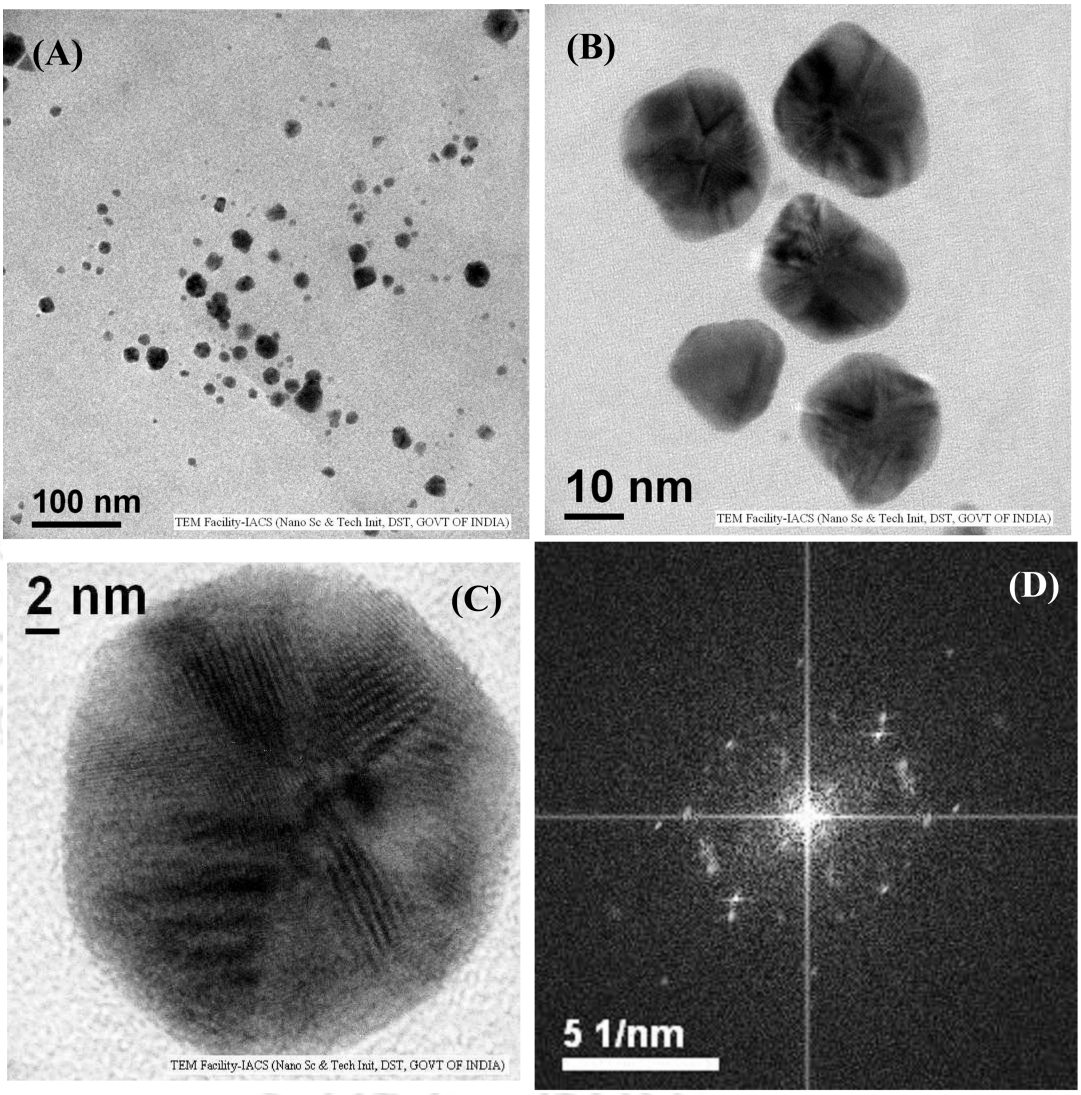


Figure 2.1.4. *TEM micrographs of samples prepared using Method 2 (A, B and C) and corresponding FFT image (D).*

There is also the apparent three dimensional "darker" growth points near the centre of the "fan". An expanded picture of (B), as shown in Figure 2.1.3C, indicates the presence of lattice fringes (due to metal) in the lighter area of the fan. Thus the whole fan is made of Au

TH-777_05612211

and surfactants (stabilizing agent) do not constitute the structures in the lighter area. It may be mentioned here that we have also observed bipodal and tripodal growth in some cases and also the formation of spherical particles. However, those cases were less prominent than the multi-branched growth. Figure 2.1.3D represents the TEM of another sample prepared under identical condition. A typical selected area diffraction (SAD) pattern of the sample in Figure 2.1.3D is also shown in inset. The lattice parameters matched with those of Au.

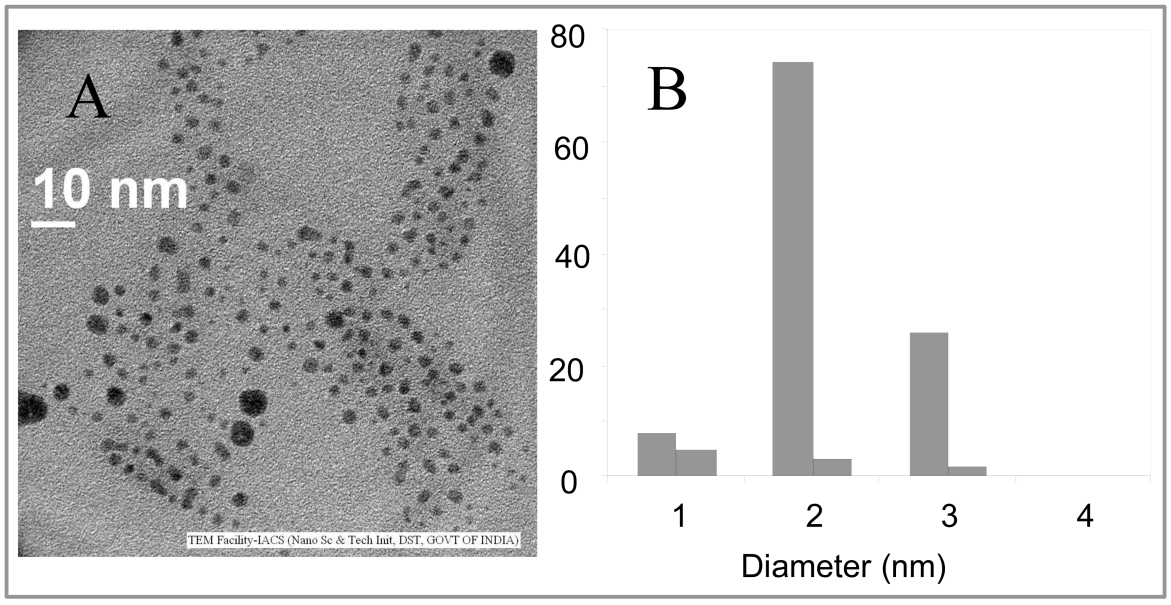


Figure 2.1.5. *TEM micrograph (A) of a sample prepared using Method 3 and corresponding particle size distribution (B). Y-axis in (B) represents relative % population.*

On the other hand, the TEM of samples prepared using Method 2 indicates formation of nearly spherical and uniform particle in the range of 10-15 nm. A closer look (Figure 2.1.4B) into the pictures reveals the formation of 'stone-like' three dimensional particles. This is consistent with the XRD of the same which shows the growth of (111) and (200) planes of the crystal. Further, a typical SAED pattern of the particles is shown in Figure 2.1.3C, which represents the formation of Au NPs.

TH-777_05612211

TEM images of Au NPs prepared using Method 3 (Figure 2.1.5) shows that generally very small particles were formed in the presence of starch as the stabilizing agent. An image in this regard is shown in Figure 2.1.5A. A typical distribution of particle sizes, shown in Figure 2.1.5B, indicates that the majority of particles formed were in the range of 2 nm sizes. In addition, there were a few larger particles, which had diameters greater than 50 nm (not shown here), possibly being the reason for the broadness and shift of the visible spectrum of Figure 2.1.1C.

It is known that shape formation in the growth of NPs could be kinetically controlled in which case the shape could evolve with time. Additionally, the shape could also be molded by the stabilizing agent or the motif of the structure based on which different shape-selected materials have been generated. A large number of methods in this regard have been reported that include biomimetic fabrication of metallic nanowires[15]. In a recent report the effect of SDS on the formation of multipod Au NPs have been described[8]. On the other hand, what we have observed indicates that it is not only the stabilizing agent but also the reaction conditions such as the reagents used are important in the formation of NPs with various shapes. Our observations demonstrated that when the reduction of $HAuCl_4$ was carried out by FAS in the presence of SDS multiply branched Au NPs were formed. On the other hand, when the same stabilizing agent was used but Na_2S was used as an additional reagent spherically shaped NPs were formed. Here, Na_2S reacts with FAS to produce FeS which then reacts with $HAuCl_4$ to produce Au NPs. Although SDS as the stabilizing agent contributed in the shape formation but the presence of sulfide in Na_2S might have helped stabilize the NPs, which would contribute towards the shape formation. As the pH of the medium was quite low (acidic), the formation of polysulfide in the medium and its subsequent role in the shape formation could possibly be discounted. Further, the presence of starch as the stabilizing agent led to the formation of small Au NPs indicating that even under the same reagent condition the product formation could finally be influenced greatly by the stabilizing agent present in the medium. The reason for the formation of smaller and

TH-777_05612211

spherical particles in starch is probably due to its hydrophobic core (helical) in the generation of NPs that are inside the core and form nearly uniform spherical particles. It is also important to mention here that there are a large number of reports with the use of SDS to generate primarily spherical shaped NPs under various experimental conditions for a number of systems[6]. Thus overall a combination of factors that involve reagents and other reaction conditions such as the stabilizing agent that finally contributes towards the shape in the formation of NPs. Also, the role of Fe^{2+} ions towards the shape formation cannot be ruled out. In the present case the reaction in the presence of SDS produced multi-branched Au NPs while in other conditions the same reaction produced spherical NPs.

2.1.4 Conclusion

In this chapter we have reported a new method of preparation of Au nanoparticles (NPs) of muti-branched and spherical shapes. $HAuCl_4$ when reduced by Fe^{2+} ions in aqueous solution, and in the presence of sodium dodecyl sulfate (SDS), produced multi-branched Au NPs including a shape that could be termed as a "nanofan". On the other hand spherical particles were produced in the presence of Na_2S and SDS or starch (instead of SDS). The essential conclusion of this chapter is that stabilizing agent and other reagents do play special roles in controlling the shape and size of the NPs produced. This is important in understanding the growth of higher order structures, which can be potentially useful with respect to tuning the spectroscopic and catalytic properties of these materials.

2.1.5 References

1. Sau, T. K.; C. J. Murphy, *J. Am. Chem. Soc.* **2004**, *126*, 8648.
2. Manna, L.; Scher, E. C.; Alivisatos, A. P. *J. Am. Chem. Soc*. **2000**, *122*, 12700.
3. Maye, M. M.; Chun, S. C.; Han, L.; Rabinovitch, D.; Zhong, C. J. J. *Am. Chem. Soc.* **2002**, *124*, 4958.

TH-777_05612211

4. Thomas, K. G.; Barazzouk, S.; Ipe, B. I.; Joseph, S. T. S.; Kamat, P. V. *J. Phys. Chem. B* **2004**, *108*, 13066.

5. Mukherjee, P.; Ahmad, A.; Mandal, D.; Senapati, S.; Sainkar, S. R.; Khan, M. I.; Ramani, R.; Pasricha, R.; Ajayakumar, P. V.; Alam, M.; Sastry, M.; Kumar. R. *Angew. Chem. Int. Ed.* **2001**, *40*, 3585.

6. Daniel, M. C.; Astruc, D. *Chem. Rev*. **2004**, *104*, 293.

7. Bae, A. H.; Numata, M.; Hasegawa, T.; Li, C.; Kaneko, K.; Sakurai, K.; Shinkai, S. *Angew. Chem. Int. Ed*. **2005**, *117*, 2066.

8. Kuo, C. H.; Huang, M. H. *Langmuir* **2005**, *21*, 2012.

9. Hao, E.; Bailey, R. C.; Schatz, G. C.; Hupp, J. T.; Li, S. *Nano Lett*. **2004**, *4*, 327.

10. Chen, S.; Wang, Z. L.; Ballato, J.; Foulger, S. H.; Carroll, D. L. *J. Am. Chem. Soc*. **2003**, *125*, 16186.

11. *CRC Handbook of Chemistry and Physics,* Weast, R. C. (Ed.), *70'th edn*. (**1989–1990**), D-151, 152.

12. Benning, L. G.; Wilkin R. T.; Barnes, H. L. *Chem Geo*. **2000**, *167*, 25.

13. Sasaki, K.; Konno, H. *Can. Mineral.* **2000**, *38*, 45.

14. Roberts, A. P. *Earth Planet. Sci. Lett*. **1995**, *134*, 227.

15. Mertig, M.; Pompe, M. *Nanobiotechnology*: *Concepts, Application and Perspectives*, C. M. Niemeyer and C. A. Mirkin (Ed.), Wiley-VCH, **2004**, p 256.

TH-777_05612211

3.1 A "Green" Chitosan-Silver Nanoparticle Composite as a Heterogeneous as well as Micro-heterogeneous Catalyst

3.1.1 Introduction

The future development of sustainable nanoscale science and technology would not only depend on overcoming knowledge barriers in developing newer principles, but also on appropriately addressing the environmental and societal concerns, especially when large-scale material production and use would be involved. The primary challenges in this regard are the maximization of usage of environmentally friendly materials and integration of the principles of "green chemistry", as far as chemistry is involved, in the production of nanoscale-based materials. In this regard, polymer-metal nanoparticle composites seem to get special attention because of their multiple application potentials in sensors[1], actuators[2], electrodes for fuel cells[3], supported micro-heterogeneous and heterogeneous catalyses[4], and in optical and optoelectronic devices[5]. Further, advantages of mechanical, optical, thermal and electrical properties of the polymer and optical, electrical and catalytic properties of the metal NPs can be suitably integrated to achieve superior performance. For example, our laboratory the first time reported the synthesis of Au nanoparticle-polyaniline composite in a single reaction condition where the composite product had higher electrical conductivity in comparison to the polymer alone[6]. There were subsequent development of methods for syntheses of polymer-metal composite nanoparticle and a polymer-TiO_2 nanoparticle thin film composite with superior photocatalytic properties[7]. In addition, it was also demonstrated that Au NP-polyaniline composite on a resin bead could act as catalyst for the oxidation of glucose with simultaneous colorimetric detection of the product[8]. Several other groups have subsequently developed various synthetic schemes for the generation of metal NP-polymer composite keeping in view appropriate applications. For example, Ballauff and coworkers[9] have reported the synthesis of several metal NP-polymer composites for

TH-777_05612211

catalysis with demonstrate of thermosensitive activity as one of the major advantages. On the other hand, Gronnow et al[10] have used expanded starch supported Pd catalyst with high activity for Suzuki, Heck and Sonogashira coupling reactions. Among the metal NPs, Ag NPs generated under various conditions, are known to be efficient catalyst for reduction of organic dyes[11] and also for the reduction of 4-nitrophenol (4NP) to 4-aminophenol (4AP)[12]. However, incorporation of Ag NPs into polymer, especially biopolymer, has not received much attention, possibly because of experimental difficulty in the syntheses of composites.

Chitosan, being a novel biopolymer, is a product of deacetylation of chitin, which is the second most abundant natural polymer in the world after cellulose. The biocompatibility and antibacterial properties of chitosan and being an environmentally friendly polyelectrolyte makes it appealing for several applications such as water treatment[13], novel fibers for textiles[14], photographic paper[15], biodegradable films[16], biomedical devices and microcapsule implants for controlled release in drug delivery[17]. Considering the physicochemical properties of Ag NPs, a composite of Ag NPs and chitosan would ideally be suited for various commercial applications, especially if generated under benign condition. Although, there are methods that are available for the synthesis of Pd NP-chitosan composite, currently there is no simple method of synthesis of a composite of Ag NP-chitosan.

In this chapter, the development of a mild one-step method of Ag NP-chitosan composite, by using chitosan as the reducing agent, at 95^{o}C and in the presence of aqueous sodium hydroxide, is reported. Interestingly, the NPs produced in the medium get attached to the chitosan and are stable for weeks without noticeable change in their properties. The NPs produced were small with sizes mostly below 5.0 nm and were found to have high catalytic activity. Also, the amount of Ag NPs produced could be easily controlled by controlling the amount of starting material ($AgNO_3$), without significant variation in sizes. The catalytic

TH-777_05612211

reduction of 4NP to 4AP by the composite using $NaBH_4$ as the reducing agent was studied, under both heterogeneous and micro-heterogeneous conditions. When the heterogeneous catalytic reaction was carried out in the presence of excess $NaBH_4$, it was observed to follow pseudo first order kinetics and the apparent rate constant depended linearly on the concentration of Ag NPs present in the composite. The turn over frequency (TOF) was observed to be $(1.5 \pm 0.3)\ X10^{-3}\ s^{-1}$ (when the reaction was carried out in heterogeneous condition). Interestingly, the composite could be used for catalyzing the same reaction at least for 10 cycles without significant loss of its activity. Transmission electron microscopic (TEM) evidences indicated that Ag NPs were present and sizes were retained even after several cycle of catalytic reductions. On the other hand, when the reaction was carried out in micro-heterogeneous conditions the rate constant was much higher.

3.1.2 Experimental Section

Materials

Silver nitrate ($AgNO_3$, 99.5 %; Merck), acetic acid (glacial, 99-100 %; Merck), chitosan of high molecular weight (75 % deacetylated; Sigma-Aldrich), sodium borohydride ($NaBH_4$, 95 %; Merck), sodium hydroxide (NaOH, 98 %; Merck) and 4-nitrophenol (95 %; merck) were used as received without further purification. Milli-Q grade water was used in all experiments.

Synthesis of Chitosan-Ag-Nanoparticles Composite

A 100 mL beaker containing 50 mL of Milli-Q water was kept in an oil bath at temperatures 93-95^{o} C with constant magnetic stirring. This was followed by addition of 0.1g of chitosan into the beaker. Freshly prepared 1.0 mL solution of 20 mM $AgNO_3$ was then added to this mixture, which was followed by addition of 100 µL of 0.3 M of NaOH. The pH of the solution was measured to be 10.4. The resultant solution turned yellow in color in about a minute, indicating the formation of Ag NPs in the medium. The reaction

TH-777_05612211

was allowed to continue for additional 10 min. In the end, powdered yellow colored solid appeared at the bottom of the beaker. The beaker was then taken out from the oil bath and cooled to room temperature. This was followed by separation and washing of the powder with Milli-Q water and the cycle was repeated for five times. The solid thus obtained was then air dried and kept for further use. The filtrate was treated with conc. HCl to check for any excess of Ag^+ present in the medium, which was negative. Thus, all of Ag^+ ions had reacted in the production of Ag NPs. In order to prepare chitosan-Ag NP composite with varying amount of Ag, the concentration of $AgNO_3$ was appropriately varied keeping all other conditions the same.

Catalysis Study

Heterogeneous condition

Investigations for the catalytic activity of chitosan-Ag NPs composite with different Ag content were pursued in the following way, using the reduction of 4NP to 4AP by $NaBH_4$ as a model reaction. In a 3.0 mL quartz cuvette, a given amount chitosan-Ag-NPs composite powder was added and this was followed by addition of 2.5 mL of 10 mM $NaBH_4$ solution. Subsequently, 25μL of 10.0 mM of 4NP was added to the mixture and the cuvette was shaken vigorously for mixing. The cuvette was then placed in a UV-vis spectrophotometer followed by monitoring time-dependent absorption at 400 nm at room temperature (23-24^o C).

Micro-heterogeneous condition

40 mg of Ag NP-chitosan composite was dissolved in 20 mL of 0.1 % (V/V) acetic acid in water. The corresponding solution of the pH was found to be 4.3. The pH of the solution was then adjusted to 6.3 by addition of NaOH solution. This stock solution was used for further catalysis studies under micro-heterogeneous condition. The resultant solution was also used for physical characterization studies of the composite. For catalysis studies, in a 3.0 mL cuvette containing 2.5 mL of freshly prepared 10 mM $NaBH_4$ solution,

TH-777_05612211

25 μL of 10 mM of 4-NP solution was added. This was followed by the addition of a specific amount of the Ag-NP-chitosan composite stock solution (2.5-15 μL of the solution). The solution was thoroughly mixed, followed by measurements of time-dependent absorption at 400 nm. It may be mentioned here that starting with higher amount of catalyst (more than 30 mg/L) lead to immediate precipitation of the same. Thus the reactions were carried out at a maximum of the above catalyst concentration. Also, during the course of the reaction the precipitation of the composite was not observed thus making the reaction condition as micro-heterogeneous.

TH-777_05612211

Analytical Measurements

UV-visible spectra of the liquid samples as well as samples used for catalytic studies were recorded using a Perkin-Elmer Lambda-25 spectrophotometer in the range of 250 to 800 nm. FT-IR spectra of chitosan and the composite powders were measured using a Perkin-Elmer Spectrum one spectrometer. Both the chitosan and chitosan-Ag NPs composite powders were mixed with KBr in order to make pellets for FTIR studies. The dynamic light scattering (DLS) measurements of the liquid samples were performed with an LB-550 (HORIBA) DLS measurement system. Transmission electron microscopy (TEM) of the particles, were performed using a JEOL-2100 equipment operating at a maximum acceleration voltage of 200 kV. The TEM samples were prepared by placing a drop of liquid sample on carbon coated copper grid (300 mesh) followed by evaporation of the solvent at room temperature.

3.1.3 Results and Discussion

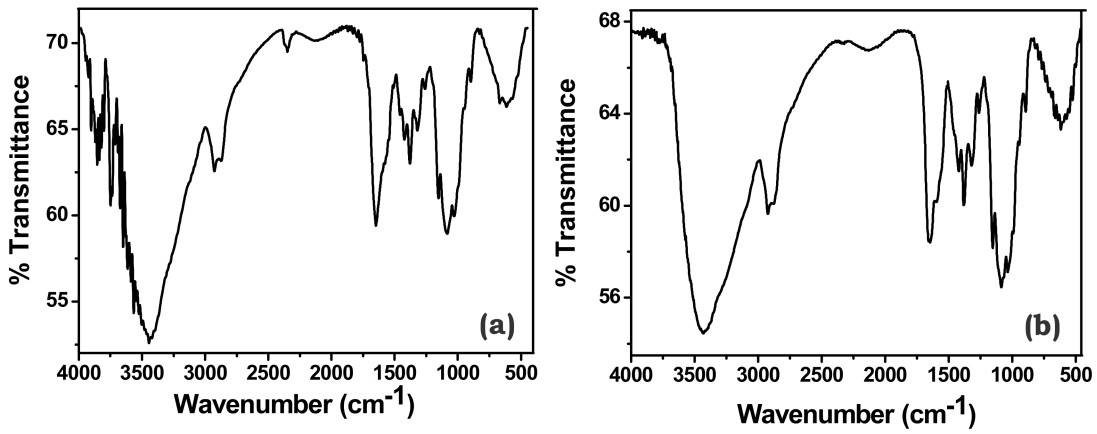
Chitosan, a well-known biodegradable polymer, consists of linear β-1, 4-linked polysaccharides similar to cellulose that is obtained by deacetylation of naturally occurring chitin. Chitosan does not have a single well-defined molecular structure. The structures can differ in molecular weight, degree of acetylation and sequence depending on whether the acetylated residues are distributed along the backbone in a random or block manner[18]. The advantage, however, lies in its significant content of primary amines and hydroxyl groups, leading the polymer to have high affinity towards metal ions, which could be adsorbed either by chelation or by ion exchange route. Several groups have taken advantage of this and reduced metal salts physisorbed onto chitosan to corresponding NPs and shown their catalytic activity by reducing chromate (using Pd), phenol (using Pd) and aromatic nitro compounds (using Ni, Cu, Cr and Zn)[19]. It was observed that chitosan powder in neutral pH condition did not react with $AgNO_3$. On the other hand in the presence of NaOH and at an elevated temperature, reduction of Ag^+ to Ag NPs could be observed as indicated by the formation of yellow colored powder. Thus under alkaline conditions, chitosan produced Ag

TH-777_05612211

NPs in the medium. Also interesting to note is that chitosan here acted as both reducing agent and also stabilizer for the NPs produced. This was further substantiated by yellow coloration in the powder with no color or characteristic spectrum (of Ag NPs) present in the solution. Further, the powder was found to be insoluble in water at pH values above 6.30, whereas clear yellow colored solution could be obtained at below that pH.

FTIR spectrum of chitosan (Figure 3.1.1 (a)) indicated the presence of substantial amount of OH and NH_2 groups, in addition to other functional groups in the polymer. This is especially indicated by the broad peak in the region 3700-3100 cm^{-1} with small peaks superimposed on it. On the other hand, when the polymer was treated with Ag^+ under aqueous alkaline condition the small structures disappeared and substantial narrowing of the peak could be observed (Figure 3.1.1 (b)). This possibly indicates the involvement of OH and NH_2 groups, in the reduction of Ag^+ to Ag, whose intensity (and thus content) decreased upon oxidation. It may be mentioned here that both the heating of the mixture at about 95º C and presence of NaOH were essential in the production of the composite as we have observed that only heating in the absence of NaOH did not produce any coloration.

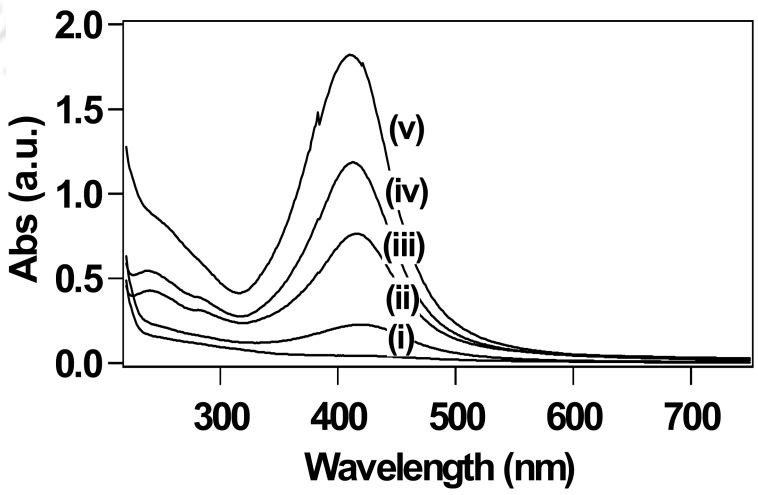
ge,



TH-777_05612211

***Figure 3.1.1**. FTIR spectrum of (a) Chitosan (CS), (b) CS-Ag NPs composite powder.*

When the yellow powder of the composite was dissolved in acetic acid and UV-vis spectrum was recorded, spectrum characteristic of the absorption due to surface plasmon resonance of Ag NPs could be observed. A collection of spectra with varying initial concentration of $AgNO_3$ are shown in Figure 3.1.2. As is clear from the figure, the spectra consisted of a single, rather sharp peak occurring in the range of 410-417 nm for all samples. It is also interesting to note that at lower concentrations of $AgNO_3$, the peak appeared at slightly higher wavelengths in comparison to those at higher concentrations of the precursor. For example, when the $AgNO_3$ concentration was kept at 0.08 mM, the peak appeared at 417 nm, while the same appeared at 410 nm when the initial concentration of $AgNO_3$ was set at 0.4 mM, along with increase in absorption intensity. This implies that when the concentration of silver ions was increased, the loading of the silver content also increased on the chitosan. However, increasing the number of Ag^+ ion lead possibly to increase in the number of NPs but not their size. It is also possible that their sized decreased with the loading. This could be due to different nucleation mechanisms operating at lower and higher Ag^+ concentrations attached to chitosan.



TH-777_05612211

Figure 3.1.2. *UV-Visible spectra of the AgNO3 treated chitosan dissolved in 0.1 % (V/V) acetic acid in water. The concentration of silver ions in the original solutions used for preparation of NPs were (i) 0.08 mM AgNO¬3 (ii) 0.16 mM AgNO¬3 iii) 0.24 mM AgNO¬3 (iv) 0.32 mM AgNO¬3 and (v) 0.4 mM AgNO¬3 respectively. The amount of chitosan used for synthesis was 0.1 g in 50*

TH-777_05612211

It is important to mention here that the excess amine and hydroxyl groups present in the chitosan polymer support the nucleation as well as stabilization of the Ag NPs formed in the process. Thus, the Ag NPs adsorbed on the surface of the polymer are prevented from further aggregation. In order to investigate the size distribution of the Ag NPs on the surface of the chitosan polymer, the TEM studies were pursued.

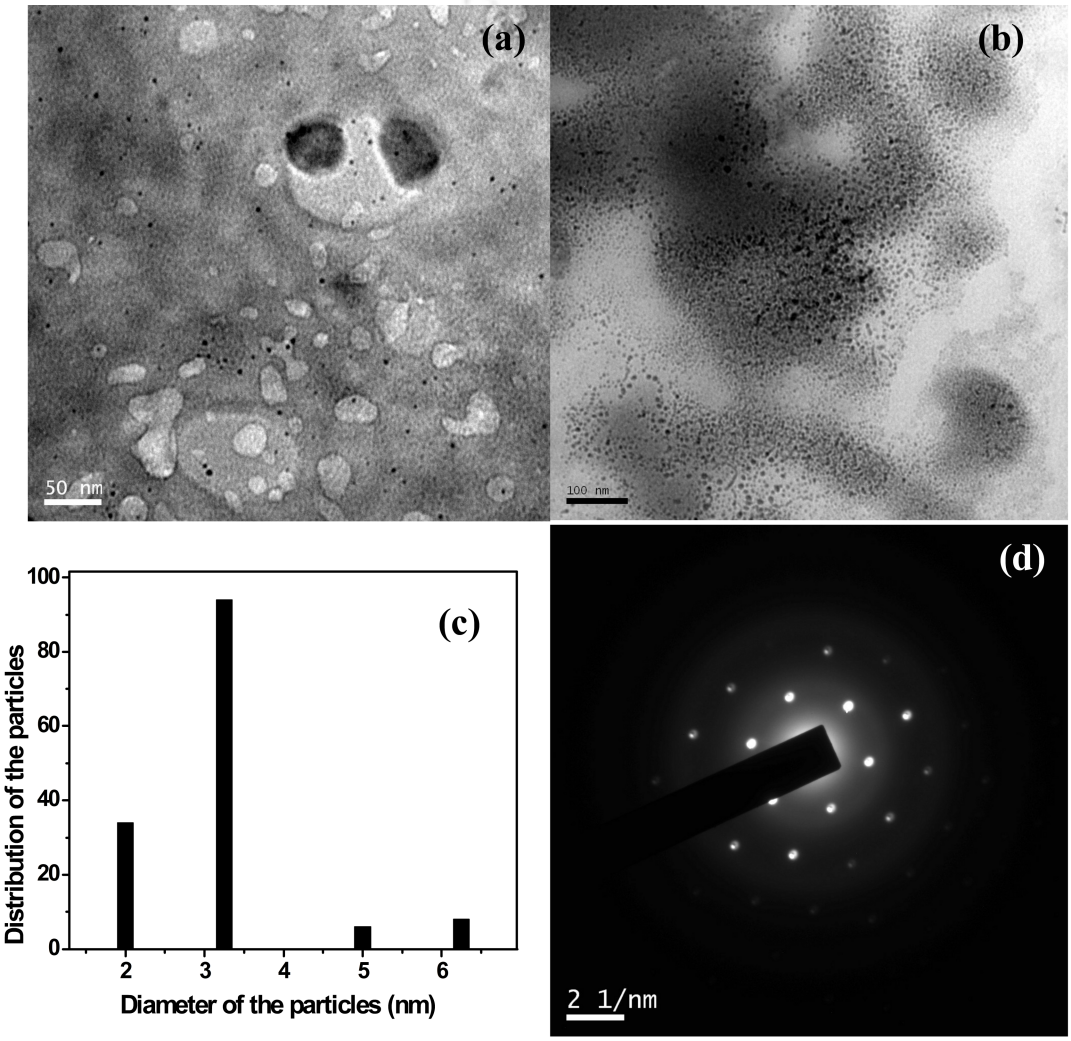
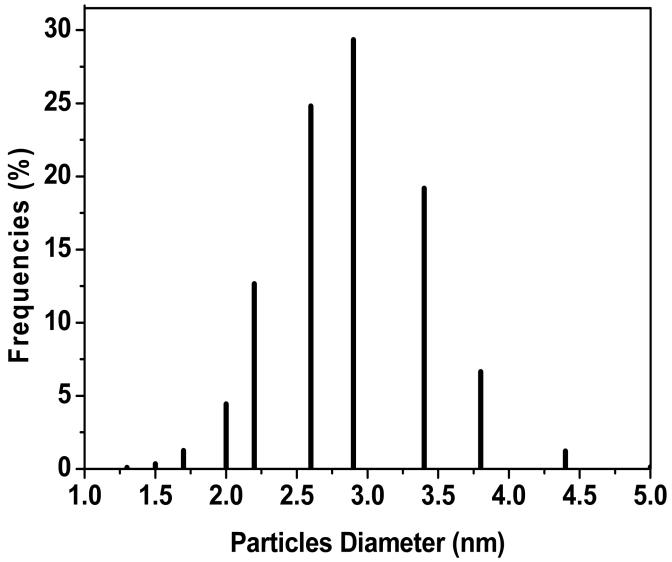


Figure 3.1.3. *(a) and (b) Transmission electron micrographs of chitosan-Ag NP composite. (c) is the particles size distribution histogram as obtained from figure 2 (a) and (d) is selected area electron diffraction pattern corresponding to a particle.*

TH-777_05612211

Typical TEM micrographs of drop cast composite are shown in Figure 3.1.3 (a) and (b) and the corresponding particles size histogram, corresponding to the micrograph 3.1.3 (a), is shown in Figure 3.1.3 (c). As is clear from the figures, small NPs were formed and deposited uniformly all over the polymer. The majority of the particles formed had sizes less than 5.0 nm. It is also interesting to note that the particles were rather uniform in sizes. The selected area diffraction (SAD) pattern of the NPs (Figure 3.1.3 (d)) consisted of a hexagonal structure of the (111) face of single crystalline Ag NPs. Further, these results correlated well with the dynamic light scattering study of the composite particles. The dynamic light scattering (DLS) measurements of the composite, dissolved in 0.1 % (V/V) acetic acid in water, also indicated the formation of small particles with nearly uniform particle size distribution. A typical particles size histogram from DLS measurements is shown in Figure 3.1.4. Clearly, more than 90% of the particles formed were of the sizes in the range of 2-4 nm with majority of the particle formed were about 3.0 nm in diameter. Thus the present method produced stable, small sized Ag NPs in the form of chitosan-Ag-NP composite with uniform and narrow particle size distributions.



TH-777_05612211

Figure 3.1.4. *The particles size distribution histogram of the Ag NPs in the composite as obtained from dynamic light scattering (DLS) measurements.*

TH-777_05612211

Also important to mention here is the observation that when chitosan-Ag NP composite was dissolved in 0.1 % (V/V) of acetic acid in water and kept for a couple of months, no discernible precipitation could be observed and there was no change in the UV-vis spectrum, indicating that these particles were also stable in solution form when present with the polymer as a composite. The ease of synthesis of chitosan-Ag NPs composite and the stability of the NPs in the composite provide opportunities for applications especially with respect to catalysis of important chemical reactions. This is especially advantageous where the NPs act as the catalyst and the adherence of the NPs to the bulk and insoluble polymer helps in recovery and thus repeated use.

The test of efficacy of the present composite in catalyzing heterogeneous chemical reactions was pursued by studying the reduction of 4-NP to 4-AP by $NaBH_4$ in the presence of the composite. The reactions have been monitored spectrophotometrically. Also, it is important to mention here that the use of excess $NaBH_4$ was necessary so that the kinetics of the reaction could be followed as a function of concentrations of Ag NPs. An aqueous solution of 4NP shows a distinct spectral profile with absorption maximum at 317 nm, which shifts to 400 nm in the presence of $NaBH_4$ due to the formation of 4-nitrophenolate ion[20]. The anionic species remain stable for weeks in absence of any other reagent. However, it was observed that in the presence of the solid chitosan-Ag NPs composite the peak at 400 nm gradually decreased with time along with the appearance of a new peak at 290 nm, which is known to be due to absorption of 4-amino phenol.[20b] A typical time dependent catalytic reduction of 4NP as followed spectrophotometrically is shown in Figure 3.1.5. As is clear from the figure, under the reaction condition, the reduction took place in about 25 min. Also important to note here is the presence of isosbestic point at 320 nm (Figure 3.1.5) indicating the formation of the product 4AP as a result of reduction from 4NP. Investigations were further pursued with respect to the rate of the reaction as a function of concentration of the catalyst (Ag NPs) in the composite. This was achieved by varying the

TH-777_05612211

amount of composite while keeping the ratio of chitosan to $AgNO_3$ keeping the same as shown in Table 3.1A. Since our observations indicated absence of Ag^+ in the medium after the formation of the composite, it is possibly safe to assume that all the Ag^+ ions present in the medium reacted to form NPs in the composite. Also, since the particle size distribution studies indicated that the NPs formed were nearly uniform in sizes and spherical in nature, the method adopted by Pikramenou et al[21] to calculate the number of particles present in each amount of composite used for catalysis was used herein. Further, the same method was used to calculate the number of surface atoms present in the NPs, which was further used for the calculations of turn over frequency (TOF).

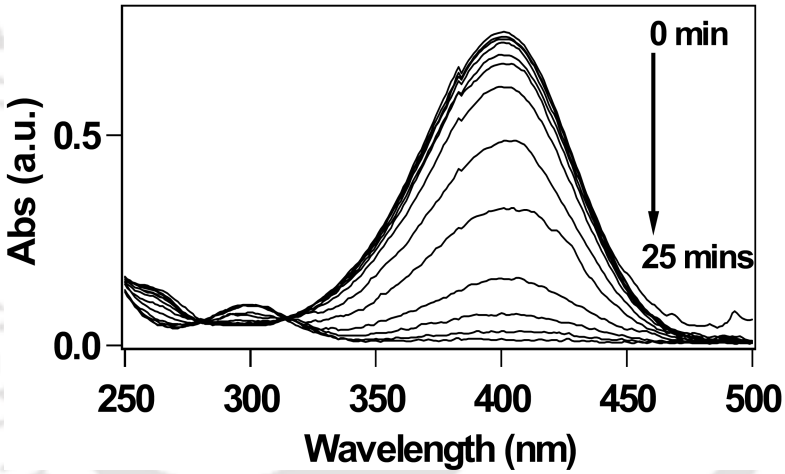


Figure 3.1.5. *UV-visible spectra of solution of 4NP measured at different time intervals in the presence of chitosan-Ag NP composite particles. The reaction conditions were as follows: [4NP] = 0.1 mM dm^{-3}, [$NaBH_4$] = 10 mM dm^{-3}, amount of chitosan-Ag NP composite powder = 2.1 mg in*

The details of the method and calculations are reported in Appendix I. For each concentration of the composite (and thereby Ag NPs) the conversion of the 4-NP to 4-AP was studied by following time dependent absorption changes of 4NP spectrophotometrically as reported before. Since absorbance of 4-NP is proportional to its concentration in the

TH-777_05612211

medium, the ratio of absorbance at time t (A) to that at t = 0 (t_0) i.e. A/A_0 could be used as the ratio of concentrations of 4-NP at time t to that t_0 (i.e. $A/A_0 = C/C_0$). The concentrations of 4-NP and $NaBH_4$ (used in excess) were kept constant for all the reactions. The amount of chitosan-Ag NPs composite used in each of these reactions is indicted in Table 3.1.A

Amount of chitosan-Ag NPs composites in unit volume of catalysis reaction mixture (g/L)	Corresponding amount of Ag present in the composite in the catalysis reaction mixture (mg/L)	Concentration of Ag in the composite in the catalysis reaction mixture ($X10^{-3}$ mol dm^{-3})
0.40	21	0.19
1.20	63	0.58
1.60	84	0.77
2.00	105	0.97
2.84	149	1.33
3.24	170	1.57
3.60	189	1.75
4.40	231	2.17
5.20	273	2.53

Table 3.1.A. *Chitosan-Ag NPs composites used in the catalysis studies and corresponding Ag NPs present in the reaction mixture. For synthesis of the composite, 0.1 g of chitosan and 0.4 mM $AgNO_3$ in 50 mL solution were used. Different amounts of the composite were taken from the*

TH-777_05612211

Also, since the concentration of $NaBH_4$ used in the reactions was in far excess of that of 4-NP the reaction can be considered as a pseudo first order reaction. The rate of the reaction is then proportional to the concentration of 4-NP alone and can be written as follows.

(1)

Here, c_t is the concentration of 4-NP at time t. It was observed that the rate of the reaction increased with the increase in the amount of chitosan-Ag NPs composite used for the reactions. A plot of the normalized concentration change as a function of time for the reduction of 4NP for various amounts of chitosan-Ag-NP composite (and thus Ag NPs) is shown in Figure 3.1.6. As is clear from the figure, the longest time taken for the completion of the reaction was 32 min when the concentration of the Ag used was 0.19 mM. On the other hand, the reaction was over in about 5 min when the concentration of the same was 2.53 mM. It is thus evident that the catalytic reaction was sensitive to the amount of Ag NPs present in the composite. Also interesting to note is that when the concentration of the catalyst was low (0.19 mM) there was significant induction period (about 13 min) in the reaction, whereas the reaction started immediately when the concentration was high (2.53 mM).

TH-777_05612211

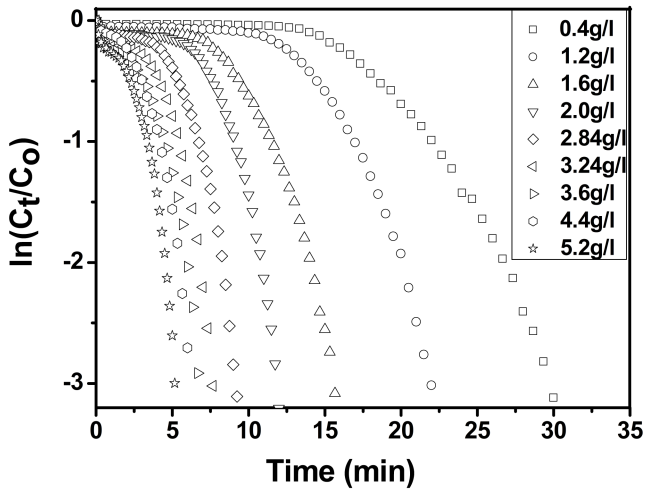


Figure 3.1.6*. Plot of the absorbance at* λ_{max} *of 4NP versus time at different amount of chitosan-Ag NP composite per unit volume. Corresponding concentrations of Ag in heterogeneous condition are given in the Table 1. The reaction conditions were as follows: [4NP]*

At the intermediate concentrations the induction period was also in between the two and decreased with the increase in the concentration of the catalyst. It may be mentioned here that the induction periods and their reduction with the concentration of the catalysts have been observed also by previous researchers working with metal NPs and have been attributed to the activation of the catalyst present in the reaction mixture[20(b), 22]. In view of the above observations, equation (1) can be rewritten as

(2)

Here is the concentration of p-nitrophenol at time , k_{app} is the apparent rate constant, which is a function of the concentration of the chitosan-Ag NPs used.

TH-777_05612211

A plot of the apparent rate constant with the concentration of the catalyst, as obtained from the $\ln(C/C_0)$ versus time plot using the data from Figure 3.1.6, is shown in Figure 3.1.7 (a). As is clear from the figure, the apparent rate constant of the reaction is linearly proportional to amount of catalyst used for the reaction. Thus equation (2) can be written as

(3)

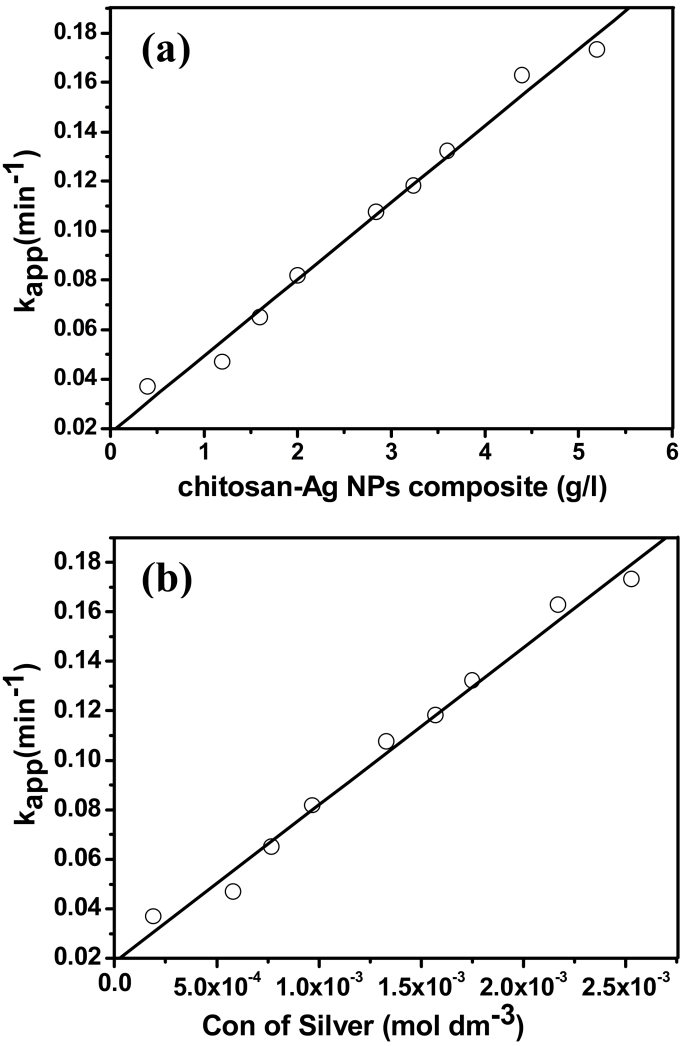
Here is the concentration of Ag present in the composite as per Table 3.1A; is the weight of the chitosan-Ag NPs present in the unit volume of the system, which was observed to increase linearly with the amount of Ag^+ in the parent salt that had been used to generate the composite (Figure 3.1.7). k_1 and k_1' are constants. Since the reaction carried out was heterogeneous and the same volume of reaction mixture was used for all the reactions the weight ( ) used herein can be assumed to be equivalent to concentration of Ag NPs ( ). The rate constant (k^1) of the reaction in the present system was calculated from the slope of the graph in Figure 3.1.7 (b), which was found to be 1.06 mol^{-1} dm^3 s^{-1}.

An important parameter indicating the efficiency of a catalyst is the turn over frequency (TOF). Since the surface atoms of the catalyst are involved in the catalysis the efficiency is related to the number of surface atoms present in the catalyst. Also, since the number of surface atoms present in NPs is high compared to its volume the efficiency is expected to be higher for NPs in comparison to the bulk catalyst, especially when the surface to volume ratio is the overriding determining factor. The TOF is defined as

(4)

TH-777_05612211

Where, M is the number of molecules (4NP here) reacted in the presence of catalyst in time *t* to produce the product and N_S is the number of surface atoms of the catalyst that is involved in the reaction. In calculating the TOF, it was assumed that the average particles size of Ag NP was 4.0 nm, which was obtained from the TEM image. Since the amount of Ag as well as the number of Ag NPs were known the number of surface Ag atoms present for each amount of composite could then be calculated. Also, the number of reactant molecules (4NP) used in each case was fixed at 1.50 x 10^{17}. Hence the TOF was calculated for each of the reaction carried out with different amount of catalyst. Table 3.1.B lists the amount of Ag NPs used, the total time taken and TOF for each reaction.



TH-777_05612211

Figure 3.1.7*. The plot of rate constant k_{app} obtained from Figure 3.1.6. Plot (a) represents rate constant k_{app} as function of amount of chitosan-Ag NPs composites normalized to the unit*

An average value of TOF was found to be 1.9 ± 0.1 s^{-1}. The calculations were performed using the total time as observed, which included the induction periods for lower concentrations of Ag NPs (and the lowest concentration data was not considered). However, if we subtract the induction time period and discount the first data (with very low concentration of catalyst) then an average value of 2.8 ± 0.4 s^{-1} was obtained for the TOF.

Table 3.1.B*. Calculation of the number of surface atoms and TOF (turn over frequency) with induction period and without induction period. The values in the rows i.e. number of Ag NPs correspond to amount of chitosan-Ag NP as in Table 1.*

No. of Ag NPs (N_{NPs}) x 10^{14}.	No. of surface atoms. (N_S) x 10^{17}	Time (s) Including induction period	Time (s) excluding induction period.	TOF (s^{-1}) x 10^3 Including induction period	TOF(s^{-1}) x 10^3 Excluding induction period.
0.60	0.37	1920	1110	2.10	3.6
1.80	1.12	1404	804	0.95	1.6
2.40	1.49	984	594	1.00	1.7
3.01	1.87	750	432	1.00	1.8
4.27	2.66	576	378	0.98	1.5
4.87	3.03	510	354	0.97	1.4
5.41	3.33	438	348	1.00	1.3
6.61	4.12	396	306	0.92	1.2
7.82	4.85	330	240	0.94	1.3

TH-777_05612211

This value is reasonable for a nanocatalyst such as small Ag NP and is consistent with literature value. One may point out that since Ag NPs are supported on the chitosan the exact number of surface atoms may not exactly be the same as calculated. However, as indicated in Table 3.1B, the consistency of the TOF value at different Ag NP concentration suggest that the effect of the support - if any - may be minimal in terms of error in the calculation.

TH-777_05612211

We were further interested in finding out the reusability of the catalyst, which is important for commercial applications. This was pursued by carrying out a set of reactions, in sequence, where the ratio of the amount of catalyst (chitosan-Ag NP composite) and the reactant (4NP) were kept nearly the same. For example, 10 mg (conc. of Ag was 1.9 mM) of the composite was taken in a cuvette with addition of 2.5 mL of a solution containing 4NP and $NaBH_4$ as before (see the caption of Figure 3.1.5). Once the reactions were over (as observed by absorbance decay of 4NP), the composite was recovered by decantation of the liquid (using a micropipette). This was followed by washing of the solid composite with Milli-Q grade water and decantation of the liquid again.

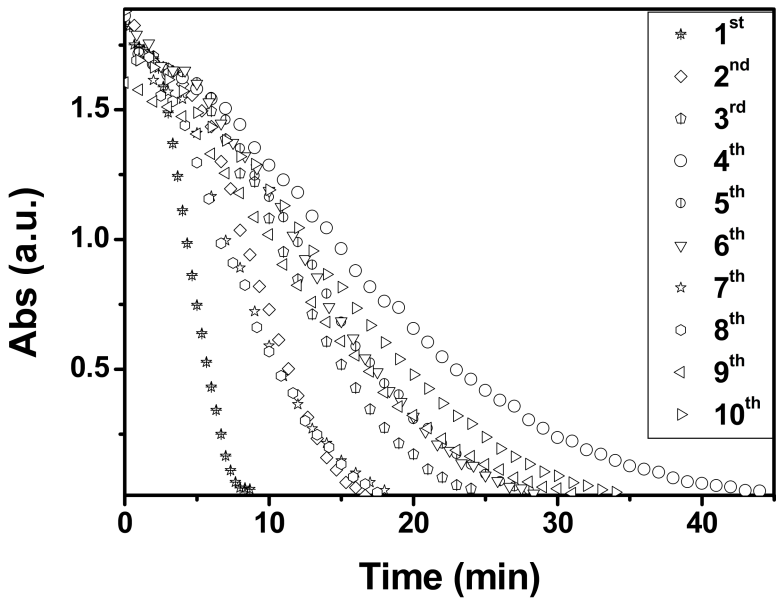


Figure 3.1.8. *Reusability of the composite catalyst as demonstrated by several cycle of reactions catalyzed by the same catalyst. The plot indicates changes in the visible absorption spectra of 4NP due the reduction to 4AP, as a function of time, for several cycles of use of the composite catalyst. The numbers on the right box indicate the cycle number in the catalysis.*

Then 2.5 mL of the same reaction mixture was added to the cuvette. The absorbance decay of 4NP with time was followed as before. The completion of the reaction was taken as the

TH-777_05612211

completion of the 2nd cycle. Similarly, the cycles were pursued for 8 more times to have 10 cycles of reaction using the same catalyst. The results are shown in Figure 3.1.8. As is clear from the figure, the catalytic activity was retained quite well even up to the tenth time. For example, when the reaction was completed in 516 s in the first cycle, it took 1716 s to be completed in the fifth cycle, while the same reaction took 1075 s in the eighth cycle. The apparent difference between the progressive cycles could be due to loss of catalyst during handling in between two cycles.

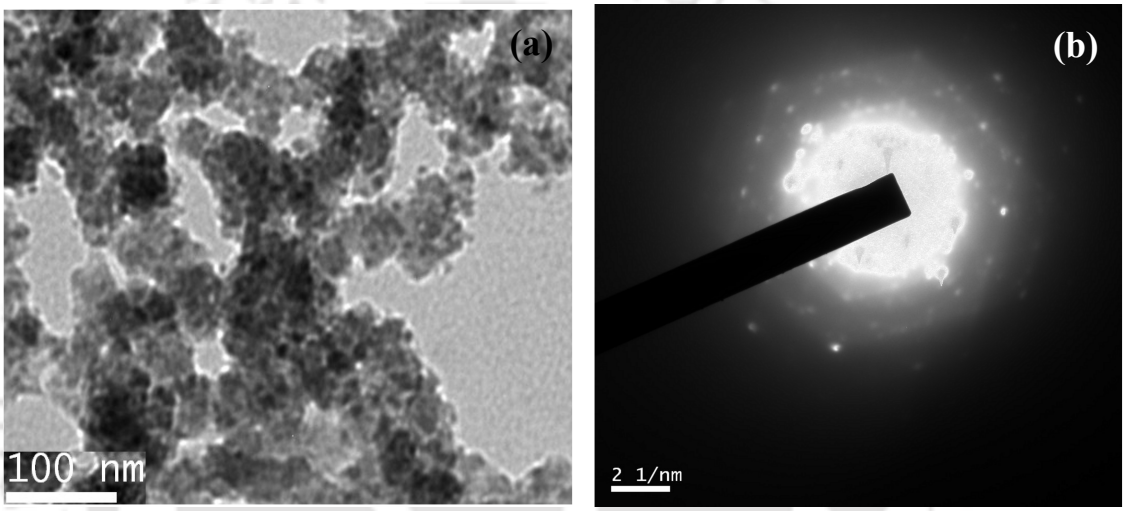


***Figure 3.1.9**. (a) TEM image of CS-Ag NPs composite powder recovered after fourth catalytic cycle (refer to Figure 6 in the manuscript). (b) Corresponding SAED pattern.*

Also, oxidation of Ag NPs and subsequent reduction by $NaBH_4$, while in the composite (in the reaction medium), may alter the average size of the particle which may also be the reason for observed differences between cycles. This means Ag NPs were stable in the composite and retained their activity. That the catalytic Ag NPs were stable and remained attached to chitosan polymer was evident from the TEM measurements of the catalyst after four cycles of catalytic reactions. A typical TEM image, shown in (Figure 3.1.9 (a)), clearly indicates the presence of small Ag NPs in the composite after the fourth cycle of operation. The SAED patterns (Figure 3.1.9 (b)) corresponding to the NPs also corroborate the presence of

TH-777_05612211

Ag NPs. These results show that metal NPs on the surface of the chitosan were not getting leached significantly during the course of the reaction. This possibly indicates that strong affinity of chitosan for Ag NPs leads to stabilization of the NPs on the surface and that might prevent the metal from leaching during the catalytic reaction. Thus we have an efficient, workable, easily recoverable Ag NP catalyst with reasonably high TOF. This is important in terms of value of a catalyst in industrial applications.

Finally, we were further interested in finding the potential of the composite as catalyst working under micro-heterogeneous conditions for increased efficiency. This would be even more advantageous if the reaction condition was such that the composite would be dispersible in the reaction mixture at a certain pH and the reaction can be carried out without catalyst getting precipitated out of the solution. Fortuitously, the Ag NP-chitosan composite was dispersible in the reaction mixture (aqueous solution) up to a pH of 6.3 and the reduction of 4NP to 4AP could be carried out under this condition using $NaBH_4$ as the reducing agent. The results of the catalysis of the conversion of 4NP to 4AP by the composite in the presence of $NaBH_4$ are shown in Figure 3.1.10. As is evident from the figure, the reduction of 4NP under micro-heterogeneous conditions was much faster than that while using the catalyst under heterogeneous conditions (Figure 3.1.6). Also, it is important to note that the concentrations of catalyst needed to carry out the same reaction (with similar concentrations of reactants) were much less when carried out in micro-heterogeneous conditions in comparison to that under heterogeneous conditions. For example, while catalyst concentrations needed under heterogeneous condition was on the order of several g/L, the same reaction could be achieved in similar times using catalyst concentrations of mg/L under micro-heterogeneous conditions. This indicates that the reaction when carried out using the composite as the catalyst under micro-heterogeneous condition is much more efficient than under heterogeneous conditions. That the reaction is faster in micro-heterogeneous condition could be explained using the concentration of metal NPs present in the medium where the rate will directly depend on the available surface area of the NPs in the medium. In that case the rate of the reaction can be expressed as

TH-777_05612211

(5)

Here C_t is the concentration of 4NP at time t, k_2 is the rate constant, S is the total available surface area of the NPs in the medium (normalized to the unit volume of the system). The validity of this approximation can be made from Figure 3.1.10, where it can be observed that increase in the concentration of the chitosan-Ag NP composite leads to rapid increase in the rate of the reaction. Also, the values of rate constants supports that the apparent rate constant k_{app} is proportional to the total surface area of the NPs and as well as concentration of composite chitosan-Ag NPs used in the system.

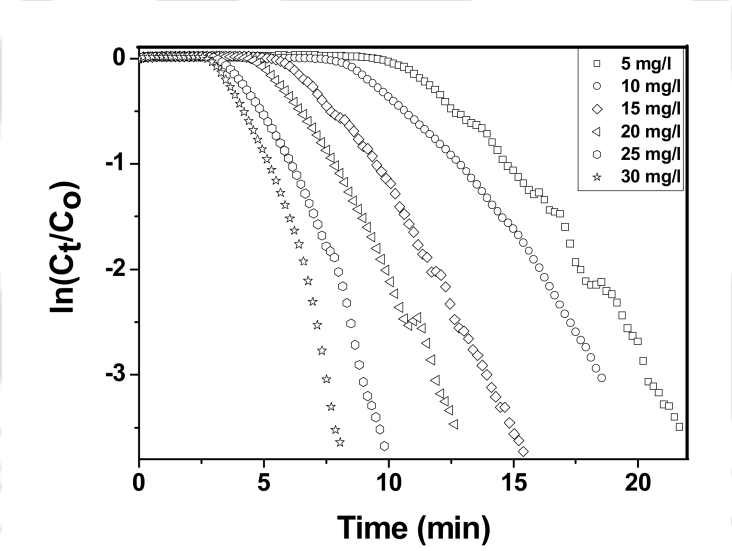


Figure 3.1.10. *The Plot of the absorbance at λ_{max} of 4NP versus time, in the presence of different amount of chitosan-Ag NP composite per unit volume. The reaction was conducted under micro-heterogeneous condition. The reaction conditions were as follows: [4NP] = 0.1 mM*

Further, the amount of chitosen-Ag NP composite used in the micro-heterogeneous reaction condition is much smaller than the heterogeneous condition. From above the observations, it

TH-777_05612211

can be concluded that the rate of the reaction in the micro-heterogeneous condition, which can be carried out with less amount of catalyst, is much faster than that under heterogeneous condition.

TH-777_05612211

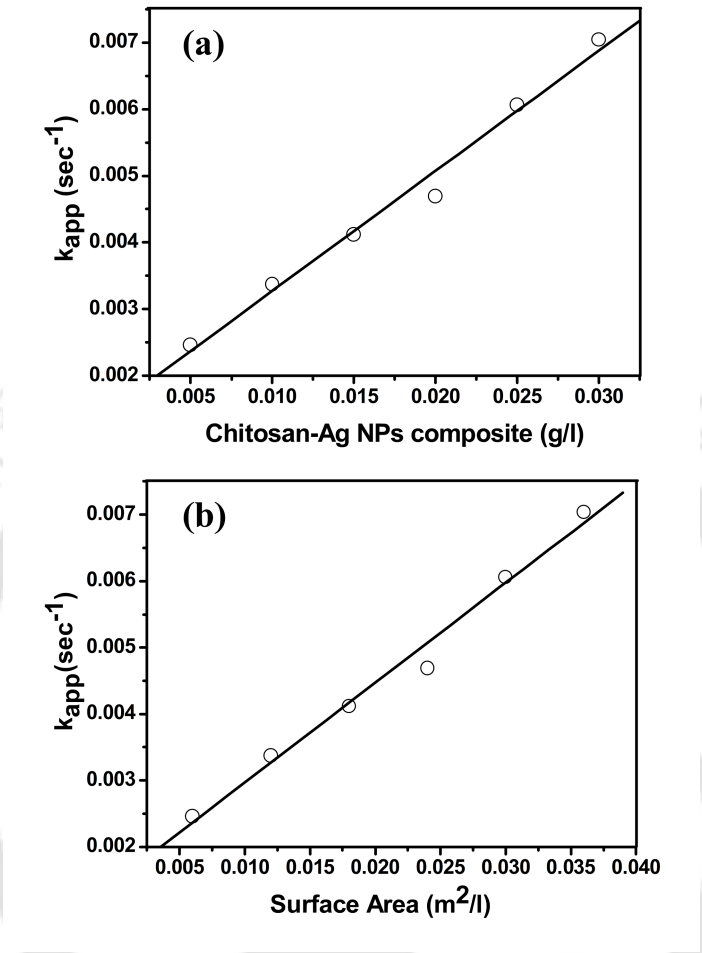


Figure 3.1.11. *The plot of rate constant k_{app} obtained from Figure 3.1.10 (reaction under micro-heterogeneous condition). Plot (a) represents rate constant k_{app} as function of amount of chitosan-Ag NPs composite and (b) is the rate constants as varied with concentration of Ag*

Finally, our observations suggest that the catalytic activity of chitosan-Ag-NP composite that has been prepared, is much higher in comparison to results available in the literature. For example, Pradhan et al[12] have used Ag NPs with an average size of *ca.* 25 nm to catalyze 4NP to 4AP using $NaBH_4$ and have obtained a rate constant $k_{app} = 2.3 \times 10^{-3}$ s^{-1} with 5.0 x

TH-777_05612211

10^{-6} mol / L Ag catalysts at 20^{o}C. The rate constant when normalized with the surface area of the catalyst was calculated to be k = 3.78X10^{-7} $s^{-1}m^{-2}L$.

On the other hand, Lu et al[22] synthesized Ag NP composite with a themosensitive polymer, having average diameter of the Ag NPs between 8 nm to 10 nm, to catalyze the above reaction. They obtained a rate constant, k = 5.2 x 10^{-2} s^{-1} m^{-2} L, higher than that obtained by Pradhan et al[12]. In the present case, with the sizes of the Ag NPs (in the composite) much smaller, the rate constant was calculated, from Figure 3.1.11 (b) to be k_2 =1.5X10^{-1} s^{-1} m^{-2} L, which is higher than the literature reports. However, considering the sizes of the NPs in the present system and also the catalyst working in the micro-heterogeneous conditions, this increase in rate constant is not surprising. The present set of results demonstrate that conditions of reaction (micro-heterogeneous versus heterogeneous), sizes of the particle (catalyst) are crucial in the catalysis involving metal NPs.

3.1.4 Conclusion

Herein, we have reported the development of a simple synthetic scheme for the generation of stable chitosan-Ag-NP composite with high catalytic activity. The NPs generated in the present method were of uniform and narrow particle sizes, with typical sizes less than 5 nm. The composite was tested for heterogeneous catalysis with Ag NPs being the active catalyst and chitosan as the support. The catalytic efficiency for the reduction of 4NP to 4AP for the composite was high with a TOF value of (1.5 ± 0.3) X 10^{-3} s^{-1}. The small particle size and thus high number of surface atoms makes the composite a rather appealing material for catalysis and other application. Further, the additional advantage of being able to use the catalyst under micro-heterogeneous conditions makes its usefulness rather appealing. To the best of our knowledge, there exists no other report of chitosan being used as a reducing agent for the production of Ag NPs as well as their stabilizer, although reports exist of functional NPs that were separately attached to chitosan for catalysis. The synthetic method, which has been developed in the present study, might be useful for further

TH-777_05612211

development of 'green' NPs synthesis in other situations. Since chitosan is biocompatible, the composite can be useful for biological applications which we are currently being pursued in the laboratory. Since, chitosan can be made in the form of beads, fibers, membranes the application potential of the composite could become even more versatile.

TH-777_05612211

3.1.5 Appendix I

Calculation of number of nanoparticles and number of surface Ag atoms

These calculations were based on the model used by J. D. Lewis, et al[21]

In 50.0 mL of water containing 0.1 g of chitosan, 1 mL of 2 X 10^{-2} mol dm^{-3} $AgNO_3$ was added. So, the final concentration of $AgNO_3$ was 4 X 10^{-4} mol dm^{-3}. After, completion of reaction, we have observed that all the Ag^+ ions were converted Ag NPs. Since the concentration of Ag^+ ion was 4 X 10^{-4} mol dm^{-3} in the original solution, this means 2.15 mg of Ag was present in 0.1 g of chitosan. So the amount of Ag nanoparticles formed in this reaction,

(eq. 1)

Where, is the Ag NPs formed on the chitosan particles, V is the final volume of the reaction, M is molar concentration of Ag^+ ion and A.wt is the atomic weight of Ag atom.

From the TEM result, it was observed that Ag nanoparticles were spherical in shape, and one can roughly write,

(eq. 2)

then

(eq. 3)

Here, $V_{cluster}$ is the volume of a cluster (nanoparticle) and V_{atom} is the volume of an atom, $R_{cluster}$ is the radius of a cluster and R_{atom} atomic radius and N is the total number of atoms within the cluster. Rearranging the eq. 2 and eq. 3, we obtain:

(eq. 4)

TH-777_05612211

Knowing the cluster radius we may also be able to calculate the surface (S) area of nanoparticles with the following equation:

(eq. 5)

For large crystals, we can calculate the number of surface atoms, N_S, directly by dividing the surface area of the cluster by the cross sectional of an individual atom, and then applying the (eq. 4):

(eq. 6)

From the TEM result we know that $R_{cluster}$ = 2 nm, and R_{atom} = 160 pm. The number of silver atom per nanoparticle was estimated using (eq. 4):

silver atom per nanoparticle.

The number of surface atoms, N_S, on single silver nanoparticle was also estimated using (eq. 6):

Silver surface atom per nanoparticles.

The fraction of silver atom on the surface of their nanoparticles is, therefore, 32 %.

Calculation of the amount of silver nanoparticles formed (N_{NP}) when 2.15 mg of Ag particles was used to make the composite particles with chitosan.

TH-777_05612211

Amount of silver particles used,

No. of silver atoms,

No. of nanoparticles in 2.15 mg of Ag particles.

Nanoparticles were formed per 2.15 mg of Ag.

3.1.6 References

1. (a) He, H.; Zhu, J.; Tao, N. J.; Nagahara, L. A.; Amlani, I.; Tsui, R. *J. Am. Chem. Soc.* **2001**, *123*, 7730. (b) Stucky, G. D. *Nature* **2001**, *410*, 885.

2. Jager, E.; Ingalis, O.; Lundstrom, L. *Science* **2000**, *288*, 2335.

3. Bashyam, R.; Zelenay. P. *Nature* **2006**, *443*, 63.

4. (a) Tsunoyama, H.; Sakurai, H.; Negishi, Y.; Tsuguda, T. *J. Am. Chem. Soc.* **2005**, *109*, 692. (b) Zhang, J.; Xu, S.; Kumacheva, E. *J. Am. Chem. Soc.* **2004**, *126*, 7908. (c) Calo, V.; Nacci, A.; Monopoli, A.; Fornaro, A.; Sabbatini, L.; Cioffi, N.; Ditaranto, N. *Organometallics* **2004**, *22*, 5154. (d) Vincent, T.; Guibal, E. *Langmuir* **2003**, *19*, 8475.

5. (a) Sih, B. S.; Wolf, O. M. *Chem Comm*. **2005**, 3375. (b) Novak, P. J.; Feldheim, L. D. *J. Am. Chem. Soc.* **2000**, *122*, 3979. (c) Atay, T.; Song, J-H.; Nurmikko, V. A. *Nano Lett*. **2004**, *4*, 1627.

6. (a) Sarma, T. K.; Chowdhury, D.; Paul, A.; Chattopadhyay, A. *Chem Comm.* **2002**, 1048. (b) Sarma, T. K.; Chatopadhyay, A. *J. Phys. Chem. A* **2004**, *108*, 7837.

7. Chowdhury, D.; Paul, A.; Chattopadhyay, A. *Langmuir* **2005**, *21*, 4123.

TH-777_05612211

8. Majumdar, G.; Goswami, M.; Sarma, T. K.; Paul, A.; Chattopadhyay, A. *Langmuir* **2005**, *21*, 1663.

9. Lu, Y.; Mei, Y.; Drechsler, M.; Ballauff, M. *Angew. Chem. Int. Ed*. **2006**, *45*, 813.

10. Gronnow, M. J.; Luque, R.; Macquarrie, D. J.; Clark, H. J. *Green chem*. **2005**, *7*, 552.

11. (a) Jana, R. N.; Sau, K. T.; Pal, T. *J. Phys. Chem. B* **1999**, *103*, 115. (b) Jiang, J-Z.; Liu, Y-C.; Sun, W-L. *J. Phys. Chem. B* **2005**, *109*, 1730.

12. Pradhan, N.; Pal, A.; Pal, T. *Colloids and surfaces, A*. **2002**, *196*, 247.

13. Kobayashi, S.; Toshitsugu, K.; Shin-Ichiro, S. *J .Am. Chem. Soc.* **1996**, *118*, 13113.

14. Shin, Y.; Yoo, D. I.; Jang, J. J. *Appl. Polym. Sci.* **1999**, *74*, 2911.

15. (a) Shigehiro, H.; Yasuo, K.; Shuntaro, K.; Testsuo, T.; Hisaya, T.; Kakuko, M.; Takeshi, Y. *Biochem. Syst. Ecol.* **1991**, *19*, 379. (b) Domare, A.; Roberts, G. A. F. *Advances in chitin science*; Andre, J., Ed.; National Taiwan Ocean University Keelung, Taiwan, **1998**.

16. (a) Dhanikula, A. B.; Panchangnula, R. *The AAPS journal*. **2004**, *6*, 1. (b) Payne, F. G.; Raghavan, S. R. *Soft matter*. **2007**, *3*, 1.

17. (a) Roy, K.; Mao, H. Q.; Huang, S. K.; Leong, K. W. *Nature Med*. **1999**, *5*, 387. (b) Bartkowiak, A.; Hunkeler, D. *Chem. Mater.* **1999**, *11*, 2486. (c) Suzuki, T.; Mizushima, Y.; Umeda, T.; Ryo, O. J. *Biosci. Bioeng.* **1999**. *88*. 194.

18. Yi, H.; Wu, L-Q.; Bentley, W. E.; Ghodssi, R.; Rubloff, G. W.; Culver, J. N.; Payne, G. F. *Biomacromolecules* **2005**, *6*, 2881.

19. (a) Hardy, J. J. E.; Hubert, S.; Macquarrie, D. J.; Wison, A. J. *Green Chem*. **2004**, *6*, 53. (b) Vincent, T.; Guibal, E. *Ind. Eng. Res. Chem*. **2002**, *41*, 5158. (c) Han, H. S.; Jiang, S. N.; Huang, M.; Jiang, J. J. *Polym. Adv. Technol.* **1996**, *7*, 704.

20. (a) Pradhan, N.; Pal, A.; Pal. T. *Langmuir* **2001**, *17*, 1800. (b) Panigrahi, S.; Basu, S.; Praharaj, S.; Pande, S.; Jana, S.; Pal, A.; Ghosh, K. S.; Pal, T. *J. Phys. Chem. C* **2007**, *111*, 4596.

TH-777_05612211

21. Lewis, J. D.; Day, M. T.; MacPherson, V. J.; Pikeramenou, Z. *Chem Comm*. **2006**, 1433.

22. Lu, Y.; Ballauff, M. J. *Phys. Chem. B* **2006**, *110*, 3930.

TH-777_05612211

4.1 'Green' Chitosan bound Silver Nanoparticles for Selective C-C bond Formation via in situ Iodination of Phenols

4.1.1 Introduction

Chemical reactions involving C-C bond formation continue to evoke research passions in the development of synthetic methods involving systems as diverse as aliphatic and aromatic compounds to complex polymers. These developments are being driven by the demands in pharmaceutical, agrochemical, polymer and even electronic industries where C-C bond formation is an important step in the designer intermediate generation, towards building complex architectures of a variety of organic molecules. As an example one can consider the case of coupling of phenols which is essential in the generation of a number of pharmacologically useful compounds such as terpenes, lignanes, tannins, flavanoids and alkaloids.[1] Further, selective C-C coupling of phenol derivatives have been used in the generation of metal complexes used as chiral metal catalysts and helical polymers.[2] Typically, coupling reactions of phenols are performed using oxidizing agents such as $FeCl_3$, ferricyanides and oxides of Pb(II), Ti(III) and V(V).[3] However, their use results in poor selectivity in the product formation and generation of mixtures of quinones, dimers, trimers and polymers. In addition, some of these reagents are environmentally hazardous for large-scale usage. Further, in many instances the selectivity in coupling is either not achieved or can be achieved through blocking appropriate positions in the aromatic ring, which require additional reagents, catalysts and not to mention the increase in the number of reaction steps and consequent yields. A new method that would involve minimum and greener reagents, reduced number of steps and that provides greater selectivity would arguably be a welcome addition to the repertoire.

Recently, a broad range of C-C coupling reactions, such as Suzuki, Heck, Sonogashira and Hiyama reactions, have been performed efficiently with the use of metal

TH-777_05612211

nanoparticles (NPs) as catalyst under homogeneous or heterogeneous condition. For example, Crooks and Co-workers[4] reported that dendrimer encapsulated Pd NPs could be used as efficient catalyst for Suzuki coupling reactions in homogeneous conditions. In addition, chitosan supported Pd NPs were used for C-C coupling under heterogeneous catalysis.[5] Separately, Au NPs and Ag NPs have been used as catalysts for oxidation and reduction of a few selected molecules.[6] Interestingly, although there have been reports of coupling reactions involving Ag NPs and Au NPs in a medium,[7] microheterogeneous coupling with high selectivity using an isolated polymer-Ag NP composite has not been reported. We have recently reported the development of a "green" chitosan Ag NP (Chit-Ag NP) composite using chitosan as both reducing as well as stabilizing agent in the presence of NaOH. The resultant composite consisted of 21.6 mg of Ag per gram of chitosan. The average size of the Ag NPs present in the composite was 4.0 ± 1.2 nm and they exhibited high catalytic efficiency for the reduction of 4-nitrophenol to 4-aminophenol, and also have high antimicrobial activities.[8] Also, the composite is soluble in water at acidic pH, while it precipitates out when the pH is turned alkaline.

In this chapter, we report the use of the Ag NPs present in the composite as an efficient catalyst, in selective C-C coupling of phenolic compounds, in the presence of molecular iodine. This is possibly the first known report on C-C coupling with Ag NPs as the catalyst. Typical reactions were carried out with phenol and a few of its derivatives as well as naphthols. The results indicate that the reaction proceeded via the formation of p-iodophenol followed by o-p coupling leading to the product. Interestingly, when the para position of phenol was blocked by a substituent then only iodination at the ortho position could be observed, without the formation of coupled products. On the other hand, in the case of naphthols *o-o* coupling could only be observed. Based on the observed results, a mechanism is proposed for the coupling reaction occurring at the surface of Ag NPs.

TH-777_05612211

4.1.2 Experimental Section

Materials

Phenol and its derivatives and iodine were purchased from Sigma-Aldrich Chemical Corporation. Absolute ethanol, Ethyl acetate (EtOAc), Hexane and dichloromethane were purchased from Merck.

Synthesis of Chitosan Ag nanoparticles (Chit-Ag NPs)

Chit-Ag NP composite was prepared by a procedure recently developed in the laboratory[7]. The details of the method are given in Chapter 3. 0.2 g of Chit-Ag NP composite powder was dissolved in 100 mL of 0.1 % (V/V) acetic acid in water. The resulting Chit-Ag NP composite solution was used as a stock solution for catalysis.

General procedure for the synthesis of the compounds

Substrates (1.0 mol dm^{-3}) were added to a solution of catalyst dissolved in a mixture of water (0.4 mL) and absolute ethanol (0.6 mL). The mixture was stirred for 1 min, followed by the addition of molecular iodine (0.6 mol dm^{-3}). The stirring was continued at room temperature until the completion of the reaction as indicated by thin layer chromatography (TLC). The reaction mixture was then poured into 10 mL of water and then extracted with dichloromethane (3 x 15 mL). The extracted organic layer was dried over anhydrous Na_2SO_4 and evaporated under reduced pressure to furnish crude product. The crude product was further purified by column chromatography, (Hexane: EtOAc (9: 1)) to provide pure product.

Analytical Measurements

NMR spectra (400 MHz for ^1H and 100 MHz for ^{13}C) were recorded using a DRX-400 Varian spectrometer with $CDCl_3$ as the solvent and Me_4Si as internal standard. Column chromatography was performed on silica gel (60 - 80 mesh) using ethyl acetate

TH-777_05612211

(Merck) and hexane (Merck) as eluent. The mass spectra were recorded using a Waters instrument (ACQUITY^{TM} UPLC) in ESI mode.

4.1.3 Results and Discussion

It was observed that when phenol was treated with molecular iodine in the presence of the catalyst 6-iodo-2,4′-bis-1,1′-phenol was formed (Scheme 4.1.1). The product was be obtained in high yield when 1.0 M of the substrate was stirred with 0.8 g/L of Chit-Ag NP composite solution at room temperature and in the presence of 0.6 M of molecular iodine. Also, the reaction was complete in 3 hrs. The concentration of Ag was 0.16 mM. The number of Ag NPs in solution was calculated to be 4.8 X 10^{16} NPs/L.[8a] The above concentration of the composite was found to be the best (with 100% yield of the product), as at lower concentrations complete conversion was not achieved and the intermediate compound (p-iodophenol) was present in the reaction mixture. For example, at 0.4 g/L and 0.6 mg/L of the composite the yields of the coupling product were 55% and 62% respectively, while p-iodophenol was formed in large excess. Plot of the product yield versus surface area of Ag NP catalyst (Figure 4.1.1) indicated rapid increase in product yield with the surface area. As is clear from the figure, at lower values of surface area, the intermediate compound was produced in high yield, whereas yield was 100% at a minimum surface area of 2.5 m^2/L. On the other hand, when the available surface area of the NPs was low the product did not form at high yield even after prolonged stirring (12 hrs). Thus it can be concluded that the total available surface area of the nanocatalyst is crucial for the formation of coupled products in the present system. Further, it may be mentioned here that when the reaction was carried out in presence of bulk Ag no coupling could be observed. Also, the intermediate (p-iodophenol) was not formed. It is known that enormous increase in surface area and surface free energy in the NP in comparison to the bulk metal make the metal NPs efficient catalysts.[9] The present results demonstrate that Ag NPs, similar to other traditional metal NPs (Pt, Pd, Rh and Ru), could be used as efficient catalyst for C-C coupling reactions.[10]

TH-777_05612211

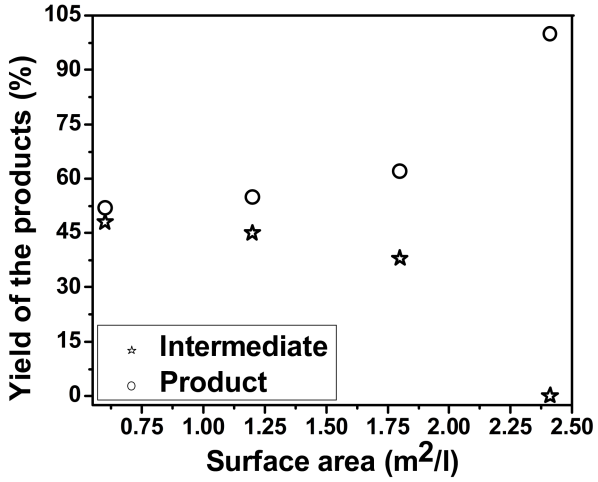
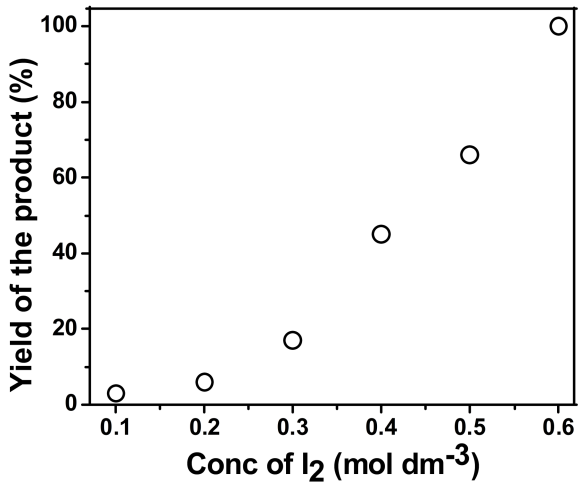


***Figure 4.1.1**. The plot of the surface area per unit volume of the total Ag NPs in the composite versus the yield of product. The concentration of I_2 was 0.6 M.*

Further, it was found that optimum concentration of molecular iodine necessary to form the coupling product with high yield (>95%) was 0.6 M, under the above reaction condition. At lower concentrations either no product was formed or product was formed with low yield, while excess starting material (phenol) was present in the reaction mixture. A plot of the product yield with the amount of iodine – shown in Figure 4.1.2 – indicates that the yield increased rapidly with the concentration of iodine, the highest being at 0.6 M. The requirement of excess iodine in the reaction could be due to the formation of its well-known complex with chitosan[11] (in the composite).



TH-777_05612211

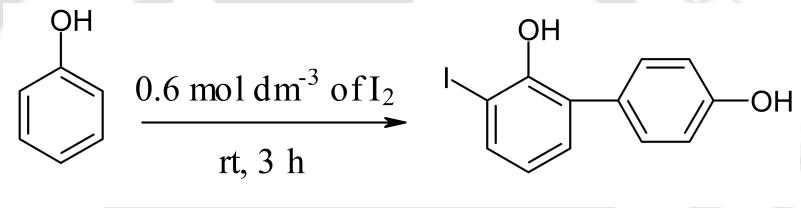
***Figure 4.1.2**. The plot of the selective coupling product of phenol with concentration of molecular iodine. The amount of the composite was 0.8 g/L.*

At lower concentrations of iodine, chitosan-iodine complex might have been formed exclusively and preferentially, rendering the availability of iodine low for reaction to occur at the surface of the Ag NP catalyst, while at higher concentrations excess iodine may be available for the formation of coupling product. It was also observed that use of iodine beyond 0.6 M led to a slurry mixture and the product could not be easily isolated and hence not pursued further in this regard. It is important to mention here that when the amount of the composite used was higher (> 0.8 g/L) - keeping the concentration of iodine constant - the yield of the coupling product decreased. The amount of the unreacted starting materials was also high (in comparison to the product) – that increased with the increasing amount of the composite (in the presence of a constant amount of iodine). Interestingly, it was observed that at the completion of the reaction (3hrs), complete conversion took place and the intermediate p-iodophenol was also consumed completely in the process (when optimum concentrations of iodine and composite were used). Thus careful choice of concentrations of iodine as well as the catalyst is important in obtaining products with high yield.

In order to have a better understanding of the mechanism of the coupling reaction and the scope of the reaction with substituted phenols, further reactions were carried out

TH-777_05612211

with ortho and para substituted phenols. The results are shown in Table 4.1A and Table 4.1B respectively. The ortho substituted phenols yielded coupling product exclusively – except for catechol - (Table 4.1A), while para substituted ones resulted in iodinated phenols instead of coupling products (Table 4.1B) under the same reaction condition. Moreover, the yields of the iodinated product of para substituted phenols were ≥ 98%. Although, the two ortho positions are available for reactions in para substituted phenols, the iodination took place only in one ortho position (Table 4.1B). Therefore, the above results clearly indicate that para position of phenols should be free and available for the coupling reaction to take place. Interestingly, ortho or para amino or nitro substituted phenols did not provide any iodinated phenol or coupling product.

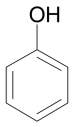
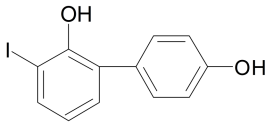
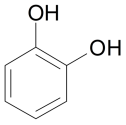
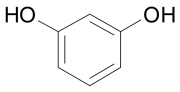
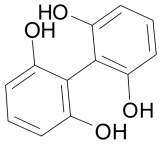
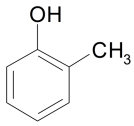
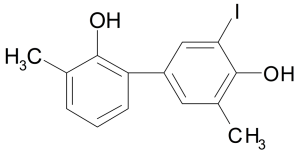
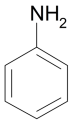
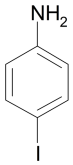


Scheme 4.1.1*. Chit-Ag NP catalyzed o-p phenolic coupling reaction.*

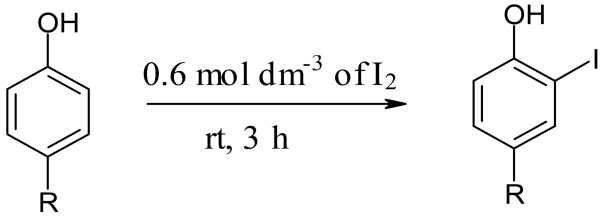
Further, 1,2-dihydroxy benzene (catechol) resulted in neither iodination nor coupling product formation even when the reaction was carried out for a relatively longer period. Additionally, in the case of naphthols, the coupling products were devoid of iodinated compounds (Table 4.1C). The product formation was through 2-2′ coupling for α-naphthol, while 3-3′ coupling occurred in β-naphthol.

Table 4.1A*. Chit-Ag NP catalyzed selective o-p phenolic coupling reaction via iodination.*

TH-777_05612211

Entry	Substrate (a)	t [h]	Product (b)	Yield [%] (a,b)
1		3		75
2		3	-	-
3		3		70
4		3		78
5		0.5		98

Recently, Temma et al reported the oxidative cross coupling of the naphthol derivatives using a chiral catalyst.[12] Their observation was that coupling of β-naphthol or β-naphthol derivatives mainly took place at the carbon nearest to the hydroxyl group. Similarly, Gao et al [13] concluded that the hydroxyl group at ortho position remains attached to the copper metal centre in the complex, leading to selective coupling in metal catalyzed reactions.



Scheme 4.1.2. *Chit-Ag NP catalyzed C-C bond formation of para substituted phenols.*

TH-777_05612211

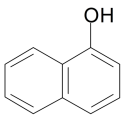
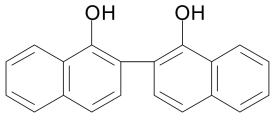
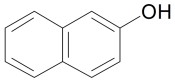
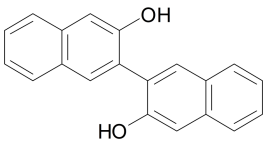
The above results demonstrated that under the present reaction conditions, C-C coupling of phenols took place between ortho and para positions of the two moieties. This was evident from the absence of coupling of the reagents in which the para positions were blocked (Table 4.1B). On the other hand, when one of the ortho positions was blocked by substitution, the coupling took place with the other free ortho position (except for the –OH substitution).

Table 4.1B. *Chit-Ag NP catalyzed coupling of p-substituted phenols.*

Entry	Substrate, R (a)	t [h]	Yield [%] (b)
1	$-CH_3$	2	85
2	$-NH_2$	3	-
3	$-NO_2$	3	-

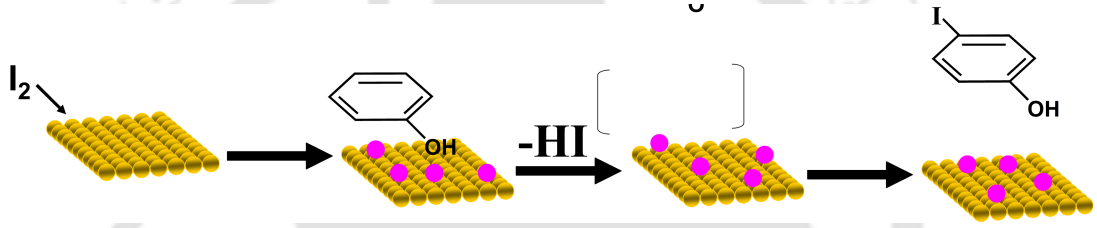
The absence of intermediate or product formation from catechol could be due to strong intramolecular hydrogen bonding between the neighboring OH groups, preventing adsorption on the surface of the NP catalyst. It can therefore be concluded that one of the ortho positions and the para position of the phenols must be free in order for the selective coupling to take place.

Table 4.1C. *Chit-Ag NP catalyzed coupling of naphthols.*

Entry	Substrate (a)	t [h]	Product (b)	Yield [%] (a, b)
1		3		83
2		3		85

TH-777_05612211

This was further confirmed by detection of p-iodophenol as the intermediate. Therefore, the above observations suggest that selective coupling of the phenols, under the present reaction conditions, took place via formation of p-iodophenol as the intermediate. At lower concentrations of the catalyst, the formation of coupled product was low, which gradually increased with increasing catalyst concentration and consequently the yield of the p-iodophenol decreased. On the other hand, at higher concentrations of the catalyst, p-iodophenol, albeit formed quickly, was converted into the coupled product. It is well-known that molecular iodine adsorbs onto the surface of bulk Ag under ultra high vacuum (UHV) condition and splits into iodine atoms.[14]

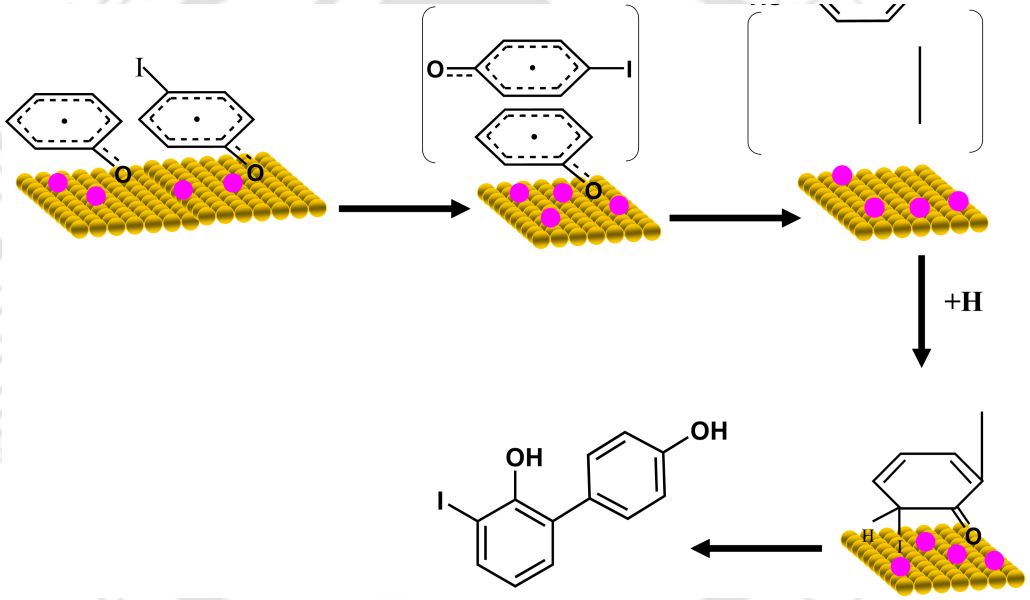


Scheme 4.1.3*. The plausible mechanistic pathway for the formation of p-iodophenols by Chit-Ag NP catalysts. Iodine on the surface is indicated by purple spheres.*

The iodine atoms generated on the surface can further react with organic moieties for iodination. Similarly, in the present experimental conditions, molecular iodine when added to chit-Ag NPs dissociates into iodine atoms, and the resulting iodine atoms remain adsorbed onto the surface of the NPs; which in turn would react with phenol adsorbed on the surface. The iodine atoms present on the surface may first abstract hydrogen from phenol leading to adsorption of phenoxyl radical on the surface. This is followed by iodination at the para position and subsequent desorption from the surface leading to the formation of p-iodophenol. The plausible process for p-iodophenol formation is schematically shown in Scheme 4.1.3. The proposed mechanism is consistent with the report that the OH group of phenol can be weakly chemisorbed onto Ag metal surface, with the ring plane nearly parallel

TH-777_05612211

to the surface[15]. Further, it is worth pointing out here that when NaI was added to the reaction mixture instead of molecular iodine, with the same amount of catalysis (0.8 g/L), there was neither formation of any iodinated product nor coupling reaction took place. This is because addition of I^- onto Ag NPs surface might result in the formation silver-iodide complex at the surface of the NPs and the resulting complex may be converted into molecular silver iodide, which is known to be catalytically inactive for selective coupling of phenols[16]. Thus iodine atoms derived from molecular iodine at the surface of Ag NPs are possibly responsible for the formation of intermediate as well as coupling products.



Scheme 4.1.4*. The plausible mechanistic pathway for the formation of selective coupling of phenol by Chit-Ag NP catalyst.*

Further, based on the results with different substituted phenols, a plausible mechanism for the formation of C-C coupled product is shown in Scheme 4.1.4. Here again, the iodine atoms present on the surface facilitate the adsorption of phenoxyl radical as well as

TH-777_05612211

p-iodophenoxyl radical on the surface. The two phenoxyl radicals subsequently form a stable species having sandwich-type geometry on the surface (Scheme 4.1.4). This geometry results in ortho-para coupling between the two with elimination of HI. This is followed by iodination at the ortho position that is nearest to the surface and the results are ortho-iodinated C-C coupled products. It has been demonstrated in other coupling reactions and from the minimum energy calculation that the sandwich-type geometry [17] between the two phenoxyl radical species as shown in Scheme 4.1.3 is the most stable form. Perkins and co-workers have shown that this sandwich-type geometry, with the staggered configuration, could lead to either the o-o coupling or o-p coupling of phenols.[18] Their observation was that at room temperature o-p coupling led to the major product formation, whereas at higher temperatures the o-o coupling was the route to the major product formation. This is consistent with our observations of selective *o-p* coupling via intermediate p-iodophenol formation at room temperature and the surface of the Ag NP played the key role in the selectivity of phenolic coupling. This conclusion is further substantiated by the works of Bent and coworkers,[19] where it was suggested that adsorbed iodobenzene molecules tilt away from surface plane and in this configuration the transient phenyl radical formed upon C-I bond dissociation has sufficient life time - possibly physisorbed in a second layer - to find and couple with another flat lying phenyl group bound directly to the Cu (111) surface. C-C coupling of phenols could be further facilitated by the excess co-adsorbed iodine atoms on the Ag NP surface, because the co-adsorbed iodine atoms on the surface can reduce the reaction barrier of phenolic coupling.[20] This is supported by the observation that the yield of o-p coupling product increased with increased amounts of adsorbed iodine. Further, in the reactions involving naphthols, iodine atoms present on the surface may facilitate the formation of napthoxyl radical, which subsequently leads to coupling with the neighboring moiety, without the formation of a sandwich complex.

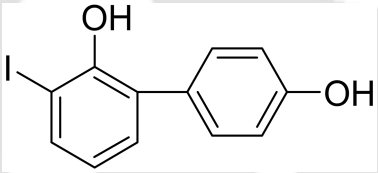
TH-777_05612211

4.1.4 Conclusion

In this chapter we have reported the use of a novel and green method in the formation of selective coupling of phenols and its derivatives using a Chit-Ag NP composite as the catalyst. Iodine atoms present on the surface of Ag NP catalyst played the major role in the formation of selective coupling via p-iodophenol intermediate. Also, the formation of stable sandwich-type geometry between phenoxyl radical and p-iodophenoxyl radical provides the key step in *o-p* coupling with high yield. The present approach is expected to open new vistas in synthetic organic chemistry; especially Ag NP catalyzed C-C coupling reactions beyond the chosen present examples.

4.1.5 Appendix I

6-Iodo-2,4′-bi-1,1′-phenol



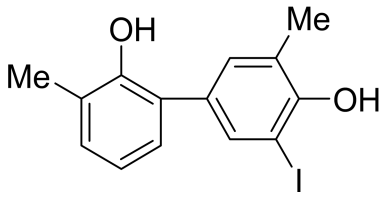
^{1}H NMR (400 MHz, $CDCl_3$): δ 3.91 (bs, 2H), 6.63 (d, *J* = 9.2 Hz, 1H), 6.84 (d, *J* = 8.4 Hz, 2H), 6.94 (t, *J* = 7.6 Hz, 1H), 7.24 (d, *J* = 8.4 Hz, 2H), 7.51 (d, *J* = 8.8 Hz, 1H).

^{13}C NMR (100 MHz, CDCl3): δ 82.77, 115.49 (2C), 118.03, 121.01 (2C), 129.88 (3C), 138.62, 153.2, 155.65.

ESIMS: 311.96.

2,2′-dimethyl-6′-iodo-6,4′-bi-1,1′-phenol

TH-777_05612211



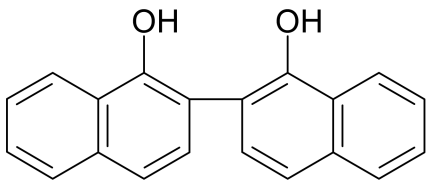
^{1}H NMR (400 MHz, CDCl3): δ 2.25 (s, 3H), 2.30 (s, 3H), 5.29 (bs, 2H), 6.58 (t, *J* = 8.0 Hz, 1H), 7.08 (d, *J* = 7.2 Hz, 1H), 7.38 (s, 1H), 7.48 (d, *J* = 8.0 Hz, 1H), 7.75 (s, 1H).

^{13}C NMR (100 MHz, CDCl3): δ 17.08, 17.38, 82.89, 122.41, 127.54, 131.71 (2C), 135.93, 140.16 (2C), 142.92 (2C), 153.24 (2C).

ESIMS: 343.02.

TH-777_05612211

2,2′-Bi-1,1′-naphthol[21]

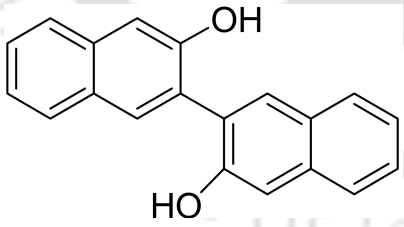


^{1}H NMR (400 MHz, $CDCl_3$) δ: 5.17 (bs, 2H), 6.74 (d, *J* = 7.2 Hz, 2H), 7.21 (t, *J* = 8.0 Hz, 2H), 7.34 (d, *J* = 8.4 Hz, 2H), 7.38 – 7.42 (m, 2H), 7.72- 7.74 (m, 2H), 8.07 – 8.10 (m, 2H).

^{13}C NMR (100 MHz, $CDCl_3$): δ: 108.86, 120.92, 121.68, 124.51, 125.49, 126.02, 126.64, 127.88, 134.94, 151.46.

ESIMS: 287.10.

3,3′-Bi-2,2′-naphthol[22]



^{1}H NMR (400 MHz, $CDCl_3$): δ 4.93 (bs, 2H), 7.11 (d, *J* = 8.8 Hz, 2H), 7.16 (s, 2H), 7.34 (t, *J* = 6.8 Hz, 2H), 7.44 (t, *J* = 6.8 Hz, 2H), 7.69 (t, *J* = 8.0 Hz, 2H), 7.77 (t, *J* = 7.2 Hz, 2H)[21].

TH-777_05612211

^{13}C NMR (100 MHz, $CDCl_3$): δ 109.76, 117.92, 123.87, 126.59, 126.76, 127.97, 129.16, 130.08, 134.76, 153.4.

ESIMS: 288.19.

4.1.6 Appendix II

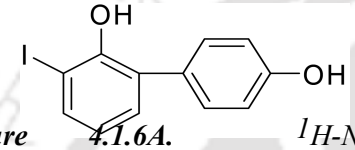
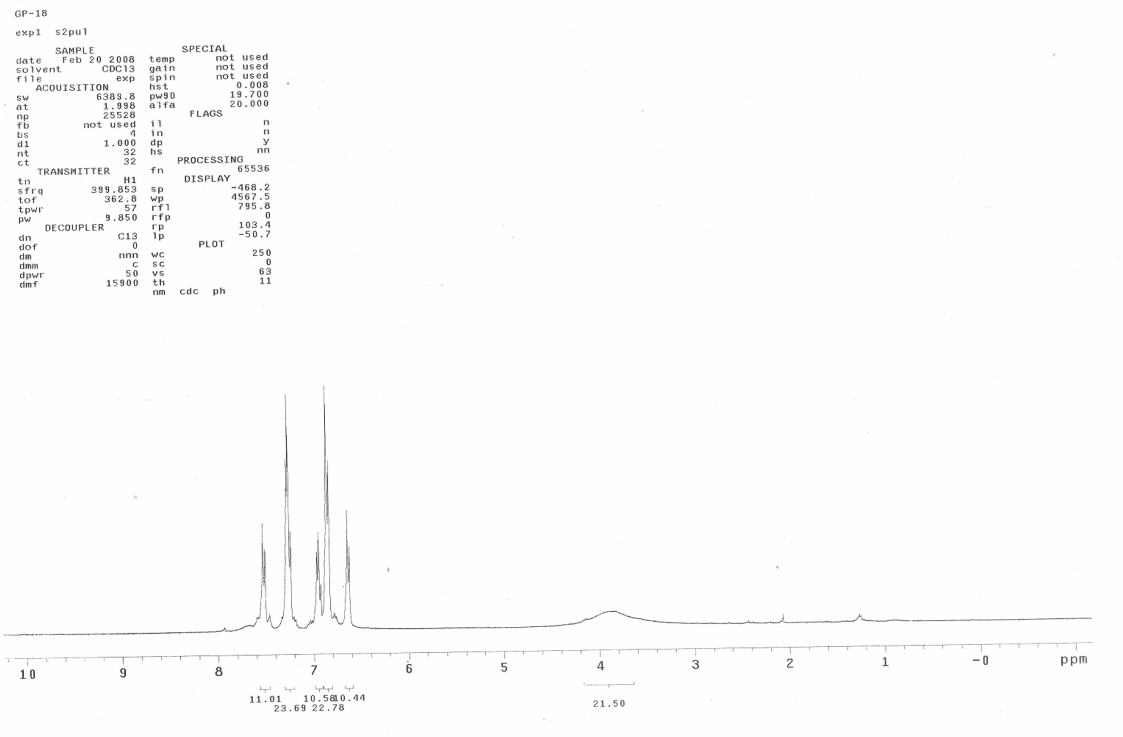
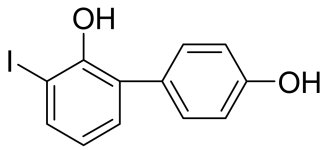


Figure 4.1.6A. *^1H-NMR spectrum of compound*



TH-777_05612211



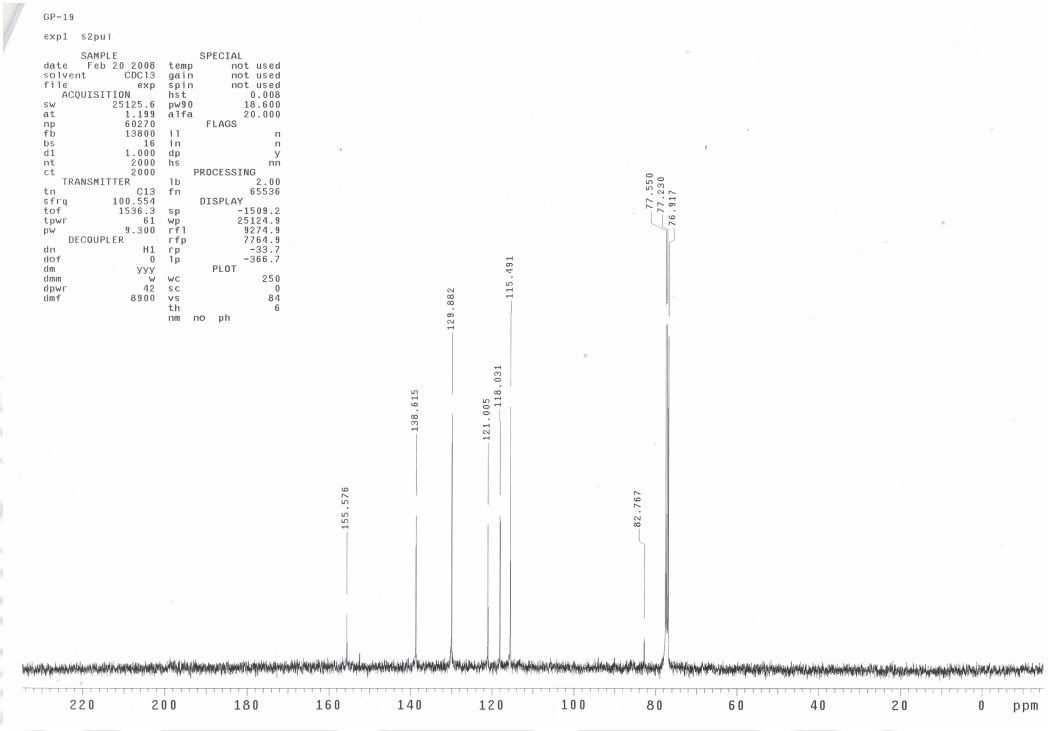
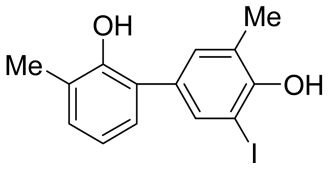


Figure 4.1.6B. *^{13}C-NMR spectrum of compound 6-Iodo-2, 4'-bi-1, 1'-phenol.phenol.*

TH-777_05612211



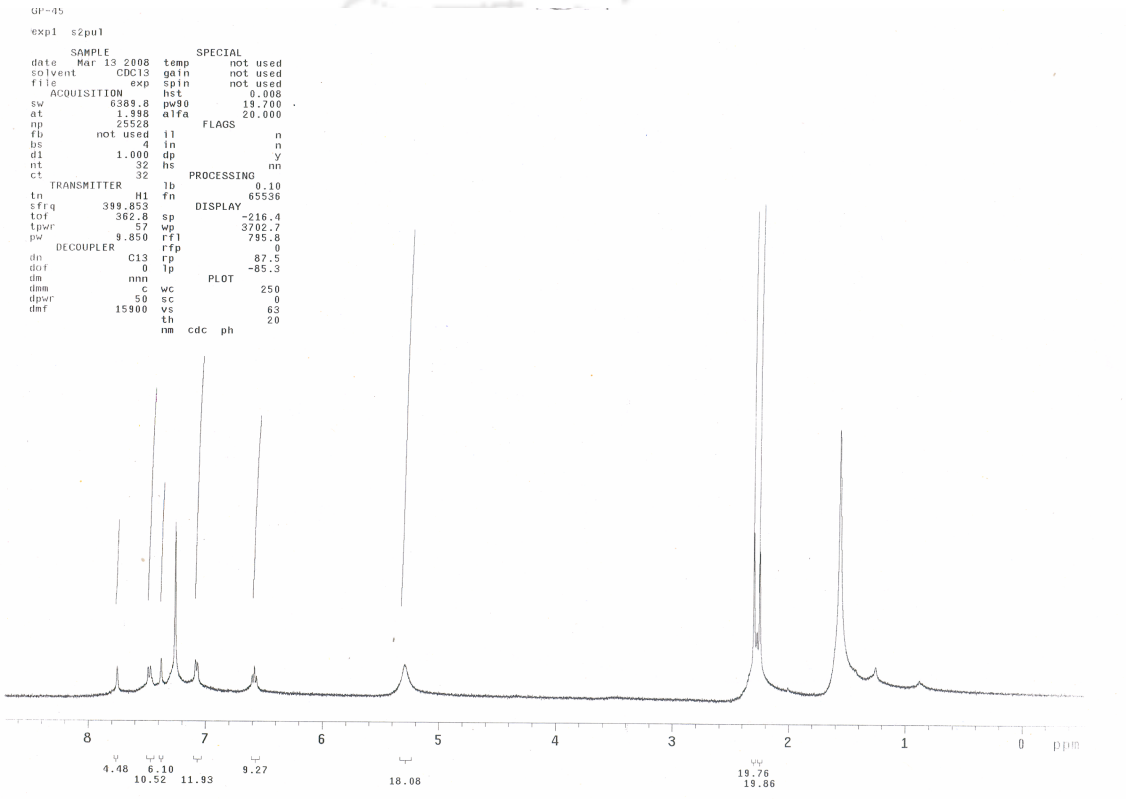
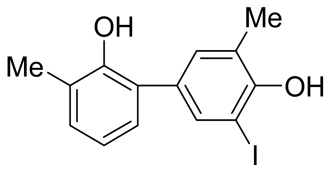


Figure 4.1.6C. *^{1}H-NMR spectrum of compound 2,2'-dimethyl-6'-iodo-6,4'-bi-1,1'-phenol.*

TH-777_05612211



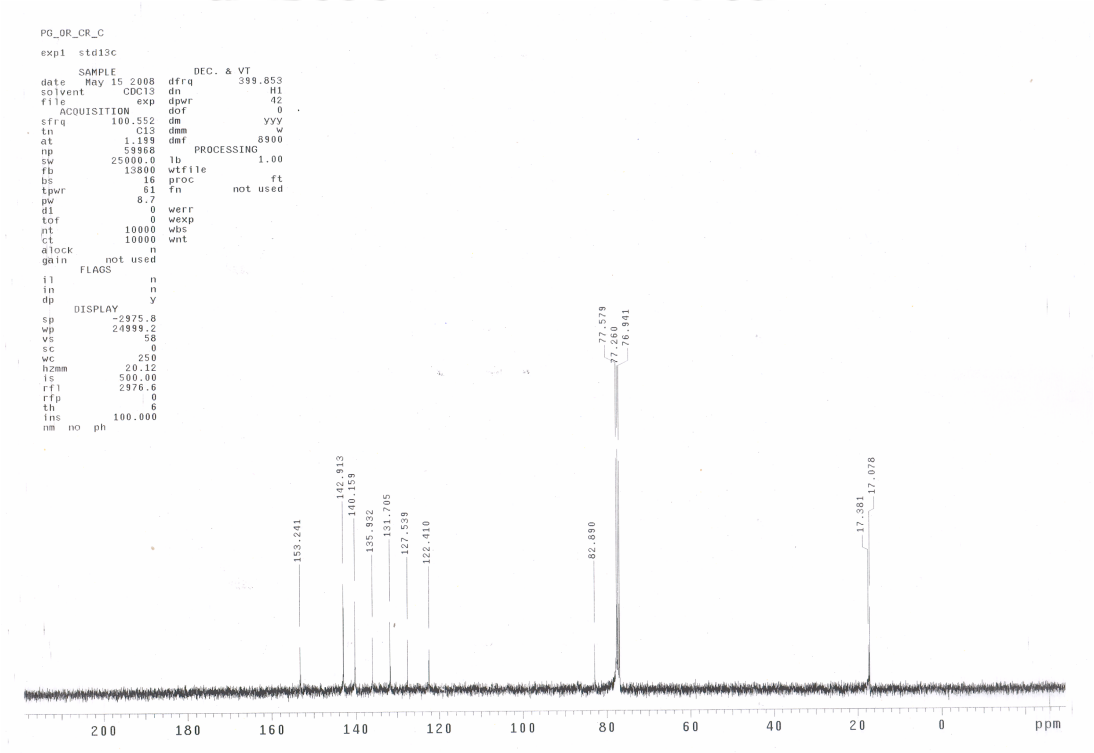


Figure 4.1.6D. *^{13}C-NMR spectrum of compound 2,2'-dimethyl-6'-iodo-6,4'-bi-1,1'-phenol.*

.

TH-777_05612211

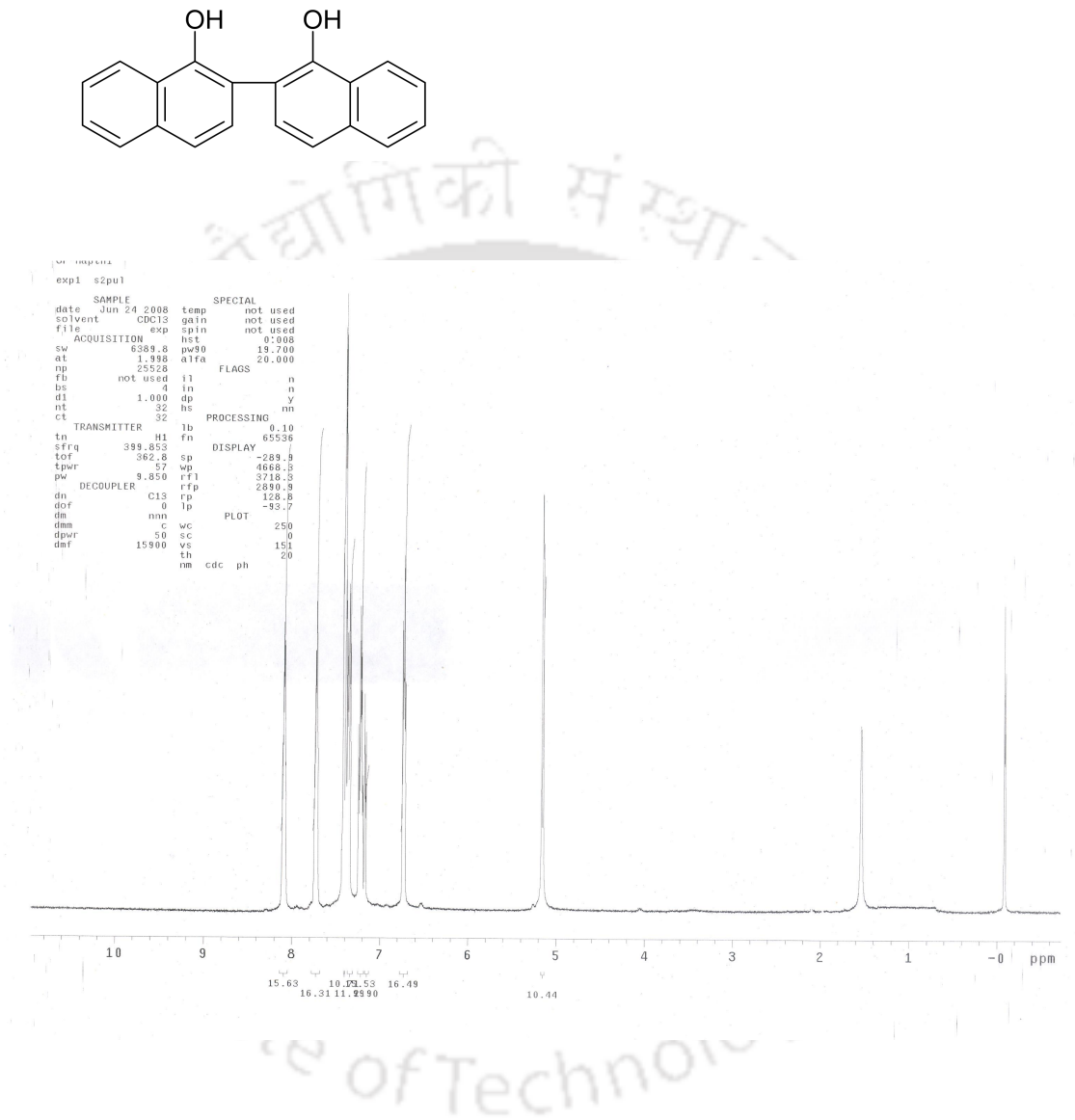


Figure 4.1.6E. *^{1}H-NMR spectrum of compound 2,2'-Bi-1,1'-naphthol.*

TH-777_05612211

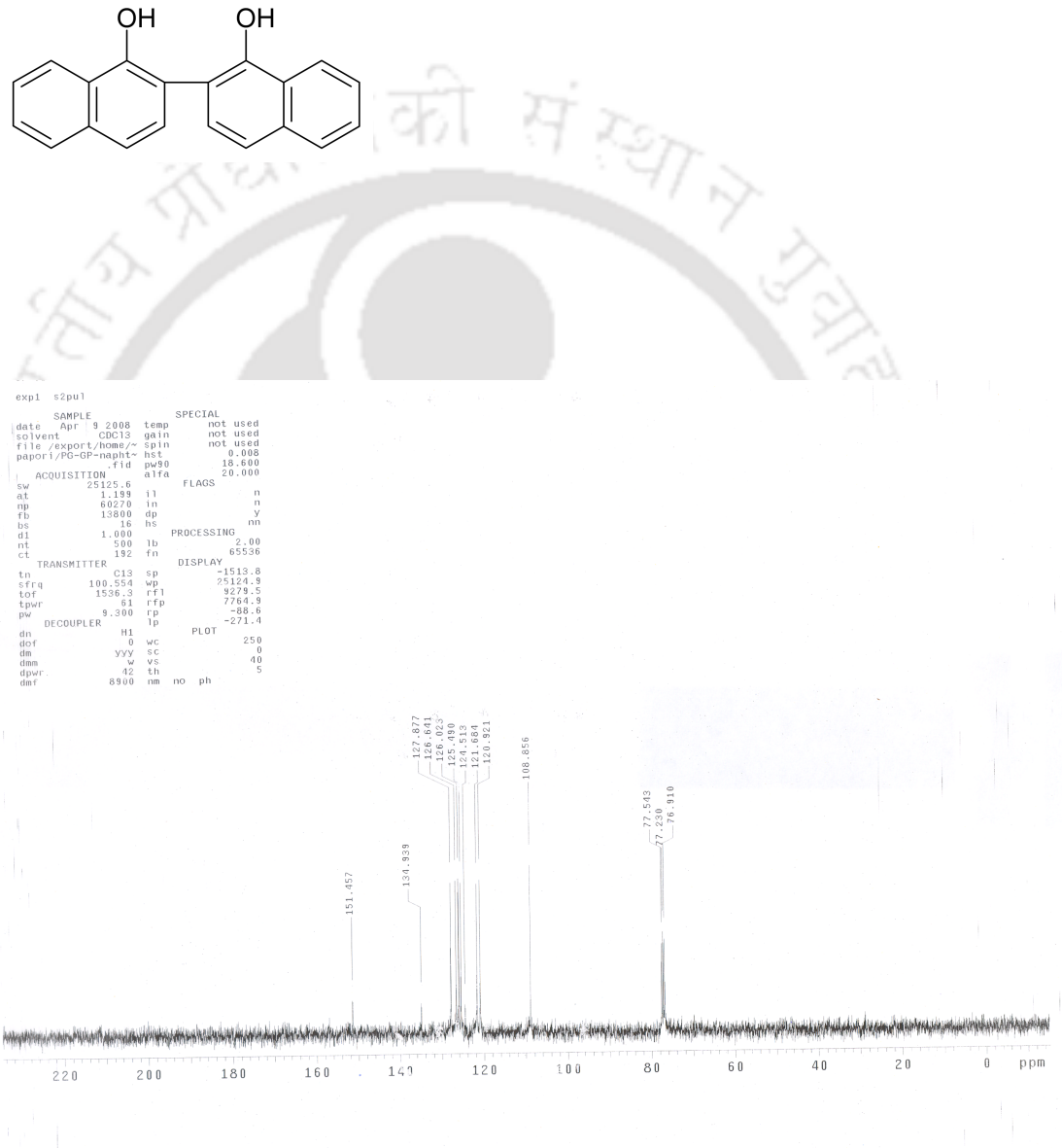


Figure 4.1.6F. *^{13}C-NMR spectrum of compound 2,2'-Bi-1,1'-naphthol.*

TH-777_05612211

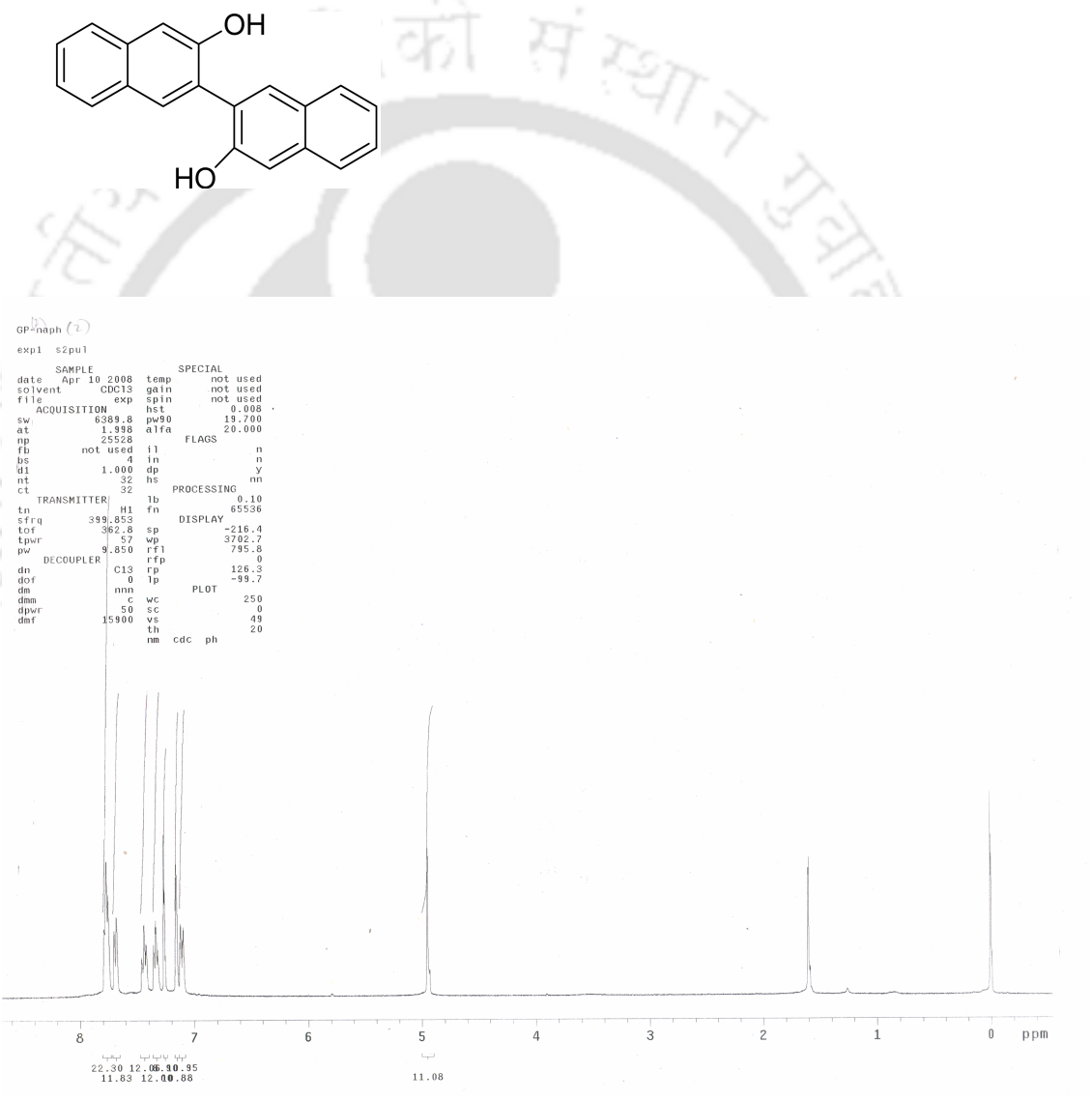
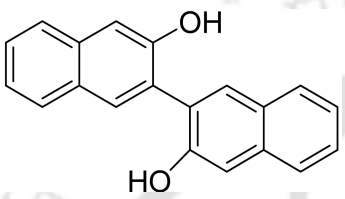
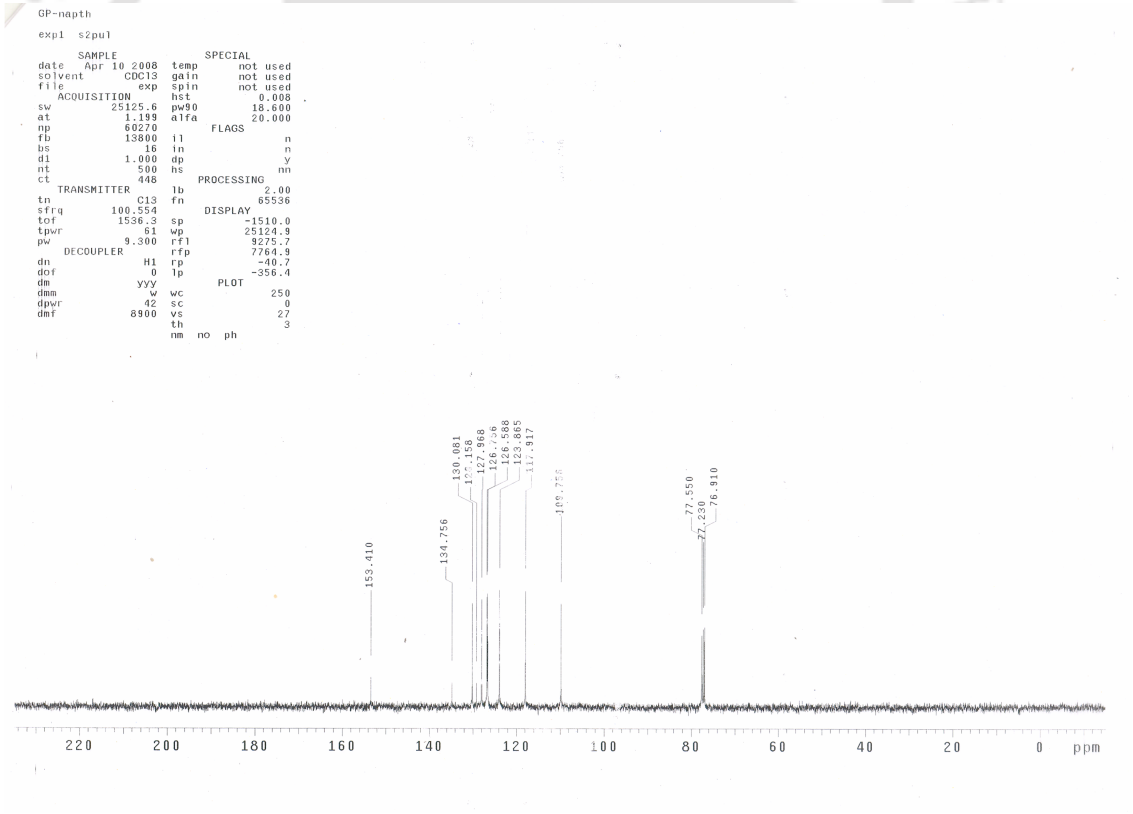


Figure 4.1.6G. *^{1}H-NMR spectrum of compound 3,3'-Bi-2,2'-naphthol.*

TH-777_05612211





TH-777_05612211

Figure 4.1.6H. *^{13}C-NMR spectrum of compound*

4.1.7 References

1. (a) Rudyanto, M.; Tomizawa, Y.; Morita, H.; Honda, T. *Org Lett.* **2008**, *10*, 1921. (b) Drochner, D.; Huttel, W.; Nieger, M.; Muller, M. *Angew. Chem. Int. Ed*. **2003**, *42*, 931. (c) Taylor, W. L.; Battersby, A. R. *Oxidative coupling of phenol*, Marcel Dekker, New York, N. Y. **1967**.

2 (a) Xie, X.; Phuan, P. W.; Kozlowski, M. C. *Angew. Chem. Int. Ed*. **2003**, *42*, 2168. (b) Kobayashi, S.; Higashimura, S. *Prog. Polym. Sci*. **2003**, *28*, 1015. (c) Whiting, D. A. *In Comprehensive Organic Synthesis*, *3*, **659** (Eds.: Trost, B. M.; Fleming, I.; Pattenden, G.), Pergamon. Oxford, **1991**. (d) Nayori, R. *Chem. Soc. Rev*. **1989**, *18*, 187. (e) Narasaka, K. *Synthesis* **1991**, 1. (f) Pu, L. *Chem Rev*. **1998**, *98*, 2405. (g) Brunel, J. M. *Chem. Rev.* **2005**, *105*, 857.

3. (a) Toda, F.; Tanaka, K.; Iwata, S. *J. Org. Chem*. **1989**, *54*, 3007. (b) Ershov, V. V.; Volod Kin, A. A.; Bogdanov, G. N. *Russ. Chem. Rev.* **1963**, *32*, 75. (c) Musso, H. *Angew. Chem.* **1963**, *75*, 965. (d) Balogh, V.; Fetizon, M.; Golfier, M. *J. Org. Chem*. **1971**, *36*, 1339. (e) Carrick, W. L.; Karapinka, G. L.; Kwiatkowski, G. T. *J. Org. Chem*. **1969**, *34*, 2388. (f) De Jong, C. R. H. I.; Van Dort, H. M.; Vollbracht, V. *Tetrahedron Lett*. **1970**, *22*, 1881. (g) Schwartz, M. A.; Holton, R. A. *J. Am. Chem. Soc*. **1970**, *92*, 1090. (h) Schwartz, M. A.; Rose, B. F.; Halton, R. A.; Vishnuvajjala, B. *J. Am. Chem. Soc.* **1977**, *99*, 2571. (i) Tomioka, K.; Koga, K.; Yamada, S. *Chem. Pharm. Bull.* **1977**, *25*, 2681. (j) Hwang, D. R.; Chen, C. P.; Uang, B. J. *Chem Commun,* **1999**, *13*, 1207.

TH-777_05612211

4. (a) Scott, R. W. J.; Wilson, O. M.; Crooks, R. M. *J. Phys. Chem. B* **2005**, *109*, 692. (b) Yeung, L. K.; Crooks, R. M. *Nano Lett.* **2001**, *1*, 14. (c) Zhao, M.; Crooks, R. M. *Angew. Chem. Int. Ed. Engl.* **1999**, *35*, 364.

5. (a) Calo, V.; Nacci, A.; Monopoli, A.; Fornaro, A.; Sabbatini, L.; Cioffi, N.; Ditaranto, N. *Organometallics* **2004**, *23*, 5154. (b) Calo, V.; Nacci, A.; Monopoli, A.; Laera, S.; Cioffi, N. *J. Org. Chem*. **2003**, *68*, 2929. (c) Gronnow, M. J.; Luque, R.; Macquarrie, D. J.; Clark, H. J. *Green Chem.* **2005**, *7*, 552.

6. (a) Astruc, D.; Lu, F.; Aranzaes, J. R. *Angew. Chem. Int. Ed.* **2005**, *44*, 7852. (b) Na, Y.; Park, S.; Ha, S. B.; Ko, S.; Chang, S. *J. Am. Chem. Soc.* **2004**, *126*, 250. (c) Wang, A. Q.; Wang, N.; Chang, C. M.; Mou, C. Y. *J. Phys. Chem. B* **2005**, *109*, 18860. (d) Wang, A. Q. ; Liu, J. H. ; Lin, S. D. ; Lin, T. S.; Mou, C. Y. *J. Catal*. **2005**, *233*, 186. (e) Lu, Y.; Mei, Y.; Drechsler, M.; Ballauff, M. *Angew. Chem. Int. Ed*. **2006**, *45*, 813.

7. (a) Yan, W.; Wang, R.; Xu, Z.; Xu, J.; Lin, L.; Shen, Z.; Zhou, Y. *J. Mol. Cata. A: Chem* **2006**, *255*, 81. (b) Sunoyama, H.; Sakurai, H.; Ichikuni, N.; Negishi, Y.; Tsukuda, T. *Langmuir* **2004** *20*, 11293.

8. (a) Murugadoss, A.; Chattopadhyay, A. *Nanotechnology* **2008**, *19*, 015603. (b) Sanpui, P.; Murugadoss, A.; Durga Prasad, P. V.; Ghosh. S. S.; Chattopadhyay. A. *Int. J. Food. Micro*. **2008**, *124*, 142.

9. (a) Murugadoss, A.; Chattopadhyay, A. *J. Phys. Chem. C* **2008**, *112*, 11265. (b) Lu, Y.; Mei, Y.; Walker, R.: Ballauff, M. *J. Phys. Chem. B* **2006**, *110*, 3930. (c) Panigrahi, S.; Basu, S.; Praharaj, S.; Pande, S.; Jana, S.; Pal, A.; Ghosh, S. K.; Pal, T. *J. Phys. Chem. C* **2007**, *111*, 4596.

10. (a) Narayanan, R.; El-Sayed, M. A. *Langmuir* **2005**, *21*, 2027. (b) Barnard, C. *Platinum Metals Rev*. **2008**, *52*, 38. (c) Yin, L.; Liebscher, J. *Chem Rev.* **2007**, *107*, 133. (d) Na, Y.; Park, S.; Han, S. B.; Han, H.; Ko, S.; Chang, S. *J. Am. Chem. Soc.* **2004**, *126*, 250. (e) Yoon, B.; Wai, C. M. *J. Am. Chem. Soc.* **2005**, *127*, 17174.

11. (a) Yajima, H.; Morita, M.; Hashimoto, M.; Sashiwa, H.; Kikuchi, T.; Ishii, T. *Int. J. Thermophys.* **2001**, *22*, 1261. (b) Shigeno, Y.; Kondo, K.; Takemoto, K. *J.*

TH-777_05612211

Appl. Polym. Sci. **1980**, *25*, 731. (c) Sashiwa, H.; Okamoto, Y.; Minami, S.; Shigemasa, Y. *Chitin and Chitosan. Res*. **1998**, *4*, 18.

12. (a) Temma, T.; Hatano, B.; Habaue, S. *Tetrahedron* **2006**, *62*, 8559. (b) Habaue, S.; Temma, T.; Sugiyama, Y.; Yan, P. *Tetrahedron Lett.* **2007**, *48*, 8595. (c) Habaue, S.; Takahashi, Y.; Temma, T. *Tetrahedron Lett.* **2007**, *48*, 7301.

13. Gao, J.; Reibenspies, J. H.; Martell, A. E. *Angew. Chem. Int. Ed.* **2003**, *42*, 6008.

14. (a) Head, J. D.; Mitchell, K. A. R.; Noodleman, L. *Surface Science* **1976**, *61*, 661. (b) Berry, G. M.; Bothwell, M. E.; Bravo, B. G.; Cali, G. J.; Harries, J. E.; Mebrahtu, T.; Michelhauge, S. L.; Rodriguez, J. F.; Soriaga, M. P. *Langmuir* **1989**, *5*, 707. (c) Paul, A. ; Jenks, C. J. ; Bent, B. E. *Surface Science* **1992**, *261*, 233.

15. (a) Solomon, J. L.; Madix, R. J. *Surface Science* 1991, 255, 12. (b) Lee, J. ; Ryu, S. ; Kim, K. *Surface Science* **2001**, *481*, 163.

16. (a) Sibbald, M. S.; Chumanov, G.; Cotton, T. M. *J. Electrochem. Soc.* **1997**, *438*, 179. (b) Wertheim, G. K.; DiCenzo, S. B.; Buchanan, D. N. E. *Phys. Rev. B* **1982**, *25*, 3020.

17. (a) Armstrong, D. R.; Cameron, C.; Nohebel, D. C.; Perkins, P. G. *J. Chem. Soc. Perkin Trans. II* **1983**, 575. (b) Armstrong, D. R.; Cameron, C.; Nohebel, D. C.; Perkins, P. G. *J. Chem. Soc. Perkin Trans. II* **1983**, 581.

18. Armstrong, D. R.; Breckenridge, R. J.; Cameron, C; Nohebel, D. C.; Pauson, P. L.; Perkins, P. G. *Tetrahedron Lett*. **1983**, *24*, 1071.

19. (a) Xi, M.; Bent, B. E. *Langmuir* **1994**, *10*, 505. (b) Bent, B. E. *Chem. Rev*. **1996**, *96*, 1361.

20. (a) Zhou, X. L.; Schwaner, A. L.; White, J. M. *J. Am. Chem. Soc.* **1993**, *115*, 4309. (b) Jenks, C. J.; Paul, A.; Smoliar, L. A.; Bent, B. E. *J. Phys. Chem*. **1994**, *98*, 572.

21. (a) Lindsten, G.; Wennerstroem, O.; Isaksson, R. *J. Org. Chem.* **1987**, *52*, 547. (b) Poutsma, M. L.; Dyer, C. W. *J. Org. Chem.* **1982,** *47*, 3367

22. Park, C. G. C.; Lee, Y.H.; Park, Y. H.; Kim, N. G.; Sik, Y. *Mol. Crys. Liq. Crystal*. **2006**, *444*, 265.

TH-777_05612211

TH-777_05612211

5.1 Stabilizer Specific Interaction of Gold Nanoparticles with a Thermosensitive Polymer Hydrogel

5.1.1 Introduction

Stimuli responsive materials such as hydrogels are important as delivery vehicles for future nanoscale drugs. The changes in size, shape and solubility in a solvent in response to changes in stimuli such as temperature, pH, ionic or other chemical and biological species make hydrogels ideal for drug delivery and controlled release of bioactive molecules and other drugs[1-3]. Interestingly, the advent of nanoscale materials in therapeutics and medical diagnostics brings about newer challenges in conjugating hydrogels with nanomaterials for targeted delivery[4-6]. In this regard, nanoparticles (NPs) could be chemically bonded to the three-dimensional structure of the gel and thus generated hybrid gel would act as both the delivery vehicle as well as the drug itself. Additionally, chemically or biologically functionalized NPs could be encapsulated to hydrogels that are held by electrostatic or van der Waals forces and the functionalized NPs could thus be released in response to a stimulus. Understanding the functioning of both kinds of hybrids is important for the development of better drugs as well as delivery systems.

Hydrogels are classified as neutral, cationic and anionic. The swelling behavior of the gels in water depends on the polymer backbone and the nature of polar groups attached to the backbone, which make the stimuli responsive properties tunable. Among the thermosensitive polymers that has been extensively studied poly (N-isopropyl acrylamide) (pNIPAm) represents an important member in the family. It has been found that, although, the lower critical solution temperature (LCST) of pNIPAm is at 32^{o}C, the same can be changed up to 60^{o}C by various degrees of copolymerization with acrylic acid (AAc)[7-15]. Furthermore, copolymerization with AAc can also cause the particles in solution to undergo a rapid and discontinuous transition, combined with a large change in volume. In addition to

TH-777_05612211

tunable LCST and large volume change accompanying transition, AAc copolymerized in the backbone of pNIPAm offers a robust architecture with the ability to respond to environmental changes in temperature, pH, ionic strengths and solvents[8-9]. These advantages have consequently contributed to the significant scientific and technological literature related to pNIPAm-AAc copolymers as environmentally sensitive delivery system[16-17].

On the other hand, recent developments in the controlled syntheses of inorganic NPs such as Au NPs and quantum dots (Qdots) bring additional potential for use of the NPs as drugs such as hyperthermia treatment with Au NPs or imaging at the intracellular level using Qdots [18-23]. However, these materials too need appropriate delivery vehicle in order for their controlled release and targeted delivery. In this respect, pNIPAm has been proposed as a stimuli responsive carrier of the NPs[24]. There have been some recent reports on the temperature-dependent study of Au functionalized pNIPAm using the surface plasmon resonance (SPR) of Au NPs[25-28]. However, these studies were limited to chemical attachment of the NPs on the polymer, by suitably modifying the backbone of the polymer. The Au NPs were generated in situ and thus their sizes and shapes were fixed. On the other hand, the versatility of Au NPs can be achieved by utilizing its tunable shapes, sizes and various functional groups that provide additional properties to the NPs. Interestingly, there have been no reports of temperature dependent interactions between functionalized Au NPs and pNIPAm polymer or its derivative. This is important as understanding the interaction between the functionalized NPs and the carrier polymer and its temperature sensitivity may play pivotal roles in drug delivery and chemical sensors of the future[29]. It is important to mention here that in the literature there are significant number of reports on using molecules and ions for the study of their interaction with hydrogels accompanying volume phase transition[30-32].

TH-777_05612211

In this chapter, we report the study of temperature dependent interactions of pNIPAm-AAc with Au NPs, functionalized by different stabilizing agents; using UV-vis spectroscopy, dynamic light scattering (DLS) based particle size analysis and transmission electron microscopy (TEM) as the probes. There were five types of systems that were investigated. The temperature dependent properties of the polymer alone, polymer functionalized Au NPs, tryptophan, thioglycolic acid or phenylalanine capped Au NPs dispersed in the polymer medium were investigated. It was observed that functionalization of the polymer with Au NPs or the presence of functionalized Au NPs affected the LCST of the polymer significantly. In this respect, we observed that more hydrophilic capping agent shifted the LCST to higher temperature. In all cases, the coi1 to globule transition occurred at above the LCST and the final particle sizes for all the systems studied here were nearly identical after the transition. Interestingly, the coil to globule transition accompanied change in the absorption maximum wavelength and also intensity in the cases involving Au NPs capped with either hydrophobic or hydrophilic groups. These results indicate that SPR of the stabilized Au NPs could act as a sensitive indicator for the change in the environment of such systems. Further, the absorption characteristics of the NPs could themselves act as clear indicators of LCST. Essentially, the results demonstrated that functionalized Au NPs could be used not only for probing LCST transitions but also the nature of the environments the polymer is in before and after the transitions. Thus, the present method could provide a fast, inexpensive and accurate approach to study the interaction between the different molecules and polymer gel by using SPR of Au NPs as the indicator.

5.1.2 Experimental Section

Materials

N-isopropyl acrylamide (NIPAm, 97% purchased from Sigma-Aldrich), acrylic acid (AAc, 99% from Sigma-Aldrich), N, N'-methylene-bis-acrylamide (MBA. 99 % from Sigma-Aldrich), potassium perdisulphate (KPS, 98% from Merck), hydrogen tetrachloroaurate ($HAuCl_4$, 17 w/w% Au in HCl from Sigma-Aldrich), L-tryptophan (99%

TH-777_05612211

from Sigma Aldrich), thioglycolic acid (98% from Sigma Aldrich), L-phenylalanine (95% from Merck) and sodium borohydride (95 %, from Merck) were used as received without further purification. Milli-Q grade water was used in all the experiments.

Synthesis of pNIPAm-AAc hydrogel

Typically, 50 mL of aqueous NIPAm (98.7 mg/mL) was taken in a 100 mL three-necked round-bottom flask. To this solution 63.0 μL of acrylic acid (0.126 % V/V) and 300.0 μL (4.9% W/V) of methylene-bis-acrylamide were added under magnetic stirring. These mixtures were kept in an oil bath; and the temperature of the solution was maintained at 70^{o}C under N_2 atmosphere. When the reaction mixtures were turned into homogeneous solution, 50.0 μL (5 % W/V) of potassium perdisulphate was introduced to this solution under the same condition and the reaction was allowed to proceed for 4 h. At the end of the period, the product was centrifuged at 20,000 rpm and washed with copious amount of water to remove the unreacted monomer as well as excess potassium perdisulphate. Finally, this hydrogel was dialyzed overnight using a Hi-Media membrane dialysis bag (12000 cut off). The dialyzed solution was again centrifuged and excess of water was removed, the hydrogel was lyophilized to obtain powdered products for subsequent use.

Synthesis of thioglycolic acid capped Au NPs

In a typical experiment 50 mL aqueous solution containing 15.0 mg of trisodium citrate which was kept in ice-water bath under constant magnetic stirring. To this solution 600.0 μL of 17.262 mM $HAuCl_4$ solution was added. This was followed by addition of 1.2 mL of 20.0 mM freshly prepared sodium borohydride ($NaBH_4$) solution. The resultant solution was dark red in color, indicating formation of Au NPs. This solution was kept under the same condition for 2 h.

In a 5 mL beaker containing 14mM of sodium hydroxide solution, 120.0 μL of thioglycolic acid was added. The solution was then slowly poured into citric acid capped Au

TH-777_05612211

NP solution prepared as above. The mixture was then stirred for 1h after which purple colored precipitation appeared. The precipitate along with the solution was subjected to centrifugation (1000 rpm at 4^{o}C). The pellet was washed with copious amount of ethanol to remove the excess of citrate ions, redispersed in 5 mL water and was used as the stock solution for further characterization studies.

Tryptophan and phenylalanine capped Au NPs

100 mL aqueous solution containing 0.1 mM of $HAuCl_4$ was mixed with 0.01g of solid $NaBH_4$. The mixture was kept under constant magnetic stirring for 2 hrs at room temperature. The color of the solution was ruby red, indicating the formation of Au NPs. This was followed by addition of 10 mL aqueous solution containing 1.0 mM of L-tryptophan to 90 mL of the above Au NP solution. The mixture was stirred for 2 hrs, after which the solution color turned red indicating possible formation of tryptophan capped Au NPs. Finally, the solution was subjected to ultra-speed centrifugation (70000 rpm/15^{o}C), and the resulting pellet was washed with copious of water to remove the excess of uncoordinated tryptophan. The pellet was redispersed in 5 mL water; the resulting solution was stable for weeks. In the preparation of phenylalanine capped Au NPs, the same procedure was followed, taking 10 mL of 9.7 mM of L-phenylalanine solution instead of tryptophan solution, which was added into 90 mL ruby red Au NP solution. All other conditions were the same as above.

Synthesis of pNIPAm-AAc stabilized Au NPs composite

300 μL of 17.3 mM $HAuCl_4$ solution was added to 50 mL of 0.04 % (W/V) polymer hydrogel solution. To this solution 600 μL of 20 mM $NaBH_4$ solution was added. This mixture was then stirred for 3 h at room temperature. The solution was then centrifuged at a high speed (20000 rpm/37^{o}C) and lyophilized to obtain powdered of composite Au NPs-hydrogel products. Finally, 10 mg of composite Au NPs-hydrogel powder was

TH-777_05612211

dissolved in 50 mL water and subsequent solution was used for further characterization studies.

Preparation of different stabilizing agent capped Au NP-hydrogel composite

Typically, in a 100 mL beaker containing 50 mL of 0.02 % polymer hydrogel solution, 2 mL of a particular stabilizing agent capped Au NP solution as prepared above was added. The resulting solution was stirred for 2 hrs which was used for further experiments. Finally, the pH of all the solutions was measured. The pH of the polymer hydrogel solution was measured to be 5.60; bare Au NP hydrogel composite solution to be 5.40, tryptophan-capped Au NP composite solution to be 5.22, thioglycolic acid-capped Au NP composite solution to be 4.69 and that for phenylalanine capped Au NP composite hydrogel solution was measured to be 5.27.

Analytical Measurements

UV-vis spectra of the polymer hydrogel, composites of polymer-Au NPs hydrogel and different stabilizing agent capped Au NPs with polymer hydrogel samples were recorded in the range of 250 to 800 nm, using a Perkin-Elmer Lambda-45 spectrophotometer with temperature controlled sample compartment. The phase transition for polymer hydrogel, composites of polymer-Au NPs hydrogel and different stabilizing agent capped Au NPs with polymer hydrogel were examined in the temperature range of 20 to 45^{o}C with a heating rate of 0.1^{o}C/min. FT-IR spectra of the samples were recorded using a Perkin-Elmer Spectrum one spectrometer. The different stabilizing agent capped Au NPs were dried as a powder and mixed with KBr, the resulting mixtures was turned into a pellet for FTIR measurements. The ^{1}H-NMR spectra of the polymer hydrogel in DMSO$_{-d6}$ (20 mg/mL) at 20^{o}C were recorded using a Varian 400 MHz spectrometer, with TMS as the internal reference. The molar mass and polydispersity of the polymer hydrogel were determined with a Waters gel permeation chromatogram (GPC) using a Waters 2410 refractive index detector. The HPLC grade of tetrahydrofuran was used as an eluent and calibrations were carried out with polystyrene

TH-777_05612211

standard. The dynamic light scattering (DLS) measurements of the polymer hydrogel, composites of polymer-Au NPs hydrogel and different stabilizing agent capped Au NPs with polymer hydrogel samples were performed with an LB-550 (HORIBA) DLS measurement system. The volume phase transition of the above liquid samples was examined with increasing temperature at heating rate of 0.1^{o}C/min. Transmission electron microscopy (TEM) of the particles, were performed using a JEOL-2100 equipment operating at an acceleration voltage of 200 kV. The TEM samples were prepared by placing a drop of liquid sample on carbon coated copper grid (300 mesh) followed by evaporation of the solvent at room temperature. The grid was then observed under the TEM.

5.1.3 Results and Discussion

pNIPAm-AAc and pNIPAm-AAc Au NP composite

It is well-known that pNIPAm, a thermosensitive polymer, undergoes a coli-to-globule transition in aqueous solution at a lower critical solution temperature (LCST) of *ca* 32^{o}C. The co-polymerization of pNIPAm with different monomers is one of the common means to alter the phase transition temperature. The nature of the co-monomer, specifically its hydrophilicity or hydrophobicity generally drives the direction of temperature shift of LCST. The choice of AAc monomer for co-polymerization stems from its easy solubility in water, bioadhesivenesss and biocompatibility[33-36]. The synthesis of pNIPAm-AAc was achieved from the free radical precipitation polymerization reaction[37]. The copolymerization of pNIPAm with AAc has been confirmed by ^{1}H–NMR using DMSO as the solvent (Figure 5.1.1).

TH-777_05612211

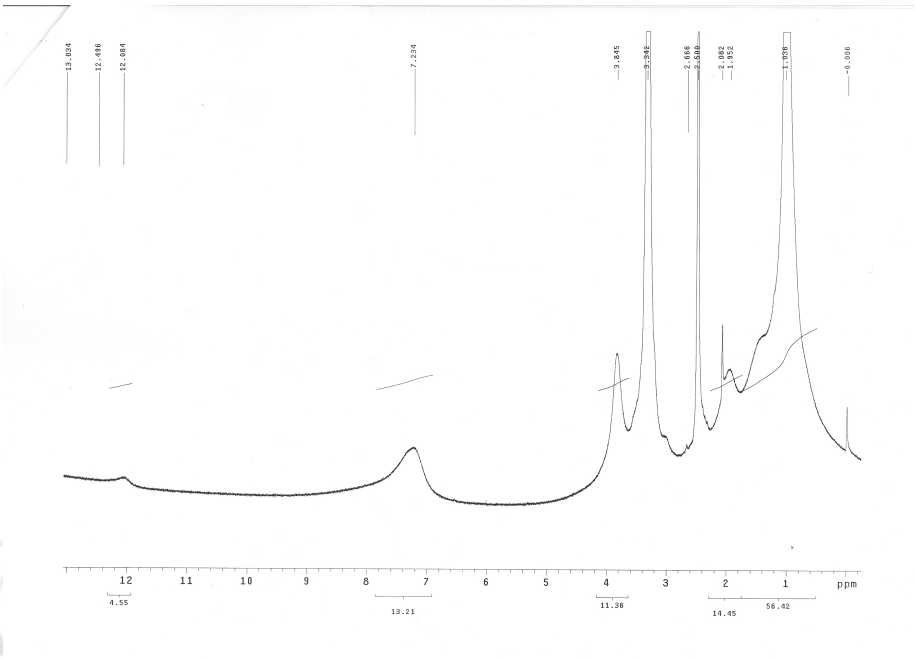


Figure 5.1.1. *^{1}H NMR spectrum of the hydrogel (at 20 mg/mL) in DMSO-$_{d6}$ solution at 25 ^{o}C.*

Figure 5.1.1 shows ^{1}H-NMR spectrum of pNIPAm-AAc. The peak at 12.04 ppm is attributed to the carboxylic acid (-COOH) proton of the acrylic acid group. The resonance for the amine proton of the amide group of the (-CO-NH) is observed at 7.234 ppm. The peak at 3.84 ppm is ascribed to the protons of the methenyl in isopropyl group. The peak at 1.92-2.66 ppm is due to the polymer backbone of the (-CH_2-CH-) protons and the peak at 1.032 ppm is the methyl proton of the N-isopropyl group. The existence of the –COOH proton in the spectrum confirmed that acrylic acid was successfully copolymerized with N-isopropyl acrylamide. The molecular weight of the polymer and their polydispersity index (PI) were measured by gel permeation chromatography.

Table 5.1A. *Molar mass of the PANIPAm-AAc hydrogel and their polydispersity obtained from*

No of Sample	Sample Name	M_n	M_w	MP	M_Z	M_{Z+1}	Polydispersity

TH-777_05612211

1	pNIPAm-AAc	5553	5553	5553	5554	5554	1.0000

The ratio of weight averaged and number averaged molecular weight was close to unity (Table 5.1A), meaning that molecular size distributions in the hydrogel were narrow. Analytical and other studies were pursued by dissolving pNIPAm-AAc as well as pNIPAm-AAc stabilized Au NPs in water at fixed compositions.

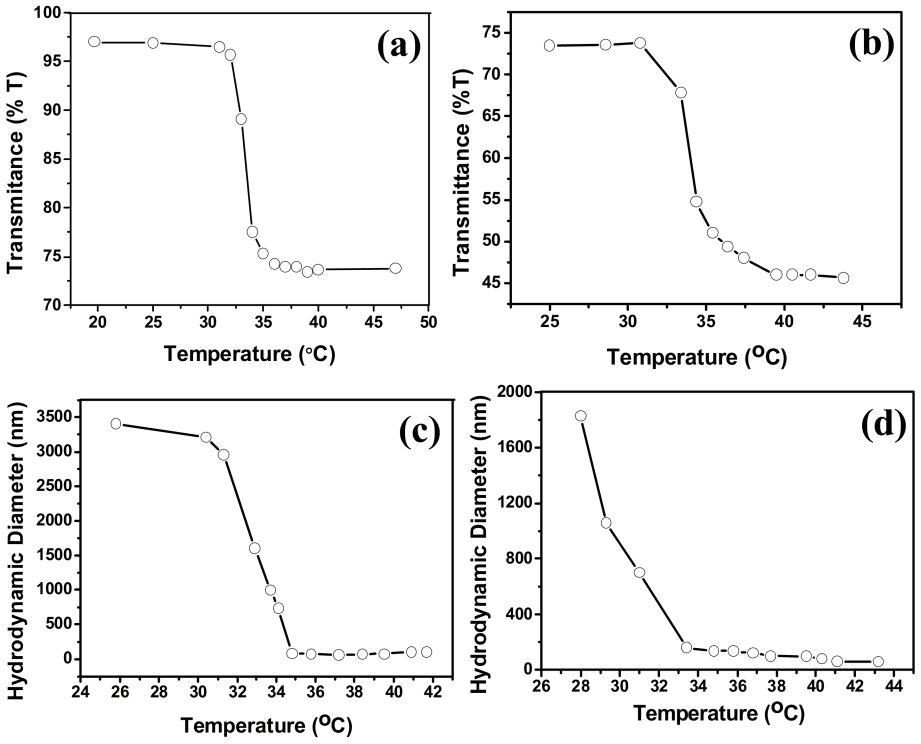


Figure 5.1.2. *(a) Optical transmittance of the pNIPAm-AAc and (b) pNIPAm-AAc stabilized Au NPs at different temperatures. Plots in (c) and (d) are dynamic light scattering based particle size analysis results of pNIPAm-AAc and pNIPAm-AAc stabilized Au NPs hydrogel at various*

TH-777_05612211

The polymer only solution was colorless and transparent at room temperature (below 30^{o}C), while the solution consisting of NP-polymer composite assumed characteristic color of Au NPs owing to their SPR absorption. The solutions became progressively opaque with increasing temperatures. Temperature dependent optical transmission of the polymer and the composite measured at the wavelength of 450 nm[38] (Figures 1a and 1b) did not vary till about 30^{o}C. However, a sharp decrease in transmittance could be observed between 32-35^{o}C and the transmission was constant beyond 35^{o}C in both the samples. The sharp decrease in transmission is associated with phase transition of the hydrogels i.e. transparent coil to opaque globule transition. Importantly, the phase transition temperature of pNIPAm-AA stabilized Au NPs (32.5^{o}C) is slightly lower than that of pNIPAm-AAc (34.3^{o}C). Also, the phase transition of the composite is not as sharp as that of the polymer alone. The interactions between the COOH groups of the polymer with Au NPs might lead to collapse of the structure at a lower temperature than that of the polymer. The temperature dependent particle size measurements of the two species indicated that the collapse of the diameters of the composite started at temperature lower than that of the polymer. Also, the reduction in diameter of the composite occurred at a slower rate than the polymer alone. The results of the particle size analysis by DLS measurements, of the pNIPAm-AAc as well as pANIPAm-AAc stabilized Au NPs, at different temperatures are shown in Figures 5.1.2 (c) and 5.1.2 (d) respectively. Interestingly, at room temperature the hydrodynamic diameter of pNIPAm-AAc polymer was measured to be 3.0 $\pm$ 0.7 μm (at 28^{o}C), while that pNIPAm-AAc stabilized Au NPs was found to be 1.8 $\pm$ 0.1 μm (at 28^{o}C). The decrease of the hydrodynamic diameter of the polymer stabilized Au NPs compared to that of the polymer could be due to the reduction of the electrostatic repulsion among the free –COO^{-} moieties[39] in the polymer hydrogel in the presence of Au NPs. The slow and early change in volume phase transition of the composite in comparison to the polymer is consistent with the results of optical transmission studies. The results of the DLS studies also indicate that Au NPs connected to the polymer lead to change in collapsing behavior of the polymer and also

TH-777_05612211

hastening the volume phase transition in the composite. It is plausible that the electrostatic interaction between the carboxylate moieties of the polymer and Au NPs lead to a structure that favors coil to globule transition at a temperature lower than that of the polymer. UV-vis spectra of the pNIPAm-AAc stabilized Au NPs at different temperatures, shown in Figure 5.1.3 consist of a single peak with absorption maximum at *ca* 530 nm. As is clear from the figure λ_{max} did not vary with temperature. At above the transition temperature the intensity of the absorption (after due consideration of the change in background) decreased slightly, which is possibly due to change in the immediate environment (and hence refractive index of the medium) [40] of the Au NPs upon collapse of the original structure. However, there was no shift in the absorption, which probably indicates that, the interaction between the carboxylate moieties and Au NPs did not change significantly upon transition to globule form.

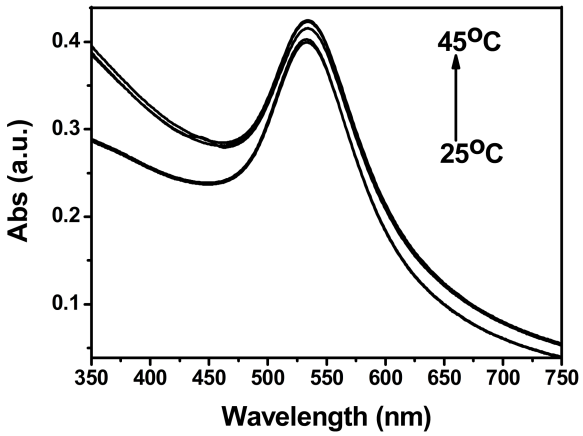


Figure 5.1.3*. The UV-visible absorption spectra of pNIPAm-AAc stabilized Au NPs at different temperatures.*

It is also interesting to note that upon increase in temperature and resulting volume phase transition of the composite there was no agglomeration of the NPs, as is clear from the UV-Visible spectra. This implies that the interaction between Au NPs and the carboxylate

TH-777_05612211

moieties of the polymer is sufficiently strong so as to prevent agglomeration due to increase in temperature, by strongly binding with COOH group of the AAc moieties that might prevent aggregation of Au NPs with increasing temperature. It is important to mention here that the temperature dependent optical as well as hydrodynamic behavior of the composite is completely reversible, indicating that the composite could represent a good model for the study of the behavior of Au NPs in thermosensitive hydrogels.

TH-777_05612211

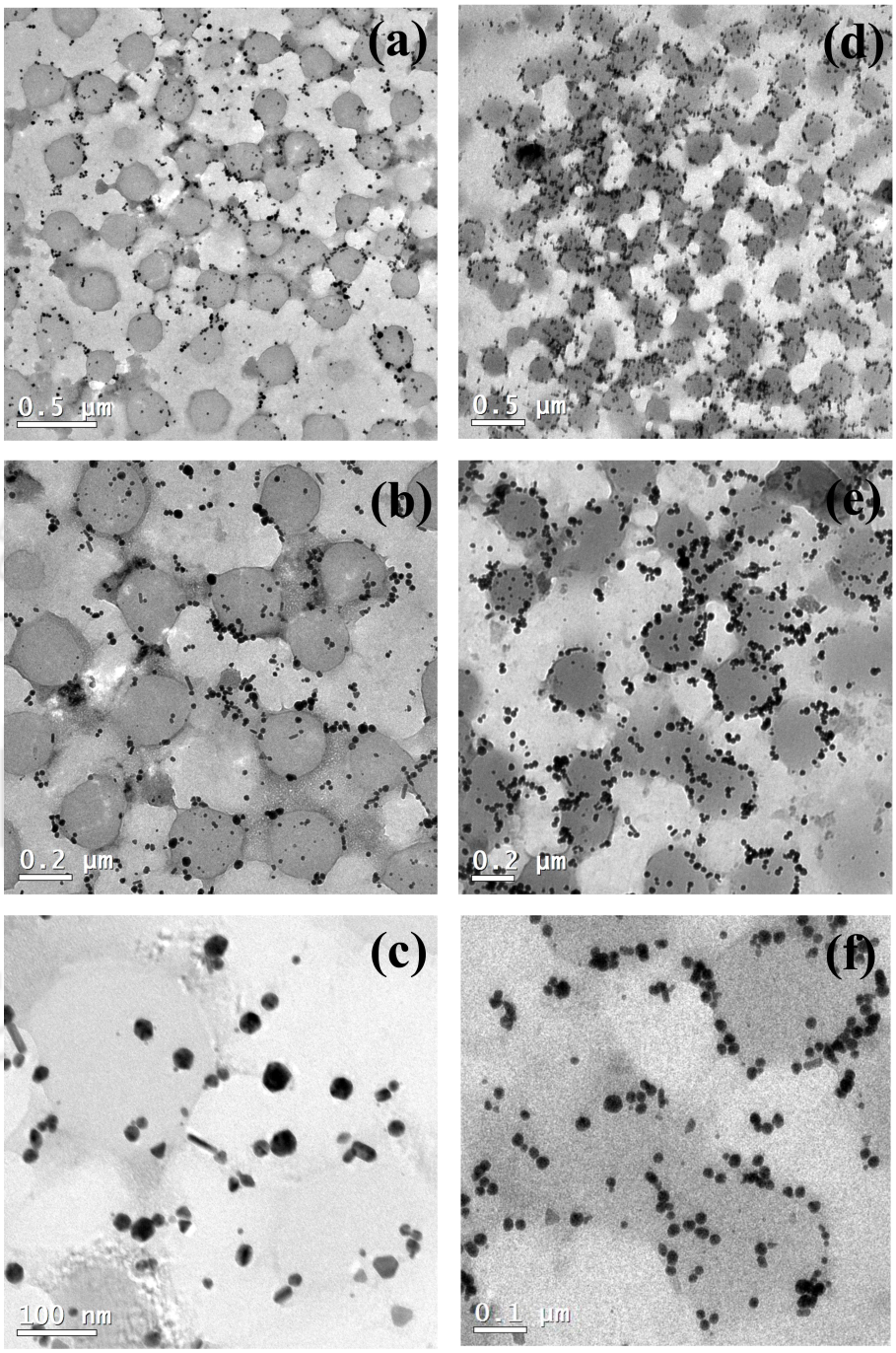


Figure 5.1.4*. The transmission electron microscopy (TEM) images of pNIPAm-AAc stabilized Au NPs at 25ºC (a); while (b) and (c) are the expanded views of (a). The plot in (d) is TEM picture of*

TH-777_05612211

Further, in order to understand the effect of swelling and de-swelling of the polymer hydrogel on the structural aspects of Au NPs, TEM measurements the polymer stabilized Au NPs were carried out. In this regard, two samples were prepared – one from a solution that was evaporated at below the phase transition temperature (at 24.3^{o}C), while the other sample was prepared by evaporation at above the phase transition temperature (at 40^{o}C). Figures 5.1.4 (a), 5.1.4 (b) and 5.1.4 (c) show different views of the TEM images of the polymer stabilized Au NPs with the sample prepared at below the LCST. As could be seen in the figures, the composite consisted of blobs of particles of about 200 nm in diameters interconnected with each other. The Au NPs (darker spots) were of 10-20 nm in sizes and were separated well from each other in the composite. The particles present in between the blobs evidenced the presence of polymer in the intervening region too. Overall, small and individual NPs connected to the polymer were present in the composite. On the other hand, the sample prepared at above the LCST also consisted of individual NPs without the presence of any significant agglomeration (Figures 5.1.4 (d), 5.1.4 (e) and 5.1.4 (f)). However, the density of the particles (Au NPs) appears to be higher in comparison to the sample prepared at below LCST. This is because at above the phase transition temperature the diameters of the polymer particles and thereby volumes were significantly reduced. This increased the apparent density of the particles. The overall structure of the polymer seems to be similar, with a slight decrease in the diameter of the blobs at higher temperature. The increases in density of the NPs on the blobs of the composite at higher temperature supports that the structure indeed collapsed into more compact globule form at the higher temperature.

As discussed before, the pNIPAm-AAc undergoes volume phase transition with a lower critical solution temperature (LCST) of 34.3^{o}C. Also, the temperature of the transition could be influenced by the presence of Au NPs as demonstrated in the preceding section. Further probe of the effect of additional agents on the volume phase transition was pursued using thioglycolic acid; tryptophan or phenylalanine stabilized Au NPs. Thioglycolic acid capped Au NPs were generated from citrate stabilized Au NPs using the ligand exchange

TH-777_05612211

method. The typical sizes of the Au NPs generated were 5.0 ±1.7 nm. The interaction of the –SH group of the thioglycolic acid with Au NPs resulted in the loss of a peak due to –SH stretching frequency at 2541cm^{-1}, which was confirmed by FTIR spectroscopy[41] (Figure 5.1.5). The acid functionalized Au NPs were then mixed with pNIPAm-AAc in aqueous solution. The composite of thioglycolic acid capped Au NPs and pNIPAm-AAc shall henceforth be referred to as pPA-thio-Au for simplicity.

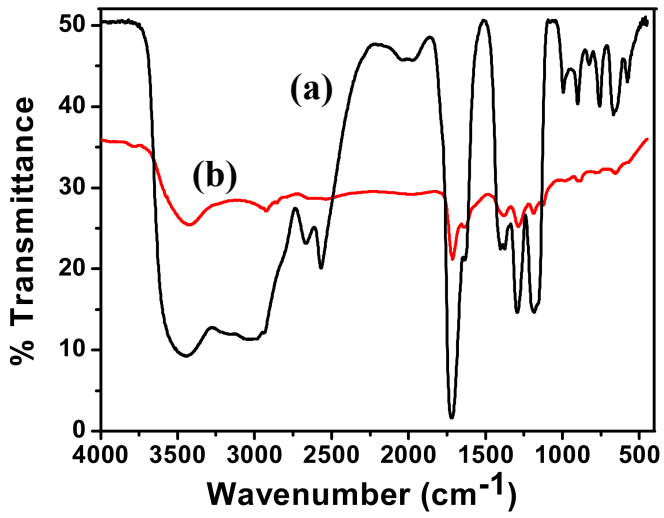


Figure 5.1.5*. (a) FTIR spectrum of thioglycolic acid only (black line) and (b) thioglycolic acid capped gold nanoparticles (red line).*

The temperature dependent UV-Vis spectra of pPA-thio-Au are shown in Figure 5.1.6 (a). The characteristic SPR band of Au NPs is present in all the spectra (at all temperatures recorded). As is clear from the spectra, the spectral characteristics changed little from 25^{o}C to *ca* 34^{o}C. Also, the absorption due to the NPs did not change in this temperature range. However, the background scattering increased significantly at above this temperature (LCST), indicating phase transition to have taken place. Interestingly, the absorption due to Au NPs alone (obtained after appropriate background correction) also changed significantly at above the LCST. The normalized absorption values were obtained as follows. The

TH-777_05612211

absorption values at 350 nm for all temperatures were first measured. That value was made to be unity for all temperatures and all other values were adjusted by dividing them with the value of absorption at 350 nm for a particular temperature. The absorption at the maximum wavelength was then taken as the absorption. Sample normalized absorption versus wavelength plots are shown in Figure 5.1.5A (a). (Refer Appendix-I,). This method of normalization is based on the works of Tenhu and coworkers.[56] A plot of normalized Au NP absorbance at 529 nm (Figure 5.1.6 (b)) indicated significant decrease in absorbance due to Au NPs at above the LCST. The value of absorbance (at λ_{max}) levels off slowly at above LCST. Also, interesting to note is the blue shift in absorption maximum (λ_{max}) with as much as 6 nm change with temperatures (Figure 5.1.6 (c)).

TH-777_05612211

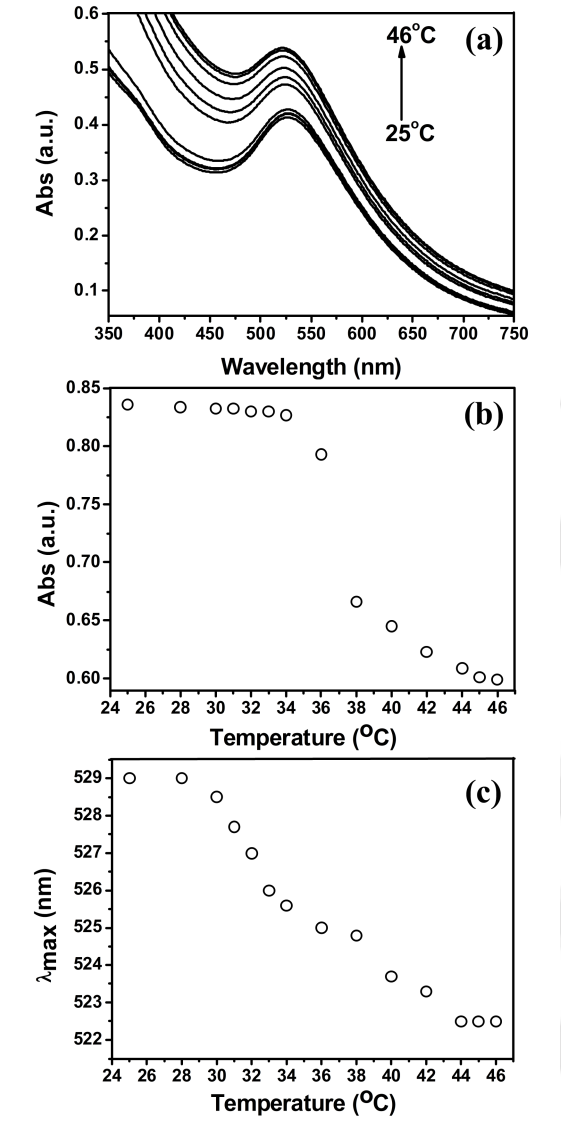


Figure 5.1.6. *(a) UV-visible spectra of pPA-thio-Au NPs with increasing temperature. (b) The plot of normalized maximum absorbance of the SPR band at different temperatures; while (c) is the temperature dependence absorption maxima (wavelength) of SPR band of Au NPs in pPA-thio-Au NPs.*

TH-777_05612211

For example, the absorption maximum was 529 nm at 25^{o}C, while at 36^{o}C the absorbance maximum shifted to 525 nm. The blue shift of absorption maximum could be ascribed to the changing dielectric constant of the medium surrounding the capped Au NPs[42-44]. In other words, when thioglycolic acid capped Au NPs were mixed with pNIPAm-AAc in aqueous solution there can be several types of interaction between the polymer and thioglycolic acid capped Au NPs.

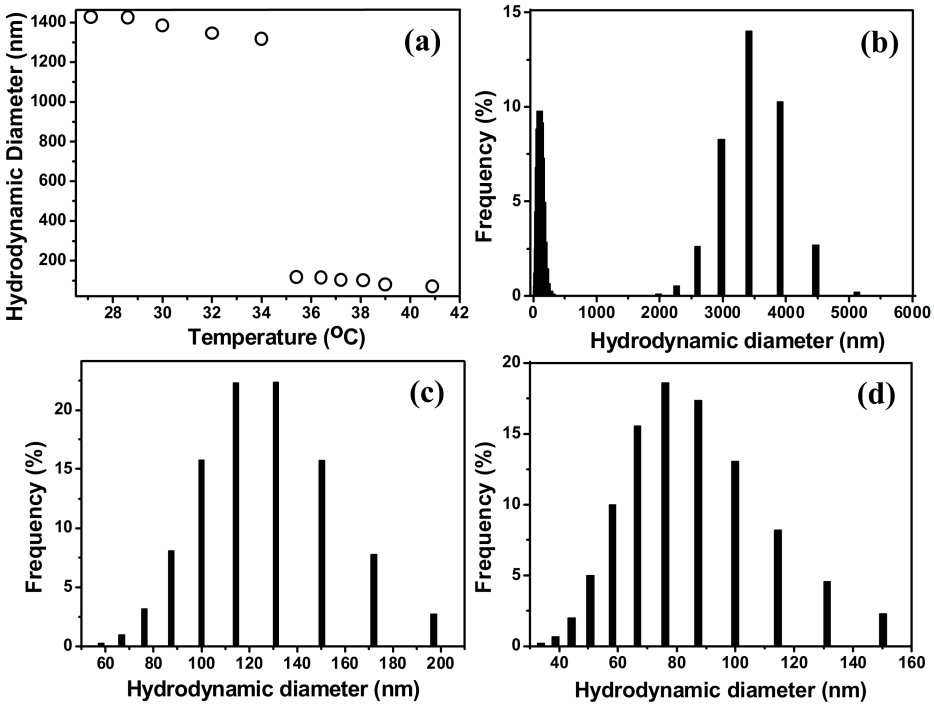
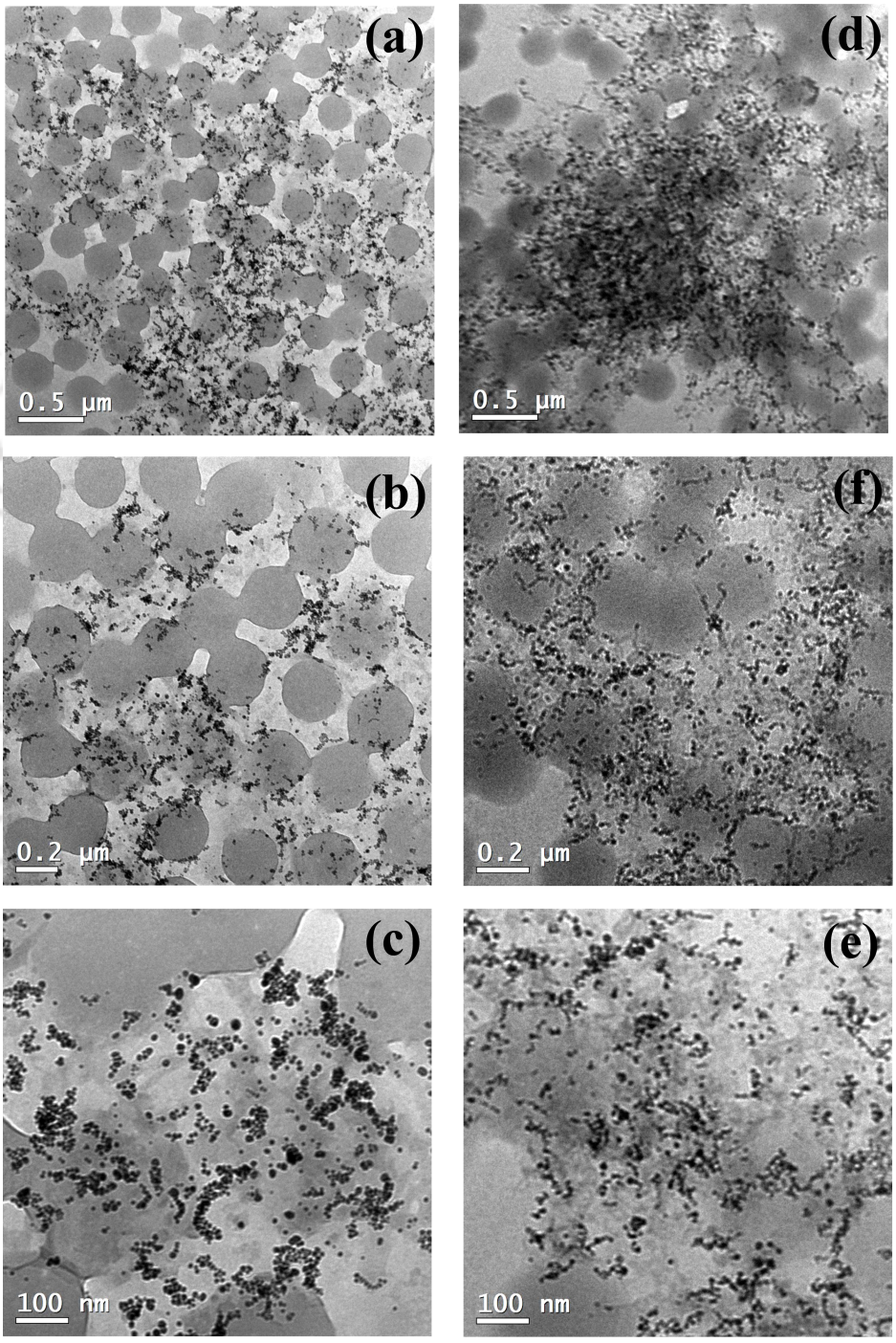


Figure 5.1.7*. (a) Temperature-dependent hydrodynamic diameters of the PPA-thio-Au NPs as measured by dynamic light scattering technique. (b) the histogram of hydrodynamic diameters of pPA-thio-Au NPs at 27oC, (c) 35.6^{o}C and (d) 39^{o}C obtained by dynamic light scattering*

This interaction might be either van der Waals or hydrogen bonding interaction (inter or intra molecular H-bonding). The polymer itself could form H-bonding among its own -COOH groups as well as with water molecules. Similarly, the -COOH groups of the

TH-777_05612211

thioglycolic acid could form H-bonds with water as well as with the polymer at below LCST.



TH-777_05612211

***Figure 5.1.8**. (a) TEM image of pPA-thio-Au NPs at 25^{o}C; while (b) and (c) are the expanded views of the picture from (a). The image in (d) is the TEM picture of the same at 40^{o}C; while (e)*

At above the LCST the polymer could possibly shrink to a form where water molecules are expelled from the network and when thioglycolic acid stabilized Au NPs are part of the polymer structures then hydrogen bonding would primarily be between the –COOH groups of the stabilizer and those (along with amide groups or –COOH group of AAc moieties) of the polymer. Thus a change in the environment might well be reflected in the observed change in the absorption characteristic of the Au NPs at above LCST. The shift in the UV-vis absorption of Au NPs indicated that the phase transition temperature here was 36^{o}C, which is different from pure polymer. The observation implies that SPR absorption of Au NPs could act as good probes for measuring the phase transition temperature of thermosensitive polymers.

Further, to understand better the volume phase transition of the pPA-thio-Au NPs, DLS measurements of the composite hydrogel were carried out at different temperature. The results are shown in Figure 5.1.7. At temperatures below LCST there were two types of particles sizes – one corresponding to the polymer with a value of 1.4 $\pm$ 0.5 μm, while the other one possibly was due to thioglycolic acid stabilized Au NPs with particles sizes of 116 $\pm$ 26 nm when measured at 27^{o}C. Thus the average particle sizes mentioned in the figures are the averages of the values, automatically reported by the software used in measuring the particle sizes. On other hand at 35.6^{o}C the sizes were reduced down to 116 $\pm$ 26 nm. The gradual change in the particle sizes at above the LCST indicates gradual deswelling of the composite in comparison to the polymer alone.

The above results suggest that at temperatures below LCST thioglycolic acid stabilized Au NPs and pNIPAm-AAc hydrogel remain as individual species in aqueous medium, where intermolecular H-bonding is predominant. When the temperature of the

TH-777_05612211

medium is increased, the intramolecular H-bonding in polymer and intermolecular H-bonding between the polymer and thioglycolic acid stabilized Au NPs are favored. At above the LCST these H-bonding provide the driving force for the formation of a composite structure consisting of Au NPs (with the stabilizer) and the polymer. The results are the formation of particles of uniform sizes and change in the SPR spectral characteristics of the Au NPs. Further, the attractive forces leading to composite formation, at above LCST, between the functionalized Au NPs and the polymer might be responsible for the changes in the SPR peak of the Au NPs. However, the above investigation of the DLS measurements shows that there will be a marked attraction between the thioglycolic acid capped Au NPs and pNIPAm-AAc polymer network and this may lead to the decrease of the hydrodynamic radius of the polymer network gel towards to the thioglycolic acid capped Au NPs sizes, with increasing the temperature of the system. This leads to the change in the λ_{max} of the SPR towards to the lower wavelength. In other words, at higher temperature the water molecules are gradually removed from polymer hydrogel and the removal induces a decrease in total volume of the polymer gel, bringing thioglycolic acid capped Au NPs very close to the polymer network leading to the blue shift of the SPR absorption of the Au NPs in the system. It must be mentioned here that all of the above behaviors have been found to be reversible with respect to change in temperature. Further, TEM analysis of the pPA-thio-Au NPs samples prepared at below the phase transition temperature (25^{o}C) and at above the phase transition temperature (40^{o}C), was pursued in order to have a better understanding of the structural transitions due to temperature increase. The results are shown in Figure 5.1.8. As is clear from the figure, at a temperature below the LCST, the Au NPs could be observed to have been dispersed rather uniformly all over the polymer (Figure 5.1.8 (a)).

TH-777_05612211

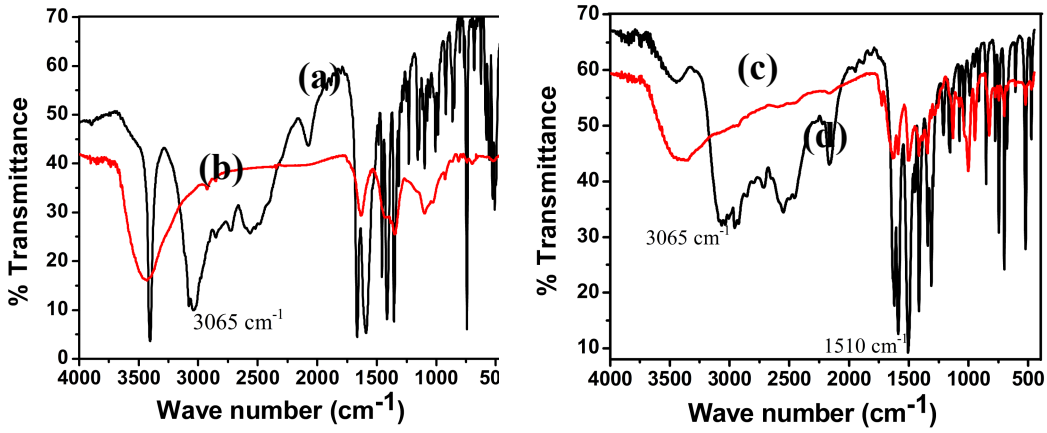


Figure 5.1.9. *FTIR spectrum of (a), (c) is bare tryptophan and phenylalanine (black lines) and (b), (d) is FTIR spectrum of tryptophan and phenylalanine capped gold nanoparticles (red lines).*

Individual Au NPs could be seen spread over the network of polymers (Figure 5.1.8 (c)) indicating uniform distribution of particles in the medium, which upon evaporation formed such structures. On the other hand, at above the LCST (at 40^{o}C), the density of the particles becomes much higher and clusters of particles could be seen deposited over the polymer (Figures 5.1.8 (d)-(f)). The average diameter of the Au NPs was found to be 8.0 ± 0.3 nm in all cases, indicating that there was no apparent agglomeration of particles. The increase in density of the particles clearly indicates the shrinking of polymer along with the functionalized Au NPs. This means that the Au NPs were bound to the polymer at above LCST, possibly through electrostatic interaction between the polymer and the stabilizers of Au NPs.

In addition to thioglycolic acid, we were interested in studying the effect of amino acids on the volume phase transition by incorporation of amino acid capped Au NPs into pNIPAm-AA hydrogel solution. Sastry and coworkers have reported that amino group binds more strongly to the surface of Au NPs than carboxylic acid group[45-47]. In addition to their

TH-777_05612211

studies, there has been several report of synthesis of different amino acid capped Au NPs, which are useful for biological applications[48-50]. The motivation has been that since the amino acids could have different side chain group - such as hydrophilic or hydrophobic, polar or non-polar – interactions of the stabilizer with biological molecules would also be different. In the present study, we have taken two different amino acids such as tryptophan and phenylalanine. Tryptophan contains hydrophilic indole moiety, while phenylalanine consists of hydrophobic phenyl ring. Thus the phase behaviors of the two different amino acid-stabilized Au NPs with the polymer, at different temperature, would be different and potentially interesting. The capping of Au NPs by amino acids has been confirmed by FTIR spectroscopy (Figure 5.1.9). Figure 5.1.9 reveals the peak at 1510 cm^{-1}, due to the symmetrical bending mode of NH_3^+, after capping with gold nanoparticles. The intensity of the peak is much decreased in both the amino acids. The broad band at 3064 cm^{-1} is ascribed to the asymmetric stretching mode of NH_3^+. This band disappeared in amino acid capped Au NPs. This indicates that both amino acids were strongly attached to the surface of the NPs by interacting with NH_3^+group. On the other hand, other functional groups of the amino acids are not affected by the presence of Au NPs. Tryptophan and phenylalanine capped Au NPs have absorption maxima at 543 nm and 519 nm respectively. For subsequent studies, the amino acid capped Au NPs were mixed in aqueous solutions containing pNIPAm-AAc hydrogel. We shall henceforth refer the resultant composites hybrid hydrogels as pPA-try-Au NPs (for pPA-AA-tryptophan capped Au NPs) and pPA-phe-Au NPs (for pPA-AA- phenylalanine capped Au NPs). Our observations as detailed below suggest that the phase transition as well as optical behavior of the two differently stabilized Au NPs are different.

TH-777_05612211

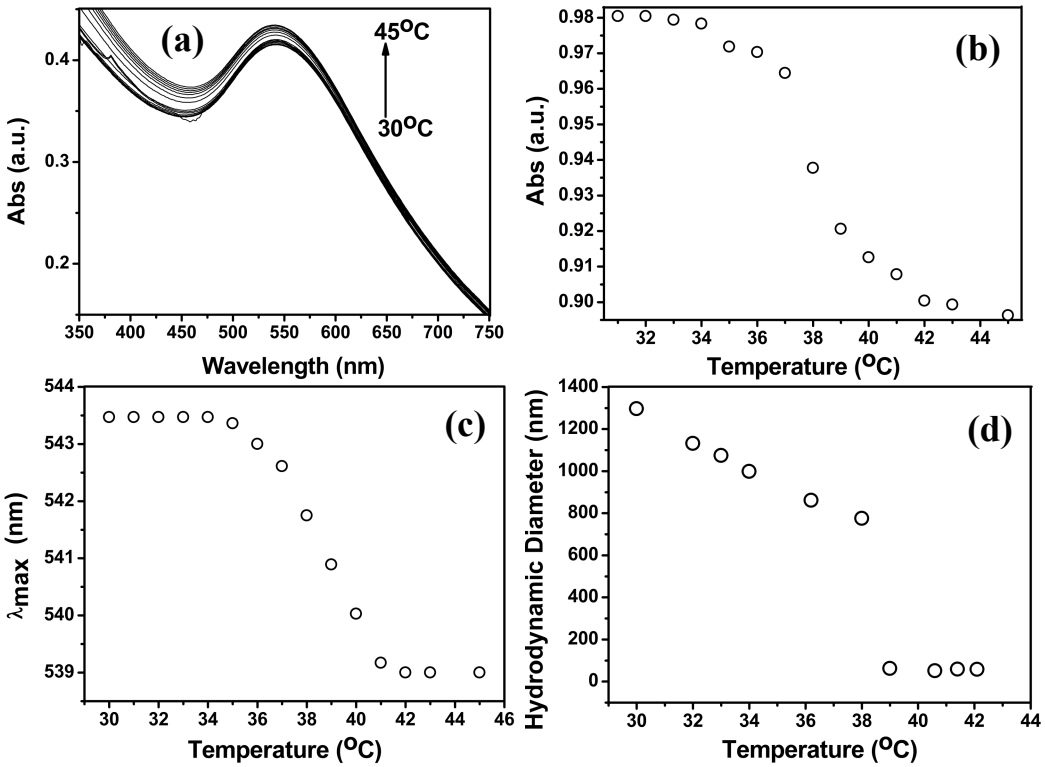


Figure 5.1.10. *(a) Temperature-dependent UV-visible spectra of pPA-try-Au NPs; while (b) is the plot of normalized absorbance at different temperatures obtained from (Figure 5.1.5A (b)), and (c) is the change of λ_{max} of the surface plasmon band of the pPA-try-Au NPs from normalized graph of Figure 5.1.5A (b). The plot in (d) is the dynamic light scattering measurement results*

The temperature-dependent UV-vis spectral changes and hydrodynamic diameters of pPA-try-Au NPs and pPA-phe-Au NPs are shown in Figures 5.1.10 and 5.1.11 respectively. The as-observed UV-vis spectra are shown in Figure 5.1.10 (a) and 5.1.11 (a) respectively. The normalized absorbances at the maxima are shown in Figures 5.1.10 (b) and 5.1.11 (b) respectively. It may be mentioned here that in order to obtain normalized absorbance from Figure 5.1.10 (a), the method similar to calculations in Figure 5.1.6 (a) was followed (Refer to Appendix-I, Figure 5.1.5A (b)). On the other hand, the normalized absorbance values at

TH-777_05612211

the maxima from Figure 5.1.11 (a) were obtained by drawing a baseline between 475 nm and 555 nm and then measuring the value of absorbance from the baseline to the maximum absorption at the λ_{max} (refer to Appendix-I, Figure 5.1.5A (c)). For the pPA-try-Au NPs composite the SPR band of Au NPs hardly changed with temperature in terms of intensity (at λ_{max}, Figure 5.1.10 (c)), while there was discernible change in the values of λ_{max} (Figure 5.1.11 (c)).

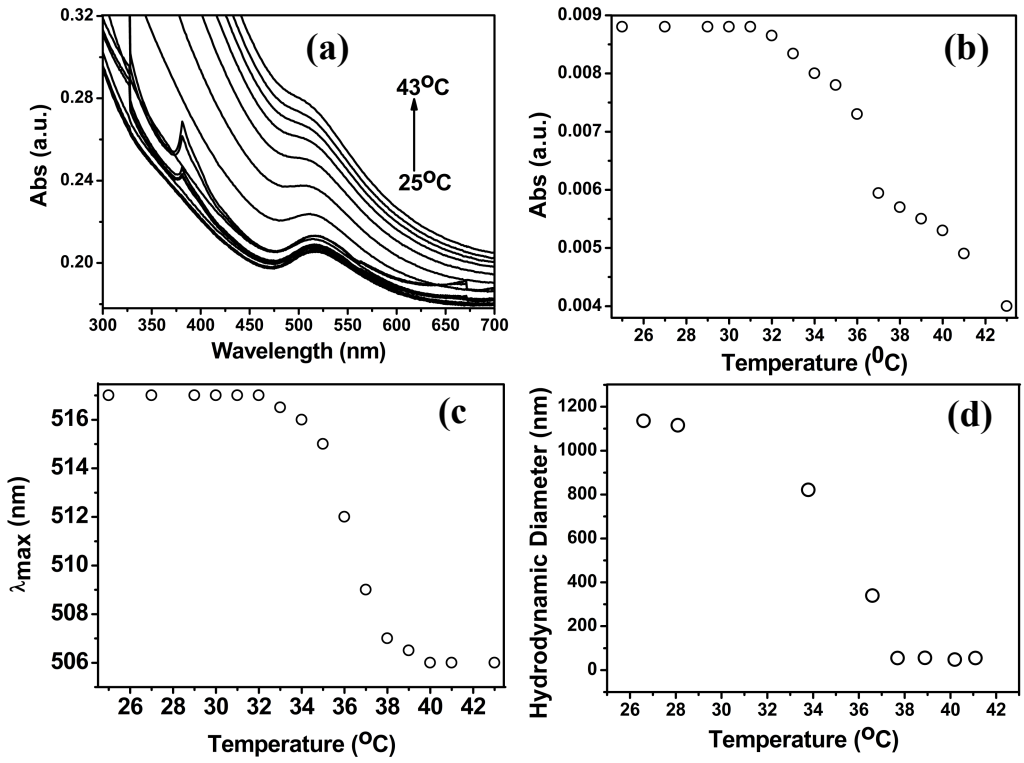


Figure 5.1.11. *(a) Temperature dependent UV-visible spectra of pPA-phe-Au NPs. The plot (b) of normalized absorbance at different temperatures is based on figure shown in Figure 5.1.5A (c) (refer to Appendix-I); while (c) is the plot of the λ_{max} of the surface plasmon band of the pPA-phy-Au NPs also calculated from Figure 5.1.5A (c). Here (d) is the average hydrodynamic*

For example, at below the transition temperature the λ_{max} of the pPA-try-Au NPs was 543 nm, while at above the phase transition temperature the λ_{max} was observed to be 539 nm. The results, however, indicate behavior similar to the ones of thioglycolic acid as the

TH-777_05612211

stabilizer, although they are less remarkable. Further, the phase transition temperature as measured from the UV-vis studies (Figure 5.1.10 (b) and 5.1.10 (c)) occurred at 39^{o}C, which is significantly higher than that of the pure polymer. In addition, the results of measurements of hydrodynamic diameters (Figures 5.1.10 (d) and 5.1.11 (d) respectively) also support the above results. Essentially, although the general behavior of the hydrophilic tryptophan moiety (in the composite) is similar to that of thioglycolic acid there are significant differences as described above, which indicates that the interaction between the polymer and the stabilized Au NPs could be substantially different at different temperatures. The H-bond that could be formed between the indole group of tryptophan and the carboxylate or amide moieties of the polymer could possibly be the reason for the behavior described above. Further evidence in support of the above conclusion came from the temperature dependent UV absorption due to Π- Π* transition of the indole moieties of the tryptophan occurring at 265 nm. It is worth pointing out that the tryptophan has absorption maxima at 278 nm, which shifted to 265 nm after the formation of stabilized Au NPs. This indicates interaction between the Au NPs and the π-electron cloud of tryptophan[51]. Figure 5.1.12 (a) shows the temperature dependent absorption spectrum of a mixture of pPA-try-Au NPs composites solutions, recorded in the range of 190 nm- 420 nm. As is evident from the figure, the band at 265 nm vanished at phase transition temperature (39^{o}C) of the pPA-try-Au NPs. It should be mentioned here that the band could again be observed when the temperature reverted back to a temperature below LCST. This observation clearly indicates that there was a significant interaction between the polymer hydrogel and tryptophane capped Au NPs, which is reversible with respect to change in temperature. It might be that encapsulation of the tryptophan moieties inside the globule of the polymer leads to vanishing of the absorption.

The results involving pPA-phe-Au NPs were remarkably different from those mentioned above. The UV-vis absorption due to SPR of Au NPs virtually disappeared with increase in temperature (Figures 5.1.11 (a) and 5.1.11 (b)). Moreover, the changes were more gradual than in the cases with the other stabilizers. The changes in the wavelength

TH-777_05612211

maxima were also significant. For example, at room temperature (25^{o}C) the λ_{max} was 517 nm, while that at 36^{o}C was shifted to 508 nm. Further, the λ_{max} shifted gradually to still lower wavelengths with increasing temperatures (Figure 5.1.11 (c)). The phase transition temperature was found to be 36^{o}C (Figures 5.1.11 (b) and 5.1.11 (c)). It is important to mention here that the volume phase transition temperatures of the systems pPA-try-Au NPs and pPA-phe-Au NPs were found to be 39^{o}C and 36.3^{o}C respectively, as obtained from temperature dependent DLS measurements (Figure 5.1.10 (d) and 5.1.11 (d)). These results are consistent with phase transition temperatures obtained from temperature dependent absorption maxima of the stabilized Au NPs.

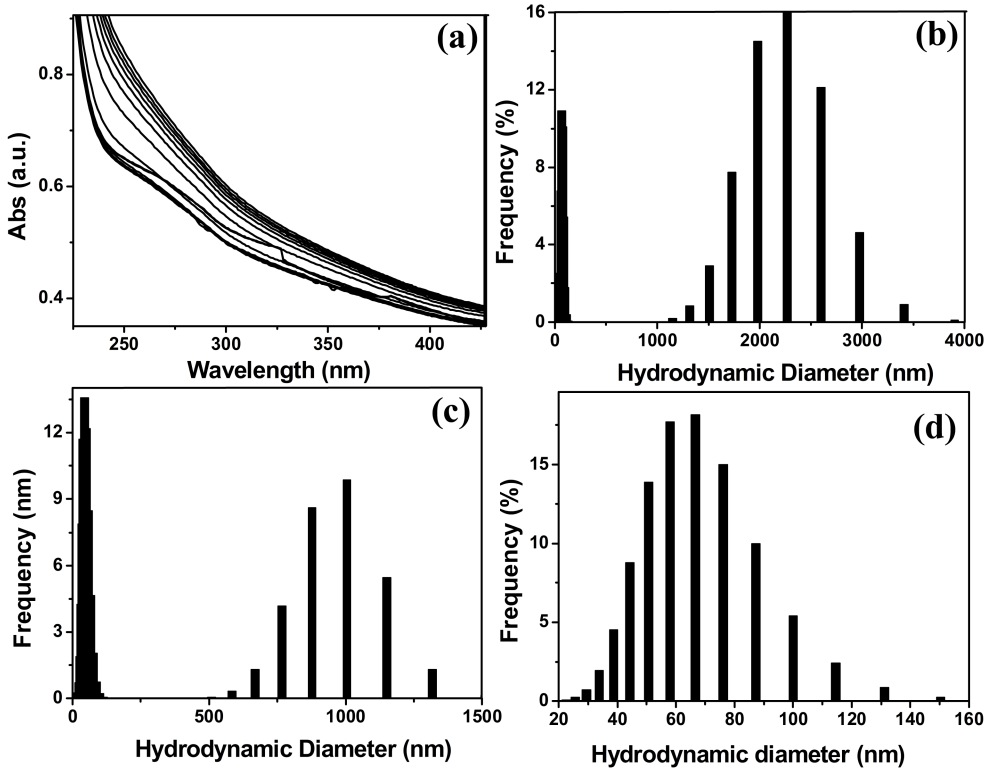


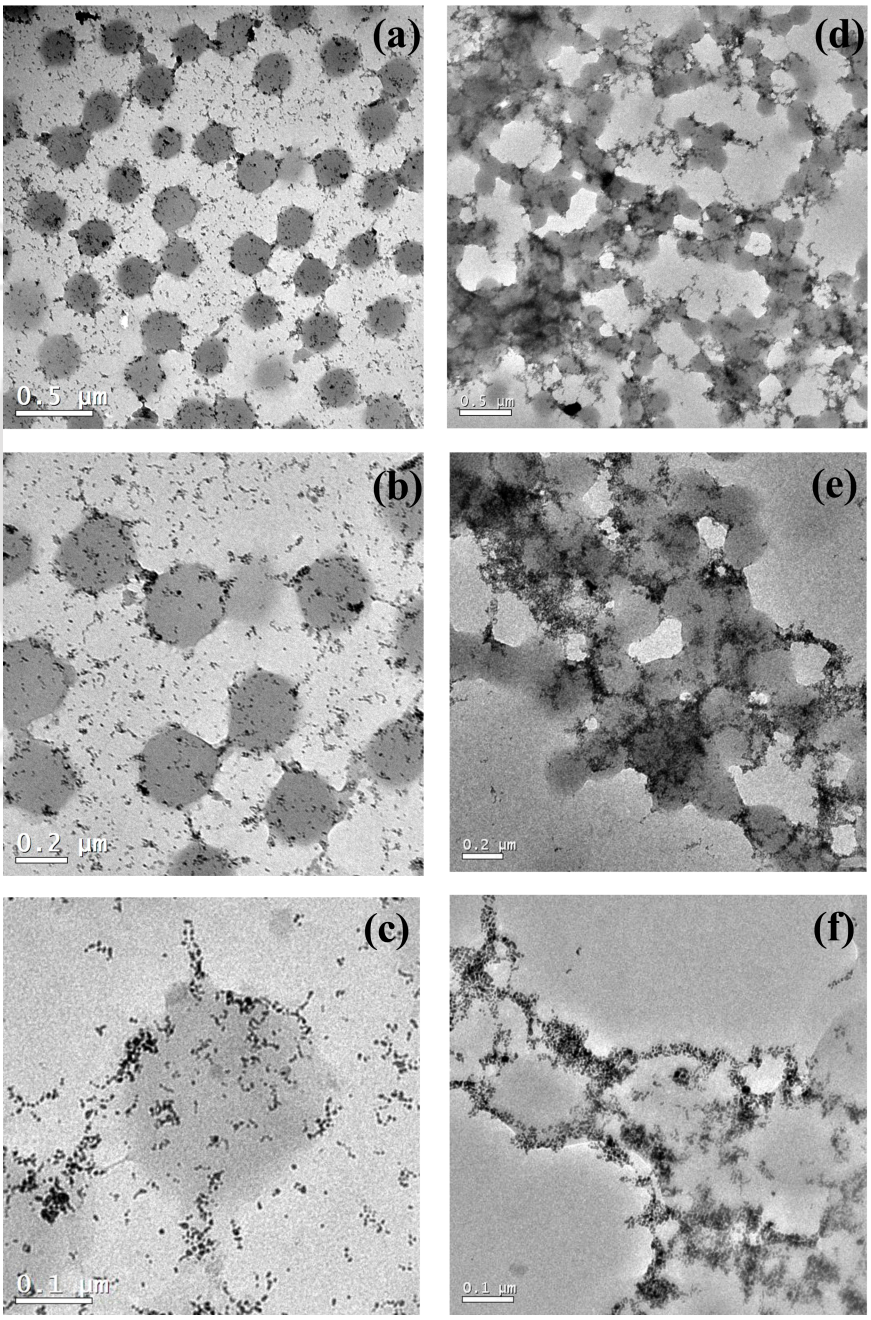
Figure 5.1.12. *(a) The UV-visible absorption spectra of pPA-try-Au NPs at different temperatures, measured in the region of 225 nm -420 nm. (b) is the histogram of hydrodymaic diameters of pPA-try-Au NPs at 30^{o}C, at 36^{o}C (c) and (d) is at 39^{o}C obtained by dynamic light scattering*

TH-777_05612211

The above results suggest that SPR absorption of Au NPs could act as a probe for understanding the nature of interactions between the stabilizer molecules and polymer hydrogel. This is especially true in establishing the LCST of the polymer hydrogel in the presence of NPs with different stabilizers. Further, a question may arise about the volume phase transition temperature of pPA-Try-Au NP composite hydrogel being higher than that of pPA-phe-Au NP composite hydrogel. This could be explained in terms of side chains of the individual amino acids. For example, tryptophan has more hydrophilic moiety of the indole ring, which can make the stronger intermolecular H-bond with polymer hydrogel, as well as with the surrounding water molecules. When the temperature is increased gradually, the intermolecular H-bond between the water and polymer and between the water and tryptophan may gradually be lost due to the thermal motion of the water molecules and consequently the volume of the pPA-try-Au NP composite hydrogel slowly shrinks (Figure 5.1.10 (d)). Luisi et al[52] reported that H-bonding interaction between the indole-water is more energetically favorable than that that of aromatic ring. They considered that H-bonding interaction between the heterocyclic ring and water is much stronger than simple aromatic benzene ring[53]. This could be responsible for higher volume phase transition temperature of the pPA-Try-Au NPs than that of pPA-phe-Au NPs composite hydrogel. This was further supported by the results of temperature dependent UV-vis spectra of NPs in both the systems. At the phase transition temperature, the SPR peak of the pPA-phe-Au NPs was more affected than that of pPA-try-Au NP composite hydrogel. This could be ascribed to the more hydrophobic nature of the phenyl ring than indole. Further, the hydrophobic interaction with the polymer is more dominant in the phenylalanine capped Au NPs, which leads to significant shift of the SPR peak in comparison to tryptophan capped NPs[40b, 42, 54]. In addition, phenylalanine contains a highly hydrophobic side residue that would have different interaction with the polymer than the highly hydrophilic thioglycolic acid or tryptophan. Also, the coil to globule transition of the polymer at above the transition temperature involves reinforced intramolecular hydrogen bonding and strong Van der Waals interactions

TH-777_05612211

(attraction) among its hydrophobic moieties[55]. This would lead to localization of the stabilized Au NPs into the hydrophobic pockets of the globule. This is probably the reason for reduced optical absorption as the NPs that are buried within the "particles" of the globule. The same may be the reason for changes in the absorption maximum.



TH-777_05612211

Figure 5.1.13. *(a) TEM pictures of pPA-try-Au NPs at 25.4oC; while (b) and (c) are the expanded view of the (a). (d) The TEM image of pPA-try-Au NPs at 40oC; while (e) and (f) are the expanded views of (d).*

Raula et al[56] have shown that both λ_{max} and absorption of the SPR peak of thermosensitive hydrogel coated Au NPs, at above the LCST changes similar to the above. The reason here has also been proposed to be due to formation of hydrophobic pocket after the collapse of the structure into globule form.

Temperature-dependent particles size histogram plot of DLS measurements of pPA-try-Au NPs and pPA-phe-Au NPs indicated specific interactions between the stabilized Au NPs and the polymer. The results are shown in Figure 5.1.12 for (pPA-try-Au NPs) and Figure 5.1.6A (Appendix-II) for (pPA-phe-Au NPs). In these cases the particles consisted of two distributions of sizes. The higher particles diameters with average values of 1.3 ± 0.8 μm and 1.15 ± 0.9 μm for pPA-try-Au NPs and pPA-phe-Au NPs respectively, in addition to lower particle diameters of values 62 ± 18 nm and 50 ± 15 nm respectively for the above. This means that polymer particles were probably dispersed separately in the medium from the stabilized Au NPs. However, since the average value of the polymer particles herein were smaller than those of polymer alone or polymer stabilized Au NPs; it is plausible that there were at least some interactions between the two. Further, at higher temperatures the particle collapsed into sizes, which are considerably less than those of all three cases discussed before. For example, at 39^{o}C the hydrodynamic diameter of the pPA-try-Au NPs was 62 $\pm$ 18 nm while pPA-phe-Au NPs showed a value of 52 $\pm$ 15 nm at 36^{o}C. This means the interactions between phenylalanine capped NPs and tryptophan capped NPs and the polymer led to globular structures with diameters smaller than that of the polymer (in its globular form) at above the LCST. Seida et al[57] reported the effect of various organic

TH-777_05612211

molecules on the nature of interaction with the polymer at above and below the phase transition temperatures. They observed that organic molecules (phenol and benzoic acid and aniline) are absorbed much into the polymer at above the phase transition due to the domination of hydrophobic interaction. This could be the reason that when the phenylalanine capped Au NPs interacted with polymer hydrogel that led to the decreasing of the hydrodynamic diameter of the pPA-phe-Au NPs than that of pPA-try-Au NPs at above the phase transition temperature. On the other hand, strong hydrophobic interactions between phenyl groups and the hydrophobic backbone of the polymer may lead to a collapsed structure that is smaller in diameter than the polymer itself. Temperature dependent TEM measurements pPA-try-Au NPs are shown in Figure 5.1.13. At below the LCST, the particles were uniformly distributed all over the solution and hence the evaporated materials had more or less uniform distributions of particles (Figures 5.1.13 (a), (b) and (c)). The NPs had typical diameters of 8.0 ± 0.6 nm. On the other hand, when the temperature was increased above LCST, the particles seem to agglomerate into the collapsed structure of the polymer. This behavior is different from the other samples where either polymer or thioglycolic acid stabilized Au NPs were used. The reversibility of the structure in solution (with respect to changes in temperature) indicates that these particles might not have agglomerated into lumps of particles only. On the contrary the interactions between the globular polymer and the stabilizers lead to some sort of collapsed structure with particles coming very close to each other in comparison to the structures obtained from polymer stabilized or thioglycolic stabilized NPs. Similar results were also observed in the case of the pPA-phe-Au NPs system (Appendix-II). The TEM pictures are shown in Figure 5.1.6B.

Qualitatively, the results mentioned above could be explained primarily by invoking two factors: hydrophobic and H-bonding interactions. In the system involving polymer capped Au NPs; there is no extraneous stabilizing agent present and hence no additional interaction between the species. Thus the results would be similar to those of polymer alone with minor variations due to the presence of Au NPs. When thioglycolic acid is used as the stabilizer; at below the LCST there would be hydrogen bonding between the stabilizer and water as well as the polymer. However, at above LCST, the hydrogen bonding between the

TH-777_05612211

carboxylate moieties of the stabilizer and the hydrophilic groups of the polymer would be favored over that with the solvent as the stable globular structure would have hydrophobic pocket and hydrophilic surfaces. Hence the final structure at above LCST may form H-bonds between the stabilizer and the polymer with stabilized Au NPs being in the pocket of the globule and the results would be different. In the case of phenylalanine stabilized Au NPs the final structure in the globule would possibly involve the stabilized NPs deeply embedded in the pocket of the globule thereby reducing even the optical absorption of Au NPs, which is different from the other cases. Finally, the general behavior involving the interactions between stabilized Au NPs and the polymer at below and above LCST is described schematically in Figure 5.1.14. Essentially, when Au NPs are stabilized by hydrophilic moieties then particles are either exposed to the aqueous medium even after the collapse (at above LCST) or embedded in the collapsed structure being bonded to the hydrophilic groups of the polymer. On the other hand, in the presence of hydrophobic stabilizers the particles are embedded deeply inside the polymer collapsed structure at above LCST.

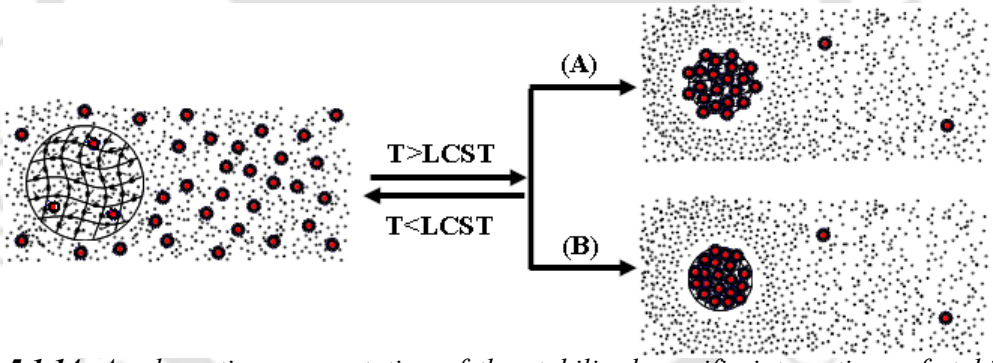


Figure 5.1.14. *A schematic representation of the stabilized specific interactions of stabilized Au NPs with the thermosensitive polymer hydrogel at below and above lower critical solution temperature (LCST). (A) and (B) represent transitions to the collapsed structure when Au NPs are stabilized by hydrophilic and hydrophobic groups respectively.*

5.1.4 Conclusion

In the present chapter, we have been able to demonstrate the use of various functional group stabilized Au NPs on the volume phase transitions of a thermosensitive polymer hydrogel. The optical properties of Au NPs stabilized with different functional groups have been used as one of the probes to understand the behavior of volume phase

TH-777_05612211

transitions in mixed systems. Particle size analysis and TEM measurements were also made to substantiate the conclusions of the observations. Essentially, when hydrophilic groups were used in the stabilizer the collapsed structures consisted of H-bonding between the stabilized Au NPs and the polymer, with little effect on the hydrophobic pocket of the globule. On the other hand, when hydrophobic group was used in the stabilizer then the observations indicated that the Au NPs along with the stabilizer were embedded deep inside the hydrophobic pocket of the globule that contributed to the drastic change in the optical absorption due to SPR of Au NPs. That amino acids were used as the stabilizing agents and their effect on the volume phase transitions of a biofriendly hydrogel would support future endeavors involving Au NPs in the drug delivery systems.

5.1.5 Appendix-I

TH-777_05612211

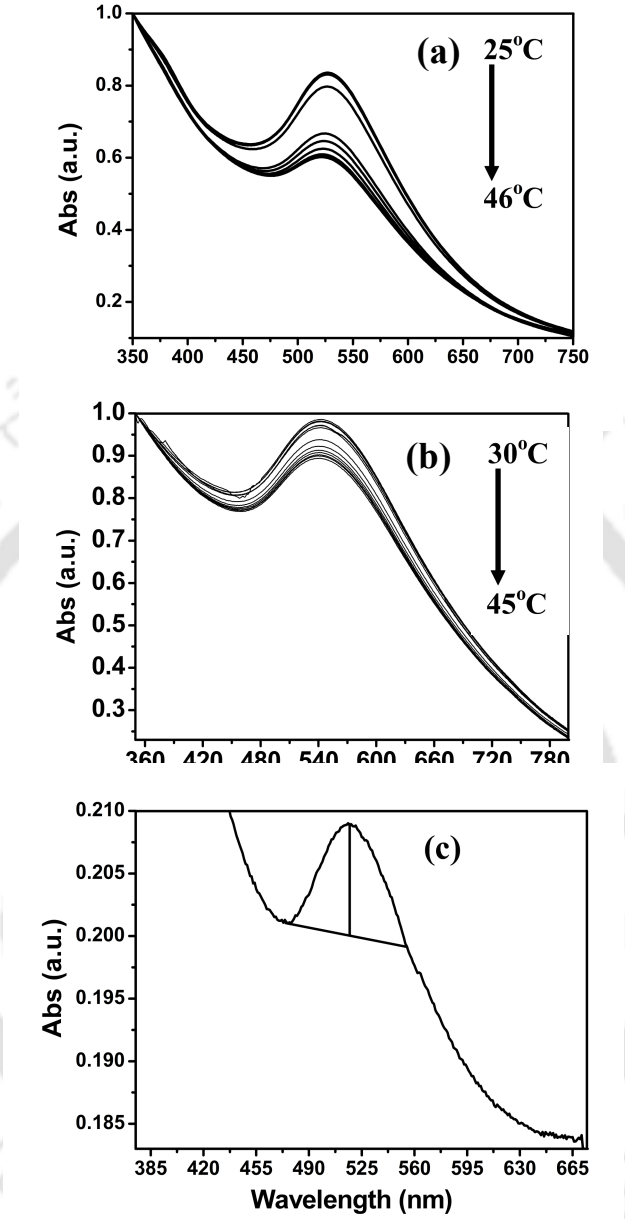


Figure 5.1.5A. *Temperature dependent normalized UV-Visible spectra of (a) pPA-thio-Au NPs, (b) pPA-try-Au-NPs and (c) pPA-phe-Au-NPs*

TH-777_05612211

5.1.6 Appendix II

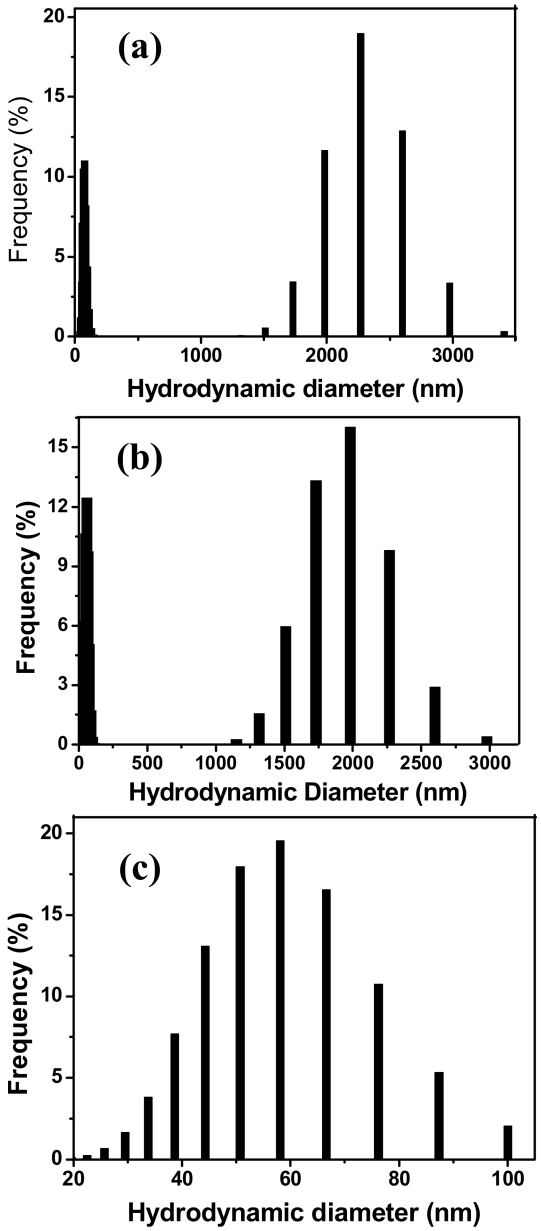


Figure 5.1.6A. *Histogram plots of hydrodynamic diameter of pPA-phe-Au NPs composite hydrogel at 26^{o}C (a), 33^{o}C (b) and (c) is 37^{o}C obtained from dynamic light scattering measurement.*

TH-777_05612211

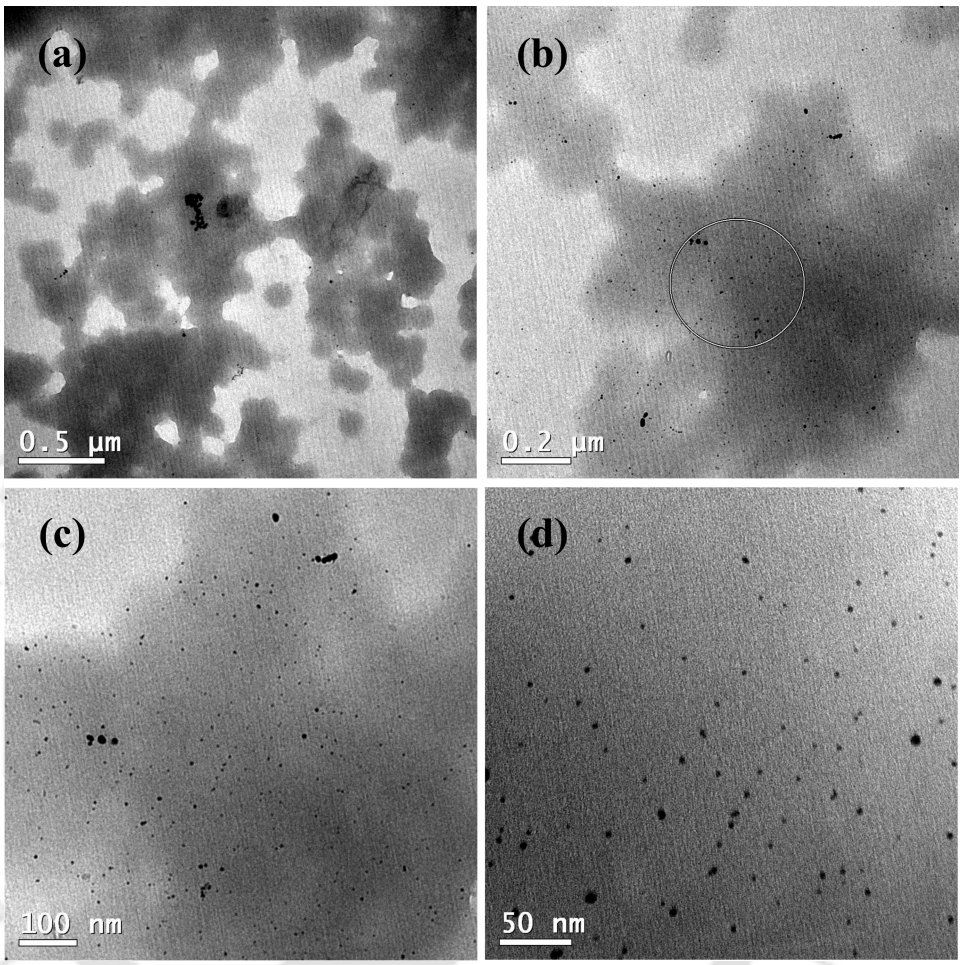


Figure 5.1.6B*(a) The TEM picture of PPA-phe-Au NPs at 40^{o}C, (b), (c) and (d) are the expanded views of (a).*

TH-777_05612211

5.1.7 References

1. (a) Saulius, J.; Naoki, M.; Ryosuke, W.; Akira, Y.; Shigeki, M.; Hiroaki, M. *Nature* **2000**, *408*, 178. (b) Haiyan, C.; Yueqing, G.; Yuzhu, H.; Zhiyu, Q. *J. Pharm. Sci and Technol.* **2007**, *61*, 303.

2. (a) Langer, R.; Tirrell, D. A. *Nature* 2004, *428*, 487. (b) Hoffman, A. S. *Adv. Drug. Deliv. Rev.* **2002**, *54*, 3.

3. (a) Peppas, N. A.; Hilt, J. Z.; Khademhosseini, A.; Langer, R. *Adv. Mater.* **2006,** *18*, 1345. (b) Vinogradov, S. V. *Curr Pharm. Des*. **2006**, *12*, 4703.

4. (a) Retama, J. R.; Zefeiropoulos, N. E.; Serafinelli, C.; Reyna, R. R.; Voit, B.; Cabarcos, E. L.; Stamm, M. *Langmuir* **2007**, *23*, 10280. (b) Robinson, I.; Alexander, C.; Lu, L. T. ; Tung, L. D. ; Fernig, D. G.; Thanh, N. T. K. *Chem Commun.* **2007***,* 4602. (c) Nora, F. J.; Sabina, A.; Silvia, J. E.; Marta, D. E. *J. Appl. Polym. Sci.* **2007**, *105*, 647.

5. (a) Malavosklish, B.; Andre, G. M.; Rachel, W. E.; Jennifer, W. L. *J Controlled Release.* **2007**, *123*, 219. (b) Chang, Y.; Su, Z. *Mater. Sci. Eng.* **2002**, *333*, 155.

6. Kondo, A.; Fukuda, H. J. *Ferment. Bioeng.* **1997**, *84*, 337.

7. Das, M.; Sanson, N.; Fava, D.; Kumacheva, E. *Langmuir* **2007**, *23*, 196.

8. (a) Snowden, M. J.; Chowdhry, B. Z.; Vincent, B.; Morris, G. E. *J. Chem. Soc., Faraday Trans.* **1996**, *92*, 5013. (b) Kim, J. H.; Lee. T. R. *Chem. Mater.* **2004**, *16*, 3647.

9. Zhou, J.; Wang, G.; Hu, J.; Lu, X.; Li, J. *Chem. Commun.* **2006**, 4820.

10. Zhang, X. Z.; Yang, Y. Y.; Wang, F. J.; Chung, T. S. *Langmuir* **2002**, *18*, 2013.

11. Zhu, M. Q.; Wang, L. Q.; Exarhos, G. J.; Li, A. D. Q. *J. Am. Chem. Soc.* **2004**, *126*, 2656.

12. Johns, C. D.; Lyon. L. A. *Macromolecules* **2003**, *36*, 1988.

13. Felton, R. H.; Pelton, H. M.; Morphesis, A.; Rowell, R. L. *Langmuir* **1989**, *5*, 816.

14. Nayak, S.; Lyon, L. A. *Angew. Chem. Int. Ed. Eng.* **2005**, *44*, 7686.

TH-777_05612211

15. Schild, H. G. *Prog. Polym. Sci*. **1992**, *17*, 163.

16. Heras Alarcon. C. D. L.; Pennadam, S.; Alexander, C. *Chem. Soc. Rev.* **2005**, *34*, 276.

17. Gan, D. J.; Lyon, L. A. *J. Am. Chem. Soc.* **2001**, *123*, 7511.

18. Christopher, L.; Amanda, L.; Naomi, H.; Jennifer, W.; Rebekah, D. *Nano Lett*. **2005**, *5*, 709.

19. Hirsch, L. R.; Stafford, R. J.; Bankson, J. A.; Sershen, S. R.; Rivera, B.; Price, R. E.; Hazie, J. D.; Halas, N. J.; West, J. L. *PNAS.* **2003**, *100*, 13549.

20. Karyakin, A. A.; Presnova, G. V.; Rubtsova, M. Y.; Egorow, A. M. *Anal. Chem*. **2000**, *72*, 3805.

21. Jain, R. K.; Stroh, M. *Nat. Biotechnol.* **2004**, *22*, 959.

22. Pathak, S.; Choi, S. K.; Arheim, N.; Thompson, M. E. *J. Am. Chem. Soc.* **2001**, *123*, 4103.

23. Storh, M.; Zimmer, J. P.; Drude, D. G.; Levehenko, T. S.; Cohen, K. S.; Brown, E. B.; Scadden, D. T.; Torchilin, V. P.; Bawendi, M. G.; Fukumura, D. *Nat. Med*. **2005**, *11*, 678.

24. (a) Lu, Y.; Mei, Y.; Drechsler, M.; Ballauff, M. *Angew. Chem. Int. Ed. Eng.* **2006**, *45*, 813. (b) Lu, Y.; Mei, Y.; Ballauff, M. *J. Phys. Chem. B* **2006**, *110*, 3930.

25. (a) Shan, J.; Tenhu, H. *Chem. Commun.* **2007**, 4580. (b) Yusa, S. I.; Fukuda, K.; Yamamoto, T.; Iwasaki, Y.; Watanabe, A.; Akiyoshi, K.; Morishima, Y. *Langmuir* **2007**, *23*, 12842.

26. Shan, J.; Nuopponen, M.; Jiang, H.; Vitala, T.; Kauppinen, E.; Kontturi, K.; Tenhu, H. *Macromolecules* **2005**, *38*,. 2918.

27. (a) Wang, B. C.; Flynn, N. T.; Langer, R. *Adv. Mater.* **2004**, *16*, 1074. (b) Karg, M.; Pastoriza-Santos, I.; Perez-Juste, J.; Hellweg, T.; Liz-Marzan, L. M. *Small* **2007**, *7*, 1222.

28. (a) Suzuki, D.; Kawaguchi, H. *Langmuir* **2005,** *21*, 12016. (b) Kazimierska, E. A.; Ciszkowska, M. *Electroanalysis* **2005**, *17*, 134.

TH-777_05612211

29. (a) Kim, J. H.; Lee, R. *Drug. Dev. Res.* **2006**, *67*, 61. (b) Holtz, J. H.; Asher, S. A. *Nature* **1997**, *389*, 829. (c) Zhao, X.; Ding, X.; Deng, Z.; Zheng, Z.; Peng, Y.; Tiang, C.; Long, X. *New. J. Chem.* **2006**, *30*, 915.

30. (a) Zhang, W.; Gaberman, I.; Ciszkowska, M. *Anal. Chem*. **2002**, 74, 1343. (b) Ma, C. S.; Zhang, W.; Ciszkowska, M. *J. Phys. Chem. B* **2001**, *105*, 10446..

31. Melnichenko, Y. B.; Kelpko, V. V.; Shilov. V. V. *Polymer* **1993**, *34*, 1019.

32. Matsukaa, S.; Ando, I. *Macromolecules* **1996**, *29*, 7136.

33. Pelton, R. *Adv. Colloid Interface Sci.* **2000**, *85*, 1.

34. Kratz, K.; Hellweg, T.; Eimer, W. *Colloids surf. A: Physicochem. Eng. Aspects.* **2000**, *170*, 137.

35. Kim, J.; Singh, N.; Lyon, L. A. *Chem. Mater.* **2007**, *19*, 2527.

36. Wei, H.; Zhang, X.; Cheng, C.; Cheng, X.; Zhou, R. X. *Biometerials* **2007**, *28*, 99.

37. (a) Khan, A. *J. Colloid and Interface Sci.* **2007**, *313*, 697. (b) Khan, A. *Mater. Lett.* **2008**, *62*, 898.

38. Zhang, J.; Chu, L. Y.; Li, Y. K.; Lee, Y. M. *Polymer* **2007**, *48*, 1718.

39. (a) Lin, C. L.; Chiu, W. Y. *J. Poly Sci. A* **2006**, *44*, 1648.

40. (a) Morones, J. R.; Frey, W. *Langmuir* **2007**, *23*, 8180. (b) Mie, G. *Ann. Phys. (Leipzig)* **1908**, *25*, 377.

41. (a) Lin, B. S.; Li, M.; Dujardin, E.; Girrard, C.; Mann, S. *Adv. Mater.* **2005**, *17*, 2553. (b) Yonezawa, T.; Kunitake, T. *Colloids surf. A: Physicochem. Eng. Aspects* **1999**, *149*, 193.

42. Ghosh, S. K.; Nath, S.; Kundu, S.; Esumi, K.; Pal, T. *J. Phys. Chem. B* **2004**, *108*, 13963.

43. Nikoobakht, K.; El-Sayed, M. A. *Langmuir* **2001**, *17*, 6368.

44. Ung, T.; Giersig, M.; Dunstan, D.; Mulvaney, P. *Langmuir* **1997**, *13*, 1773.

45. (a) Joshi, H.; Shirude, P. S.; Bansal, V.; Ganesh, K. N.; Sastry, M. *J. Phys. Chem. B* **2004**, *108*, 11535. (b) Joshi, H.; Bhumkar, D. R.; Joshi, K.; Pokharkar, V.; Sastry, M. *Langmuir* **2006**, *22*, 300.

TH-777_05612211

46. Selvakannan, P. R.; Mandal, S.; Phadtare, S.; Pasricha, R.; Sastry, M. *Langmuir* **2003**, *19*, 3545.

47. Mandal, S.; Selvakannan, P. R.; Phadtare, S.; Pasricha, R.; Sastry, M. *Proc. Indian, Acad Sci. (chem. Sci*) **2002**, *114*, 513.

48. Zhong, Z.; Luo, J.; Ang, T. P.; Highfield, J.; Lin, J.; Gedanken, A. *J. Phys. Chem. B* **2004**, *108*, 18119. (b) Nayak, N. C.; Shin, K. *J. Nanosci Nanotech.* **2006**, *6*, 1.

49. Polavarapu, L.; Xu, Q. H. *Nantechnology* **2008**, *19*, 075601.

50. Phadtare, S. ; Kumar, A. ; Vinod, V. P.; Dash, C. V.; Rao, M.; Shukla, P. G.; Sivaram, S.; Sastry, M. *Chem. Mater.* **2003**, *15*, 1944.

51. Selvakannan, P. R.; Mandal, S.; Phadtare, S.; Gole, A.; Pasricha, R.; Adyanthaya, D.; Sastry, M. *J. Colloid Interface Sci.* **2004**, *269*, 97.

52. Stoller, E. J.; Gelpi, J. L.; Velankar, S.; Golovin, A.; Orozco, M.; Luisi, B. F. *Structure, Function and Bioinformatics* **2004**, *57*, 1.

53. (a) Van, T. M.; Price, S. L.; Clary, D. C. *Chem Phys Lett.* **2000,** *311*, 253. (b) Carney, J. R.; Hagemeister, F. C.; Zwier, T. S. *J. Chem Phys.* **1998**, *108*, 3379.

54. (a) Mulvaney, P. *Langmuir* **1996**, *12*, 788. (b) Ung, T.; Liz-Marzan, L. M.; Mulvaney, P. *J. Phys. Chem. B* **2001**, *105*, 3441.

55. Zhu, M. Q.; Wang, L. Q.; Exarhos, G. J.; Li, A. D. Q. *J. Am. Chem. Soc.* **2004**, *126*, 2656.

56. Raula, J.; Shan, J.; Nuopponen, M.; Niskanen, A.; Jiang, H.; Kauppinen, E. I.; Tenhu, H. *Langmuir* **2003**, *19*, 3499.

57. Seida, Y.; Nakano, Y. *J. Chem. Eng. Jpn.* **1996**, *29*, 767.

TH-777_05612211

6.1 Acetanilide Mediated Reversible Assembly and Disassembly of Au Nanoparticles

6.1.1 Introduction

Organizations of nanoscale particles into well-defined superstructures are currently being addressed –among others - by self-assembly using electrostatic forces or molecular bonds and by using template-based approaches[1-5]. These are important for their applications where collective properties of the nanoparticles (NPs) would be utilized. For example, assembly of NPs and the associated physical property changes have been used in sensing heavy metal ions, DNA hybridization and other biomolecular events[6-11]. Molecularly programmed assembly of NPs holds the key to further applications encompassing chemistry, biology, material science and optoelectronics. Chemistry, especially the use of 'soft' interactions, offers the possibility of molecular level control over reversible assembly and disassembly of NPs in solution[12-17], a large part of which remains much to be explored. Molecularly controlled assembled NPs would not only offer newer materials with tunable properties but may also reveal a great deal about the nature of molecular interactions between the NPs and the assembling molecules and the formation of hierarchical structures.

In this chapter, the work on the use of sparingly soluble acetanilide in the reversible assembly and disassembly of Au NPs in water is reported. The primary control parameter, in the assembly formation, is the concentration of acetanilide in the medium, which also acted as the reducing agent as well as the stabilizer for the NPs. Two different ways have been used to achieve the assembly formation. The first method involved simultaneous synthesis and assembly of spherical NPs using various amount of acetanilide during synthesis. In the other method, minimum acetanilide concentration was first used in the preparation of spherical Au NPs. This was followed by addition of various amount of acetanilide in order to obtain controlled organization of NPs. The results obtained were similar. The optical

TH-777_05612211

properties of the NPs and their assemblies were commensurate with the amount of acetanilide present in the medium. Further, the assemblies of NPs could be disassembled into individual NPs using ultrasonic waves and further reassembled into superstructures by concentrating the redispersed particles. The results reported herein indicate the possibility of molecular level control on the organization of NPs in aqueous media.

6.1.2 Experimental Section

Materials

Hydrogen tetrachloroaurate ($HAuCl_4$, 17 % Au in HCl as purchased from Sigma-Aldrich), and Acetanilide (99 %, from Merck), were used as received without further purification. Milli-Q grade water was used in all the experiments.

Synthesis of Au Nanoparticles using Acetanilide

Method-I

The method involved the use of various amounts of acetanilide at the time of synthesis. Typically, to five 30 mL vials - each containing 10 mL of Milli-Q grade water - 10 mg, 20 mg, 30 mg, 40 mg and 50 mg acetanilide were added. The concentrations of acetanilide in the vial were thus 7.29 mM, 14.58 mM, 21.87 mM, 29.16 mM and 36.45 mM respectively. The vials were then heated to 90^{o}C in order to dissolve acetanilide. This was followed by addition of 20 μL of 17.26 mM of $HAuCl_4$ to each solution while they were still being heated. These reaction mixtures were then kept on a hot plate under slow boiling condition for 5 min. The resulting solutions appeared red in color, indicating possible formation of Au NPs. The red colored solutions were then taken out from the hot plate and cooled to room temperature. The solutions were used for further characterization studies. The pH of all of the resulting solutions was measured to be 3.5. It was also observed that while the solutions containing initially 7.29 mM, 14.58 mM, 21.87 mM of acetanilide were stable for 3-4 days, those containing 29.16 and 36.45 mM of acetanilide were stable for only

TH-777_05612211

a day after which visible precipitation could be observed. However, if the pH of the solutions were changed to 7.0 - after synthesis - they were stable for a couple of weeks without occurrence of observable precipitations.

Method-II

This method involved the synthesis of Au NPs with minimum amount of acetanilide followed by addition of various excess amounts of acetanilide. Five 30 mL vials, each containing 20 mg of acetanilide (14.58 mM) in 10 mL milli-Q water, were kept on hot plates at 90^{o}C. To each of the solutions, 20 μL of 17.26 mM of $HAuCl_4$ was then added. This was followed by keeping the reaction mixtures on the hot plate under slow boiling condition for 5 mins, after which the solutions turned red. The solutions were then taken out of the hot plate, immediately followed by addition of appropriate amount of acetanilide so that the total concentrations of acetanilide in the vials were 18.95 mM, 23.30 mM, 27.71 mM, 32.07 mM and 36.45 mM respectively. These solutions were then kept at room temperature for 30 min before use. The pH of the resulting solution was found to be 3.5. The solutions, as such, were used for further characterization studies.

Disassembly of Au NPs

0.5 mL portion each of the Au NP solutions, containing the highest concentration of acetanilide (36.45 mM) and as prepared using Method-I and Method-II above, was taken in a 30 mL vial. To each of these two vials, 4.5 mL of milli-Q water was added. The solution appeared nearly colorless with slight violet tint. UV-vis absorption spectra of the solutions were recorded. They were then kept in an ultrasonication bath (Elma, Model: D-78224, Singen / Htw at 35 KHz) for 3 h. The resulting solution was violet in color and the UV-vis absorbance spectrum consisted of a single peak at 535 nm, with enhanced absorption value. On the other hand, the solution obtained from Method-II still did not show any color change. However, after sonication for a total of 8 h, the solution appeared violet (weak) in color and

TH-777_05612211

the UV-visible absorbance spectrum consisted of one major peak at 540 nm with a small hump at 650 nm. Both the solutions were used for further TEM analysis.

Reassembly of Au NPs

Twenty four, identically prepared solutions as reported above for the preparation of disassembly of Au NPs mad using Method-I, were mixed in a 30 mL vial, which was then subjected to ultracentrifugation at 70,000 rpm at 15^{o}C for 15 mins. Finally, the pellet was collected and then washed with copious amount of water with centrifugation after each wash. This process was repeated for three times. The pellet was then redispersed in 3 mL water. The 0.8 mL of redispersed sample was diluted with 1.7 mL water. The pH of the solution was adjusted to 3.5 by adding 10 μL of ~1M hydrochloric acid. The total volume of the solution was made to be 2.5 mL. To this solution, 20 mg of acetanilide was added. The mixture was kept on a hot plate and slowly boiled for 3 mins. The solution was brought to room temperature and further kept for 30 mins before pursuing UV-visible absorption and TEM studies.

Analytical Measurements

UV-vis absorption spectra of the samples were recorded using a HITACHI model U-2800 UV-visible spectrophotometer in the range of 300 to 1100 nm. The ^{1}H-NMR spectra of acetanilide as well acetanilide capped Au NPs in $CDCl_3$ were recorded using a Varian 400 MHz spectrometer, with TMS as the internal reference. The dynamic light scattering (DLS) measurements of the liquid samples were performed with an LB-550 (HORIBA) DLS measurement system. Transmission electron microscopy (TEM) measurements were performed using JEOL-2100 equipment operating at an acceleration voltage of 200 kV. The TEM samples were prepared by placing a drop of liquid on carbon coated copper grid (400 mesh) followed by evaporation of the solvent at room temperature.

TH-777_05612211

6.1.3 Results and Discussion

When 34.5 μM $HAuCl_4$ was treated with 7.29 mM acetanilide (at boiling condition) UV-vis spectrum (Figure 6.1.1 (A) (a)) characteristic of spherical Au NPs with a single peak having maximum at 551 nm was observed. TEM measurements of the sample indicated the presence of spherical NPs in the solution (Figure 6.1.1 (B)) with diameters of about 20 nm, although there was substantial number of NPs with diameters less than 10 nm. On the other hand, when increasing amount of acetanilide was used, the UV-vis spectra consisted of two surface plasmon resonance (SPR) peaks – the transverse one at 551 nm - while the longitudinal one appeared at increasingly higher wavelengths when larger amounts of acetanilide was used (Figure 6.1.1 (A) (c)-(e)). For example, at the acetanilide concentrations of 21.87 mM, 29.16 mM and 36.45 mM the second peak appeared at 698 nm, 750 nm and 754 nm respectively. It is also important to mention that the peak at 551 nm remained constant for all of the above samples. TEM measurements (Figures 6.1.1 (C) and 6.1.1 (D)) indicated the formation of necklace–like assemblies of NPs at higher acetanilide concentrations.

TH-777_05612211

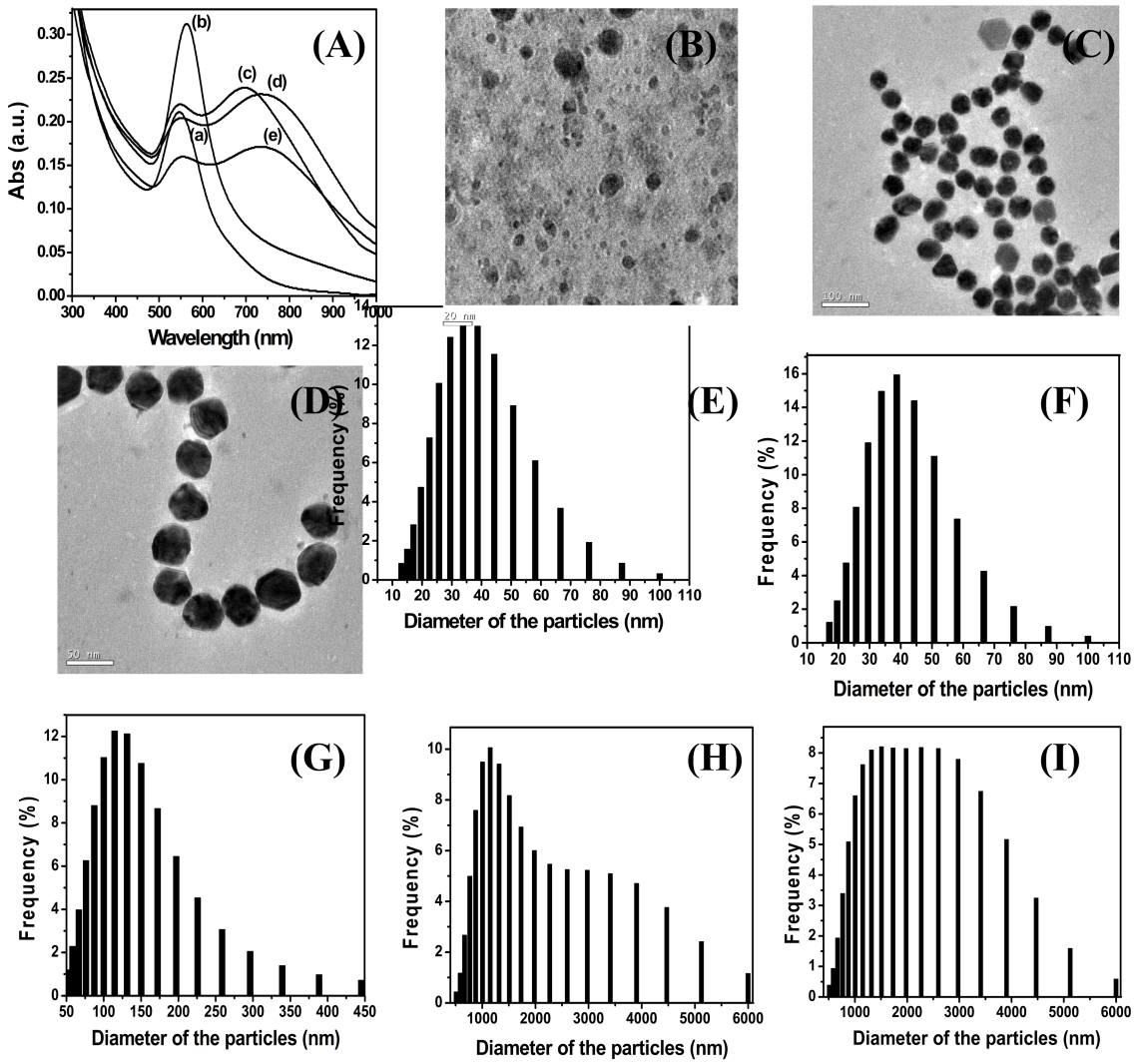


Figure 6.1.1. *(A) UV-vis spectra of Au NPs prepared with acetanilide concentrations of 7.29mM (a), 14.58mM (b), 21.87mM (c), 29.16mM (d) and 36.45mM (e) respectively. The samples were prepared using Method-I. (B) TEM picture of Au NPs from solution corresponding to (A (a)); scale bar 20 nm. (C) TEM graph of solution corresponding to (A (e)); scale bar 100 nm and (D) is an expanded view of (C); scale bar 50 nm. (E-I) Dynamic light scattering measurements of particles*

TH-777_05612211

The length of the chains increased with increasing acetanilide concentration. Also, branching of structures from a single head to several linear arrays could be observed. Interestingly, there was no formation of rods or other structures indicating that the extent of associations of NPs, which depended on the amount of acetanilide present in the medium, was responsible for the observed spectra in the present conditions.

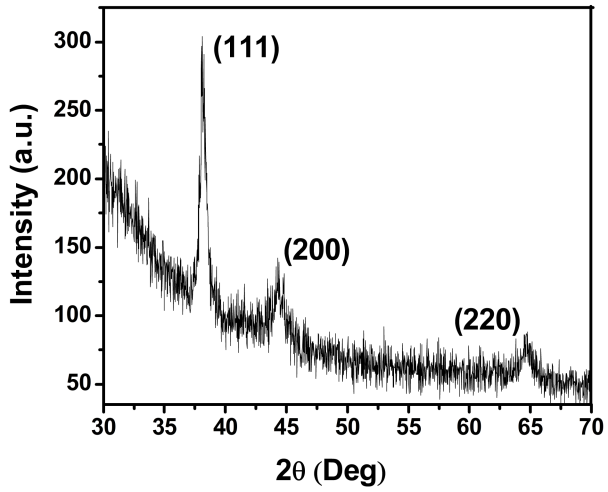


Figure 6.1.2. *X-ray diffraction pattern of evaporated solution corresponding to sample (e) prepared using Method-I.*

X-ray diffraction (XRD) measurements also indicated the formation of Au NPs in the solution (Figure 6.1.2) as well as present in the assemblies. Further, dynamic light scattering (DLS) measurements of the above solutions showed that at the lowest concentration of acetanilide the particles formed were small with 30-40 nm in average diameter (Figure 6.1.1 (E)). However, with increasing concentration of acetanilide the average sizes shifted to increasingly higher values (Figures 6.1.1 (F) - 6.1.1 (I)) of several microns. The observations indicate that in the presence of increasing amount of acetanilide longer assemblies in the medium were formed. In other words, as the acetanilide concentration was increased the number of particles involved in each assembly, which were responsible for the occurrence of the longitudinal plasmon resonance peak, had also increased. Thus with the increase of

TH-777_05612211

assembly size the longitudinal absorption maximum shifted to increasingly higher values. This is due to self-assembly of Au NPs into linear chain like arrays, where the length of the linear chain increases with increasing concentration of acetanilide (Figure 6.1.3). Also, Au NPs present in the each array were in close proximity of each other and possibly were separated by acetanilide molecular layers, which lead to the progressive shifting of longitudinal SPR peak into higher wavelength due to strong uniaxial coupling along the linear arrays[18].

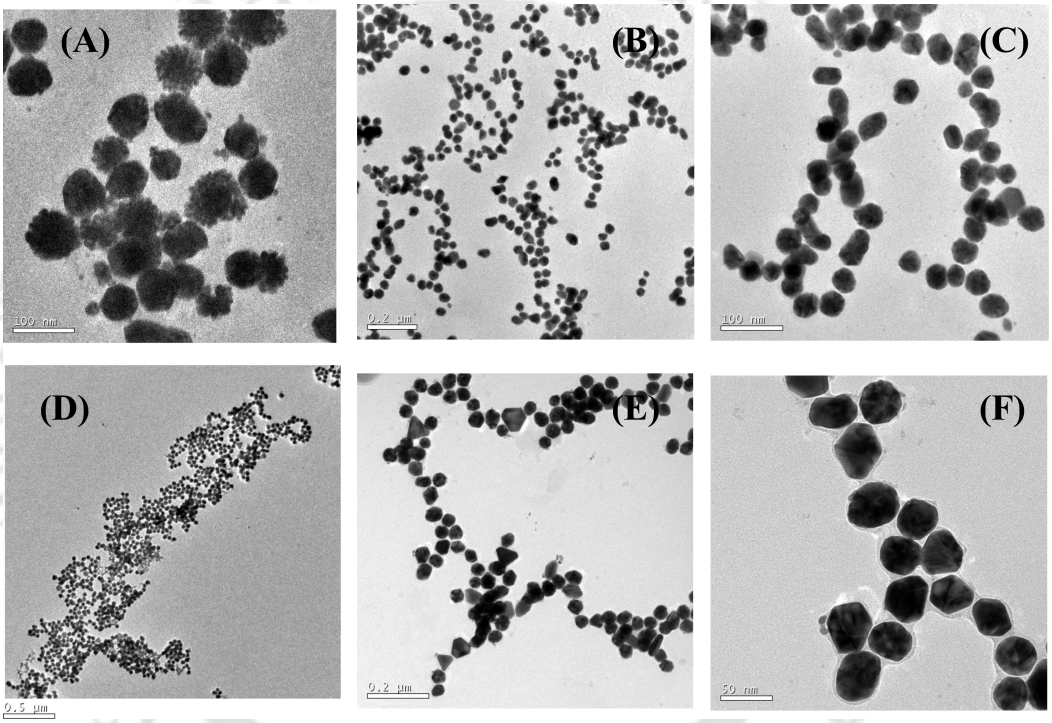


Figure 6.1.3 *Additional TEM images as obtained from samples prepared using Method-I (corresponding UV-vis spectra are shown in Figure 1 (A), in the manuscript). (A) TEM picture of Au NPs from solution corresponding to Figure 1 (A(b)), (B) TEM graph of solution corresponding to Figure 1 (A(c)). (C) is an expanded view of (B). (D) is the TEM image corresponding to the sample with absorption shown in Figure 1 (A(e)); (E) is another view taken from the same sample*

TH-777_05612211

Further, these assemblies were quite stable in the medium as simple dilutions of the samples did not dissociate. For example, when 0.5 mL of the sample corresponding to that mentioned in Figure 6.1.1 A(e) was diluted with water to 4.5 mL, the UV-vis spectrum (Figure 6.1.4 (A)) did not change other than lowering of the intensity of the bands due to dilution. However, when the diluted solution was subjected to ultrasonication for 3 h, the longitudinal peak vanished and the intensity of the transverse peak enhanced (Figure 6.1.4 (B)). TEM evidence (Figure 6.1.4 (C)) showed that the assemblies were indeed converted into individual particles.

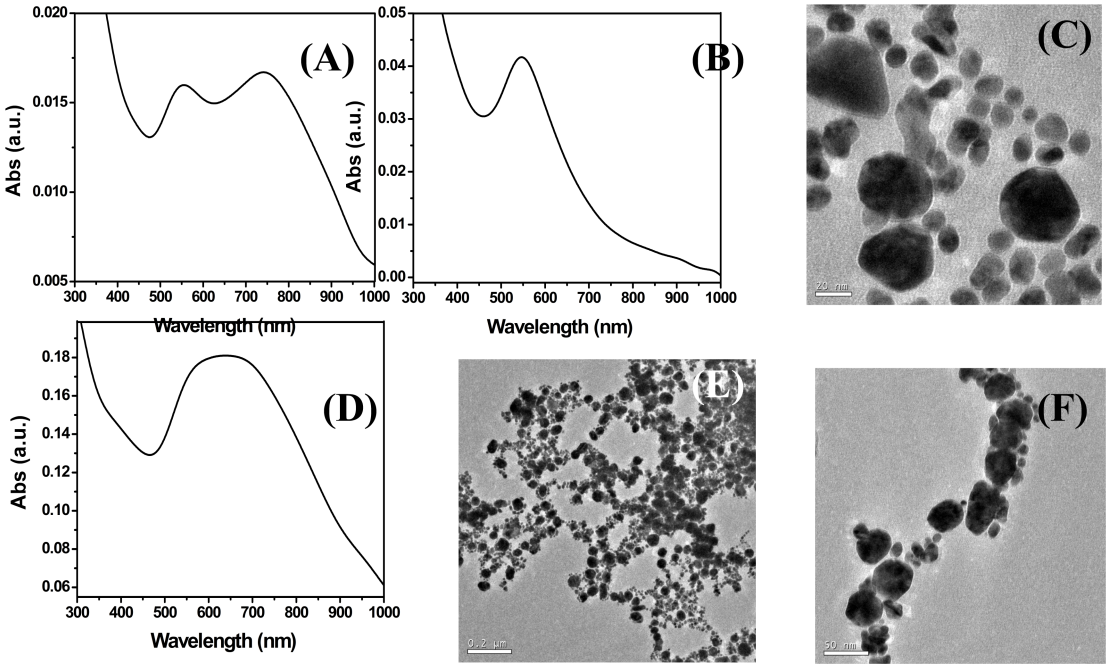


Figure 6.1.4. *(A) UV-vis spectrum of diluted solution corresponding to that in Figure 6.1.1 (A) (e)). (B) UV-vis spectrum of solution in (A) after sonication. (C) TEM picture of solution corresponding to that in (B); scale bar 20 nm. (D) UV-vis spectrum of the solution with reassembled NPs. (E) TEM picture corresponding to sample in (D; scale bar 200 nm). (F) An expanded view of (E); scale bar*

TH-777_05612211

The sizes of the disassembled particles were consistent with the original non-assembled individual particles. It may be mentioned here that when the pH of the as prepared solution (corresponding to Figure 6.1.1 (A) (e)) was changed to 8.62, there was no change in the UV-vis spectrum (Figure 6.1.5) of the assembly indicating that making the solution alkaline had no effects on the assembly. Interestingly, when the ultrasonicated solution was concentrated by centrifugation and then additional acetanilide was added, assembly formation could again be observed. The UV-vis spectrum (with the appearance of the second peak at 690 nm) and corresponding TEM image, as shown in Figures 6.1.4 (D) and 6.1.4 (E) – 61.4 (F) respectively, clearly supported the formation of reassembly.

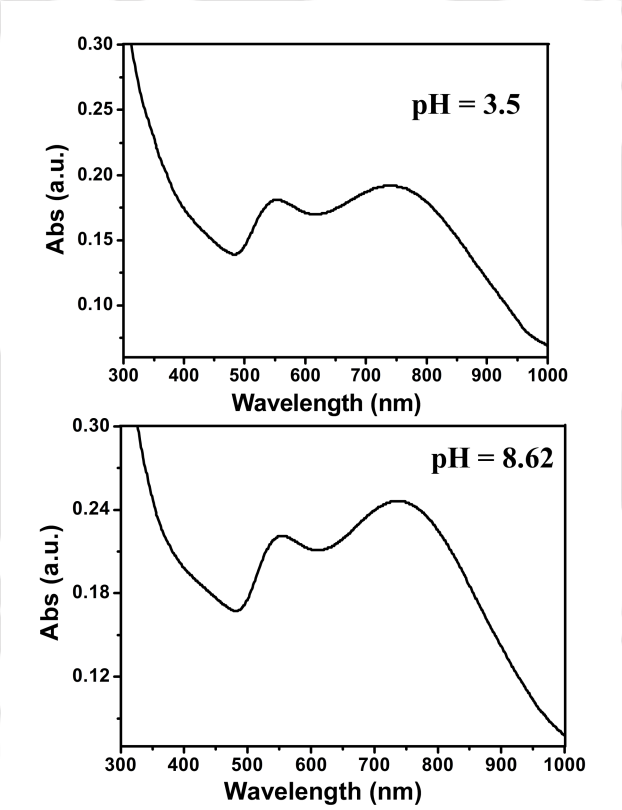
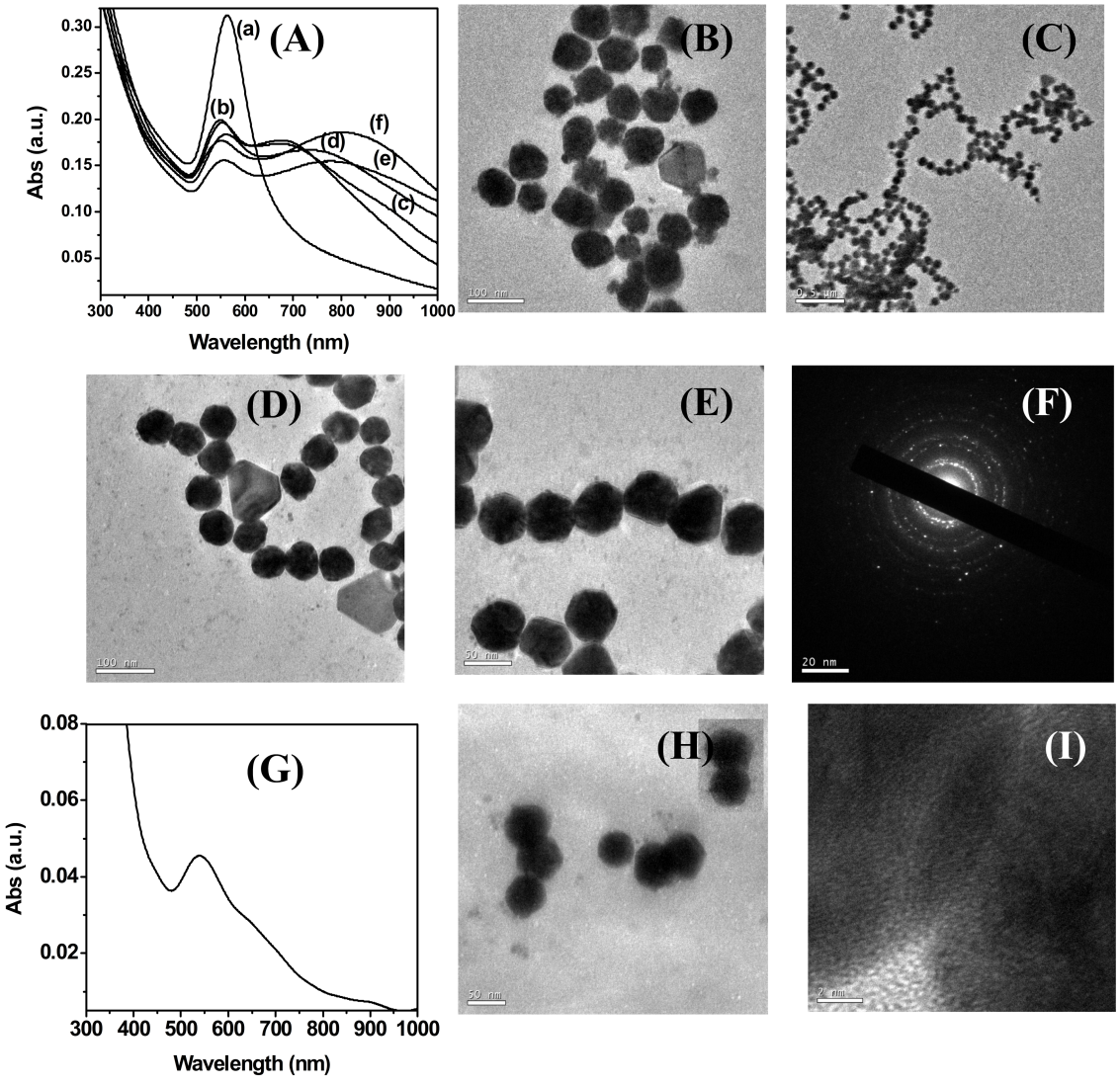


Figure 6.1.5. *UV-visible spectrum of a solution similar to that of the assembly shown in Figure 6.1.1(A) (e) corresponding to pH 3.5 and that of the same at pH 8.62*

TH-777_05612211

We have also observed that when Au NPs were synthesized with the lowest concentration of acetanilide (with the formation of spherical NPs; Figure 6.1.6 (A) (a)) and additional acetanilide was added subsequently, assembly formation could also be observed with the appearance of a characteristic second peak, at a higher wavelength, depending on the amount of additional acetanilide present in the medium (Figures 6.1.6 (A) (b)-(f)). TEM measurements (Figures 6.1.6 (B) – (F)) also indicated that the spherical NPs formed at the lowest acetanilide concentration self-assembled into superstructures upon addition of acetanilide. The self-assembled NPs could be again disassembled by dilution followed by ultrasonication as described before.



TH-777_05612211

Figure 6.1.6. *(A) UV-visible spectra of Au NPs prepared with acetanilide using Method-II. The concentrations of acetanilide in the final solutions were (a) 14.58mM, (b) 18.95mM, (c) 23.30mM, (d) 27.71mM, (e) 32.07mM and (f) 36.45mM respectively. (B) TEM picture of Au NPs from solution corresponding to (A (a)). (C) TEM picture of corresponding solution (A (e)). (D) and (E) Expanded views of (C). (F) SAED picture of Au NPs obtained from (C). (G) UV-vis spectrum of solution in (A (e)) after dilution followed by ultrasonication. (H) TEM picture of particles*

The UV-vis spectrum and TEM image of the disassembled particles are shown in Figures 6.1.6 (G) and (H) respectively. Interestingly, while the transverse plasmon resonance peak was enhanced at the end of ultrasonitation and the longitudinal peak intensity decreased substantially, however, it was persistent albeit very weak. TEM studies also indicated that there was the presence of small number of fused particles in addition to single spherical particles. A better view of the fusion is shown in the high-resolution TEM (HRTEM) image in Figure 6.1.6 (I), and which clearly demonstrates the fusion of the NPs. This indicates that during the process of self-assembly - in the presence of excess acetanilide - some of the NPs were fused while most of them remained separated by the intervening acetanilide layers. It is important to mention that when the NP-containing solution (self-assembled at higher concentration of acetanilide) was diluted and not subjected to ultrasonication there was no change in the absorption spectra for days indicating the stability of the assembly even under dilution condition.

TH-777_05612211

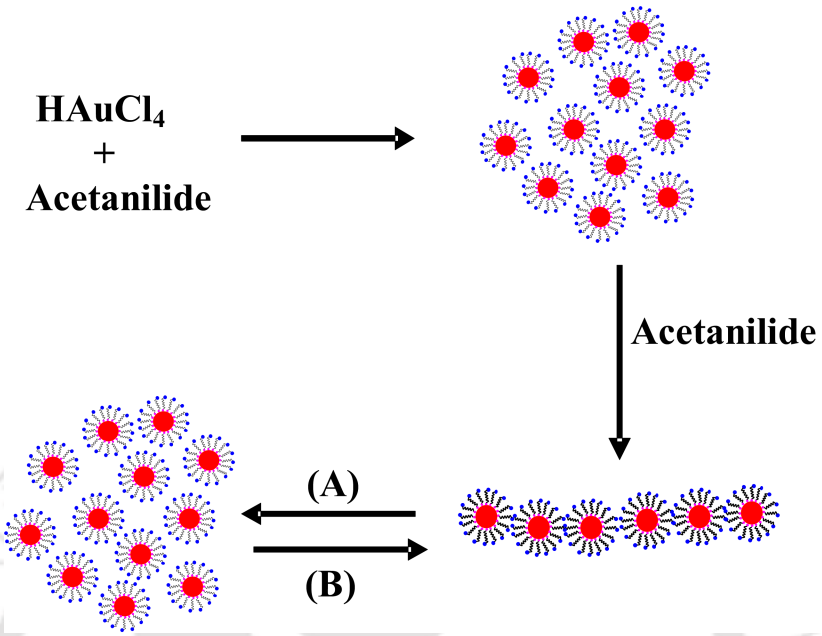


Figure 6.1.7. *A schematic representation of formation of assembly and disassembly of Au NPs using acetanilide as a mediator. Here (A) represents solution dilution followed by ultrasonication*

TH-777_05612211

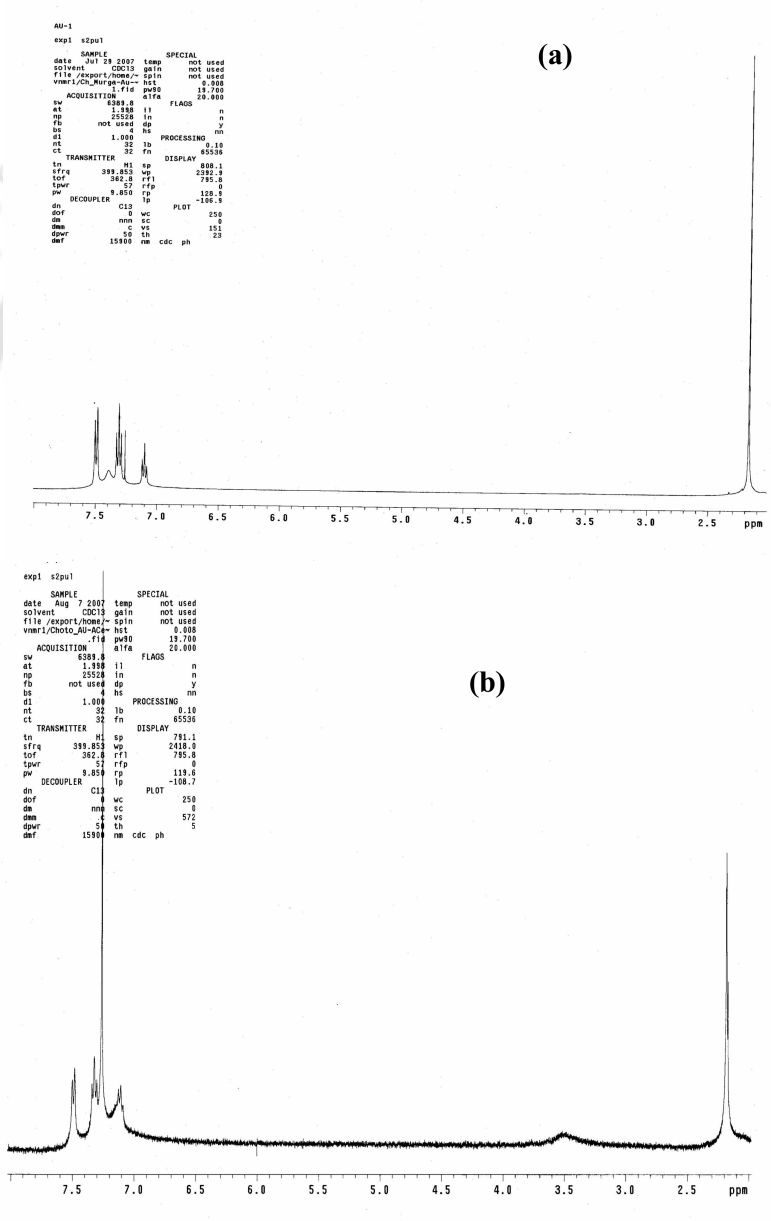
On the other hand, when the disassembled NP solution was concentrated by centrifugation and acetanilide was added, formation of self-assembly could again be observed as was evidenced by UV-Vis spectroscopy (not shown here). The overall outcome of observations of the present studies is represented schematically in Figure 6.1.7.

The above results demonstrate the formation of unusual self-assembled Au NPs in chain like arrays in the absence of any extraneous template, other than the sparingly soluble acetanilide, whose properties in aqueous solution possibly lead to the formation of the structures associated with the assemblies. The linear arrays, which are responsible for the associated uniaxial coupling of isotropic surface plasmon of the NPs, lead to the local field enhancement along the Au NPs chain, resulting in the appearance of the longitudinal band at higher wavelengths in the UV-vis spectra[19-20]. Moreover, the length of the chain-like arrays increases with the solution concentration of acetanilide thus increasing the number of NPs associated with each assembly, which in turn increases the wavelength of longitudinal excitation. Further, with increased concentration of acetanilide a number of bifurcations and enclosed loops are produced, extending the network of interconnected Au NPs chains (Figure 6.1.3). These extended network formation, while accommodating a larger number of interconnected NPs, does not lead to further change in the length of the one-dimensional arrays of NPs, which can be associated with the constant peak position related to the longitudinal plasmon resonance. In brief, at higher concentrations of acetanilide the length of the chain does not necessarily increase; they branch out instead. It is worth mentioning here that at even higher concentrations of acetanilide precipitation occurred (due to insolubility of acetanilide) thus preventing further studies in this regard.

In order to understand the formation of assemblies of Au NPs involving acetanilide, proton NMR spectra of a sample consisting of linear chain like arrays of Au NPs were recorded. The acetanilide capped Au NPs prepared using the highest concentration of

TH-777_05612211

acetanlide (36.45 mM) in Method-I was allowed to settle by keeping at room temperature for one day after its preparation.



TH-777_05612211

Figure 6.1.8. *^{1}H NMR spectrum of pure acetanilide (a) acetanilide capped Au NPs (b) dispersed*

The precipitate was collected and washed with water for five times to remove the excess, uncapped acetanilide. The excess water in the precipitate was removed by lyophilization. The powder of acetanilide capped Au NPs was then dispersed in $CDCl_3$, which was used for recording NMR spectrum. Figure 6.1.8 (a) shows the proton NMR spectrum of acetanilide. Three different types of peaks are seen in the spectrum. The peak at 2.15 *ppm* is due to methyl protons attached to the carbonyl group of acetanilide and the proton of secondary amine group attached to phenyl occurred at 7.40 *ppm*. In addition, multiple peaks appeared in the region between at 7 and 7.6 *ppm* due to aromatic protons of acetanilide. On the other hand, Figure 6.1.8 (b) shows the proton NMR spectrum of acetanilide capped Au NPs. It was observed that peak at 7.40 *ppm* of pure acetanilide (due to amine proton) had shifted to high field at 3.52 *ppm* and is possibly due to protonation in the presence of acid. Further, two singlet peaks appeared at 2.174 *ppm* and 2.185 *ppm*. One of them could be due to methyl protons of protonated acetanilide that is bound to NPs, while the other one could be due to acetic acid produced due to partial hydrolysis in the presence of acid. Thus the protonated acetanilide molecules that are bound to the surface of the Au NPs in the medium, lead to the creation of local excess cationic charge at higher concentration of acetanilide, resulting in the formation of asymmetric distribution of charge on the surface of the NPs[19]. This possibly results in the formation of dipoles involving asymmetric deposition of protonated acetanilide on the negatively charged surfaces of the NPs. In other words, when the concentration of acetanilide is gradually increased, the extrinsic dipolar interaction increases progressively; and when this interaction become strong enough to overcome the interparticles electrostatic repulsive forces, the formation of uniaxial organization of Au NPs into linear chain like array takes place. In addition, the interparticle cohesion within the chains and networks could further be reinforced by the hydrophobic moieties of benzene ring present in the surface bound acetanilide molecules providing overall stability to the arrays (Figure 6.1.8 (b)). At the lowest concentration of acetanilide it is plausible that stabilized

TH-777_05612211

NPs were well dispersed in water and thus stable individual spherical NP could be obtained. At concentrations higher than the solubility at room temperature (1 mg mL^{-1}), the individually stabilized NPs that were produced at boiling conditions, would self-assemble when cooled to room temperature. In this way self-assembly into linear or other superstructures would be more stable at higher concentrations of acetanilide. Thus the formation of necklace-like chains of NPs could be possible. The molecular forces responsible for the association prevents the breakage of the structures under simple dilution as the interaction between the NPs and protonated acetanilide may be higher than the one provided by the solvent to the stabilized NPs. On the other hand, when the solution is diluted and subjected to ultrasonication these structures break into single particles as the forces holding the assembly may not be sufficient enough to survive the energy of ultrasonic waves, favoring reformation of spherical Au NPs surrounded by protonaed acetanilide, which is already at lower concentration (due to dilution of the original solution).

6.1.4 Conclusion

In a nutshell, we have presented a facile way of using 'soft interactions' in the formation of assembly and disassembly of Au NPs stabilized by sparingly soluble acetanilide in water, and with controllable optical properties of the assembly by tuning the concentration of the stabilizing agent alone. This is different from all previous methods where the concentration of the parent salt or additional reagent (seed) was used as the control parameter in generating the assembly. Further investigations are needed to understand the complete mechanism of assembly and disassembly formations and applications. Also, another important application of the assembled NPs, which is systematic generation of Au NPs-polyaniline composite from the different assemblies, will be reported subsequently. The present work hopefully would not only pave the way for molecular tuning of nanoparticle assembly but also systematic generation of hybrid assemblies with controllable material properties.

TH-777_05612211

6.1.5. References

1. Kalsin, A. M.; Fialkowski, M.; Paszewski, M.; Smoukov, S. K.; Bishop, K. J. M.; Grzybowski, B. A. *Science* **2006**, *312*, 420.

2. Leunissen, M. E. ; Christina, G. C. ; Antti-Pekka, H.; Royal, C. ; Alfons, V. B. *Nature* **2005**, *437*, 235.

3. Jackson, A. M.; Hu, Y.; Silva, P. J.; Stellacci, F. *J. Am. Chem. Soc.* **2006**, *128*, 11135.

4. Tang, Z. Y.; Kotov, A. N. *Adv. Mater.* **2005**, *17*, 951.

5. Li, H.; Park, S. H.; Reif, H. R.; LeBean, T. H.; Yan, H. *J. Am. Chem. Soc.* **2004**, *126*, 418.

6. Taton, A. T.; Mirkin, C. A.; Letsinger, L. R. *Science* **2000**, *289*, 1757.

7. Storhoff, J. J.; Lazarides, A. A.; Music, C. R.; Mirkin, C. A.; Letsinger, R. L.; Schatz, G. C. *J. Am. Chem. Soc.* **2000**, *122*, 4640.

8. Jin, R.; Wu, G.; Li, Z.; Mirkin, C. A.; Schatz, G. C. *J. Am. Chem. Soc.* **2003**, *125*, 1643.

9. Liu, J.; Lu, Y. *J. Am. Chem. Soc.* **2003**, *125*, 6642.

10. Liu, J. ; Lu, Y. *J. Floures.* **2004**, *14*, 343.

11. Kim, Y.; Johnson, C. R.; Hupp, J. T. *Nano Lett.* **2001**, *1*, 165.

12. Jung, Y. J. ; Lee, K-B.; Kim, Y-G.; Choi, I. S. *Angew. Chem. Int. Ed.* **2006**, *45*, 5960.

13. Tian, L.; Shi, C.; Zhu, J. *Chem Commun*. **2007**, *37*, 3850.

14. Mallia, V. A.; Vemula, P. K.; John, G.; Kumar, A.; Ajayan, M. P. *Angew. Chem. Int. Ed*. **2007**, *46*, 1.

15. Warner, M. G.; Hutchison, J. E. *Nat. Mater*. **2003**, *2*, 214.

16. DeVries, G. A.; Brunnbauer, M.; Hu, Y.; Jackson, A. M.; Long, B.; Neltner, B. T.; Uzun, O.; Wunsch, B. H.; Stellacci, F. *Science* **2007**, *315*, 358.

17. Wang, G.; Murray, R. W. *Nano Lett.* **2004**, *4*, 95.

18. Lin, S.; Li, M.; Dujardin, E.; Girard, C.; Mann, S. *Adv. Mater.* **2005**, *17*, 2553.

TH-777_05612211

19. Liao, J.; Zhang, Y.; Yu, W.; Xu, L.; Ge, C.; Liu, J.; Gu, N. *Colloid and Surface A*. 2003, *223*, 177.

20. Shipway, A. N.; Lahav, M.; Gabai, R.; Willner, L. *Langmuir* **2000**, *16*, 8789.

6.2 Surface Area Controlled Differential Catalytic Activities of One Dimensional Chain-Like Arrays of Gold Nanoparticles

6.2.1 Introduction

In the previous section, acetanilide molecule was used to synthesize Au NPs and their subsequent formation of self assembly. However, the method inherently limits the organization of NPs in terms of choice of constituent particle sizes. This could be avoided by organization of presynthesized NPs (by using other known reagents and stabilizers) using acetanilide for organization only. Herein we report the use of sparingly soluble acetanilide to organize citrate stabilized Au NPs into 1D chain-like array of superstructures in water. Interestingly, the extent of organization i.e. the length or branching of arrays could be controlled by the concentration of acetanilide. Our observations suggest that the presence of strong electric dipole coupling on the surface of Au NPs along with reduction of electrostatic repulsion forces between the citrate stabilized Au NPs - by introducing protonated acetanilide - facilitated the formation of linear superstructures. More interestingly, the organized Au NPs were catalytically active and the extent of activity depended on the level of organization. The catalytic activities were tested by reduction of 4-nitrophenol (4NP) into 4-aminophenol (4AP) using excess sodium borohydride. The effective surface areas of the

TH-777_05612211

Au NPs in the organized assemblies were then calculated from the rate constants of the above reactions. The results indicate that the effective surface area for catalysis decreased linearly with the concentration of acetanilide. The present experimental observations also indicate that the assembled NPs were fused together in the presence of excess borohydride, which also contributed towards the reduction of effective surface areas.

6.2.2. Experimental Section

Material

Hydrogen tetrachloroaurate ($HAuCl_4$, 17 % Au in HCl as purchased from Sigma Aldrich), tri sodium citrate (99% from Merck), acetanilide (99 %, from Merck), sodium borohydride ($NaBH_4$, 95 %; Merck), and 4-nitrophenol (95 %; Merck) were used as received without further purification. Milli-Q grade water was used in all the experiments.

Table 6.2A. *The different concentrations of acetanilide added into citrate capped Au NPs.*

Amount of acetanilide in 10 mL water (mg)	Concentration of acetanilide in 10 mL water (mM)	Con of acetanilide after mixing 1 mL citrate ion capped Au NPs. (mM)
5.0	3.7	3.2
7.5	5.5	4.8
10.0	7.4	6.4
12.5	9.2	8.0
15.0	11.1	9.7
17.5	13.0	11.3
20.0	14.8	13.0
22.5	16.6	14.5
25.0	18.5	16.2

TH-777_05612211

27.5	20.3	17.7
30.0	22.2	19.4

Synthesis of citrate stabilized Au NPs

Typically, 15.0 mg of trisodium citrate was added to 50 mL water in a 100 mL conical flask and the mixture was stirred under ice-cold conditions, followed by the addition of 600.0 μL of 17.3 mM of $HAuCl_4$. 1.2 mL of freshly prepared 10.0 mM sodium borohydride solution was slowly added to the reaction mixture under stirring condition. Finally, the stopper was tightly closed and the stirring was continued for 2 hrs more under the same condition. After 2 hrs, the color of the solutions appeared ruby-red, indicating formation of Au NPs. The pH of the solution was found to be 4.0.

TH-777_05612211

Preparation of acetanilide solution

A given amount of acetanilide was added to 10 mL water and this mixture was heated at 90^{o}C to dissolve all the solid acetanilide. Finally, the solution was brought to room temperature. The final pH of the solution was made to be 3.0 by addition of 20 µL of 0.226 M HCl to the mixture. The amount of acetanilide and final concentration of acetanilide for various mixtures are given in Table 6.2A.

Mixing aqueous acetanilide with citrate capped Au NPs

Several samples of 1.0 mL of the above citrate ion capped Au NPs solution (2.477 X 10^{15} particles / L) were taken in 30 mL vials. Aqueous acetanilide solutions of different concentrations were slowly added to different vials containing the Au NPs. The mixtures were kept at room temperature for 30 min. The final pH values of the solutions were measured to be 3.5. The solutions were used for all studies. The final concentrations of acetanilide in the above solutions are given in Table 6.2A. Precipitation was observed when the concentration of acetanilide in the solution exceeded 16.2 mM. However, in all the other solutions containing lower amount of acetanilide, no visible precipitation could be observe even after a day.

Catalytic study

Catalytic studies were performed within 2 hrs of addition of aqueous acetanilide to citrate capped Au NPS solutions. 100.0 µL of each of the Au NP (2.477 X 10^{14} particles/L) solutions containing acetanilide were added to 2.5 mL solution containing freshly prepared 10.0 mM of sodium borohydride and 0.1 mM of 4NP solution. The mixture was shaken once for thorough mixing and then kept in the sample compartment of a UV-vis spectrophotometer. Time dependent UV-vis absorption was recorded at 400 nm. The studies were performed at room temperature.

TH-777_05612211

Characterization study

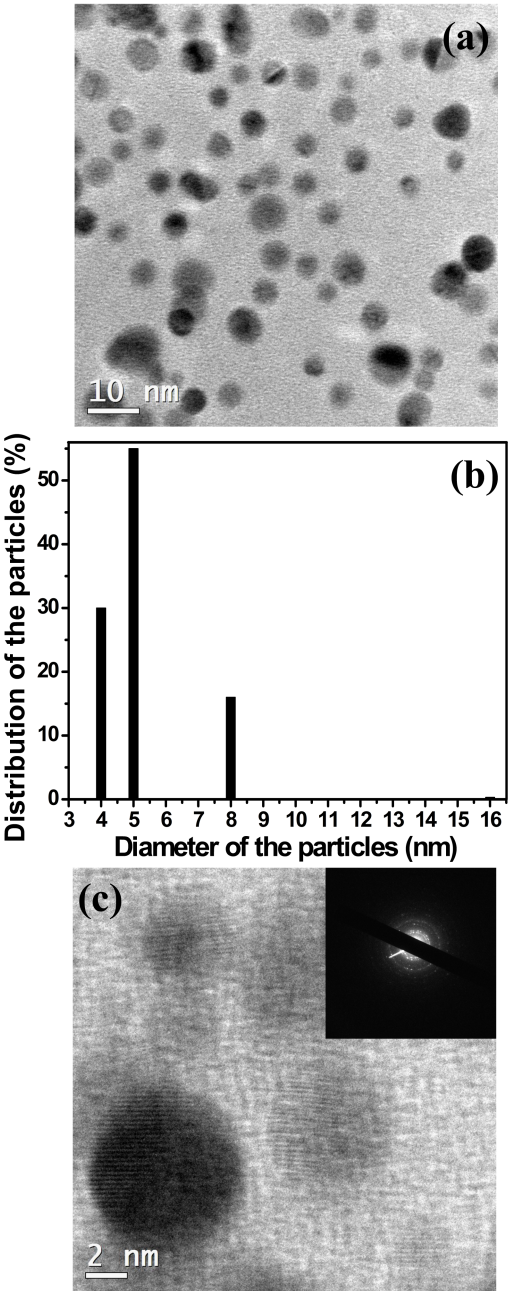
UV-vis absorption spectra of the samples were recorded, using a Hitachi model U-2800 or Perkin Elmer model Lambda 35 UV-visible spectrophotometer, in the range of 300 to 1100 nm. FT-IR spectra of the pure acetanilide and acetanilide treated citrate capped Au NPs were measured using a Perkin-Elmer Spectrum One spectrometer. For acetanilide treated citrate stabilized Au NPs, the following procedure was followed for sample preparation. After addition of acetanilide (19.4 mM) into citrate ion capped Au NPs, the solution was subjected to centrifugation at 15000 rpm and at 20^{o}C. The pellet was washed with water. The cycle was performed thrice before collecting the pellet, which was air-dried and then mixed with KBr to record FTIR spectrum. Similarly, solid acetanilide was mixed with KBr to make a pellet for FTIR measurement. FTIR spectra were recorded in the region of 4000-400 cm^{-1}. TEM measurements were performed using a JEOL-2100 equipment operating at an acceleration voltage of 200 kV. The TEM samples were prepared by placing a drop of liquid on carbon coated copper grid (400 mesh) followed by evaporation of the solvent at room temperature.

6.2.3 Result and Discussion

Citrate stabilized Au NPs prepared by sodium borohydride method in the presence of trisodium citrate, produced particles with uniform sizes. TEM image, shown in Figure 6.2.1 (a) indicated the formation of spherical particles with average diameter 5.0 $\pm$ 1.7 nm (Figure 6.2.1 (b)). A high resolution TEM (HRTEM) image, which is shown in Figure 6.2.1 (c) indicates that the particles were in spherical in nature. The UV-vis spectrum of the Au NPs consisted of a single peak with maximum at 527 nm, which is characteristic of spherical Au NPs. Addition of aqueous solution of acetanilide into citrate ion capped Au NPs (2.48 X 10^{15} particles / L) led to change in color of the solution from red to pale pink and finally to blue with progressive increase in the concentration of acetanilide. Figure 6.2.2 shows the UV-vis spectra of Au NPs in the presence of various concentrations of acetanilide. The spectra were recorded 30 min after addition of acetanilide. As is evident from the figure, the

TH-777_05612211

spectrum consisted of a single peak at 527 nm at the lowest concentration of acetanilide (3.2 mM).



TH-777_05612211

Figure 6.2.1. *(a) Transmission electron micrograph (TEM) of citrate capped Au NPs prepared by sodium borohydride method. (b) Histogram of particle size distribution of citrate ion capped Au NPs. (c) High resolution TEM (HRTEM) picture of a few particles shown in (a) and the inset in (c) is the selected area electron diffraction pattern of the particles.*

When the concentration was increased broadening of the peak started to occur until the concentration was 6.4 mM. However, upon further addition of acetanilide (8.0 mM - 11.3 mM) a second peak appeared at 650 nm, as a shoulder to the first peak. On the other hand, when acetanilide concentration was further increased to 13.0 mM or higher a clear second peak at 700 nm appeared in addition to a slightly red-shifted first peak at 535 nm. The results thus indicate that addition of excess acetanilide led to appearance of a peak due longitudinal SPR. Further, the peak due to the transverse SPR of Au NPs was not affected much by the change in concentration of acetanilide. The results also imply that at increasing concentrations of acetanilide, the number of Au NPs involved in the linear assembly formation increased progressively. However, after a certain concentration of acetanilide no change in the peak due to longitudinal SPR could be observed. This may be due to additional Au NPs that might not be available for increasing the length of the assembly. The results indicate that the particles were self-assembled into unidirectional chain-like array of superstructure, which is responsible for the formation of longitudinal SP band at higher wavelength owing to the strong uniaxial coupling along the linear array.[1]

TH-777_05612211

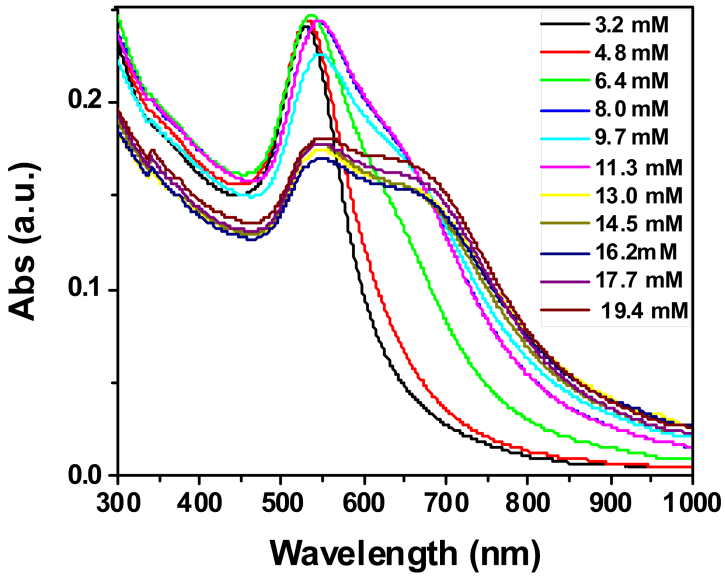


Figure 6.2.2. *The UV-Visible spectra of citrate capped Au NPs with different concentration of acetanilide. The numbers in the inset table indicate the concentration of acetanilide in the medium.*

Further, in order to understand the formation of self-assembly of Au NPs, TEM measurements were carried out from samples containing citrate capped Au NPs with different concentrations of acetanilide.

TH-777_05612211

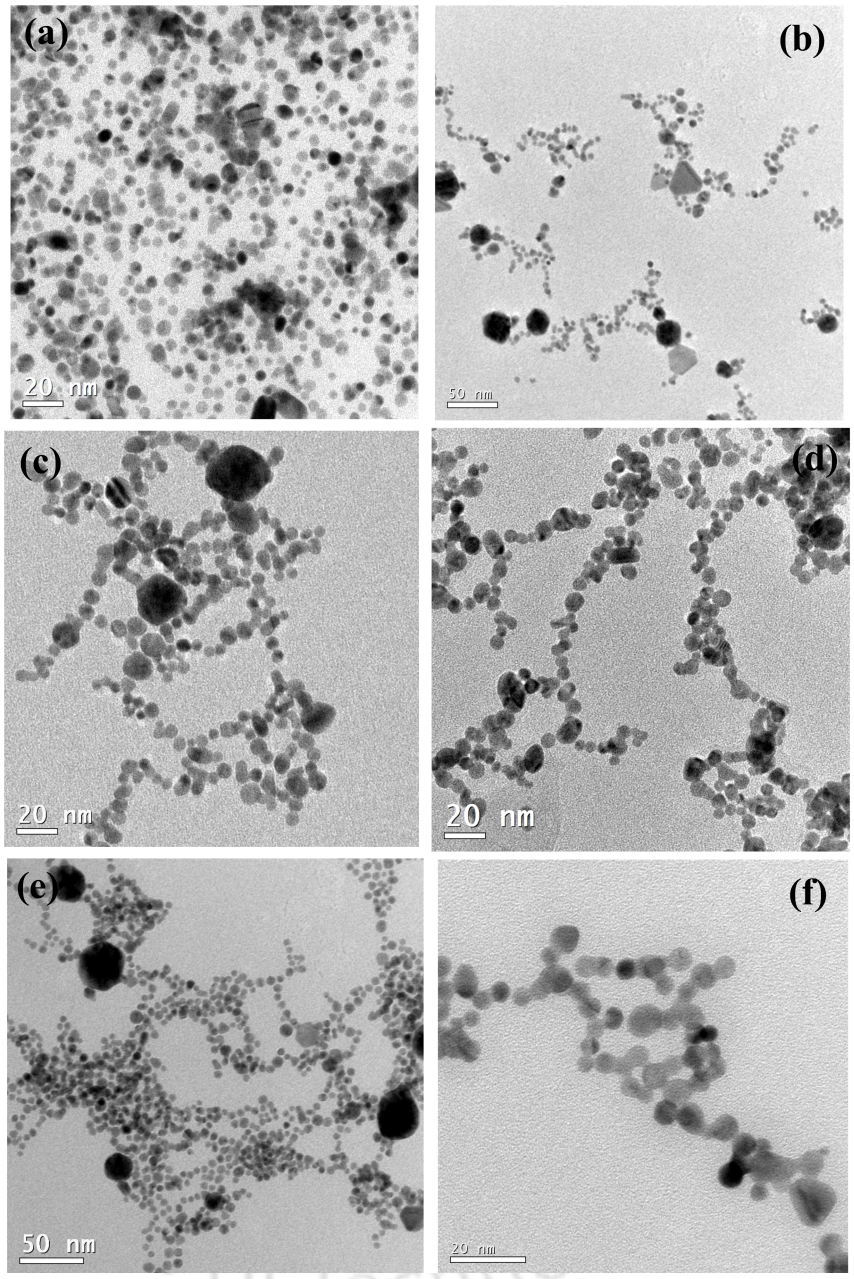


Figure 6.2.3. *TEM images of citrate capped Au NPs in the presence of different concentration of acetanilide. The concentrations of acetanilide in the samples were as follows: (a) 3.2 mM, (b) 4.8 mM, (c) 9.7 mM, (d) 13.0 mM and (e) and (f) 19.4 mM.*

The results are shown in Figure 6.2.3. At the lowest concentration of acetanilide, the particles were dispersed rather uniformly in the medium without any major orderly arrangement other than evaporation induced aggregation of Au NPs (Figure 6.2.3 (a)).

TH-777_05612211

However, at increased concentrations of acetanilide formation of linear arrays could be observed (Figures 6.2.3 (b), 3 (c) and 3(d)). The results suggest that the length of the assemblies increased with the increase in concentration of acetanilide For example, at 4.8 mM - 9.7 mM acetanilide concentrations the assemblies were typically of 50-150 nm in length, whereas at 19.4 mM the lengths were more than 100 nm. It is also interesting to note that at higher concentrations the branching of the arrays was more prominent than further increase in the length of the assembly. For example, at 6.4 mM concentration of acetanilide, 77% of the assemblies were linear, while the rest were branched assemblies (Figure 2.2.5A; Appendix I). On the other hand, at 19.4 mM of acetanilide 80% branched assemblies were present, while the number of linear assemblies was reduced to 20%. The details of concentration dependent branch formation are given in Table 6.2B.

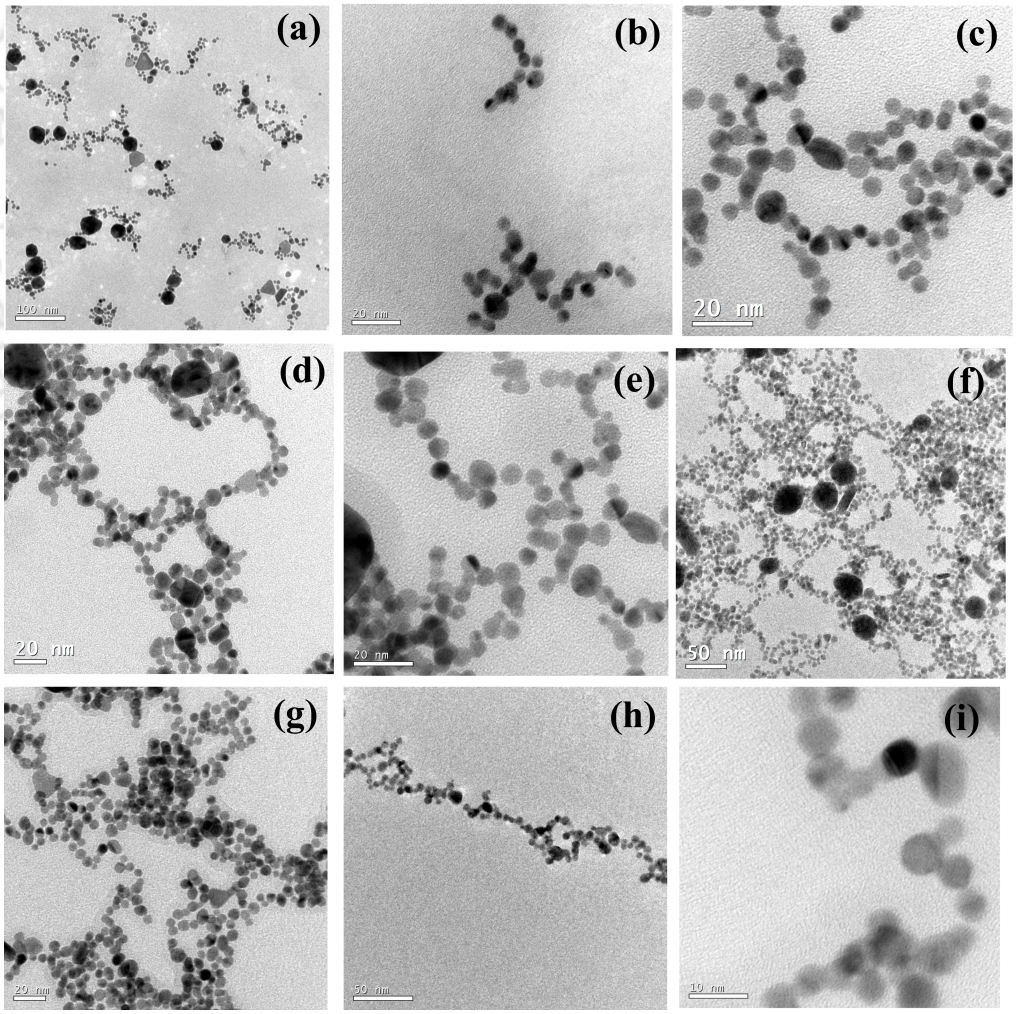
***Table 6.2B**. Branching of linear assemblies of Au NPs in the presence of increasing concentration of acetanilide. Refer to Appendix-II.*

Concentration of acetanilide (mM)	Linear chains (%)	Branches (%)
3.2	-	-
6.4	77	23
9.7	53	47
19.4	20	80

Additionally, at higher acetanilide concentrations formation of loops from the extended arrays could also be observed. That led to the formation of interconnected networks of particle assemblies (Figures 6.2.4 (e) and (f)). HRTEM measurements indicated that the organization of NPs by excess acetanilide led to linear superstructures consisting of fused

TH-777_05612211

and non-fused particles. The number of fused particles and non-fused particles had no apparent correlation with the concentration of acetanilide present in the medium. Further, in order to understand the role of the acetanilide molecules on the assembly formation, FTIR spectroscopic measurements of acetanilide treated citrate capped Au NPs (Figure 6.2.5 (b)) were carried out. The broad peak in the region of 1647 cm^{-1} is due to the characteristic peak of amide-I stretching vibration. The low intensity peak around 1547 cm^{-1} is attributed to the amide-II, N-H band. Besides that, additional peaks that appeared in the region of 1500 cm^{-1} and 1600 cm^{-1} correspond to the aromatic ring and a broad peak in the region of 3300-3400 cm^{-1} is due to the N-H stretching vibration.



TH-777_05612211

***Figure 6.2.4**. TEM images of citrate ion capped Au NPs treated with different concentrations of acetanilide. The concentration of acetanilide for the sample in (a) and (b) was 4.8 mM, (c), (d) and (e) was 13.0 mM, and (f), (g), (h) and (i) was 19.4 mM. (b) is an expanded version of (a); (d) and (e) are expanded views of (c) and (g), (h) and (i) are expanded views of (f).*

Further, it has been proposed that the peaks at 1500 cm^{-1} and 1600 cm^{-1} could be due to symmetric and asymmetric deformations of protonated –NH group of acetanilide.[2a] The result implies that acetanilide molecules were bound to the surfaces of the Au NPs. In an earlier set of experiments (refer to previous section) we have observed that Au NPs could be generated by reaction of acetanilide with $HAuCl_4$, followed by formation of linear superstructures in the form of assembled Au NPs.[2b] However, that method produced Au NPs with broad size distribution, which could not be used effectively for surface area controlled catalytic activity studies. Interestingly, the results also support the stabilization of Au NPs by acetanilide. Proton NMR studies of the acetanilide stabilized Au NPs revealed that protonation of acetanilide in the stabilized Au NPs.[2b] This is reasonable considering the fact that the medium in the experiments was acidic.

TH-777_05612211

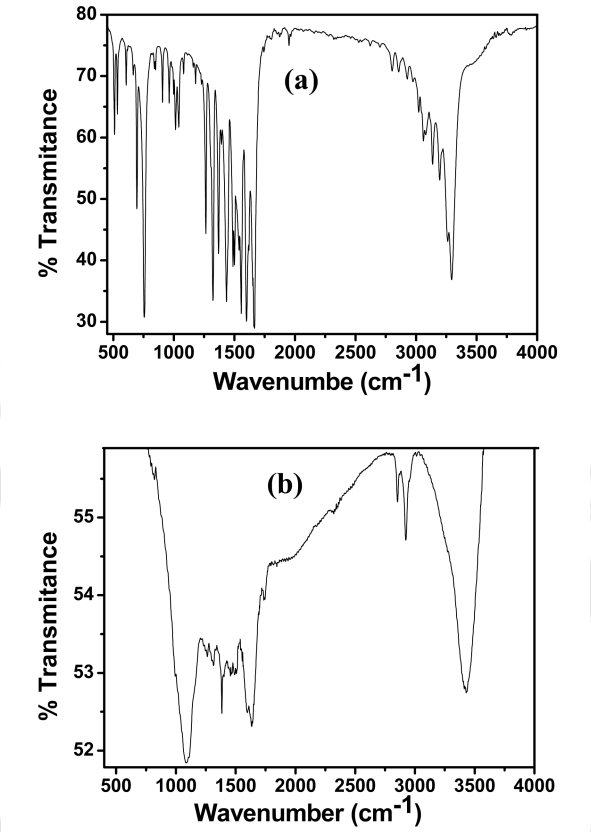


Figure 6.2.5. *FTIR spectrum of acetanilide (a) and (b) is that of the citrate stabilized Au NPs treated with acetanilide.*

The above results demonstrate that protonated acetanilide organized citrate stabilized Au NPs into linear superstructures. It is interesting to note that Au NPs even though stabilized by citrate could be organized by acetanilide in the acidic medium. The negatively charged citrate stabilized Au NPs may interact with positively charged protonated acetanilide leading to structures that would favor strong dipolar coupling for extending the structures. This in turn may lead to the formation of linear superstructures via orientation of the dipoles. At higher acetanilide concentrations the formation of branched structures would be favored as the Au NPs being symmetrical in nature may constitute multiple nucleation centers from the same particles into different direction. The particle would then act as the nucleation head of the branched structures. It is important to mention here that van der

TH-777_05612211

Waals interaction between the benzene rings of acetanilide may also play a critical role in the formation of organized assembly.[3-4] According to the Lin et al, [5] the formation of 1-D superstructure of the Au NPs is favored by the spatial portioning of the citrate/MEA (2-mercaptoethonol) on the Au NPs surface. Their conclusion was that the presence of mixed citrate/MEA stabilization shell is a prerequisite for the uniaxial organization of Au NPs into short chains by inducing extrinsic dipolar interactions. On the other hand, Wang et al[6] reported that formation of permanent electric dipole moment among the Au NPs may originate from the non-uniform distribution of the stabilizers on the surface of the NPs due to the different crystallographic faces present on the Au NPs. This could possibly be a reason for uniaxial organization. In the present scenario addition of acetanilide into citrate capped Au NPs may partially remove capping molecules (citrate ions) which would be replaced by protonated acetanilide molecules. The preferential replacement could be decided by the nature of faces present on the crystal.[2a] This would lead to the formation of a dipole which may cause preferential alignment of neighboring Au NPs. At higher acetanilide concentrations, the dipolar interaction alone may not be prominent.[7] However, pi-pi interactions between the benzene rings could possibly lead to aggregation in the form of branched head.

We were further interested in finding the catalytic activities of the assemblies formed under different acetanilide concentrations. This could possibly shed light on the available catalytically active surface area of Au NPs in an assembly and its variations across the assemblies. We have chosen a well-known reaction involving reduction of 4NP to 4AP by sodium borohydride,[8] catalyzed by Au NPs present in different assemblies generated in the present experimental conditions. Also, as the reduction of 4NP by excess $NaBH_4$ is negligible in comparison to that in the presence of Au NPs, the catalysis could be followed quantitatively. Further, since the concentration of borohydride was used in excess, the reaction could be considered pseudo first-order with respect to the concentration of 4NP. The rate equation can be written as[9]

TH-777_05612211

(1)

Here, k_{app} is the apparent rate constant, which can be assumed to be proportional to the total available surface area(s) of assembled Au NPs (per unit volume of the reaction mixture). C_t is the concentration of 4NP at time t, and k is the rate constant normalized to the surface area (*s*) of the Au NPs. The conversion of 4NP into 4AP was measured by the time-dependent decay of absorbance at 400 nm. It is worth pointing out here (as mentioned before) that appearance of the absorbance maximum at 400 nm is due to the formation of 4-nitrophenolate ion, which occurred immediately after addition of $NaBH_4$ to the system.[10]

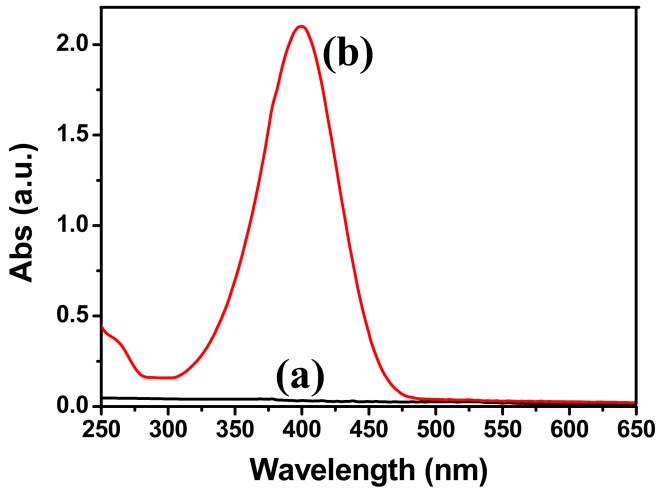


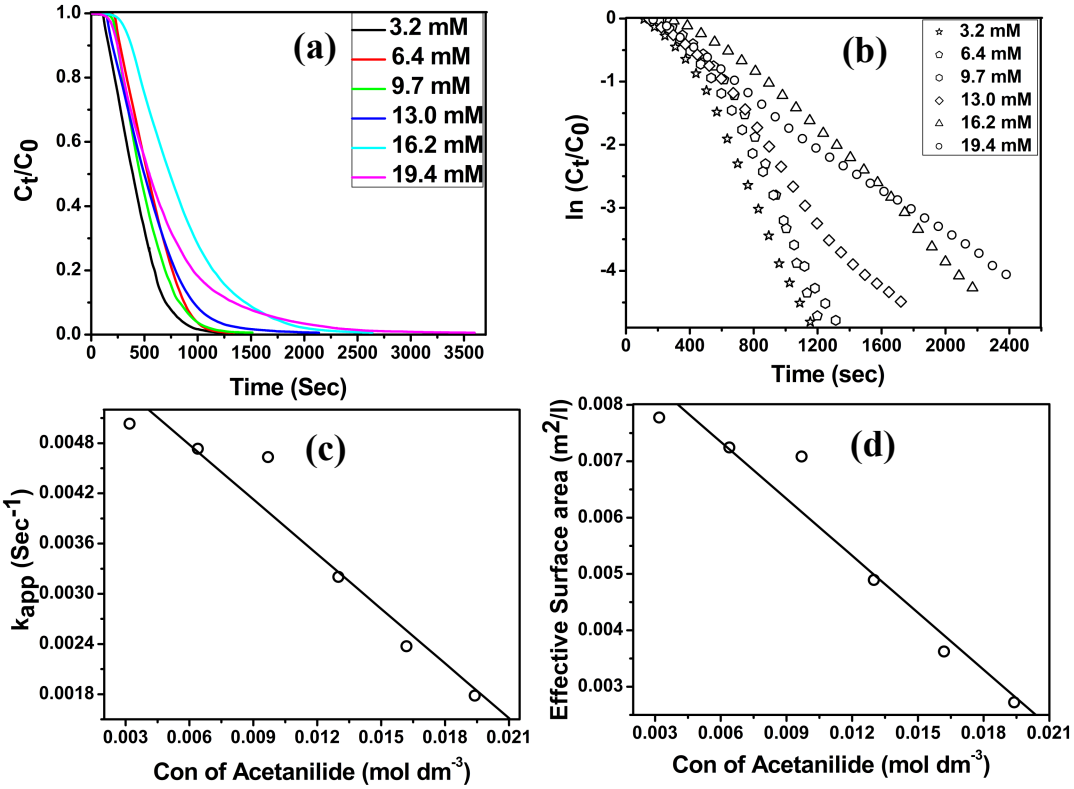
***Figure 6.2.6**. Absorption spectra (a) of Au NPs ((2.477 X 10^{14} particles/L)) in the presence of $NaBH_4$*

TH-777_05612211

Further, since the amount of Au NPs used for catalysis in all the samples was small (significantly diluted from the original sample), the absorption due to them in the region of probe was negligible and hence did not interfere with the present set of studies. The UV-vis spectra of diluted Au NPs (with concentration being same as that in the catalysis media) treated with $NaBH_4$ and that of the same after addition of 4NP are shown in Figure 6.2.6. The results clearly demonstrate the fitness of the present method of following decay kinetics of 4NP using UV-vis spectroscopy, in the presence of very small quantities of Au NPs. Since the absorbance of 4NP is proportional to its concentration in the medium, the ratio of absorbance at time t (A) to that t = 0 (A_o), i.e. A/A_0, could be used as the ratio of concentration of 4NP at time t to that at t_0 (i.e., $A/A_o = C/C_o$). As shown in Figure 4a, the logarithm of rate of decrease in the concentration of 4NP is close to being linear with time indicating first order decay. This is true for all the samples. However, what is interesting to note is that the rate of decay of concentration of 4NP was related to the amount of acetanilide that was originally present at the time of formation of assembly; the higher was the concentration the slower was the rate of decay. Moreover, in some of the reactions the presence of induction period was apparent, which could be due to time taken for the activation of catalyst (assembled Au NPs). Similar behavior with NP catalyst has been observed previously by other groups.[11] It is important to remember that at the time of formation of assembly as well as for the catalysis studies the total number of Au NPs was constant (2.48×10^{14} particles/L). This means the rate of decay of 4NP was directly related to the nature of assembly formed in the medium. The longer was the assembly or higher was the number of branched assemblies, the slower was the rate of decay of 4NP. For example, when the acetanilide concentration was 3.2 mM the reaction was over in 1275 s. However when the concentrations were 6.4 mM, 9.7 mM, 13.0 mM, 16.2 mM and 19.4 mM the times of reaction completion were 1342 s, 1513 s, 2138 s, 2634 s and 3600 s respectively. The results are shown in Figure 6.2.7 (a). The results indicate a linear dependence of k_{app} on the concentration of acetanilide (Figure 6.2.7 (b)). The results shown in Figures 6.2.7 (b) and 6.2.7 (c) were further used to calculate the effective surface areas of assemblies that were

TH-777_05612211

involved in the catalysis. The individual graphs were subjected to linear fit for obtaining a value of K_{app}. The surface areas were then calculated using equation (1). In order to pursue this, the particle sizes of the sample with as-prepared citrate stabilized Au NPs were taken as 5.0 nm and particles were assumed to be spherical. The total surface area of all the particles present in the medium was then calculated (Appendix II). This provided a value of rate constant (k) which was found to be 0.6532 m^{-2} L s^{-1}. It may be pointed out here that when the experiments were carried out in absence of acetanilide but by diluting the Au NPs as above, the rate of the reaction was slower. For example, instead of adding 7.0 mL of acetanilide at different concentrations, 7.0 mL of water was added into the citrate ion capped Au NPs (pH 3.5).



TH-777_05612211

Figure 6.2.7*. (a) The normalized decay of 4NP absorbance with time at 400 nm catalyzed by Au NPs in different assemblies. The numbers in the panel indicate the concentration of acetanilide. (b) Plot of ln (Ct/C_0) of 4NP with time. The numbers in the inset indicate the concentration of acetanilide in the medium. (c) The plot of apparent rate constant with different concentration of acetanilide and (d) is plot of effective surface area versus acetanilide concentration.*

TH-777_05612211

The resulting Au NPs were then subjected to the catalytic reduction of 4NP into 4AP under the same condition. The rate of the reaction was found to be slower than that with the one treated with 3.2 mM acetanilide prior to catalysis (with the same total Au NPs per volume). A comparison of the catalytic decay of 4NP by Au NPs in the absence and presence of 3.2 mM acetanilide, shown in Figure 6.2.8, clearly indicate the difference in the catalytic decay rate. TEM results indicate that at the reaction pH (i.e. at 3.5) considerable agglomeration of the Au NPs (in absence of acetanilide) took place thereby reducing the effective surface area for catalysis (Figure 6.2.9). In brief, the presence of acetanilide provides an easy control of reaction surface area in the form of linear assemblies of the Au NPs, whereas in absence of the same the Au NPs agglomerated into lumps of particles.

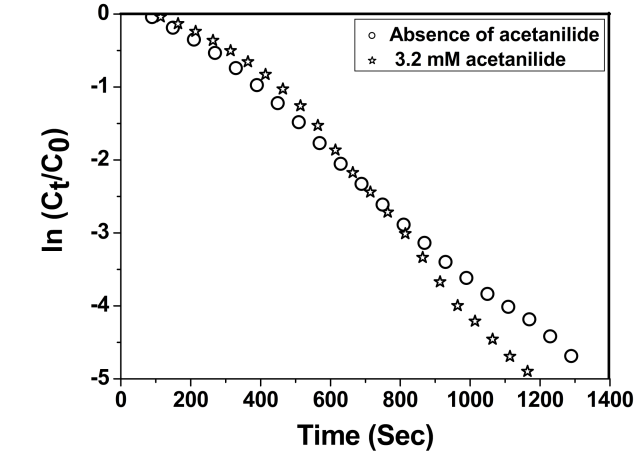


Figure 6.2.8. *Catalytic decay of absorbance of 4NP by Au NPs in the presence and absence of 3.2 mM acetanilide. Other reaction conditions were the same.*

The effective surface areas of all the assemblies were then calculated and the results are plotted in Figure 6.2.7 (d). The figure certainly indicates that the surface area available for catalysis in the assemblies was linearly proportional to the concentration of acetanilide, and the effective surface area decreased with increasing concentration of acetanilide. This observation shows that catalytic activity at a given temperature depends on the total available surface area (S) of the Au NPs. This is reasonable when we consider that the

TH-777_05612211

catalysis takes place on the surface of the Au NPs.[9a] Ballauff et al reported that the catalytic activity is strongly dependent on the total available surface (S) of the NPs present in the unit volume of the system.[12] Recently, we have reported that the apparent rate constant (k_{app}) linearly increases with increasing the number of metal NPs (of same size and shape) in the system.[13]

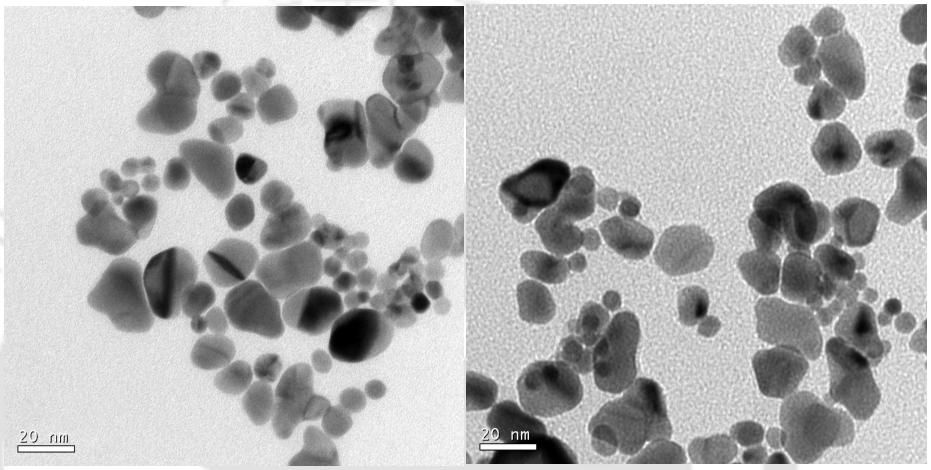


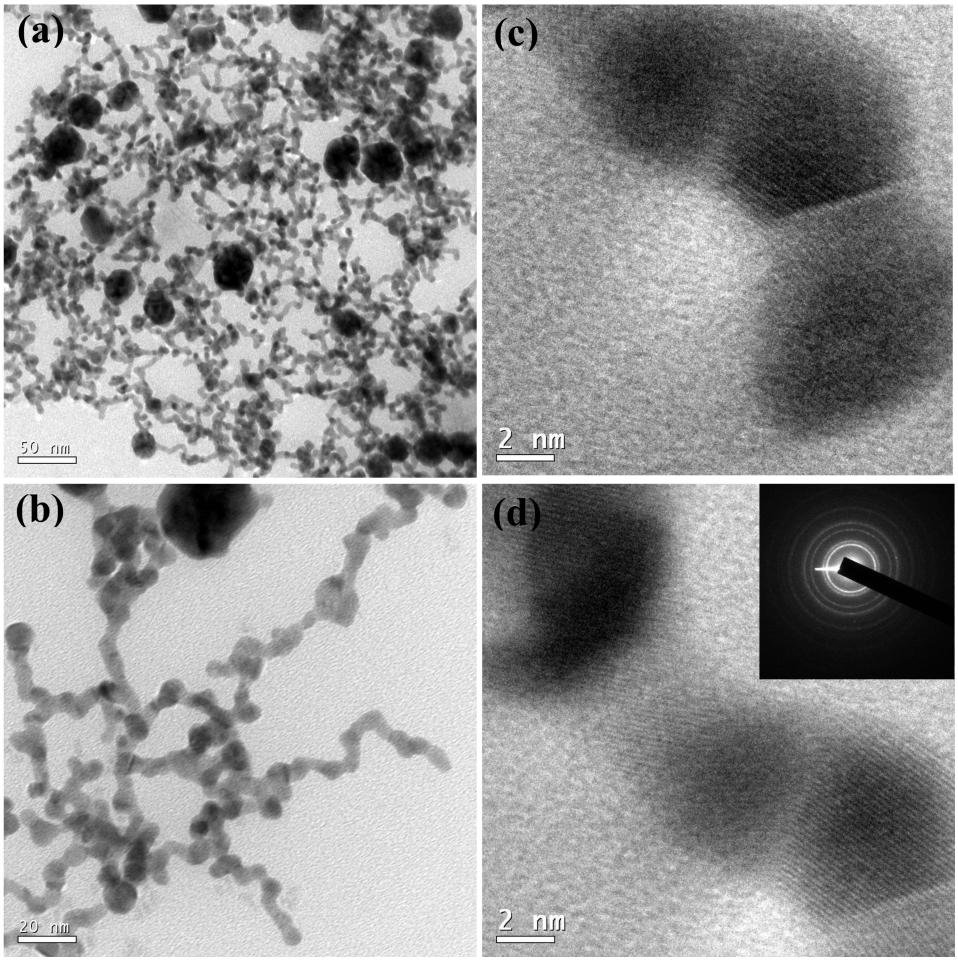
Figure 6.2.9. *Typical transmission electron microscopic images depicting the agglomeration of GNPs in the reaction medium into lumps of particles, in the absence of acetanilide.*

In the present investigation, the results suggest that catalytic activity of Au NPs – which is related to the total available surface area of the NPs - could be affected when the Au NPs are self-assembled into linear chain-like networks. Longer is the network or more branched is network of assembly slower is the rate of catalytic reaction.

Investigation of the morphology of the assembly of Au NPs after catalysis indicated the formation of fibrous structures in the process. TEM images of the assemblies of Au NPs, formed with 16.2 mM acetanilide and recorded after completion of the catalytic reaction are shown in Figure 2.6.10. Clearly, the assemblies led to the fiber formation due to fusion of the NPs keeping the original motifs generated during the assembly formations retained in the

TH-777_05612211

fibers. More interestingly, the structures indicate that in solution the assemblies were truly one-dimensional, with occasional branched structures and not other forms of two-dimensional assemblies that the TEM images (Figure 6.2.3) before fusion might otherwise suggest. In other words, the agglomeration of particles seen in TEM images in Figure 6.2.3 could be the result of evaporation, whereas in solution the structure of the assembly is one-dimensional. Further, HRTEM images shown in Figures 6.2.10 (c) and (d) indicate that the particles were fused together along the same faces. This is evident from the lattice fringes observed across two fused particles. Thus the fibers were made of assembled Au NPs and no organic molecule was present in between the particles.



TH-777_05612211

Figure 6.2.10. *(a) TEM images of the assembly after catalysis, (b) is the expanded view of (a) and (c) and (d) are the high resolution images of (a). The insert in (d) is the selected area electron diffraction pattern of the fibers. The concentration of acetanilide used in this study was 16.2 mM.*

TH-777_05612211

From the lattice fringes of the fused particles, when lattice plane spacing was calculated a value of d = 0.23 nm was obtained.[14-15] This value corresponds to the spacing of the (111) faces of GNP, which shows that particles in the assemblies were fused along (111) faces. SAED patterns of the nanofibers (Figure 5d; inset) consisted of diffraction due to (111), (200), (220) and (311) places of Au.[2a]

Another question may arise about the time of formation of the fibers from the self-assembled arrays of Au NPs in the medium. This is important as that would define the nature of effective surface area available for catalysis during the course of the reaction. Our observations indicate that addition of $NaBH_4$ to the assemblies led to the fusion of Au NPs in the assemblies. This could be similar to observations by Tang and coworkers in which they found that fusion of NPs occur via partial removal of stabilizers.[16] Typical TEM images corresponding to fibers formed upon addition of $NaBH_4$ to an assembly of Au NPs (with acetanilide concentration being 16.2 mM) are shown in Figure 6.2.7A ((a)-(c)). The figure clearly indicates that the nature of fibers formed upon addition of $NaBH_4$ is the same as that observed after completion of the reaction. Control experiments with 4NP and 4AP did not show any agglomeration of particles ruling out their contribution in the fiber formation (Figure 6.2.7B: Appendix-III). Also, TEM images recorded from samples taken from catalysis reaction mixture at 5 min, 10 min and 30 min intervals were found to be identical (Figure 6.2.7A (d)-(f)) and of the same shape and dimensions of those formed upon addition of $NaBH_4$. The results show that during the course of the reaction there is no change in shape, size or morphology of the fibers. Therefore the catalyses carried out in all the experiments reported here were due to fibers formed upon fusion of Au NPs. Their overall length and effective surface areas were responsible for the differences in the rate of the reaction observed herein.

TH-777_05612211

6.2.4 Conclusion

We have reported a simple and facile method to generate linear chain-like networks of superstructures by addition of acetanilide into spherical citrate ion capped Au NPs. In solution the superstructures were stable in the formed of assembled Au NPs. Upon addition of $NaBH_4$ the Au NPs were fused leading to the formation of nanofibers based on the motifs of the original assemblies. The length of the nanofibers and their branches were dependent on the concentration of acetanilide present in the assembling medium. Interestingly, the effective surface areas of the assemblies were linearly dependent on the concentration of acetanilide. The rates of the reactions were dependent on the available surface area which was indirectly dependent on the concentration of acetanilide. It may be mentioned here that poisoning of metal catalyst by amine is known and may also contribute to overall reactivity. However, fusion of Au NPs into fiber could be the primary reason for the reduced catalytic activity. Essentially the present method offers a way of controlling effective catalytic surface areas of catalytically active Au NPs through the formation of assembly followed by the formation of fibers. The molecular properties of acetanilide were responsible for the organization into one-dimensional assemblies.

TH-777_05612211

6.2.5 Appendix I

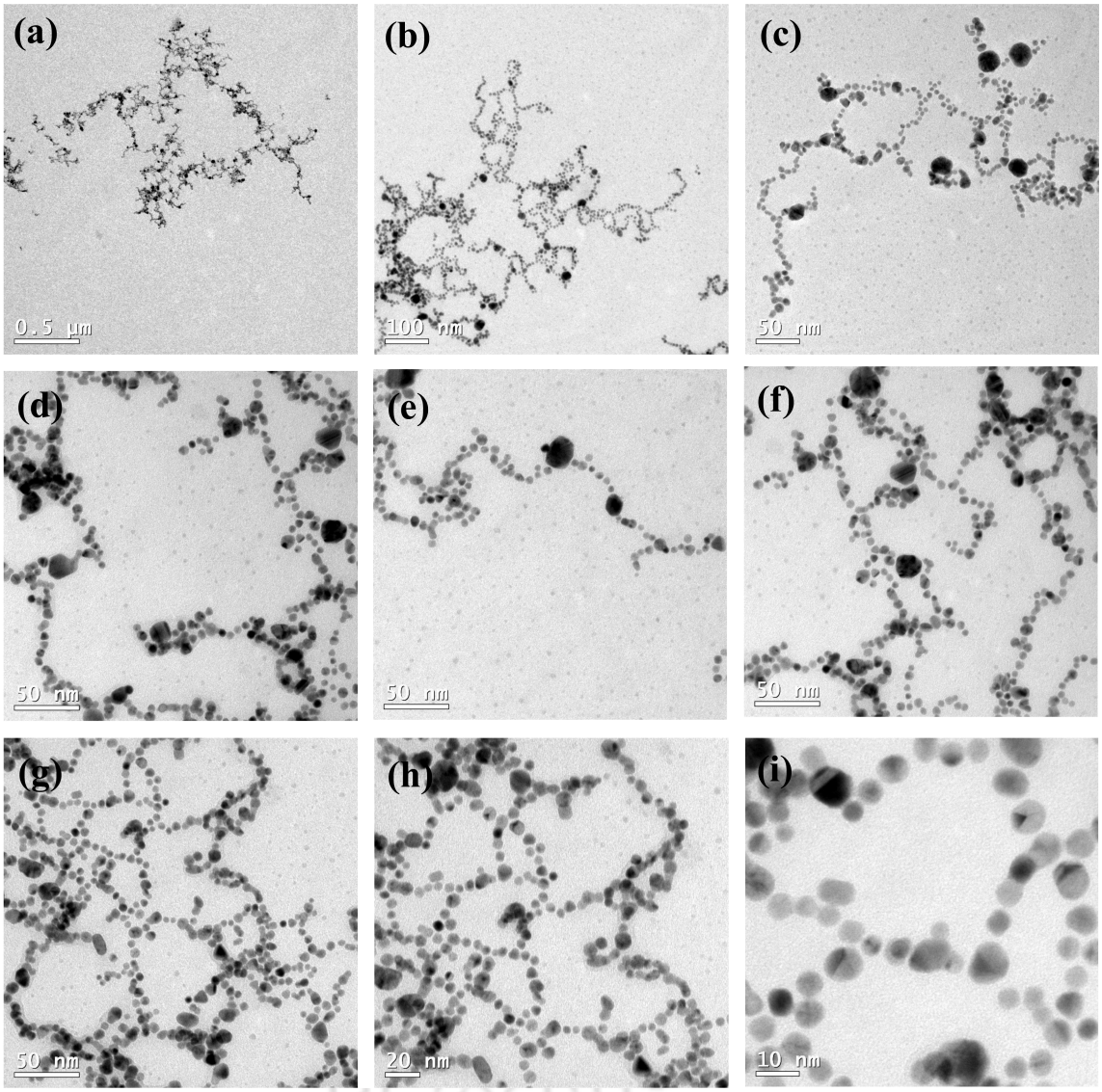


***Figure 6.2.5A**. TEM images of assembly of Au NPs formed in the presence of 6.4 mM of acetanilide and citrate capped Au NPs. (a) is the assembly of Au NPs at lower magnification, (b) to (i) are different magnifications of the image (a). These figures were used to calculate the percentage of linear and branched structures present in the assembly.*

TH-777_05612211

Calculation of percentage population of linear and branched assembly

In order to estimate the percentage of linear assembly versus branched assembly formation, the following procedure was adopted. At lower concentrations of acetanilide the length of assemblies were rather small (less than 200 nm). From a low resolution TEM image, linear assemblies without any branching were counted as linear. When more than one linear assembly was joined together by a head then it was considered a branch assembly. The number of such assemblies was calculated as the number of branched assembly. At higher concentrations of acetanilide the length of assemblies was rather long (greater than 100 nm). In these cases, from the low resolution TEM, the number of branched heads was taken as branched assembly, whereas long (greater than 50 nm) assemblies (in the larger assembly) were considered as linear assemblies. Thus the two percentages were calculated.

TH-777_05612211

6.2.6 Appendix II

Calculation of number of nanoparticles and fraction of surface atoms using a spherical cluster approximation model [13, 17].

(eq. 1)

Where, is the weight of the Au particles in the medium, V is the final volume of the reaction, M is molar concentration of Au^{3+} ion and A.wt is the atomic weight of Au atom.

, V= 51.8 mL, M= Final concentration of $HAuCl_4$, 2.0 X 10^{-4} mol/l, A. wt = 196.97 g/mol.

Here, an excess of sodium borohydride was used for the reduction of Au^{3+} to Au NPs. Hence it can be assumed that all of $HAuCl_4$ was converted to Au NPs.

From this solution, 1.0 mL of Au NPs was taken and added to 7.0 mL acetanilide solution (with a particular concentration of acetanilide). The weight of Au NPs (same as Au) in 8.0 mL solution was 4.924 X 10^{-6} g/mL. From this solution, 0.1 mL of Au NPs was used for the catalysis study.

The weight of the Au NPs in the final 0.1 mL solution was 4.924X10^{-7} g

From the TEM results, we observed that Au nanoparticles were spherical in shape, and we can roughly write[1, 2],

(eq. 2)

then

(eq. 3)

Here, $V_{cluster}$ is the volume of a cluster (nanoparticle) and V_{atom} is the volume of an atom, $R_{cluster}$ is the radius of a cluster and R_{atom} atomic radius and N is the total number of atoms within the cluster. Rearranging **eq. 2** and **eq. 3**, we obtain:

TH-777_05612211

(eq. 4)

Knowing the cluster radius we may also calculate the surface (S) area of nanoparticles with the following equation:

(eq. 5)

Calculation of the amount of gold nanoparticles formed (N_{NP}) when 4.924 X 10^{-7}g of Au particles was used in catalysis.

The average diameter of the gold nanoparticles was assumed to be 5.0 nm. The number gold atoms per particles are 6077 (reference 41).

Amount of gold particles used,

No. of gold atoms,

.

No. of nanoparticles in 4.924X10^{-7} g of Au particles.

Nanoparticles were formed per 4.924X10^{-7} g of Au.

TH-777_05612211

Surface area per unit volume

2.477×10^{11} NPs were added to 2.5 mL solution containing 4-nitrophenol (4-NP) and excess sodium borohydride solution.

for spherical Au NPs.

Calculation of effective surface area of the Au NPs.

The reaction was found to be pseudo first order with respect to 4-NP.

So,

For uniformly dispersed spherical Au NPs in the presence of lowest concentration of acetanilide. The rest of the values of effective surface area were calculated using this value of k and from the equation above.

Table 6.2.6A*. Results of apparent rate constants and effective surface areas.*

Con of acetanilide (mM)	k_{app} (S^{-1}) ($X\ 10^3$)	Effective Surface area (m^2/l) ($X\ 10^3$)
3.2	5.03	7.77
6.4	4.73	7.24
9.7	4.63	7.08
13.0	3.20	4.89
16.2	2.37	3.62
19.4	1.78	2.72

TH-777_05612211

TH-777_05612211

6.2.7 Appendix III

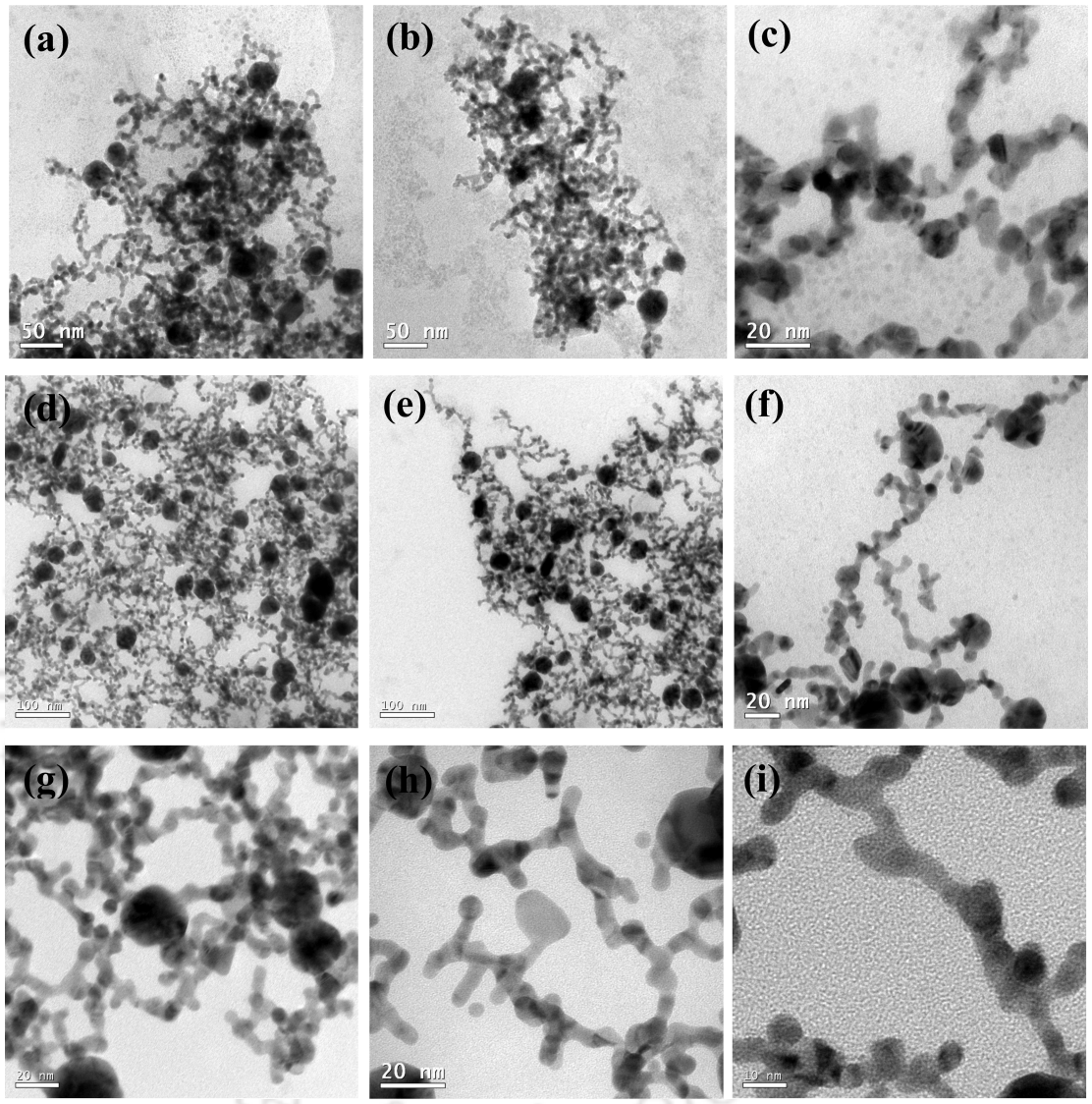


***Figure 6.2.7A**. (a) and (b) are the TEM images of the nanofibers obtained after addition of 2.5 mL of 10 mM NABH¬4 to Au NPs solution used for catalysis studies. (c) is the expanded view of (b). (d) and (e) are the images of nanofibers recorded from the solution of catalysis mixture after 5 min of addition of reagents. (f) to (i) are expanded views of (e) under different magnifications. The concentration of acetanilide used in this study was 16.2 mM.*

TH-777_05612211

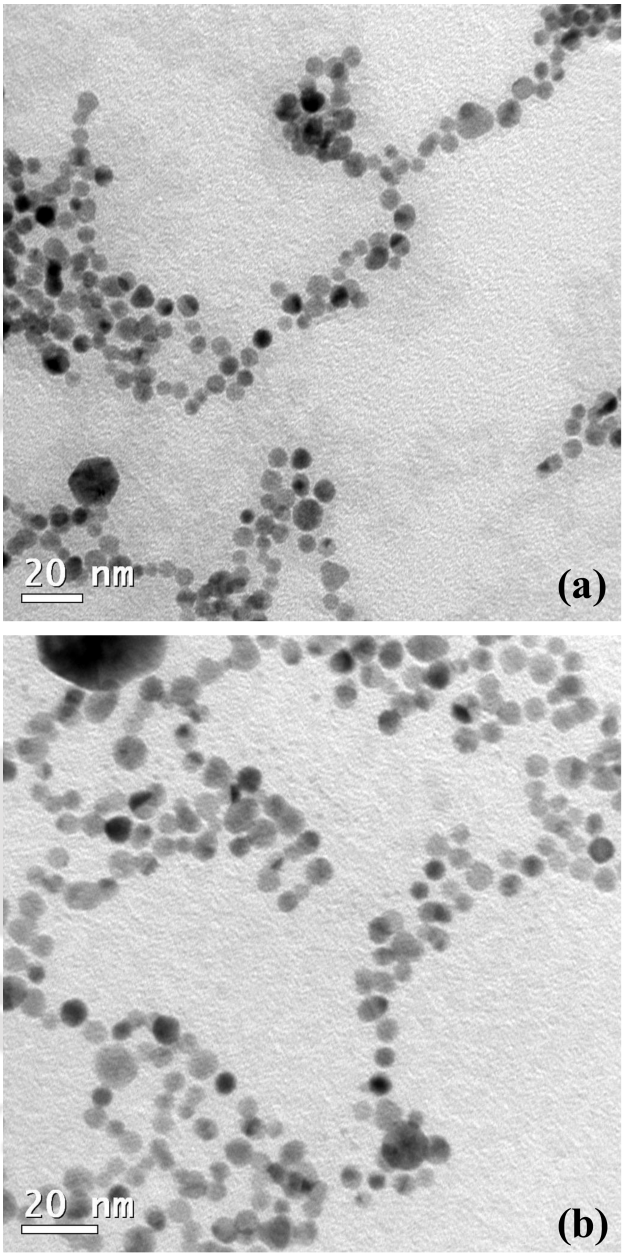


Figure 6.2.7B. *TEM images of Au NP assemblies treated with (a) 0.1 mM 4-aminophenol and (b) 0.1 mM 4-nitrophenol respectively.*

TH-777_05612211

6.2.8 References

1. (a) Liao, J. H.; Zhang, Y.; Yu, W.; Xu, L.; Ge, C.; Liu, J.; Gu, N. *Colloids surf. A* **2003,** *379*, 261. (b) Liz-Marzan, L. M. *Langmuir* **2006**, *22*, 32. (c) Mulvaney, P. *J. Phys. Chem. B* **2001,** *105*, 3441.

2. (a) Polavarapu, L.; Xu, Q-H. *Nanotechnology* **2008,** *19*, 075601/1. (b) Murugadoss, A.; Kar, M.; Chattopadhyay, A. *J. Colloid Interface Sci*. **2008,** *324***,** 230.

3. Teranishi, T.; Haga, M.; Shiozawa, Y.; Miyake, M. *J. Am. Chem. Soc.* **2000,** *122*, 4237.

4. Kumar, A.; Mandal, S.; Mathew, S. P.; Selvakannan, P. R.; Mandale, A. B.; Chaudhari, R. V.; Sastry, M. *Langmuir* **2002,** *18*, 6478.

5. Lin, B. S.; Li, M.; Dujardin, E.; Girrard, C.; Mann, S. *Adv. Mater.,* **2005,** *17*, 2553.

6.Wang, L.; Wei, G.; Sun, L.; Song, Y.; Yang, T.; Sun, Y.; Guo, C.; Li, Z. *Nanotechnology* 2006, *17*, 2907.

7. Shipway, A. N.; Lahav, M.; Gabai, R.; Willner, I. *Langmuir* **2000,** *16*, 8789.

8. (a) Lu, Y.; Mei, Y.; Drechsler, M.; Ballauff, M. *Angew. Chem. Int. Ed.* **2006**, *45*, 813. (b) Esumi, K.; Isono, R.; Yoshimura, T. *Langmuir* **2004**, *20*, 237. (c) Vincent, T.; Guibal, E. *Langmuir* **2003,** *19*, 8475.

9. (a) Panigraphi, S.; Basu, S.; Praharaj, S.; Pande, S.; Jana, S.; Pal, A.; Ghosh, S. K.; Pal. T. *J. Phys. Chem. C* **2007**, *111*, 4596. (b) Mei, Y.; Sharma, G.; Lu, Y.; Ballauff, M. *Langmuir* **2005**, *21*, 12229.

10. (a) Antipov, A. A.; Sukhorukov, G. B.; Fedutik, Y. A.; Hartmann, J.; Giersig, M.; Mohwald, H. *Langmuir* **2002**, *18*, 6687. (b) Pradhan, N.; Pal, A.; Pal, T. *Langmuir* **2001**, *17*, 1800.

11. (a) Lu, Y.; Mei, Y.; Walker, R.; Ballauff, M.; Drechsler, M. *Polymer* **2006**, *47*, 4985. (b) Praharaj, S.; Nath, S.; Ghosh, S.; Kundu, S.; Pal, T. *Langmuir* **2004,** *20*, 9889.

TH-777_05612211

12. Lu, Y.; Mei, Y.; Ballauff, M. *J. Phys. Chem. B* **2006**, *110*, 3930.

13. Murugadoss, A.; Chattopadhyay, A. *Nanotechnology* **2008**, *19*, 015603/1

14. Pong, B. K.; Lee, J. Y.; Trout, B. L. *Langmuir* **2005**, *21*, 1159.

15. Xie, J.; Zhang, Q.; Lee, J. Y.; Wang, D. I. C. *J. Phys. Chem C* **2007,** *111*, 17158.

16. Tang, Z.; Kotov, N. A.; Giersig, M. *Science* **2002,** *297*, 237.

17. Lewis, J. D.; Day, M. T.; Mac Pherson, V. J.; Pikeramenou, Z. *Chem Commun*. **2006**, 1433.

TH-777_05612211

7.1 Acetanilide as a Precursor for Shape and Size Selective Polyaniline-Au Nanoparticle Composites

7.1.1 Introduction

Recent research endeavors in the area of conducting polymers are leading to discovery of newer methods of generation of nanoscale shape and size selective polymers and their composites especially with metal nanoparticles (NPs). For example, significant research efforts are being put in the field of nanoscale composite materials which consist of inorganic metal nanoparticles (NPs) and conducting polymers such as polyaniline (PANI), polypyrrole (PPy) and polythiophene (PT).[1-5] It has been realized that composites could be superior vis-à-vis polymers or NPs, in terms of their combined mechanical, electrical, electronic, optical and chemical properties[6-8] and thus would be amenable to important application such as electrodes for batteries, non volatile memory devices, immunodiagnostic assay, sensors and actuators.[9-12] Nanoscale composites would take the advantages a few steps further owing to their size-dependent properties and easier processing opportunities.[13] Among the composite materials, polyaniline-Au NP (PANI-Au NP) composites have attracted extraordinary attention due to their ease of synthesis, environmental stability, tunable conductivity and unique doping/dedoping chemistry.[14-18] It must be mentioned here that there are significant number of recent works on composites of PANI with Ag NPs, Cu NPs or semiconductor NPs.[19-22] Interestingly, in all the works related to the composites of PANI, aniline has primarily been used as the monomer, although there are reports of derivatives of aniline for the synthesis of polymer. However, aniline is a known carcinogen. It tends to be unstable and polymerize easily in the presence of light and oxidizing species; and the control over particle size in the polymerization could only be achieved in the presence of templates such as micelles and other polymers that form particular structures in

TH-777_05612211

solution. The challenges could be overwhelming when the generation of size and shape selective nanoscale polymers or composites is sought.

An alternative monomer that has evaded attention is acetanilide - which is a solid and non-toxic. Acetanilide has unique advantages over aniline because of its environmental and solvent stability and is amenable to functionalization using well-established synthetic schemes. Thus selective derivative formation could possibly be achieved for the generation of polymers or composites with desired properties. However, its low solubility in water makes it a difficult choice for bulk polymerization. Nonetheless, when it comes to the formation of nanoscale structures as a result of polymerization the low solubility could actually be advantageous. We have taken advantage of the low solubility and consequent structure formation of acetanilide in water, in order to generate systematic shape and size selective PANI-Au NP nanoscale composites in water, which we report in this chapter.

We have recently observed that HAuCl4 when treated with acetanilide generated spherical Au NPs and their assemblies at various concentrations of acetanilide.[23] These structures are completely reversible and their optical properties are commensurate with the level of assembly formation, which could be controlled by controlling the concentration of acetanilide. Interestingly, when polymerized specific structure formations could be observed, which were exclusively dependent on the concentration of acetanilide. Our observations indicate that when the concentration of acetanilide was low spherical Au NP-polymer composites were formed in the medium. At higher concentrations, these individual particles gave way to assembly of composite particles. At still higher concentrations, nanofibers of the composite were formed. Optical properties of the composite were those of the polymer and they indicate that different oxidation states of the polymer were formed depending on the concentration of acetanilide, when the concentration of $HAuCl_4$ was kept constant. Also, acid-base behaviors of the composites were completely reversible. All the composites were stable in aqueous solutions for couple of weeks - without the need of additional stabilizer-indicating the presence of well-dispersed nanocomposites. Transmission electron

TH-777_05612211

microscopy (TEM) measurements indicated the presence of well-dispersed Au NPs in all the composites with various densities depending on the amount of acetanilide used as the precursor.

7.1.2 Experimental Section

Materials

Hydrogen tetrachloroaurate (HAuCl4-, 17% Au in HCl as purchased from Sigma-Aldrich), acetanilide (99 %, from Merck), and ammonium peroxidisulphate (99% from Merck) were used as received without further purification. Milli-Q grade water was used in all the experiments.

Synthesis of Au Nanoparticles using Acetanilide

Typically, to seven 30 mL vials, each containing 10 mL of water, 10 mg, 20 mg, 30 mg, 40 mg and 50 mg acetanilide respectively were added. The concentrations of acetanilide in the vial were thus 7.3 mM, 14.6 mM, 21.9 mM, 29.2 mM, 36.5 mM, 43.7 mM and 51.0 mM respectively. The vials were then heated to 90^{o} C in order to dissolve acetanilide. This was followed by addition of 20 µL of 17.26 mM of HAuCl4 to each solution while they were still being heated. These reaction mixtures were then kept on a hot plate under slow boiling condition for 5 mins. The resulting solutions appeared red in color. This indicated possible formation of Au NPs. The red colored solutions were taken out from the hot plate and cooled to room temperature. The solutions were used for further studies.

Synthesis of shape selective composites of PANI-Au NPs

8.0 mL of each of the above (Au NPs in acetanilide) solutions was taken in a 25 mL beaker. To this beaker, a given amount of concentrated hydrochloric acid was added, followed by stirring for 5 mins. A given amount of solid ammonium peroxydisulphate (APS) was slowly added to each sample and the stirring was continued till appearance of green precipitate. The concentration of acetanilide and APS and amount of hydrochloric acid and

TH-777_05612211

total time to complete the reaction are given in the Table 7.1A. The green precipitate from the each sample was collected by centrifugation and washed with copious amount of water and was then subjected to further centrifugation to remove excess APS and the other oligomers. Finally, the green color precipitates thus obtained were dispersed in distilled water using ultrasoncation for 10 mins. The solutions were found to be stable for a month without appearance of any precipitate or change of color.

Table 7.1A. *The final concentrations of all reactant, reagents and total time for the formation of PANI-Au NPs composites in the reaction medium.*

Exp: Name	Con of Acetanilide (mM)	Amount of con HCl added (mL)	Con of APS (mM)	Total time (hrs)
Exp: 1	06.87	0.5	7.7	58
Exp: 2	13.30	0.77	15.0	48
Exp: 3	19.10	1.17	21.6	30
Exp: 4	24.58	1.50	27.6	26
Exp: 5	29.58	1.87	33.3	21
Exp: 6	34.14	2.24	38.5	16
Exp: 7	38.45	2.61	43.3	14

TH-777_05612211

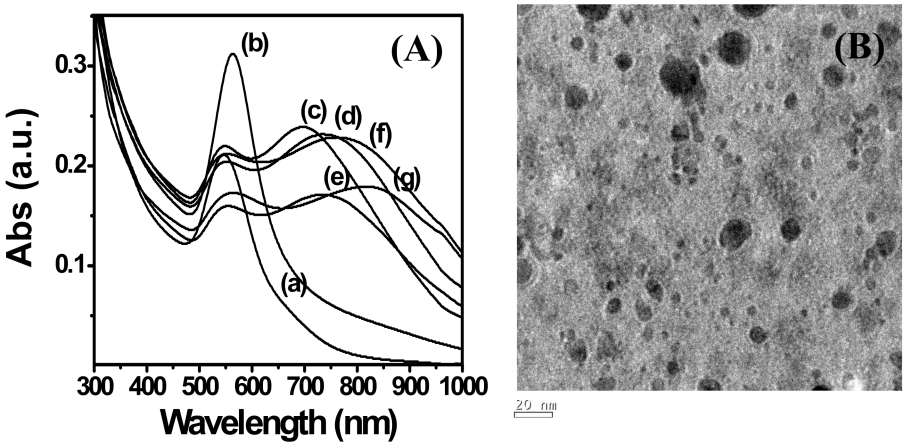
Analytical Measurements

UV-vis spectra of the samples were recorded using a HITACHI model U-2800 spectrophotometer in the range of 200 to 1100 nm. FT-IR measurements were performed using a Perkin-Elmer FTIR (Spectrum One) spectrometer. The sample for FTIR measurements was prepared by air-drying each of the solutions on a glass slide followed by mixing with KBr in order to make pellet, which was used for recording spectra. All the measurements were carried out under ambient conditions. Transmission electron microscopy (TEM) measurements were performed using JEOL-2100 equipment operating at a maximum acceleration voltage of 200 kV. The TEM sample was prepared by placing a drop of liquid on carbon coated copper grid (400 mesh) followed by evaporation of the solvent at room temperature.

TH-777_05612211

7.1.3 Results and Discussion

Acetanilide is sparingly soluble in water at room temperature and the solubility increases with temperature. We have observed that at 90^{o}C, aqueous acetanilide (at 7.3 mM concentration) when mixed with HAuCl4 results in the formation of red color. UV-vis spectrum (Figure 7.1.1 (A)) of the solution consists of a single peak at 545 nm, indicating the formation of Au NPs in the medium. TEM measurement indicated the formation of spherical NPs with sizes in the range of 10-20 nm (Figure 7.1.1 (B)). When the concentration of acetanilide was kept at 14.6 mM, 21.9 mM, 29.2 mM, 36.5 mM, 43.7 mM and 51.0 mM, keeping the concentration of HAuCl4 constant, a second peak appeared in the UV-vis spectrum of each of the above mixtures, in addition to the first peak at the above wavelength. The wavelength of absorption maximum of the second peak increased with increasing concentration of acetanilide, with the values appearing at 698 nm. 750 nm, 754 nm, 780 nm and 829 nm respectively at the concentrations mentioned above. TEM measurements indicated the formation of linear assemblies of NPs with increasing chain length at higher concentrations. The average particle size of the NPs constituting the assembly was the same as those formed at the lowest acetanilide concentration.



TH-777_05612211

***Figure 7.1.1**. (A) UV-vis spectra of Au NPs prepared with acetanilide concentrations of 7.3 mM (a), 14.58 mM (b), 21.87 mM (c), 29.16 mM (d), 36.45 mM (e), 43.74mM (f) and 51.03mM (g) respectively. (B) TEM picture of Au NPs from solution corresponding to A (a).*

The details of these results have been discussed in Chapter 6. Interestingly, when additional conc. HCl was added to each of these solutions the second peak vanished and the intensity of the first peak increased. This indicted that the assemblies dissociated into constituent spherical particles at higher acidity. Since the assemblies were broken and consequently had no role in the formation of PANI-Au NP composite, the details of the above results are omitted here.

Further, when APS was added to a solution containing excess acid treated Au NPs, which was generated by reaction of 14.6 mM of acetanilide and $HAuCl_4$, green coloration of the solution was observed. UV-vis spectrum (Figure 7.1.2 (A)) of the solution consisted of peaks at 430 nm and 816 nm. In addition, there was another peak occurring in the region of 285-320 nm. These peaks are characteristic of polyaniline that was formed in the medium. For the samples with initial acetanilide concentrations of 21.9 mM and 29.2 mM, the intensity of the peaks increased (in comparison to when starting with 14.6 mM of acetanilide) indicating formation of increased amount of PANI under the reaction condition. On the other hand, when the concentrations of acetanilide were kept at 36.5 mM or 43.7 mM, a new peak appeared at 620 nm in addition to other peaks. The absorption peak in the range of 285-320 nm is due to the two different Π- Π^* transitions of the benzenoid ring and transition from the low lying orbital of the Π_q orbital (quinoid ring system) respectively.[24] Further, when the initial concentration of acetanilide was kept at 51.0 mM or higher, the intensity of the peak at 816 nm was increased with concomitant gradual decrease of the peak at 620 nm. It has been proposed that the peak at 620 nm is due to partially protanated form of emaraldine salt and the peak at 816 nm can be attributed to the interchain charge

TH-777_05612211

transition of polaran- Π^* transition.[25] This is possibly due to the insufficient amount of acid present in the medium at the time of polymerization reaction.[26a, 26d] The above results indicate that PANI was formed in the medium for all the samples, possibly in the form of PANI-Au NP composite. However, the level of oxidation of PANI depended on the amount of acetanilide present at the initial stage (as revealed from the UV-vis spectroscopic measurements). For example, PANI, generated at the lowest concentrations of acetanilide (14.6 mM), consisted of both benzenoid and quinoid form as the amount of acid present was excess. However, at the concentrations of 36.5 mM 43.7 mM, both the benzenoid and qunoid forms were formed but the level of protonation is different from that at the lowest concentration of acetanilide generated PANI.

TH-777_05612211

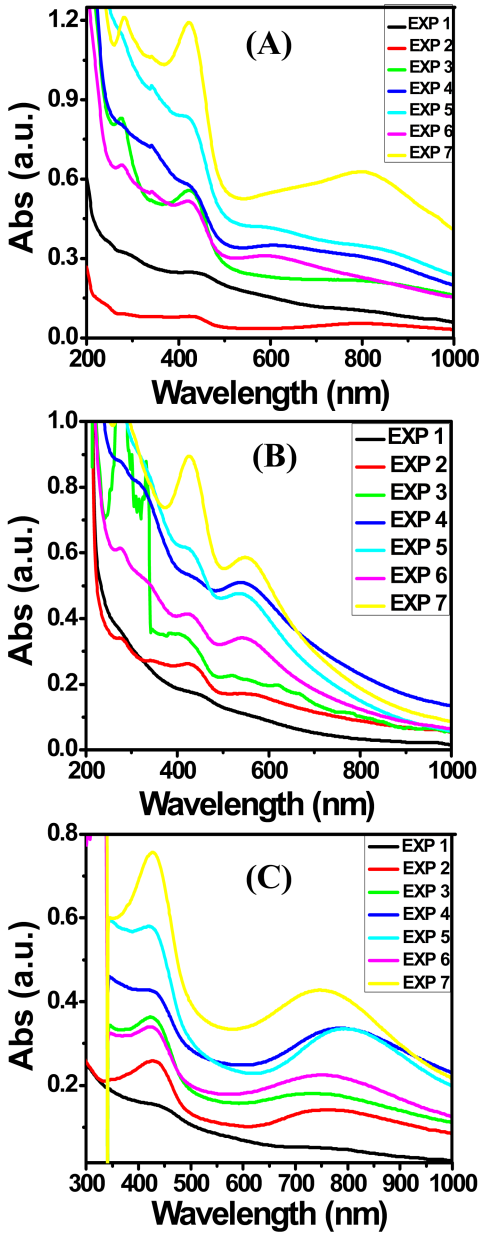


Figure 7.1.2. *(A) The UV-Visible spectrum of composite PANI-Au NPs with different concentration of acetanilide in the presence of AuNPs. (B) After NaOH treated with (A), (C) Again HCl treated with (B).*

TH-777_05612211

When the polymers formed in presence of Au NPs and under different acetanilide concentrations, were further treated with base (at pH =12.0) all of them were converted to emeraldine base form as was evident from the UV-vis spectra shown in Figure 7.1.2 (B). In all the spectra, the peak characteristic of the base form appeared at 585 nm. Further, when they were treated with acid (pH = 2.3) all of the polymers were converted into emeraldine salt form with characteristic peak at around 800 nm (Figure 7.1.2 (C)). These experimental results suggest that the PANI formed under the reaction conditions and in the presence of Au NPs could reversibly be converted between emeraldine salt and base form by treatment with acid and base respectively. The results indicate that the optical and possibly electrical characteristics of PANI were retained when generated from acetanilide and in the presence of Au NPs. In other words, the polymers, formed in the presence of Au NPs and starting with acetanilide as the monomer, are acid-base sensitive and the polymers generated in all samples were the highly conductive emaraldine PANI.[27]

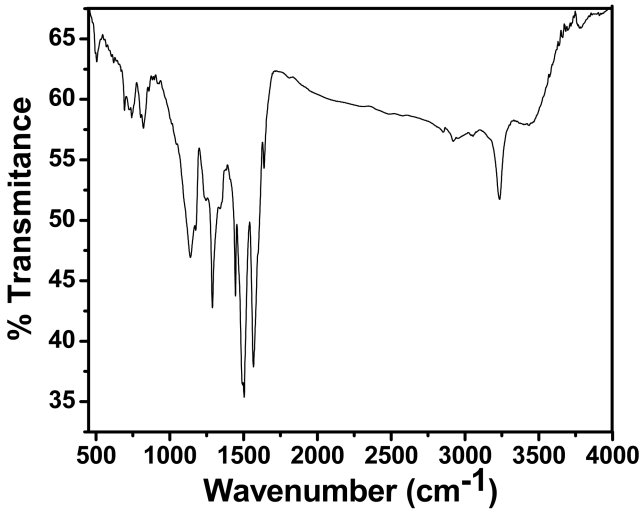
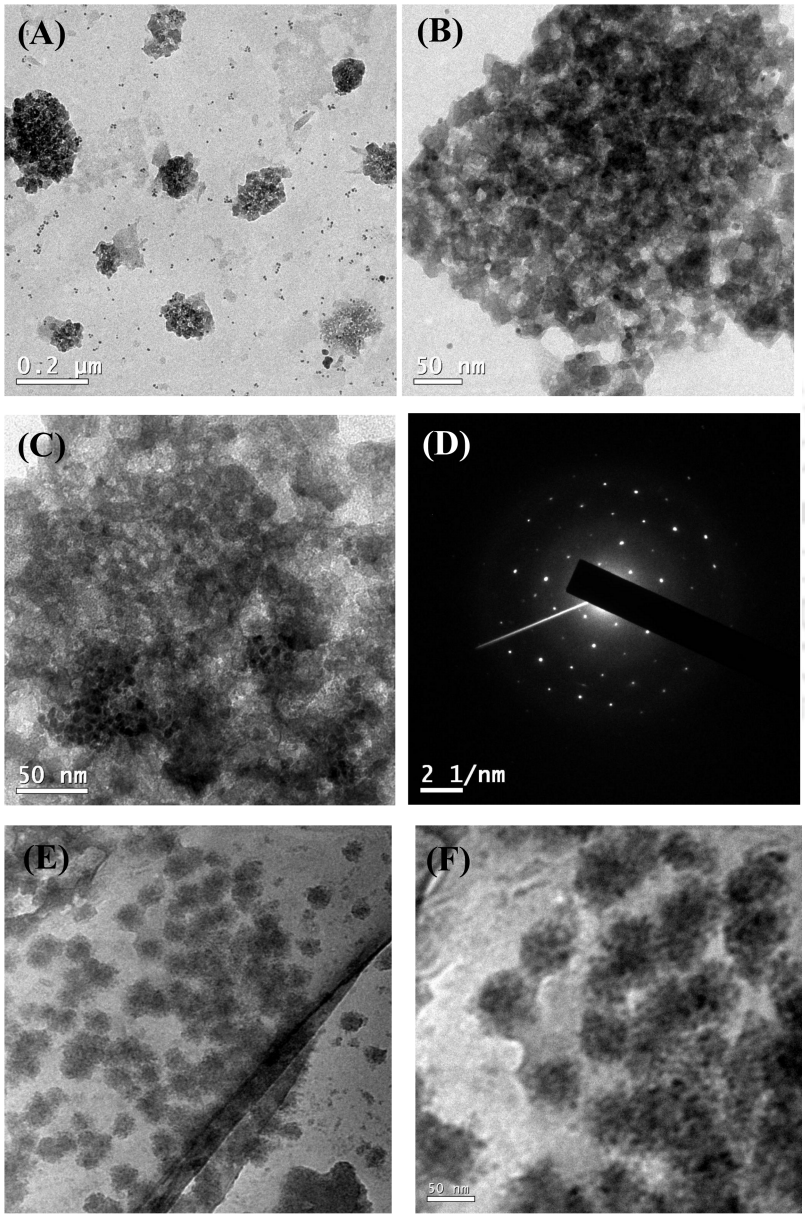


Figure 7.1.3. *FTIR spectrum of PANI-Au NPs composite of the corresponding sample Exp: 5*

TH-777_05612211

Further evidence for the formation composite PANI-Au NPs, came from FTIR measurements which were carried out for all the samples produced at various initial acetanilide concentrations. A typical FTIR spectrum corresponding to Exp: 5 is shown in Figure 7.1.3.



TH-777_05612211

Figure 7.1.4. *The transmission electron microscopy of PANI-Au NPs composites, (A) TEM images obtained from EXP:1 (B) and (C) are expanded view of (A), (D) SAED is obtained from figure (C) and image(E) is obtained from Exp:2 and (F) is expanded view of (E)*

The spectrum consists of a peak in the region of 3500-3200 cm^{-1}, which can be attributed to be due to the N-H stretching vibration and the peak occurring at 3000-2800 cm^{-1} is due to aromatic C-H stretching vibration. On the other hand, the absorption peak at 1636 cm^{-1} is characteristic of N=C- stretching mode of quinoid ring. The band at 1565 cm^{-1} and 1497 cm^{-1} are due to the deformation mode of the quinoid and benzene ring. The vibration peak at 1287 cm^{-1} is attributed to protonated C-N group, which is possibly responsible for the interaction of Au NPs with PANI. The absorption band at 1136 cm^{-1} is due to the in-plane bending vibration of C-H, while C-H out of plane deformation mode occurred at 814 cm^{-1}. Thus the peaks present in the FTIR spectrum indicate the formation PANI in the medium.[13a] Similar FTIR spectra were obtained for the other composites prepared at different initial acetanilide concentrations. In brief, PANI-Au-NP composites were formed in all the samples prepared with different amount of acetanilide.

Interestingly, further investigation of the products by TEM revealed the formation of various structures of the polymer-Au-NP composite depending on the initial concentration of acetanilide. For example, at the lowest concentration of acetanilide (7.3 mM) used small, spherical raspberry-like nanoparticles were formed.[28] The sizes were 200 nm or less in diameters. The particles composed of PANI as well as Au NP-PANI composite. The results are shown in Figure 7.1.4 (A). When the concentration of the acetanilide was 14.6 mM, formation of continuous structures - where the raspberry-like particles seem to have been connected by polymer - could be observed (Figure 7.1.4 (B)). SAED patterns indicated the presence of Au NPs in the particles. When the concentration of acetanilide was kept at still higher value (36.5 mM) then formation of continuous nanofibers of the polymer was favored

TH-777_05612211

with intermittent presence of Au NPs along with the polymer in the form of raspberries embedded in the continuous fibers (Figure 7.1.5). At even higher concentrations the continuous fiber formation (of the composite) was favored (Figure 7.1.6).

The incorporation of metal and semiconductor NPs into the conjugated polymers such as PANI is of special interest, as the interactions between the NPs and the polymer may play significant role in tuning the properties of the composite.[29] The application potential would be better if the size and shape of the composites could be controlled at the nanoscale. Although, there are several reports on the preparation of shape and size selective nanocomposites of Au NP-PANI in the presence of stabilizing agents and or templates,[30] there is, however, no report on the synthesis of stable aqueous dispersion of the nanoscale composites themselves. This is where acetanilide played crucial role in the present method of synthesis of stable size and shape-selected nanocomposites. The low solubility of acetanilide in water in conjunction with nucleation centers created by the presence of Au NPs possibly resulted in the shape and size selection of nanoparticles and fibers of the composite.

TH-777_05612211

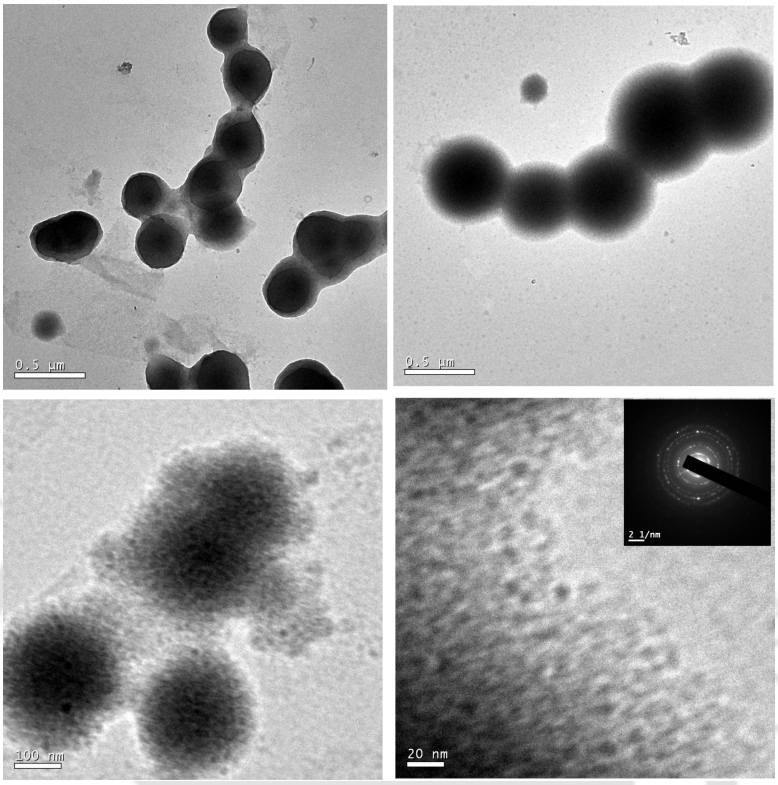


Figure 7.1.5*. (A), (B) and (C) are the transmission electron microscopy of PANI-Au NPs composites of EXP: 5 and (D) is the expanded view of (C). The inset figure of SAED is obtained*

Also, our results suggest that the polymer formed under different conditions, starting with acetanilide, was the same as PANI. This is possibly due to dissociation of acetanilide into anilinium ions in the presence of excess acid, which resulted into the formation of PANI in the same way as is starting with aniline as the monomer. At the lowest acetanilide concentrations there are a large number of independent sites where the growths of the polymer and composite take place simultaneously

TH-777_05612211

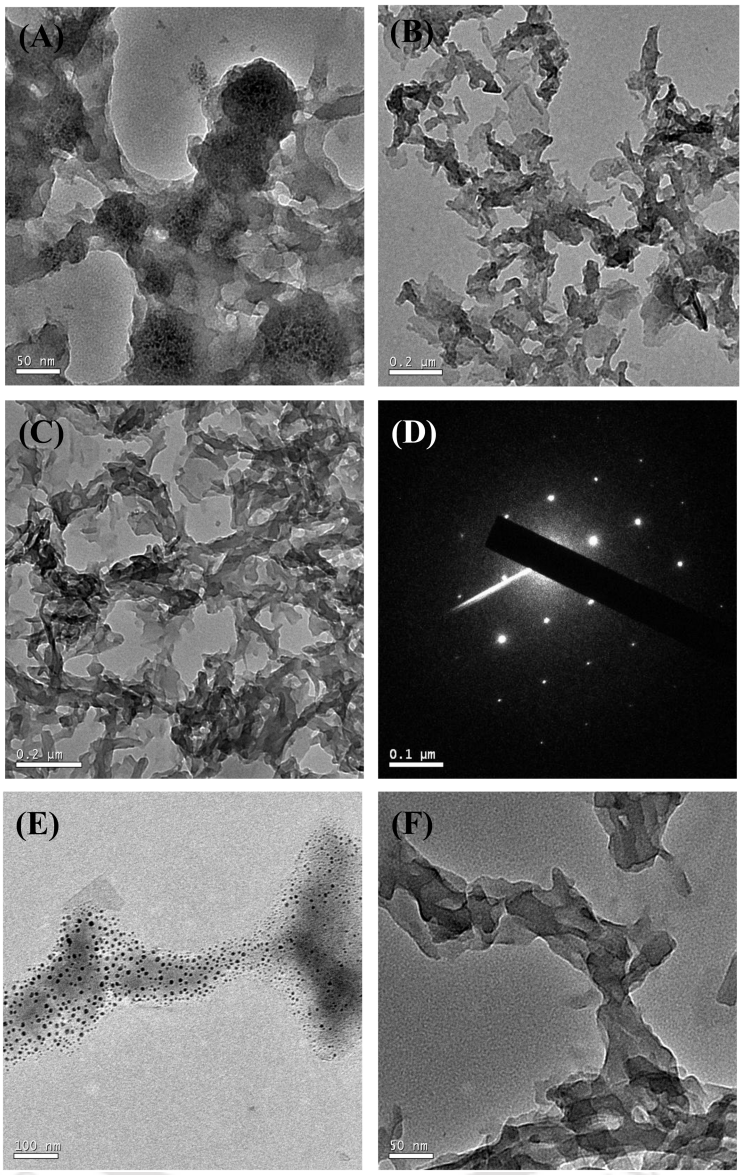


Figure 7.1.6*. (A) is the transmission electron microscopy of PANI-Au NPs composites of EXP: 4. (B) and (C) is the TEM images obtained from EXP 6 and (D) is the corresponding SAED picture. The image (E) is obtained from another part of the same spmple of EXP: 6 and (F) is the image obtained from EXP: 7*

As the concentration of monomer is low (anilinium ions from acetanilide) the polymers or composites remain in particulate forms rather than forming a continuous polymer film or fiber. This is due to the fact that there is not enough monomer to have the formation of

TH-777_05612211

continuous fibers or films. This is commensurate with the observations in Figure 7.1.4 (A). When the concentration of the monomer is increased the additional anilinium ions present in the medium contribute towards forming continuous structures by joining the particulate structures. This gave rise to structures corresponding to that shown in Figure 7.1.4 (B). It is important to note that at 36.5 mM of acetanilide concentration there were a large number of nucleation sites present in the medium and there was enough monomer present for the formation of raspberry-like structures joined by polymer fibers (Figure 7.1.5). Upon further increase in concentration of the monomer the continuous fiber formation due to polymerization begins to dominate over the discrete nucleation sites (Figure 7.1.6 (A)), even though the presence of a large nucleation sites is still evident. Interestingly, when the concentration of acetanilide was still higher the continuous fiber formation dominated over discrete nucleation, which is evident from Figure 7.1.6 (B), (C) and (E). However, at the concentrations of 43.7 mM there are the presence of micron-long individual fibers (Figure 7.1.6 (F)) where structures of the raspberries were conserved, however, the particles were not spherical. Their typical diameters were about 100 nm. When the concentration of acetanilide was kept at even higher values (51.0 mM or higher) only nanofiber formation could be observed. This is because at higher anilinium concentrations, the individual nucleation sites do not exist as the monomers, whereas they are present everywhere in sufficient numbers so as to form continuous fibers of the composite.

TH-777_05612211

7.1.4 Conclusion

In brief, we have taken advantage of the low solubility and stability of acetanilide in developing a new method of synthesis of PANI-Au NP nanoscale composites. The method allowed the synthesis of the composite with size and shape selectivity. Formation of Au NPs as a result of reduction of $AuCl_4^-$ by acetanilide resulted in the generation of nucleation sites around which the polymerization of anilinium ions could take place. At the lowest concentration of acetanilide spherical isolated nanoscale particles of polymers and composites were observed to have been formed. At higher concentrations the particles seem to have been merged to form micronscale structures consisting of composites. At still higher concentrations continuous fibers with diameters in the nanoscale were formed. The composites consisted of PANI and the optical and acid-base characteristics of the composites resembled those of emeraldine form of PANI. In addition, the present method offers composites that are water soluble and stable for months without forming any precipitate at the bottom of the container, and thus overcomes the fundamental challenges of insolubility and intractability associated with PANI and its composite. This is important from the point of application in large-scale environmentally friendly industrial scenario. Further, this method does not need any extra control, solvent or any special condition to make the nanoscale composites of Au NPs and PANI. The knowledge obtained from this work may pave various ways of systematic development of three-dimensional water-soluble metal NP-polymer composites with tunable electrical, optical and chemical properties.

7.1.5 References

1. Huang, J.; Kaner, R. B. *Nature* **2004**, *3*, 783.

2. Sih, B. C.; Wolf, M. O. *Chem. Coomun*. 2**005**, 3375.

3. (a) Xu, J.; Wang, J.; Mitchell, M.; Mukherjee, P.; Jeffries-El, M.; Petrich, J. W.; Lin, Z. *J. Am. Chem. Soc*. **2007**, *129*, 12828. (b) Hu. W. M.; Kumar, S.; Lee, A.; Felorzabihi, N.; Shen, L.; Zhao, F.; Froimowicz, P.; Scholes, G. D.; Winnik, M. A. *J. Am. Chem. Soc*. **2008**, *130*, 9481.

TH-777_05612211

4. Feng, X.; Huang, H.; Ye, Q.; Zhu, J,-J.; Hou, W. *J. Phys. Chem. C* **2007**, *111*, 8463.

5. Herrikhuyzen, J. V.; George, S. J.; Vos, M. R. J.; Sommerdijk, N. A. J. M.; Ajyaghosh, A.; Meskers, S. G. J.; Schenning, A. P. H. J. *Angew. Chem. Int. Ed*. **2007**, *46*, 1825.

6. Lahav, M.; Weiss, E. A.; Xu, Q.; Whitesides, G. M. *Nano Lett*. **2006**, *6*, 2166.

7. Park, S.; Lim, J.-H.; Chung, S.-W.; Mirkin, C. *Science* **2004**, *303*, 348.

8. Bongnitzk, M.; Hou, H.; Ishaque, M.; Frese, T.; Hellwing, M.; Schwarte, C.; Schaper, A.; Wendorff, J. H.; Greiner, A. *Adv. Mater*. **2000**, *12*, 637.

9. Hunag, J.; Virji, S.; Weiller, B. H.; Kaner, R. B. *J. Am. Chem. Soc*. **2003,** *125*, 314.

10. Wang, H.-L.; Gao, J.; Sansinena, J.-M.; McCarthy, P. *Chem. Mater*. **2002**, *14*, 2546.

11. Xie, D.; Jiang, Y.; Pan, W.; Li, D.; Wu, Z.; Li, Y. *Sens. Actuators B* **2002**, *81*, 158.

12. Kaneko, M.; Nakamura, H. *J. Chem. Soc., Chem. Commun*. **1985**, 346. (a) Tseng, R. J.; Hunag, J. X.; Ouyang, J. Y.; Kaner, R. B.; Yang, Y. *Nano Lett*. **2005**, *5*, 1077. (b) Liu, J.; Tian, S.; Knoll, W. *Langmuir* **2005**, *21*, 5596.

13. (a) Sanjanlal, P. R.; Sreeprasad, T. S.; Nair, S.; Pradeep, T. *Langmuir* **2008**, *24*, 4607. (b) Li, W.; Wang, H. L. J. *J. Am. Chem. Soc*. **2004**, *126*, 2278. (c) Huang, J.; Kaner, R. B. *Angew. Chem. Int. Ed.* **2004**, *43*, 5817. (d) Huang, K.; Zhang, Y.; Long, Y.; Yuan, J.; Han, D.; Wang, Z.; Niu, L.; Chen, Z. *Chem.-Eur. J*. **2006,** *12*, 5314.

14. MacDiarmid, A. G. *Angew. Chem. Int. Ed*. **2001**, *40*, 2581.

15. Chiang, J. C.; MacDiarmid, A. G. *Synth. Mat*. **1986**, *13*, 193.

16. Xia, Y. N.; Wiesinger, J. M.; MacDiarmid, A. G.; Epstein, A. *J. Chem. Mater*. **1995**, *7*, 443.

17. Majidi, M. R.; KaneMaguire, L. A. P.; Wallace, C. G. *Polymer* **1994**, *35*, 3113.

18. Sarma, T. K.; Chattopadhyay, A. *Langmuir* **2004**, *20*, 4733.

TH-777_05612211

19. Oliveria, M. M.; Cvasttro, E. G.; Canestaro, C. D.; Zanchet, D.; Ugarte, D.; Roman, L. S.: Zarbin, A. J. G. *J. Phys. Chem. B* **2006**, *110*, 17063.

20. Kumar, R. V.; Mastai, Y.; Diamant, Y.; Gedanken, A. *J. Mater. Chem*. **2001**, *11*, 1209.

21. Toney, A.; Topka, M.; Uluski, R.; Wood, C. *Langmuir* **2008**, *24*, 9727.

22. Lu, X.; Yu, Y.; Chen, L.; Mao, H.; Zhang, W.; Wei, Y. *Chem. Commun*. **2004**, *13*, 1522.

23. Murugadoss, A.; Chattopadhyay, A. J. *Colloid and Interface Sci*. **2008**, *324,* 230.

24. (a) Jang, J.; Ha, J.; Lim, B. *Chem. Commun*. **2006**, 1622. (b) Huang, W. S.; MacDiarmid, A. G. *Polymer* **1993**, *34*, 1833.

25. (a) Sarma, T. K.; Chattopadhyay, A. *J. Phys. Chem. A* **2004**, *108*, 7837. (b) Venancio, E. C.; Wang, P.-C.; MacDiarmid, A. G. *Synth. Met*. **2006**, *156*, 357.

26. (a) Neoh, K. G.; Young, T. T.; Looi, N. T.; Kang, E. T. *Chem. Mater*. **1997**, *9*, 2906. (b) Zhang, W. J.; Feng, J.; MacDiarmid, A. G.; Epstein, A. J. *Synth. Met*. **1997**, *84*, 119. (c) Albuquerqu, J. E.; Mattoso, L. H. C.; Balogh, D. T.; Faria, R. M.; Masters, J. G.; MacDiarmid, A. G. *Synth. Met*. **2000**, *113*, 19. (d) Cao, Y.; Smith, P.; Heeger, A. J. *Synth. Met*. **1989**, *32*, 263.

27. Sarma, T. K.; Chowdhury, D.; Paul, A.; Chattopadhyay, A. *Chem. Commun*. **2002**, 1048.

28. Shiigi, H.; Yamamoto, Y.; Yoshi, N.; Nakao, H.; Nagaoka, T. *Chem. Commun*. **2006**, 4288.

29. (a) Pillalamarri, S. K.; Blum, F. D.; Bertino, M. F. *Chem. Commun*. **2005**, 4584. (b) Advincula, R. C. *J. Dispersion Sci. Technol*. **2003**, *24,* 343. (c) Smith, J. A.; Josowicz, M.; Janata, J. *Phys. Chem. Chem. Phys*. **2005**, *7*, 3614.

30. (a) Choi, S. J.; Park, S. M. *Adv. Mater*. **2005**, *17*, 1547. (b) Wei, Z. X.; Zhang, Z. M.; Wan, M. X. *Langmuir* **2002**, *18*, 917. (c) Yang, Y. S.; Wan, M. X. *J. Mater. Chem*. **2002**, *12*, 897. (d) Chiou, N.-R.; Lee, L. J.; Epstein, A. J. *Chem. Mater*. **2007**, *19*, 3589. (e) Yoshida, K.; Shimomura, T.; Ito, K.; Hayakawa, R. *Langmuir* **1999**, *15*, 910.

TH-777_05612211

TH-777_05612211

8.1 Concentration Dependence and Specificity in the Amino acid Induced Assembly of Gold Nanoparticles

8.1.1 Introduction

The ordered arrangement of nanomaterials into one dimensional (1D) superstructures have gained tremendous importance in many areas of research, inspired by the potential applications in nanoscale devices such as plasmonic nanowaveguides,[1] surface plasmon based biosensors,[2] single electron transistors,[3] nanoelectronics[4] and nanomagnetics.[5] However, such applications using the properties of nanomaterials require precise control over their particle size and shape, interparticle spacing and organization geometry. Over the past decades, different kinds of techniques have been used to generate assembled the nanomaterials. For example, electron beam lithography,[6] focused ion beam lithography,[7] soft lithography[8] are some of the techniques that have been used to obtain organized arrays of nanomaterials on solid surfaces. On the other hand, in liquid phases, electrostatic interaction,[9] hydrogen bonding,[10] hydrophobic interactions[11] are some of the natural forces that are available for use in the organization of nanoparticles (NPs). Additionally, template directed assemblies using biomolecules such as DNA and proteins,[12] tobacco mosaic virus[13] and bacteriophage[14] have also been used for the generation of organized arrays. Although, the biosystems provide alternate opportunities for assembly of NPs, they may not be able to offer precise and varied controls as their structures and biochemical constituents are largely 'fixed', even though genetic recombinant technology offers versatility in this regard.[15] However, programmed assembly of nanomaterials using molecular forces in liquids offers an attractive cost-effective alternative that could have far reaching consequences in chemistry, biology, material science and optoelectronics.[16] Further, molecularly controlled assembled NPs may provide newer properties that might otherwise not be attainable using other means. For example, Nakata et al reported

TH-777_05612211

molecularly controlled formation of chains of superparamagnetic NPs having higher blocking temperature compare to their individual constituents.[17] Further, the generation of 1D nanomaterials via molecular interations would not only reveal a great deal about the interactions themselves, the molecule themselves could contribute towards catalytic, electric, magnetic and optical properties of the assembled nanomaterials.[18] This approach could also stimulate preparation of nanowires and nanofibes that are formed through the linear arrangement of individual NP.[19, 18a] Among the nanomaterials, the one dimensional assembly of metal NPs especially Au NPs and their associated collective vectorial properties are of particular interest in nanoelectronics, optoelectronics and biosensor devices.[20] However, unlike magnetic and semiconductor NPs, the self-assembly of Au NPs into 1D chain-like array is very tricky because it does not have any intrinsic electric dipoles, which is a prerequisite for the formation of uniaxial organization of 1D chain-like array of NPs.[21] To overcome this difficulty, the Au NP surface should have heterogeneity in charge distribution, which can possibly be achieved either through non-uniform spatial distribution of capping ligand on different crystallographic faces or nanoscale separation in mixed ligand stabilization layer, which could be responsible for the driving force for the assembly of NPs into 1D linear superstructures.[22] Recently, Sardar et all showed that asymmetrically functionalized Au NPs can self-assemble into linear 1D chain-like array of supperstryctures and they have also reported that ligand shell on the Au NPs surface plays an important role for controlling the interparticle distance in the 1D Au NP chain.[23] Mann and coworkers have produced the linear or branched chain like array of Au NPs by ligand exchange method.[24] Recently, our group has reported that linear or branching chain like array of Au NPs can also be produced by ligand exchange of citrate molecules with protonated acetanilide molecules. We observed that the length of the chain or number of branching of Au NPs chain was dependent on the concentration of acetanilide.[18a] The results have further motivated us to study the effect of amino acid molecules on the formation of linear chain-like array of Au NPs. The primary motivation has been that since the amino acids could have different side chain group - such as hydrophilic or hydrophobic, polar or

TH-777_05612211

non-polar – interactions of the stabilizer with biological molecules would also be different. The organization of Au NPs in linear chain arrangement by using biomolecules such as amino acids would be of high potential impact in the fields of biosensor and drug delivery other than molecular building of superstructures. The driving force is that at lower pH, the amine group at the α-carbon can bind to the Au NP surface that may induce self assembling of Au NPs into either linear or branched chains of Au NPs.

In this chapter, we report on the investigation of the effect of amino acids on the assembly formation of citrate-stabilized spherical Au NPs into 1-D chain-like superstructures. The nature of the assembly formed and associated optical properties were found to be dependent on the concentration of amino acid as well as the nature of the side chain group present in the amino acid. It was observed that to a solution of Au NPs when increasing amount of an amino acid was added the characteristic peak at 527 nm gradually diminished in intensity, while a second peak appeared at higher wavelength, the manximum of which progressively shifted to longer wavelength with increasing concentration. The changes were highly specific to the amino acid present in the medium. For example, when lysine or tryptophan was used, micromolar quantity of the acid was enough to induce a large-scale organization. On the other hand, when phenylanine or glutamine was used milli-molar quantities of amino acids were required to observe significant changes in the absorption spectra. Thus the assembly formation could not only be useful for identification of amino acids but also may be used to estimate their solution concentrations. In addition, 1D chain of necklace-like Au NPs converted into nanofibers when excess hydrophilic amino acid was used. On other hand, at higher concentration of hydrophobic amino acids, the necklace-like Au NPs did not get transformed into nanofibers. Our observations suggest that the nature of the side chains present in the amino acids with their functional groups may play an important role for controlling the interparticles interaction and their subsequent fusions in the amino acid assembled Au NPs chain.

TH-777_05612211

8.1.2. Experimental Section

Materials

Hydrogen tetrachloroaurate ($HAuCl_4$, 17 % Au in HCl as purchased from Sigma Aldrich), tri sodium citrate (99 % from Merck), acetanilide (99.5 %, from Merck), sodium borohydride ($NaBH_4$, 95.5 %; Merck), L-lysinemonohydrochloride, L-tyrosine and L-tryptophan (99.5 %, from Merck), L-phenylalanine and glutamine (99.9 %, from sigma Aldrich) were used as received without further purification. Milli-Q grade water was used in all the experiments.

Synthesis of citrate stabilized Au NPs

Citrate stabilized Au NPs were prepared following the reported procedure.[18a] Briefly, aqueous $HAuCl_4$ was reduced by sodium botohydrate in the presence of trisodium citrate. The final pH of the solution was found to be 4.0.

Table 8.1A. *The final concentrations of citrate stabilized Au NP containing amino acid solution.*

Conc of phenylalanine (m mole dm^{-3})	Conc of Tryptophan (μ mol dm^{-3})	Conc of tyrosine (m mol dm^{-3})	Conc of glutamine (m mol dm^{-3})	Conc of Lysine (m mol dm^{-3})
0.97	1.40	0.06	5.70	0.018
1.89	2.81	0.13	6.84	0.036
2.75	4.22	0.20	7.89	0.054
3.56	5.63	0.26	8.86	0.073
4.32	7.04	0.33	9.77	0.091
5.04	8.45	0.40	10.6	0.11
5.72	9.86	0.46	11.4	0.12
6.37	11.2	0.53	12.1	0.14
6.98	12.6	0.60	12.8	0.16
7.56	14.0	0.66	13.4	0.18
8.11	15.5	0.73	14.0	0.20
8.64	18.3	0.80	14.6	0.22

TH-777_05612211

Preparation of amino acids solution

25 mg, 10 mg, 25 mg and 20 mg of L-phenylalanine, L-tyrosine, L-glutamine and L-lysine respectively were separately added to 30 mL vials containing 5.0 mL water each. L-phenylalanine and L-tyrosine solutions were slowly warmed in hot plate to dissolve. The solutions were then brought to room temperature. The other two amino acids dissolved in water at room temperature. The final concentrations of the amino acids in the solutions were 30.26 Mm for L-phenylalanine, 10.74 mM for L-tyrosine, 34.2 mM for L-glutamine and 27.36 mM for L-lysine respectfully. Finally, the pH of the solution was made to be 3.42 by addition of 20 μL of 0.23 M HCl to this mixture. In addition, tryptophan solution was prepared by the following method. Typically, 5.0 mg of L-tryptophan was dissolved in 10 mL water. From this solution, 2.0 mL was taken to dilute with 8.0 mL water so that final concentration of the L-tryptophan is 0.60 mM. Finally, the pH of the solution was made to be 3.42 by addition of 20 μL of 0.23 M HCl to the mixture.

TH-777_05612211

Mixing aqueous amino acids with citrate stabilized Au NPs

Several samples of 3.0 mL of the above citrate ion capped Au NPs solutions were taken in 30 mL vials. Aqueous amino acids solutions of different concentrations were slowly added to different vials containing the Au NPs. The mixtures were kept at room temperature for 30 min. The final pH values of the solutions were measured to be 3.45. The solutions were used for all studies. The final concentrations of all the amino acids in the above solutions are given in Table 8.1A. In the solutions containing the lower amount of amino acids there was no visible precipitation even after a day, but at higher concentration precipitation was observed in 20 min.

Characterization study

UV-vis absorption spectra of the samples were recorded, using a Varian model Carry 50 Bio or Perkin Elmer model Lambda 35 UV-visible spectrophotometer, in the range of 200 to 1100 nm. FTIR spectra of the pure acetanilide and acetanilide treated citrate capped Au NPs were measured using a Perkin-Elmer Spectrum One spectrometer. For amino acids treated citrate stabilized Au NPs, the following procedure was followed for sample preparation. After addition of amino acid (6.98 mM for L-phenylalanine, 15.5 μM for L-tryptophane, 0.66 mM for L-tyrosine, 13.4 mM for L-glutamine and 0.20 mM for L-lysine) into citrate ion capped Au NPs, the solution was subjected to centrifugation at 15000 rpm and at 20^{o}C. The pellet was washed with water. The cycle was performed thrice before collecting the pellet, which was air-dried and then mixed with KBr to record FTIR spectrum. Similarly, all solid amino acids were mixed with KBr to make a pellet for FTIR measurement. FTIR spectra were recorded in the region of 4000-400 cm^{-1}. Transmission electron microscopy (TEM) measurements were performed using a JEOL-2100 equipment operating at a maximum acceleration voltage of 200 kV. The TEM samples were prepared by placing a drop of liquid on carbon coated copper grid (400 mesh) followed by evaporation of the solvent at room temperature.

TH-777_05612211

8.1.3. Result and discussion

Citrate stabilized Au NPs, prepared based on our earlier reported method,[18a] were produced in uniform dispersion with the characteristic peaks of surface plasmon band observed at 527 nm. Addition of aqueous solution of different amino acids into citrate stabilized Au NPs showed changes in the color of the solution from red to faint purple and then purple and the solutions finally turned into blue color with further increase in concentration of amino acids. Figures 8.1.1 (A) and (D) shows the UV-vis spectra of the solution after addition of different concentrations of phenylalanine and lysine into citrate stabilized Au NPs solution. The spectra were recorded 30 min after mixing. The spectra revealed that upon increasing the concentrations of either of the amino acids, the SPR band first broadened, which upon further increase in concentration gave rise to two peaks – one near the original peak, while the second peak appeared at higher wavelength. For example, at the concentration of 6.37-7.00 mM the peaks occurred at 682 nm and 700 nm for phenylalanine, while that for lysine (73 μM) appeared at 684 nm. The peak at longer wavelength is due to longitudinal surface plasmon (LSPR) of Au NP and this can be ascribed to the formation of linear chain-like assembly of the NPs. The LSPR band position increased with increase in concentration. Interestingly, after certain concentrations (8.64 mM for phenylalanine and 0.12 mM for lysine) there was no further change in the peak position. The observations indicate that while increasing the concentration of amino acids the number of Au NPs involved in the assembly increased, however, after certain concentration there was no change as all NPs might have been involved in the assembly formation and there was no change in the structure of the assembly. Further, similar observations were made with other amino acids, which are tryptophan, tyrosine and glutamine. However, the observations with different amino acids suggest that the formation of 1D chain assembly of Au NPs and associated optical properties were not only dependent on the concentrations of amino acids but also on the nature of the side chain group present in the amino acid. For example, when lysine, tryptophan and tyrosine were used micromolar quantities of the acid was enough to induce a large scale organization and appearance of the LSPR band. On the other hand, when phenylanine and glutamine were used milli-molar quantities of amino acids were required to

TH-777_05612211

achieve significant changes in the absorption spectra (Appendix-I). These observations imply that changes of the optical absorption spectra of Au NPs are highly specific to the amino acid present in the medium.[25]

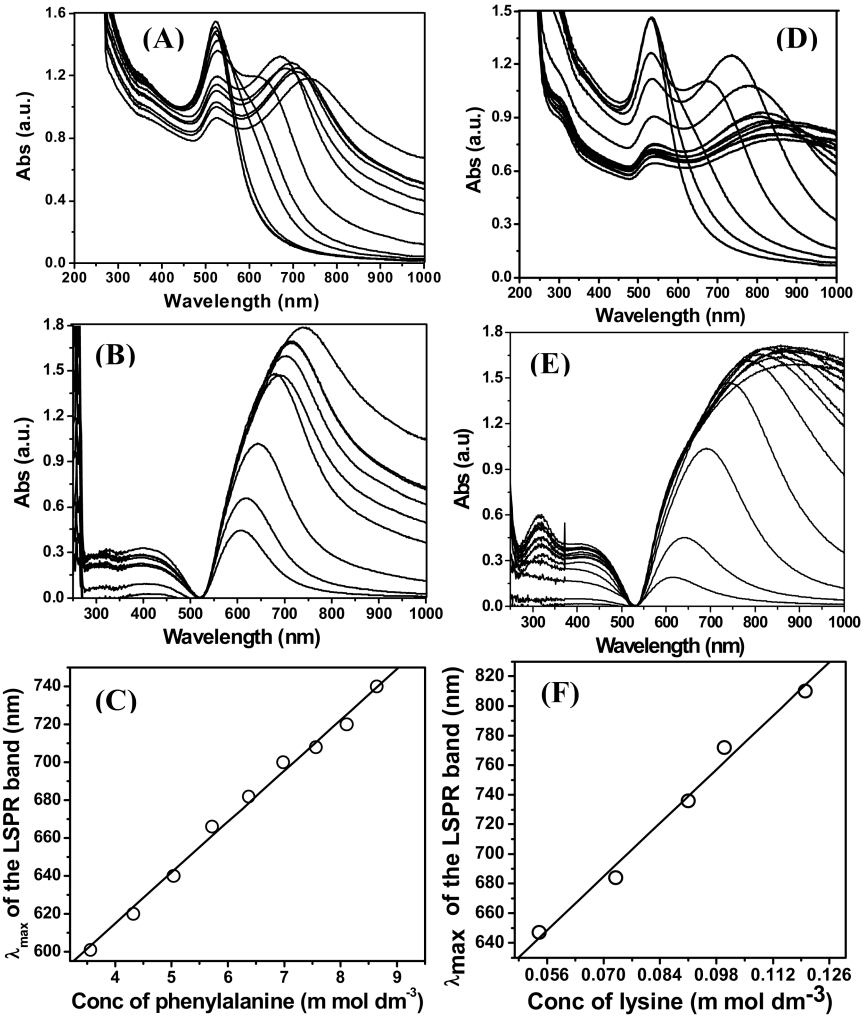


Figure 8.1.1. *(A) and (D) are the UV-Visible absorption spectra upon addition of different concentrations of L-phenylalanine and L-lysine into citrate stabilized Au NPs solution. (B) and (E) were obtained after normalization of graphs (A) and (D) and then subtraction of absorption maxima at 527 nm. (C) and (F) are the plot of shifting of the LSPR band of the citrate stabilized Au NPs with concentration of L-phenylalanine and L-lysine solution.*

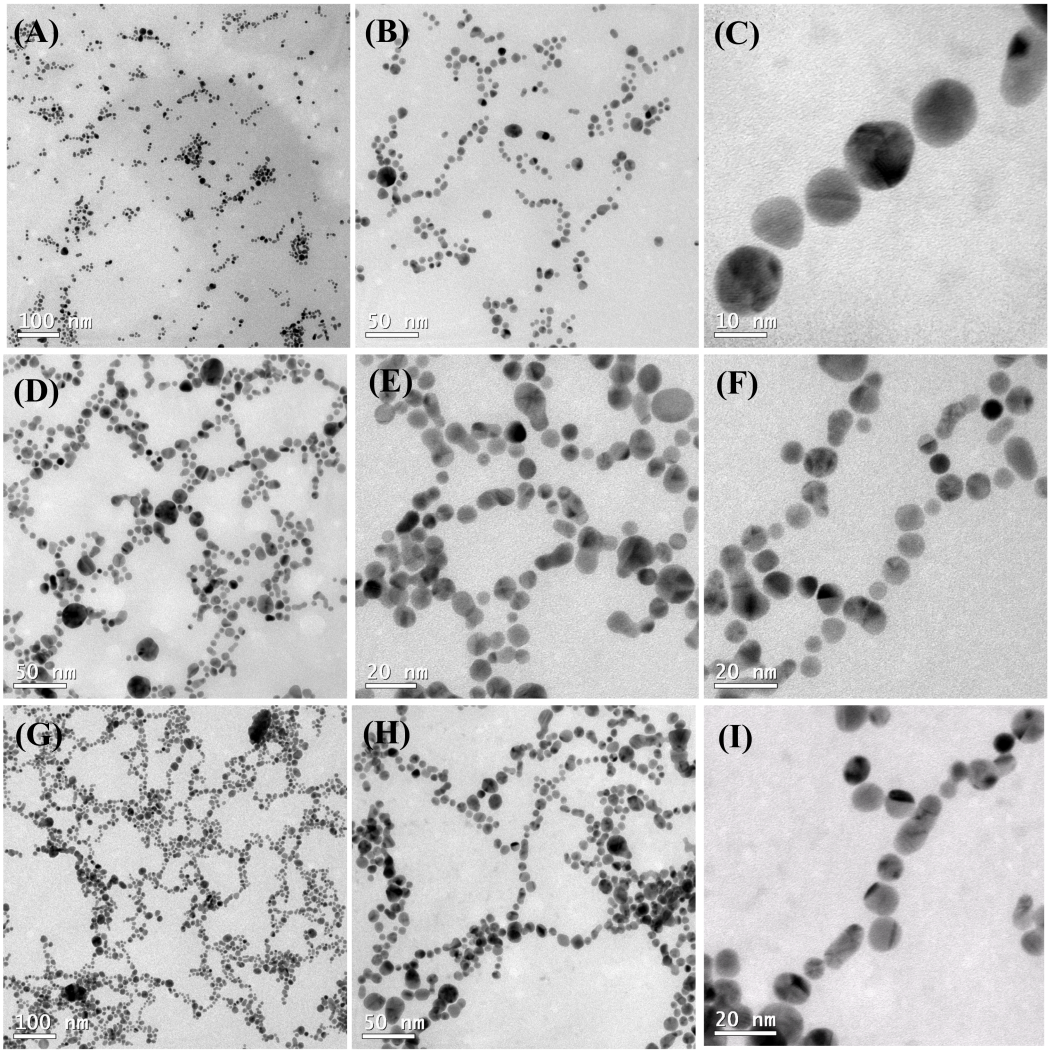
TH-777_05612211

Further we were interested to find a correlation between the optical absorption spectra of amino acids induced chains of Au NPs assembly versus concentrations of different amino acids. This would allow the development of a simple method of finding the concentration of amino acid present in a medium. This was pursued by normalization of the obtained absorption spectra of different amino acid treated citrate stabilized Au NPs, followed by subtraction of the spectrum due to Au NPs (in absence of amino acid) with absorption maximum at 527 nm. This resulted into plots of absorption with wavelength maxima of LSPR band of the Au NPs assembly (Figures 8.1.1 (B) and (E)). From the graphs, plots of shift in the wavelength maximum of LSPR versus the concentration of each amino acid present in the solution were obtained, which were straight lines (Figures 8.1.1 (C) and (E)) and (Appendix-I). Further, the observations also indicate that some of the amino acids led to aggregation of Au NPs than the other at lower concentrations. For example, tryptophan and tyrosine show (Figures 8.1.1A, (A) and (D): Appendix-I), higher changes in the absorption intensities of the LSPR band of the Au NPs, with less shifting of the wavelength maximum. On the other hand, in the case of phenylalanine or lysine treated Au NPs both the intensities and wavelength maximum changes more with concentrations of the amino acids. The sensitivity of the absorption and wavelength maxima of Au NPs with respect to the addition of different amino acids indicate a newer way of estimation of concentration of the amino acid, in addition to its specificity.

Further, in order to understand the growth of chain formation and morphology of the 1D chain of Au NPs assembly, we have carried out TEM measurements of different amino acid treated citrate stabilized Au NPs at various concentrations of amino acids. Figure 8.1.2 shows the TEM images of the NPs at different concentration of phenylalanine. As is clear from the figure, at the lowest concentration of phenylalanine (4.32 mM) the particles were assembled into liner 1D chain-like array of structures. At this concentration, there were still particles that were not involved in the assembly formation (Figure 8.1.2 (A) and (B)). When the concentration of phenylalanine was increased (for example, 5.72 mM) the number of particles involved in the assembly was more, which also subsequently increased the length of the chains of Au NPs assembly (Figure 8.1.2 (D) and (E)). Further at still higher

TH-777_05612211

concentrations of phenylalanine used, the 1D chains of assembly formed branched structures (Figure 8.1.2 (G) and (H)). The results imply that addition of phenylalanine into citrate capped Au NPs, led to self-assembled linear chains of assembly and the number of particles involved in the assembly increased with increasing the concentration of the amino acid. High resolution TEM images show (Figure 8.1.2 (C), (F) and (I)) that Au NPs although were close to each other, there was gaps between two neighboring NPs.



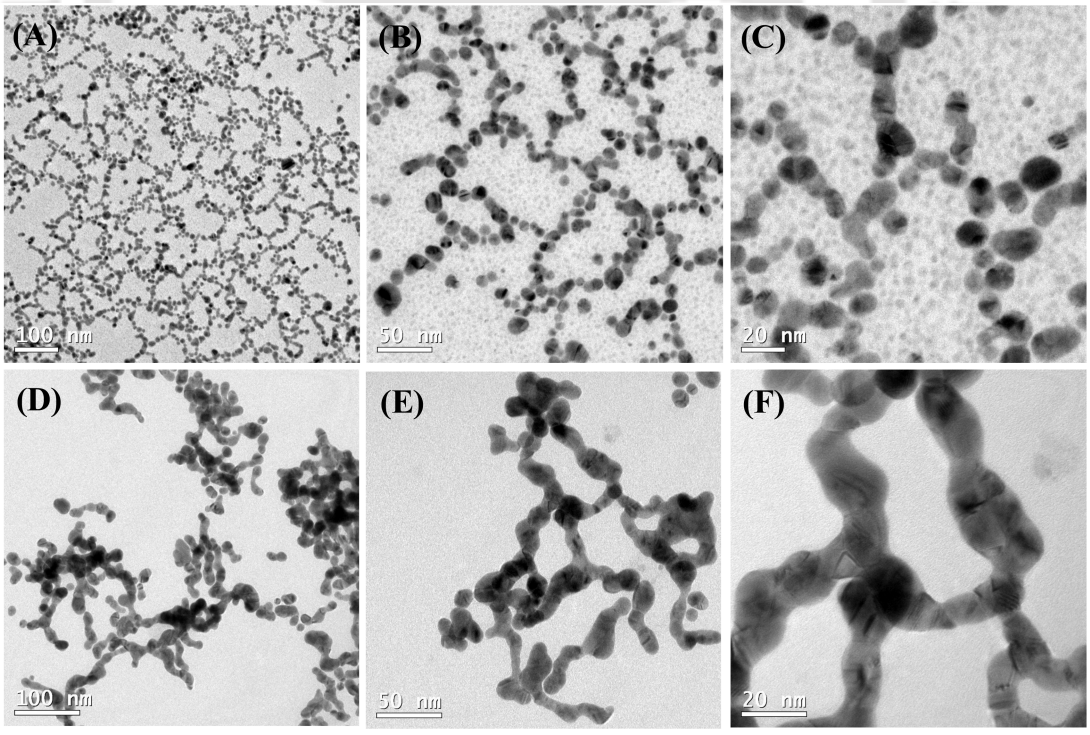
TH-777_05612211

***Figure 8.1.2**. Transmission electron micrograph (TEM) image of citrate capped Au NPs (A) in the presence of 4.32 mM of phenylalanine; (B) and (C) are the expanded views of (A). (D) is in the presence of 5.72 mM, (E) and (F) are the expanded views of (D). (G) is in the presence of 8.11 mM of phenylalanine, (H) and (I) are the expanded views of (G).*

The observation demonstrates that while adding the phenylalanine in to citrate stabilized Au NPs, the phenylalanine molecules are captured on the surface of the Au NPs that subsequently leads to the formation self-organized 1D chain of assembly of the NPs. Further, the benzene ring on the phenylalanine backbone may reinforce the formation of assembly of Au NPs into linear chains. This is further supported by the observations of assembly formation using tyrosine. Figure 8.1.6A (Refer: Appendix-II) shows the changes in the spectra of Au NPs upon addition of different amounts of tyrosine into citrate stabilized Au NPs. The results show that at considerably low concentration (0.2 mM) of tyrosine the particles were assembled into either linear chain or branching of chains of Au NPs occurred. Slight increase in the concentration of tyrosine causes dramatic increase of assembling of Au NPs. At the highest concentration (0.46 mM) used herein formation of large aggregation of Au NPs occurred. The large aggregation of Au NPs assembly appeared in the form of linear chains with concurrent branching of arrays (Figure 8.1.6A (E) and (F): Appendix-II). In these structures the particles were in close contact with each other, however, maintaining interparticle distance to suggest that stabilizing molecules were present in the intervening region. This could due to the presence of tyrosine molecules in between the NPs, where both the benzene ring and OH group (through H-bonding) contribute to the stability of the structures. Hence the observation of longitudinal plasmon resonance band at longer wavelength, due to the uniaxial organization of Au NPs into linear chain-like array of superstructures, which could be responsible for interparticles coupling of surface plasmon of the individual Au NPs along the linear chains.[24, 26] However, it is interesting to note that the amount of tyrosine molecules required for the formation of assembly is much less compared to that required while using phenylalanine. This might be due to contributions of the side chain groups of those amino acid molecules in the formation of linear assembly, which will be discussed later in this section.

TH-777_05612211

On the other hand, when lysine (0.054 mM) was added to citrate stabilized Au NPs the particles self-assembled into linear chain-like array of superstructures (Figure 8.1.3), some of which were found to be fused to each other unlike previous cases of simple assembly formation. Further increasing concentration (0.1 mM) of lysine led to complete fusion of the NP, which appeared as interconnected fibers rather than assembly of NPs (Figure 8.1.3 (D) and (E)). Also interesting to note was that assembling of the Au NPs in the presence of lysine occurred at much lower concentration (of the amino acid) in comparison to that using phenylalanine. Further, at low concentrations of lysine, all Au NPs are might be self-assembled into either linear chains or branched chains of Au NPs, most of which might not have been fused; however, the self-assembled Au NPs start fusing with each other gradual increase in the concentration of lysine and then finally formed the nanofibers. UV-vis spectra of lysine added NPs also support the formation of assembly of NPs with increasing concentration of the amino acid.



TH-777_05612211

***Figure 8.1.3**. Transmission electron microscopy (TEM) images of citrate capped Au NPs (A) in the presence of 0.054 mM of lysine; (B) and (C) are the expanded views of (A). (D) is in the presence of 0.11 mM, (E) and (F) are the expanded views of (D).*

This could be due to the fact with gradually increasing the concentration of lysine, the Au NPs started to self-assemble, the process further continuing with increasing the concentration of lysine. The process results in the appearance of the second peak and increase in the wavelength maximum of LSPR band. After certain concentration of lysine (0.054 mM), the Au NPs involved in the assembly start to fuse with each other, while free NPs continue to assemble, and the process is completed at higher amino acid concentration.

The above observations suggest that not only is the amino acid concentration important in the assembly of Au NPs into linear superstructures, the nature of the acid with its residues plays important role in this regard. This forms the basic of concentration specific organizations. Further evidence of the above observation comes from studies with glutamine. TEM results are shown in Figure 8.1.7A (Appendix-III), which demonstrates the effect of the amino acid of different concentrations on the citrate stabilized Au NPs. The figures clearly shows that at lower concentration of glutamine (7.89 mM), assembly formation took place; however, the number of particles involved in the assembly was small (Figure 8.1.7A (A) and (B): Appendix-III). On the other hand, when the concentration was increased gradually the number of particles involved in the assembly also increased leading to the formation linear and / or branched chains of Au NPs. The assemble particles get fused with each other along the chain, at higher concentrations of glutamine (10.6 mM or higher). Further, increasing the concentration of the glutamine leads to formation of either longer chain or particles or branching took place accompanied by fusion of them. The behavior of assembly formation followed by fusion of particles using glutamine is similar to that using lysine. However, what is interesting is that the concentrations needed to induce the assembly formation in both the cases are different. For example, 0.054 mM of lysine was needed to form the well organized assembly Au NPs either in linear chain or branched chain form. On

TH-777_05612211

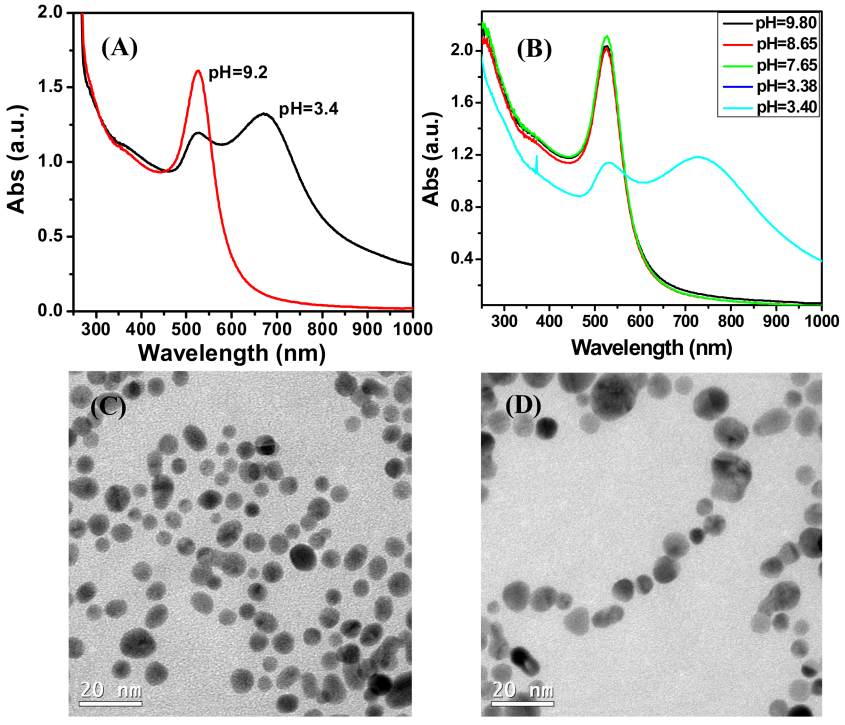
the other hand, 10.6 mM of glutamine was needed for the same assembly process to have taken place. This means that the nature of side chain present in the amino acid plays an important role in the formation of assembly of Au NPs. The difference in the side chains lead to the difference in the concentrations needed for the assembly formation and also the appearance of the second peak followed by it shift. Also, the same reason may be applicable for the difference in the position of the LSPR band at the highest concentrations of the amino acids. The same reason may be behind the fusion of the assembled NPs in the presence of specific amino acids, whereas it is not there in other cases. The amino acids that have been used here have either hydrophobic side chains or hydrophilic ones.

While protonated amine and carboxylate groups results in the attachment of amino acids to the citrate stabilized Au NPs, they also contribute to the formation of dipoles that involves citrates and amino acids (protonated) that partially replaces some of the stabilizers. In addition, weak interactions such as H-bonding, van der Waals and hydrophobic interactions may also contribute to the formation of linear assembly as well as fusion of the assembled NPs in some cases. While, both kinds of side chains led to the formation of assembly, it is interesting to note that amino acids with hydrophilic side chains led to the fusion of the assembled NPs. Even more interesting to note is the fact that while lower concentration of lysine could induce assembly and fusion, considerably higher concentrations of glutamine was required for the same.

Further, studies were pursued with citrate stabilized Au NPs by addition of different concentrations of tryptophan. In this regard, although tryptophan has nonpolar side chain, its behavior might be different due to the presence of the indole moiety. The indole moiety is hydrophilic and thus might lead to behavior similar to lysine or glutamine. The observations indicate that at lower concentrations of tryptophan (for example 5.63 μM), the Au NPs were assembled into linear structure (Figure 8.1.8A: Appendix-III) and albeit formation of branched structures were also present. The interparticle distances between Au NPs in the assembled structures were larger in comparison to that when glutamine or lysine was used in the assembly formation. Interestingly, when the concentration of the tryptophan was gradually increased (to 11.2 μM) the particles seem to have come closer together (Figure

TH-777_05612211

8.1.8A (C) and (D): Appendix-IV) and there were adhesion of adjacent particles i.e. two neighboring particles were close to each other with almost no gaps in between them. Finally, the arranged particles formed nanofibers at even higher concentration of tryptophan (18.3 μM). High resolution TEM images of the samples prepared with the highest concentration of tryptophan treated citrate stabilized Au NPs indicated that the particles were fused into each other in the chains of Au NPs assembly (Figure 8.1.8A (F): Appendix-IV). The above TEM results are commensurate with the UV-vis study of citrate stabilized Au NPs solution at different concentrations of tryptophan. Importantly, the amount of tryptophan required for the self-assembly of Au NPs is very less (1.0 to18.0 μ M) in comparison to that used for lysine or glutamine. The results suggest that the cross-linking interaction between the indole groups may be responsible for the enhancement of assembly formation at lower concentration of tryptophan molecules in the solution. Further, the interparticles interaction between the indole moieties containing benzene ring may reinforce the assembly formation of Au NPs into 1D chain-like structure.



TH-777_05612211

Figure 8.1.4. *(A) and (B) are the UV-Visible spectra recorded upon addition of lysine and phenylalanine at different pH to the citrate stabilized Au NP. (C) TEM image of addition of phenylalanine at pH=9.03 and (D) is the TEM image at pH=3.38*

There have been many reports are available in the literature related to the binding of amino acids to Au NPs. For example, Sastry et al reported that at physiological pH, the amine group (that is attached to the α-carbon to the amino acids) can bind to Au NPs surface via strong interaction and they have also reported that protanated amine group can also bind electrostatically to Au NPs surface.[27] According to zhong et al, at lower than physiological pH (3.20 to 5.60), the amino acids can bind strongly with Au NPs and they have also reported that the formation of the linear organization of Au NPs is dependent on the pH of the medium.[28] On the other hand, the organization had no control in the unidirectional growth of Au NPs assembly. Recently, Xu and co-workers have shown that the formation of linear chain-like Au NPs assembly is dependent on the amount of glutamic acid used in the medium, when Au NPs were synthesized in a single-step by using sodium borohydride as the reducing agent for $HAuCl_4$.[29] To the best of our knowledge there is no report on the systematic organization of Au NPs into linear chain-like superstructure by using the properties of different amino acid molecules. More recently, we have found that protonated amine group (p-amino acetanilide) can exchange the citric acid on the Au NPs surface and the extent of replacement of the citric acid can be controlled by controlling the concentration of protanated amine molecules. In order to understand the pH dependence of the assembly formation experiments were pursued by UV-vis spectroscopy and TEM studies with lysine and phenylalanine. The results are shown in Figures 8.1.4 (A) and (B). It is interesting to observe that at higher pH, there is a single SPR band of the Au NPs; however, when pH of the solution was decreased to a value of 3.40, there was an additional peak at longer wavelength, which is due to the LSPR band of the Au NPs. Further, results of TEM investigations of samples with phenylalanine added to citrate stabilized Au NPs at different pH are shown in Figure 8.1.3 (C) and (D). The images clearly show at lower pH, the Au NPs

TH-777_05612211

were self-assembled into linear chain-like array of superstructure, whereas individual particles were present at higher pH. At higher pH, the protonated form of amino acids is not present. This does not favor dipole formation needed for uniaxial arrangement of particles. In addition, electrostatic repulsion between the COO^- of the amino acid and citric acid molecules on the surface of the Au NPs may not favor arrangements of neighboring particles. Hence the particles remain as uniformly distributed individual ones.

In order to understand the role of amino acid molecules for organization of Au NPs in 1D chain, we have carried out the FTIR analysis of the amino acid treated citrate stabilized Au NPs. Figure 8.1.5 shows the FTIR spectra of samples consisting of added phenylalanine or lysine into citrate stabilized Au NPs. The characteristics band in the region of 1400-1600 cm^{-1} and 3436 cm^{-1} due to COO^- stretching and N-H asymmetric stretching vibration confirmed the presence of amino acids in the treated samples (Figure 8.1.5 (B and D)). The bands at 1081 cm^{-1} and 703 cm^{-1} are ascribed to the presence of benzene ring.

TH-777_05612211

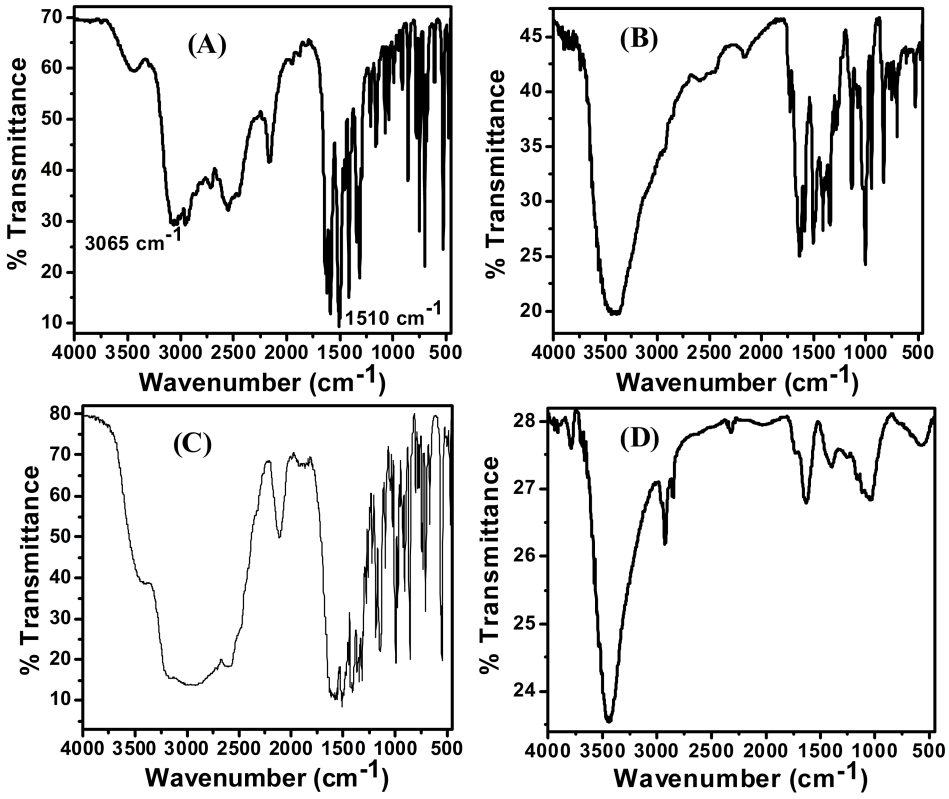
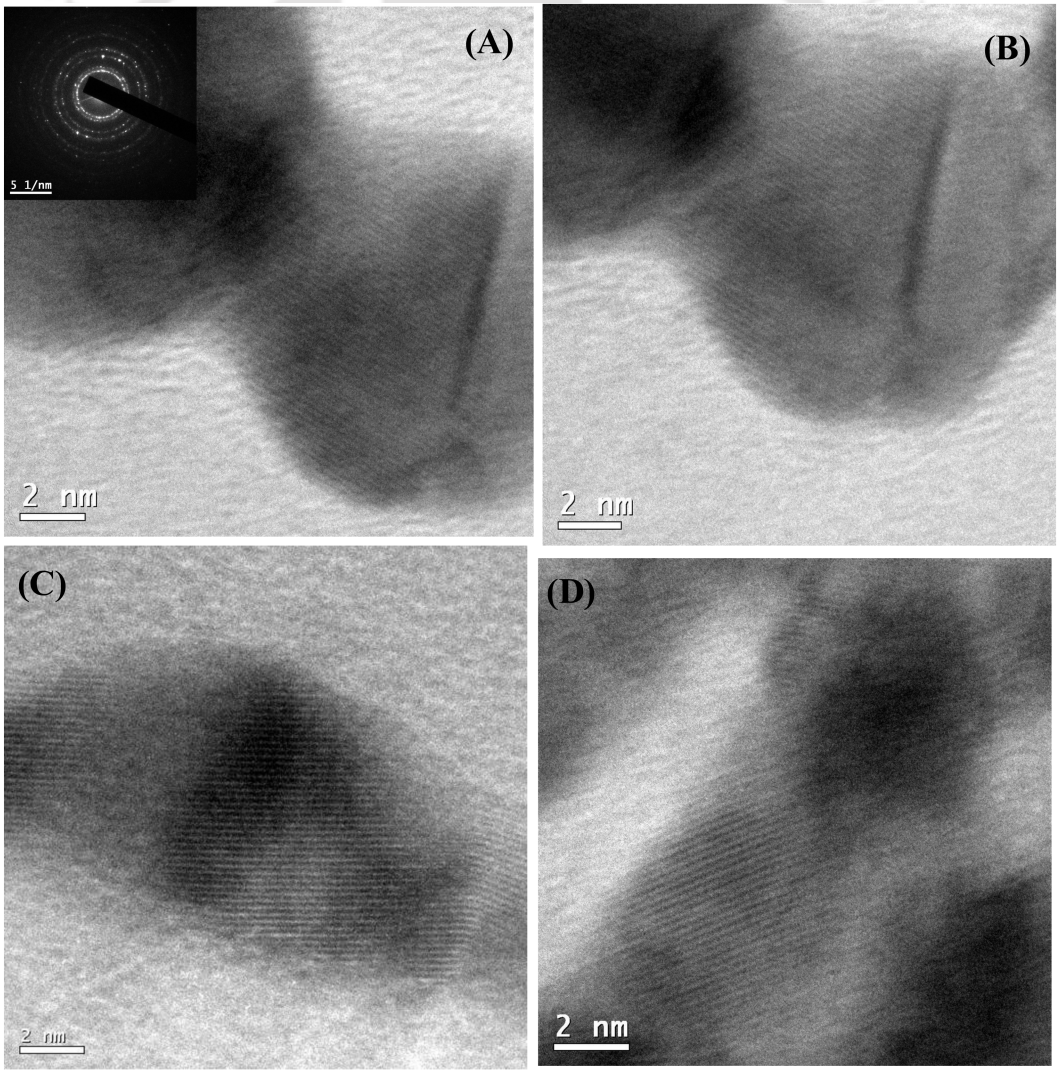


Figure 8.1.5. *FTIR spectra of (A) and (C) are those of pure phenylalanine and lysine respectively, (B) and (D) are those of phenylalanine and lysine treated citrated stabilized Au NPs.*

The bands at 1160 cm^{-1}, 1128 cm^{-1}, 1098 cm^{-1} and 2916 cm^{-1} are the characteristic vibration modes of C-C stretching and CH_2 asymmetric stretching. Further, the peaks at 1510 cm^{-1} and 3065 cm^{-1} are due to symmetric deformations and asymmetric stretching vibration of protonated $–NH_2$ group of amino acids. Interestingly, we observed that the intensity of the asymmetric deformation band of $–NH_3^+$ (1510 cm^{-1}) was decreased (Figure 8.1.9 Appendix-V) in amino acid treated citrate stabilized Au NPs. Further, the intensity of asymmetric stretching mode of protanated $–NH_2$ at 3065 cm^{-1} significantly decreased and in

TH-777_05612211

some of the amino acids, the band at 3065 cm^{-1} is completely vanished (Figure 8.1.4 (B) and Figure 8.1.9A (D), (E) and (F): Appendix-V) upon treatment with the NPs.[29, 30] This observation clearly indicates that protanated amine group in the amino acids strongly interact with the citrate stabilized Au NPs. Further evidence of the above observation - the FTIR spectrum of all the amino acids treated citrate stabilized Au NPs - are shown in Appendix-V. Therefore, the above results implies that upon addition of amino acids into citrate stabilized Au NPs at pH=3.4, the citrate molecules are effectively exchanged by amino acids (at least partially) leading to the formation asymmetric charge distribution on the surface of the Au NPs, which is a prerequisite for extrinsic dipole-dipole interaction on the surface of the Au NPs.



TH-777_05612211

***Figure 8.1.6**. (A) and (B) are the high resolution TEM images of 0.11 mM of lysine treated citrate stabilized Au NPs. The inset in (A) is SAED picture of corresponding nanofibers. (C) is due to 12.41 mM glutamine treated citrate stabilized Au NPs and (D) is due to 18.63 μM of tryptophan treated citrate stabilized Au NPs*

Moreover, the protonated amino acids, which are strongly bound on the specific crystallographic facets of the Au NPs, may induce dipolar interactions among the Au NPs in the solution and that causes the unidirectional growth of the Au NPs in the solution. In other words, when protonated amino acids molecules interact with citrate stabilized Au NPs, the amino acids molecules are non-uniformly distributed on the surface of the Au NPs (after partially replacing the citrates), leading to the formation of one dimensional array of structures. According to Liz-Marzan and coworkers, non uniform distribution of stabilizer molecules on the surface of the Au NPs induces the strong dipole-dipole interaction, which could be responsible for the organization of Au NPs into linear arrays.[31] Our observations also suggest that addition of protonated amino acid molecules into citrate stabilized Au NPs possibly creates the polarity on the Au NPs surface, upon which a few Au NPs interact to form short chains. These short chains of arrays of NPs agglomerate further at higher amino acid concentrations to form larger arrays. At certain amino acid concentrations the growing of the long chain array is limited and formation branched arrays and finally interconnected network of assembly formation are thermodynamically favored. This may be due to the creation of extra entropy contribution, which favors the formation of branched structures.[21b, 32] Further, the interparticle cohesion within the chains and networks could be reinforced by hydrophobic moieties of the benzene ring present in the surface bound amino acids (phenylalanine and tyrosine molecules).[11b] The understanding of the interparticles interaction and cross-linking reactivity in the unidirectional assembly of Au NPs is one of the important focuses of current research interests.[33] This is especially true, when amino acids are involved in the assembly of Au NPs and the assembling behaviors depend on the functional groups and side chains of the acids. Our observation suggests that in the presence of hydrophobic amino acids such as phenylalanine and tyrosine, the particles

TH-777_05612211

are assembled either in linear array of chain or branched chains without the presence of fusion among the particles. On the other hand, in the presence of lysine, glutamine or tryptophan molecules, at the lowest concentrations of the acids, the particles are assembled into necklace chain-like arrays and the get fused and finally long chains of nanofiber (including branched ones) are formed. This indicates that amino acids with hydrophilic or polar side chains are causing the formation of nanofiber, while the ones with hydrophobic side chain does not lead to the formation of nanowires. In order to understand the fusion of Au NPs in 1D chain better, we have carried out high resolution TEM analysis of the samples treated with lysine, glutamine and tryptophane amino acid, which are shown in Figure 8.1.6. Essentially the images show that the fibers consist of fused particles with continuous lattice fringes along the plane of fusion. When the lattice plane spacing was calculated a value of d= 0.236 nm was obtained, which corresponds to the spacing of (111) faces of Au NPs.[19,18a,29,34] Further, the selected area electron diffraction pattern (SAED) of the nanofibers, which is shown in inset of Figure 8.1.5 (A) have well defined crystallographic facets and the electron diffraction pattern due to (111), (200), (220) and (311) faces of Au NPs.[18a,34] Thus the observations strongly suggest that more hydrophilic amino acids such as lysine and glutamine induce the fusion of the Au NPs to each other and fusion of the particles occurred along (111) faces of the crystallographic planes; and at higher concentration these fused particles indeed to form nanofiber. Xu and coworkers suggested that the attachment of Au NPs leading to the formation of the chains might be driven by the chemical bond formation between the structurally similar surfaces of the Au NPs. Our observations indicate that the more hydrophilic amino acids such as lysine and glutamine molecules may be bound very weakly on the (111) facets of the Au NPs surfaces. It is worth to mention that the binding ability between the amine group of the amino acids and Au NPs surfaces is different for different facets and especially on the (111) faces is relatively weaker compared to other ones.[29,35] According to kotto and coworkers, the strong dipole-dipole interaction leading to the formation of arrays followed by removal of stabilization shell on the pearl-necklace assembly of NPs by organic solvents may be responsible for the formation of nanowires. [36]

TH-777_05612211

Our observations imply that addition of higher concentrations of hydrophilic amino acid molecules into citrate stabilized Au NPs causes the removal of weakly bound amino acids (which are highly soluble in water) on the Au NPs and leading to the formation of nanofibers through fusion of NPs. On the other hand, addition of non-polar or hydrophobic amino acids that are sparingly soluble in water, leads to a structure that would minimize Gibbs energy including hydrophobic interaction. This would be favorable with amino acids being in between the NPs rather than being in the solution (as they are lowly soluble), in addition to being present along the sides of the chain. In other words, although hydrophobic amino acids are weakly bound to the (111) facets of the Au NPs, they may not be removed from the Au NPs after assembly, because solvation energy is not available to overcome the interaction of weakly bound amino acids on the surface of the Au NPs. The interparticle interactions among the phenylalanine or tyrosine molecules in the arrays (and present in the intervening region of the NPs) could be driven by strong Π- Π interaction between the benzene rings present in the acids. This leads to maintaining interparticle spacing along the chains of Au NPs assembly and fusion of particles does not take place.

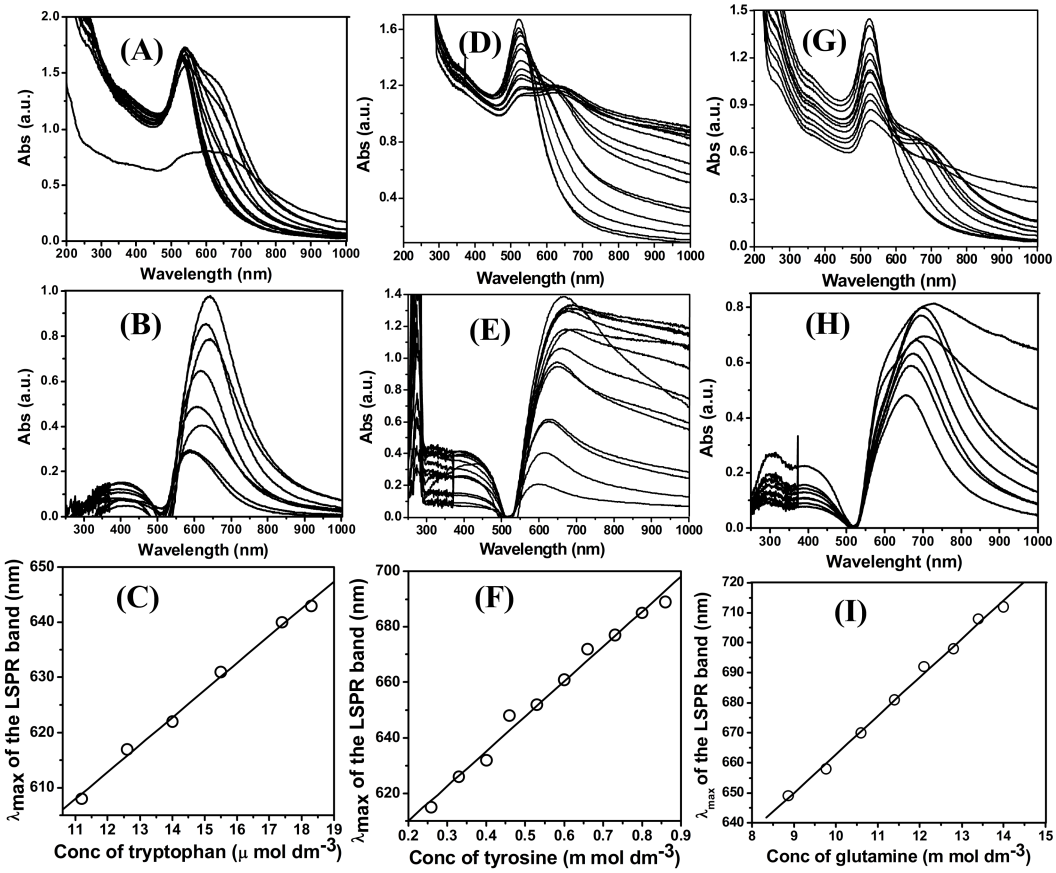
8.1.4. Conclusion

We have developed a facile method of preparation amino acid mediated one dimensional assembly of linear chain-like array of superstructures. The formation of linear array of Au NPs depended on the nature of the amino acid and its concentration in the medium. Our observations suggest that amino acids with hydrophilic side chains produce long chain Au nanofiber via the formation of necklace-like chains of Au NPs assembly. On the other hand, the ones with hydrophobic side chains produced necklace-like assembly of Au NPs without the presence of any fusion among the NPs. The optical properties of assembled Au NPs produced in the forms of 1D chain and fibers were dependent on the side chains of the amino acids. This may also provide newer ways of estimation of amino acids concentration in the solution. Additionally, the present method paves the understanding of the interparticle interaction involving both hydrophobic and hydrophilic moieties present in

TH-777_05612211

the stabilizers. The present approach is expected to be of potential interest in future bionanodevice based applications.

8.1.5. Appendix-I



TH-777_05612211

***Figure 8.1.5A**. (A), (D) and (G) are the UV-Visible absorption spectra recorded after addition different concentration of L-tryptophan, L-tyrosine and L-glutamine respectively into citrate stabilized Au NPs solution. (B), (E) and (H) were obtained after normalization of graphs (A), (D) and (G) respectively, followed by subtraction of absorption maxima at 527 nm. (C), (F) and (I) are the plots of shifting of the LSPR band of the citrate stabilized Au NPs with various concentrations of L-phenylalanine and L-lysine solution.*

8.1.6. Appendix-II

TH-777_05612211

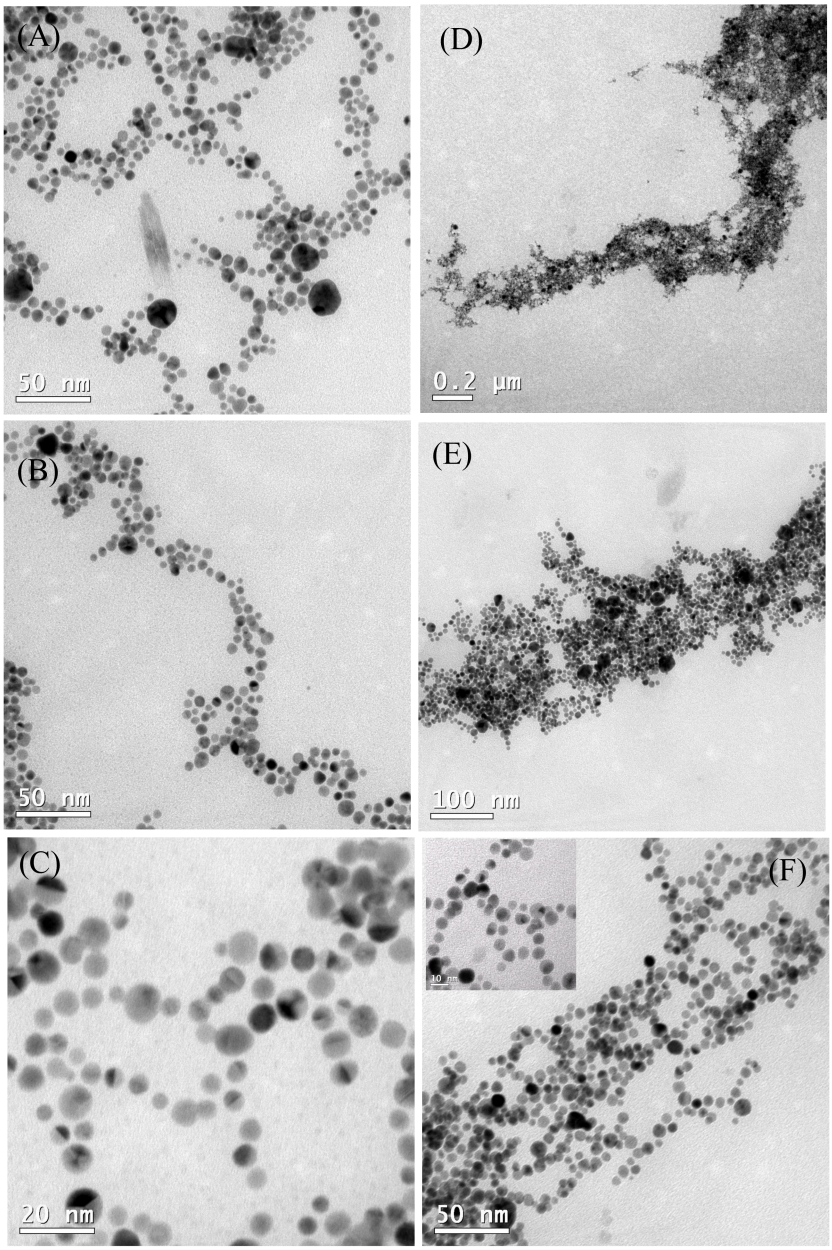


Figure 8.1.6A. *Transmission electron micrograph (TEM) image of citrate capped Au NPs (A) in the presence of 0.20 mM of tyrosine; (B) and (C) are other views of the same sample. (D) is in the presence of 0.46 mM, (E) and (F) are the expanded views of (D). The inset is the expanded view of (F)*

TH-777_05612211

8.1.7. Appendix-III

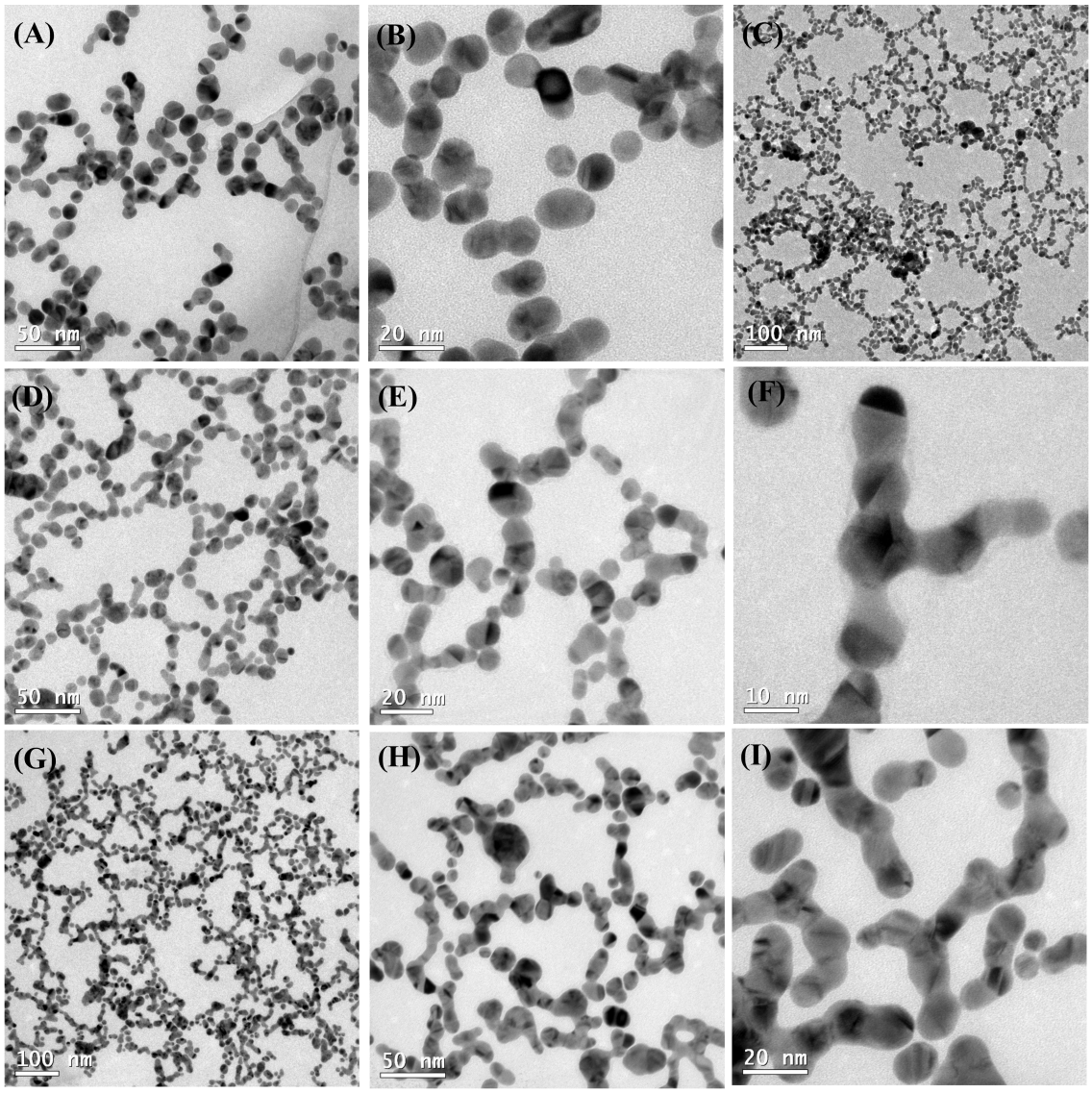
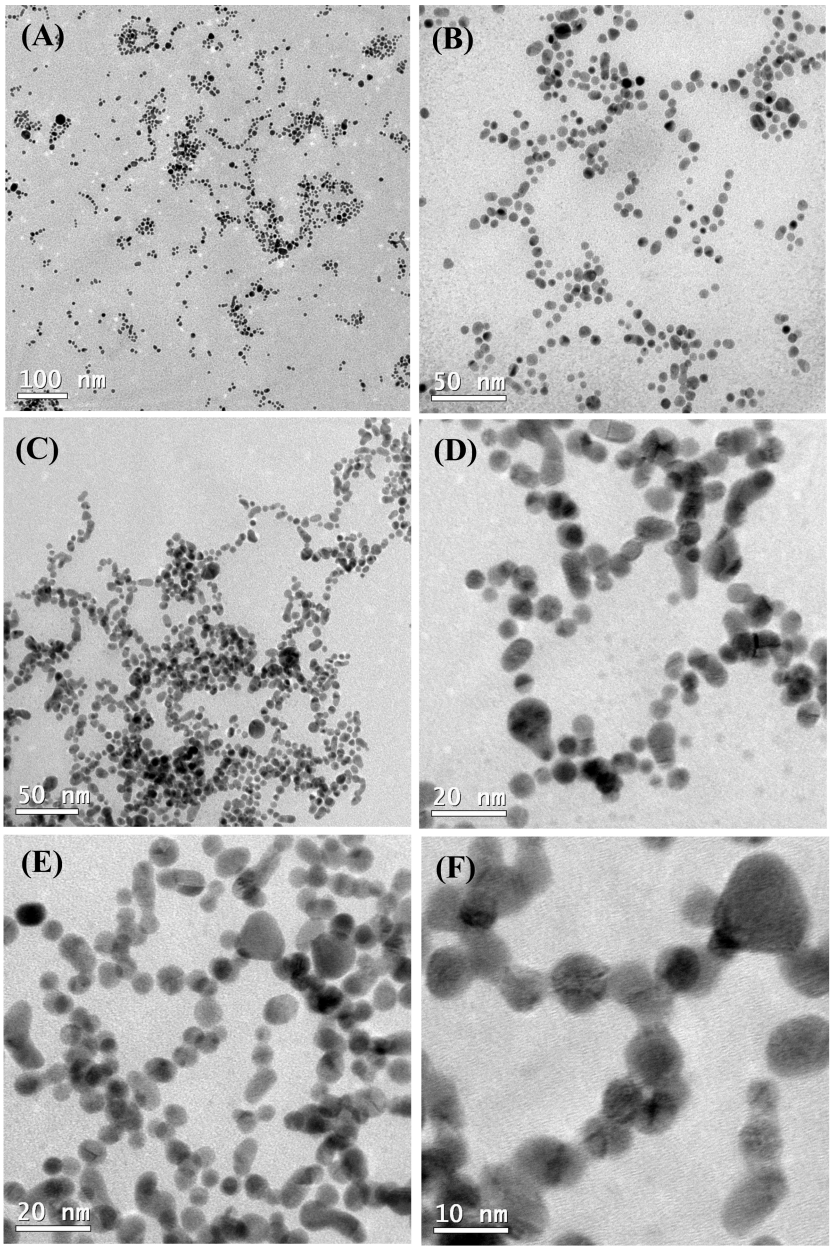


***Figure 8.1.7A**. Transmission electron microscopy (TEM) image of citrate capped Au NPs (A) in the presence of 7.89 mM of glutamine; (B) is the expanded view of (A). (C) is in the presence of 10.6 mM, (D), (E) and (F) are the expanded views of (C). (G) was obtained in the presence of 12.8 mM of glutamine, (D), (H) and (I) are the expanded views of (G)*

TH-777_05612211

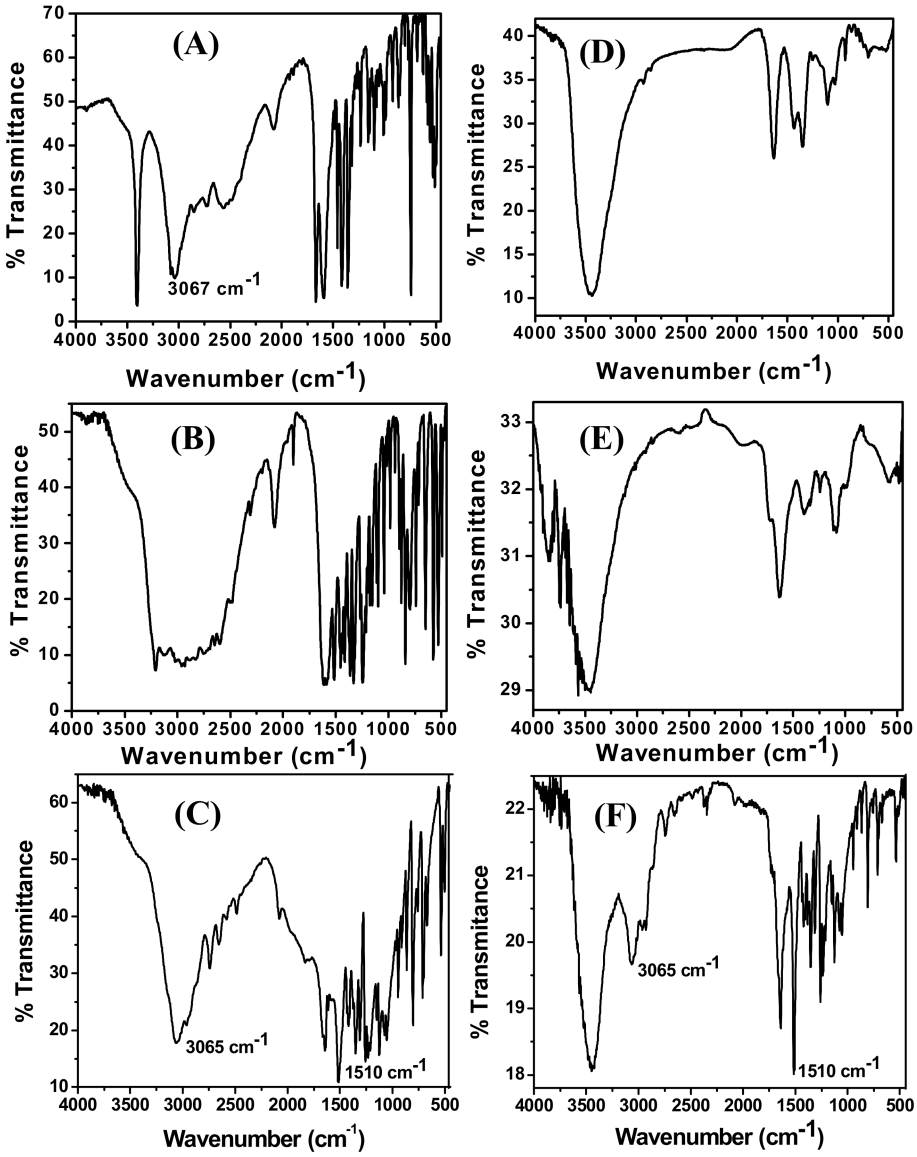
8.1.8. Appendix-IV



TH-777_05612211

***Figure 8.1.8A**. Transmission electron microscopy (TEM) image of citrate capped Au NPs (A) in the presence of 5.63 μM of tryptophan; (B) is the expanded view of (A). (C) was recorded in the presence of 11.2 μM, (D) is the expanded view of (C). (E) is in the presence of 18.3 μ and (F) is the expanded view of (E).*

8.1.9. Appendix-V



TH-777_05612211

***Figure 8.1.9A**. (A), (B) and (C) is the FTIR spectra of pure tryptophan, tyrosine and glutamine and (D), (E) and (F) are the corresponding amino acids treated citrate stabilized Au NPs.*

TH-777_05612211

8.1.10. References

1. Mair, S. A.; Kik, P. G.; Atwater, H. A.; Meltzer, S.; Harel, E.; Koel, B. E.; Requicha, A. A. G. *Nat. Mater*. **2003**, *2*, 229.

2. Sudeep, P. K.; Joseph, S. T. S.; Thomas, K. G. *J. Am. Chem. Soc*. **2005**, *127*, 6516.

3.Klein, D. L.; Roth, R.; Lim, A. K. L.; Alivisatos, A. P. McEuen, P. L. *Nature* **1997**, *389*, 699.

4. (a) Alivisatos, A. P. *Science* **1996**, *271*, 933. (b) Gardner, C. L.; Apps, R.; Russell, A. J. *High Power Microwaves* **1995**, *1*, 12. (c) Chen, J.; Wiley, B. J.; Xia, Y. *Langmuir* **2007**, *23*, 4120.

5. (a) Singh, H.; Laibinis, P. E.; Hatton, T. A. *Nano Lett*. **2005**, *5*, 2149. (b) Klokkenburg, M.; Vonk, C.; Claesson, E. M.; Meeldijik, J. D.; Erne, B. H.; Philipse, A. P. *J. Am. Chem. Soc*. **2004**, *126*, 16706.

6. Barnes, W. L.; Dereux, A.; Ebbessen, T. W. *Nature* **2003**, *424*, 824.

7. Wallraff, G. M.; Hinsberg, W. D. *Chem. Rev*. **1999**, *99*, 1801.

8. (a) Xia, Y.; Whitesides, G. M. *Annual Review of Material Science* **1998**, *28*, 153. (b) Xia, Y.; Whitesides, G. M. *Angew. Chem. Int. Ed*. **1998**, *37*, 550.

9. Kalsin, A. M.; Fialkowski, M.; Paszewski, M.; Smoukov, S. K.; Bishop, K. J. M.; Grzybowski, B. A. *Science* **2006**, *312*, 420.

10. Kinge, S. S.; Calama-Crego, M.; Reinhoudt, D. N. *Langmuir* **2007**, *23*, 8772.

11. (a) Teranishi, T.; Haga, M.; Shiozawa, Y.; Miyaka, M. *J. Am. Chem. Soc*. **2000**, *122*, 4237. (b) Kumar, A.; Mandal, S.; Mathew, S. P.; Selvakannan, P. R.; Mandale, A. B.; Chaudhari, R. V.; Sastry, M. *Langmuir* **2002**, *18*, 6478.

12. (a) Braun, E.; Eichen, Y.; Sivan, U.; Ben-Yoseph, G. *Nature* **1998**, *391*, 775. (b) Djalali, R.; Chen, Y.; Matsui, H. *J. Am. Chem. Soc*. **2002**, *124*, 13660.

13. Dujardin, E.; Peet, C.; Stubbs, G.; Culver, J. N.; Mann. S. *Nano Lett*. **2003**, *3*, 2437.

14. Mao, C. B.; Flynn, C. E.; Hayhurst, A.; Sweeney, R.; Qi, J. F.; Georgiou, G.; Iverson, B.; Belcher, A. M. *Natl. Acad. Sci. USA* **2003**, *100*, 6946.

TH-777_05612211

15. (a) Niemeyer, C. M.; Ceyhan, B.; Hazarika, P. *Angew. Chem. Int. Ed*. **2003**, *42*, 5766. (b) Park, S.-J.; Lazarides, A. A.; Mirkin, C. A.; Letsinger, R. L. *Angew. Chem. Int. Ed*. **2001**, *40*, 2909.

16. Kannan, B.; Kulkarani, R. P.; Majumdar, A. *Nano Lett*. **2004**, *4*, 1521.

17. Nakata, K.; Hu, Y.; Bakr, O.; Stellacci, F. *Adv. Mater*. **2008**, *9999*, 1

18. (a) Murugadoss, A.; Chattopadhyay, A. *J. Phys. Chem. C* **2008**, *112*, 11265. (b) Maye, M. M.; Lim, S. I.-I.; Luo, J.; Rab, Z.; Rabinovich, D.; Liu, T.; Zhong, C.-J. *J. Am. Chem. Soc*. **2005**, *127*, 1519.

19. Wang, L.; Wei, G.; un, L.; Liu, Z.; Song, Y.; Yang, T.; Sun, Y.; Guo, C.; Li, Z. *Nanotechnology* **2006**, *17*, 2907.

20. (a) Kang, Y.; Erickson, K. J.; Taton, T. A. *J. Am. Chem. Soc*. **2005**, *127*, 13800. (b) Tang, Z. Y.; Kotov, N. A. *Adv. Mater*. **2005**, *17*, 951.

21. (a) Zhang, Y. X.; Zeng, H. C. *J. Phys. Chem. B* **2006**, *110*, 16812. (b) Tlusty, T.; Safran, S. A. *Science* **2000**, *290*, 1328.

22. (a) Jackson, A. M.; Myerson, J. W.; Stellacci, F. *Nat. Mater*. **2004**, *3*, 330. (b) Johnson, C. J.; Dujardin, E.; Davis, S. A.; Murphy, C. J.; Mann, S. *J. Mater. Chem*. **2002**, *12*, 1765.

23. Sardar, R.; Shumakar-parry, J. S. *Nano Lett*. **2008**, *8*, 731.

24. Lin, S.; Li, L. M.; Dujardin, E.; Girard, C.; Mann, S. *Adv. Mater*. **2005**, *17*, 2553.

25. (a) Zhang, F. X.; Han, L.; Israel, L. B.; Daras, J. G.; Maye, M. M.; Ly, N. K.; Zhong, C.-J. *Analyst* **2002**, *127*, 462. (b) Lim, I.-I.; Ip, W.; Crew, E.; Njoki, P. N.; Mott, D.; Zhong, c.-J.; Pan, Y.; Zhou, S. *J. Phys. Chem. B* **2007**, *23*, 826.

26. Storhoff, J. J.; Lazarides, A. A.; Mucic, R. C.; Mirkin, C. A.; Letsinger, R. L. *J. Am. Chem. Soc*. **1998**, *120*, 1959.

27. (a) Joshi, H.; Shirude, P. S.; Bansal, V.; Ganesh, K. N.; Sastry, M. *J. Phys. Chem. B* **2004**, *108*, 11535. (b) Selvakannan, P. R.; Mandal, S.; Phadtare, S.; Pasricha, R.; Sastry, M. *Langmuir* **2003**, *19*, 3545.

TH-777_05612211

28. (a) Zhong, Z.; Luo, J.; Ang, T. P.; Highfield, J.; Lin, J.; Gedanken, A. *J. Phys. Chem. B* **2004**, *108*, 18119. (b) Zhong, Z.; Patskovskyy, P.; Bouvrette, P.; Luong, J. H. T.; Gedanken, A. *J. Phys. Chem. B* **2004**, *108*, 4046.

29. Polavarapu, L.; Xu, Q.-H. *Nanotechnology* **2008**, *19*, 075601.

30. (a) Tobita, M.; Yasuda, Y. *J. Phys. Chem C* **2008**, *112*, (DOI: 10.1021/jp803195e). (b) Michailescu, G.; Olenic, L.; Pruneanu, S.; Bratu, I.; Kacso, I. J. Optoele. *Adv. Mater*. **2007**, *9*, 756.

31. Giersig, M.; Pastoriza-Santos, I.; Liz-Marzan, L. M. *J. Mater. Chem*. **2004**, *14*, 607.

32. Zilman, A.; Tlusty, T.; Safran, A. *J. Phys. Condens. Matter* **2003**, *15*, S57.

33. (a) Perepichka, D. F.; Rosei, F. *Angew. Chem. Int. Ed*. **2007**, *46*, 6006. (b) DeVries, G. A.; Brunnbaur, M.; Hu, Y.; Jackson, A. M.; Long, B.; Neltner, B. T.; Uzun, O.; Wunsh, B. H.; Stellacci, F. *Science* **2007**, *315*, 358. (c) Lim, I.-I.; Zhong, C.-J. *Gold Bulletin* **2007***, 40*, 1.

34. Xie, J.; Zhang, Q.; Lee, J. Y.; Wang, D. I. C. *J. Phys. Chem. C* **2007**, *111*, 17158.

35. Pong, B. K.; Lee, J. Y.; Trout, B. L. *Langmuir* **2005**, *21,* 11599.

36. Tang, Z.; Koto, N. A.; Giersig, M. *Science* **2002**, *297*, 237.

TH-777_05612211

TH-777_05612211

9.1 Ascorbic Acid as a Mediator and Template for Assembling Metallic Nanoparticles

9.1.1 Introduction

Further developments in near future in the frontiers of nanoscale science and technology would depend on ability to organize zero, one and two-dimensional nanostructures into hierarchical higher order functional structures. In this regard, presently there are a few of methods - chemical as well as physical – available for the organization of nanoscale structures into desirable assemblies. For example, Pan et al[1] generated nanobelts of semiconducting oxides such as those of Zn, Sn, In, Cd and Ga by evaporating the corresponding metal oxide powders at high temperatures. On the other hand, Kotov and coworkers[2,3] have demonstrated that Se, Te and CdTe nanowires could be prepared by chemical decomposition of parent nanoparticles (NPs) after depletion of the stabilizers. Further, a significant number of chemical and biochemical methods have been developed to obtain inorganic nanowires (NWs) and peptide nanotubes either by templated or templateless self-assembly[4-7]. Directed self-assembly using physical forces such as electric field, or microscopic fluid flow has also proved to be effective in obtaining nanoscale one-dimensional structures on a substrate[8,9]. Also, there are several protocols for DNA-templated assembly of NPs into organized two and three-dimensional structures[10-12]. Interestingly, tobacco mosaic virus has also been used in organizing NPs into potential electronic devices.[13]

There are a growing number of chemical methods that are being used to organize inorganic NPs into corresponding metal NWs[14-19], resulting into dispersions of metal NWs with typical dimensions of a few hundred nanometers. The NWs, suspended in a medium, might have limited use due to the inherent difficulty in processing them into useful devices as such. Also, it would be desirable to have the assembly of NPs turned into longer wires,

TH-777_05612211

where the constituents of the wire would ideally be NPs of the metal, with the retention of at least some of the properties of the nanoscale dimensions even in the organized structure that has an otherwise larger dimension. Further, if these assemblies are made of hundreds of micrometers long (or even longer) they would be scientifically intriguing, technologically challenging with enormous application potential. Additionally, if they can easily be isolated and manipulated in their solid state then they would be even more usefulness. This could be the basis of large-scale organization of heterostructures with components whose properties would primarily be decided by their nanoscale structures.

In this chapter, we report a new method of assembling metallic NPs into millimeter - scale fibrous superstructures using L-ascorbic acid (AA). AA has been used here as the precursor for the generation of fibers, reducing agent and assembly of NPs into fiber bundles. AA is known to get oxidized and degrade into several products one of which is the polymerization in aqueous solution[20-22,24]. It has been observed by us that under acidic condition, the polymerization leads to fiber formation, which has been used in the present applications. Subsequently, it was observed that these fibrous structures could act as the template for deposition of metallic NPs, such that those of Pt, Au and Ag NPs prepared separately, by addition of the fibers into the NP-dispersed medium. AA has also been used as a precursor to generate metallic NPs from their parent salt and concomitant organization into three -dimensional fibrous structures. For example, in the presence of AA, Au NPs were produced in the medium, which subsequently led to formation of assemblies. Typically, it took about 6 days to form fiber bundles with dimension of about 5 mm diameter disc. The fiber bundles could easily be transferred to surfaces like glass, aluminum and carbon coated copper grids, and subsequent analytical measurements could be made using the transferred samples. UV-vis spectroscopy, X-ray diffraction (XRD), scanning electron microscopy (SEM) and TEM measurements established the formation of fiber-like structures revealing the association of the NPs into these structures. Also, we observed that the Au NPs –polymer composite fibers were electrically conducting, with a promise of fabricating futuristic devices.

TH-777_05612211

TH-777_05612211

9.1.2 Experimental Section

Materials

Hydrogen tetrachloroaurate ($HAuCl_4$, 17 % Au in HCl purchased from Sigma-Aldrich), silver nitrate ($AgNO_3$ 99.5 % from Merck), platinum (II) chloride ($PtCl_2$ > 71 % from Fluka - Aldrich), sodium borohydride ($NaBH_4$ > 95 %, from Merck), L- ascorbic acid (99 %, from Merck) and sodium hydroxide (NaOH, 98 %, from Merck) were used as received without further purification. Milli-Q grade water was used in all the experiments.

Generation of AA Fiber

30.65 mg of L-ascorbic acid was dissolved in 10 mL water so that the final concentration of the solution was 17.26 mM. The pH of the solution was measured to be 3.12. This solution was kept at room temperature for four days after which fiber formation could be observed. The fibers appeared colorless. The fiber formation was allowed for two more days after which the fiber bundle was taken out of the solution, cleaned with water, air-dried and was used for further analysis and applications.

Generation of Au NP-AA Composite Fiber

40 μL of 17.26 mM of $HAuCl_4$ was dissolved in 10 mL water so that the final concentration of $HAuCl_4$ was 0.07 mM. To this solution freshly prepared 80 μL of 0.20 M of L-ascorbic acid was added. The final concentration of L-ascorbic acid in this solution was 1.60 mM. The resultant solution immediately turned purple in color indicating the formation of Au NPs. The color finally turned red in 15 min. The pH of the solution was measured to be 3.06. The solution was kept at room temperature for a few days. The fiber formation could be observed by naked eye on the 6^{th} day. The color of the fiber appeared reddish. This fiber was kept in this solution till the color of the solution vanished, which typically took 25 days and the fibers grew further. The fiber bundle was then taken out of the solution and washed four times and was air-dried for further characterization studies.

TH-777_05612211

Generation of Pt NP-AA Composite Fiber

7 mg of $PtCl_2$ powder was dissolved in 25 mL water so that the final concentration of the solution is 1.05 mM. 5 mL of this solution was added to 10 mL water and this was followed by addition of 600 μL of 20 mM sodium borohydrate solution. The resultant solution immediately turned brown, indicating the formation of Pt NPs. To this solution a single fiber bundle obtained from AA was added and the fiber containing solution was tightly sealed. The fiber was kept in the solution for five days, after which the fiber appeared dark brown in color. The fiber was then taken out from the solution and washed with water three times and was finally air-dried for further characterization studies.

Deposition of Au NPs on AA Fiber Bundle

To a 10 mL aqueous solution of 0.069 mM $HAuCl_4$, 150 μL of 20.0 mM of freshly prepared sodium borohydrate solution was added. The resultant solution color was red. After allowing an elapse of 1 h, a previously generated AA-degraded polymer fiber was carefully placed inside the solution and this was kept at room temperature for six days. The fiber was then red in color indicating that Au NPs were deposited on fiber of AA polymer. There were no visible precipitates from the solution. The fiber was then taking out of the solution and washed with water three times and was air-dried for further characterization studies.

Deposition of Ag NPs on AA Fiber Bundle

To 10 mL water containing 0.08 mM $AgNO_3$ 10 μL of 20.00 mM of freshly prepared $NaBH_4$ solution was added. This immediately resulted into formation of yellow color with possible generation of Ag NPs. This solution was kept at room temperature for 1 h and to this solution a fiber bundle of AA polymer (previously prepared) was added and this was kept at room temperature for six days. The fiber was then yellow in color indicating that Ag NPs were deposited on fiber of AA polymer.

TH-777_05612211

The fiber was then taken out of the solution and washed with water two or three times and was air-dried for further characterization studies.

Analytical Measurements

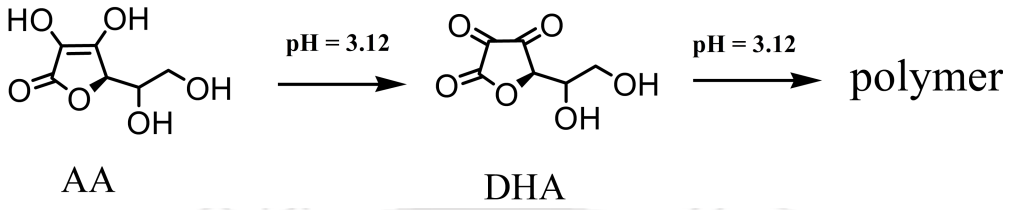
UV-vis spectra of the samples were recorded using a Perkin-Elmer lambda-25 spectrophotometer in the range of 200 to 1100 nm. As the starting AA concentration was high for the AA (only) fiber formation, a dilute solution was prepared in order to measure the typical absorption spectrum of AA. For this, the concentrated solution after keeping for 12 days was diluted to 0.14 mM to record UV-vis spectrum. FT-IR spectra of the AA-fibers were measured using a Perkin-Elmer Spectrum one spectrometer. AA fiber as well as Au NPs -AA composite fibers were dried under ambient conditions. They were then individually mixed with dry KBr in order to make pellets for recording FTIR spectra. All the measurements were carried out under ambient conditions. X-ray diffraction (XRD) pattern of the dried Au NPs - AA polymer, placed on a microscope glass slide, was recorded using a Bruker Advance D8 XRD machine (Cu α source at 1.5406 Å wavelength), in thin film mode. Transmission Electron Microscopy (TEM) of the fiber, placed on carbon coated copper grids, was performed using JEOL (Model 1200EX) equipment operating at a maximum acceleration voltage at 120 kV. Scanning electron microscopy (SEM) of the fibers on Al or Cu stubs was performed using LEO scanning electron microscope (model 1430 VP). Electrical conductivity measurements of the as-prepared composite fibers were recorded on a glass slide using a Keithley nanosource meter.

9.1.3 Results and Discussion

AA under acidic condition is known to get oxidized to produce dehydroascorbic (DHA) acid. Further oxidation is possible in the presence of an oxidizing agent such as hydrogen peroxide, into oxalate and α, β, γ-trihydroxybutyric acid[23, 25, 26].

TH-777_05612211

On the other hand, DHA is known to get transformed into 2, 3-diketo-gulonic acid (DKG), which itself produces a host of products[27-30], and among them polymerization has been observed as one of the pathways (Scheme 9.1.1 below).



Scheme 9.1.1. *A scheme for the polymerization of ascorbic acid*

When AA was kept under acidic condition, it probably was self-oxidized into DHA and then DKG that led to the formation of fibrous structure with time as a result of polymerization. Time-dependent UV-vis absorption spectra of the solution of ascorbic acid (Figure 9.1.1) showed that the initial absorption peak at 264 nm (recorded immediately following the solution preparation) corresponds to known AA absorption. However, when the solution was kept for 12 days the peak shifted to 253 nm. This blue shift has earlier been attributed to the formation of, among other products, DHA, which may also be the case herein. The absorption band at 264 nm is due to the π- π^* transition of the C=C moiety of AA[24b]. When AA is oxidized to DHA, the band shifted to lower wavelength at 253 nm which is possibly due to the presence of C=O. The absence of the band at 264 nm indicated the oxidation of AA. Thus the observations suggest the formation of the various products, which is consistent with literature reports[23]. It is interesting to mention here that upon allowing the solution to stand for about 6 days colorless fibrous structures appeared at the bottom of the vials. These fibers were ready to be lifted out of the solution in the form of bundles and were further analyzed by SEM, typical micrographs of which are shown in Figures 9.1.2 (a) and (b). As is clear from the figures a network of fibers were formed with diameters of about 1-4 μm and length of each section spanning about 40 μm. These fibers were rather smooth

TH-777_05612211

and did not appear to be formed from the agglomeration of smaller particles (Figure 9.1.2 (b)). In other words, elongated and branched polymers were formed systematically, from smaller fibers into larger ones with time, that lead to the formation of branched fibers with about 5 mm diameter.

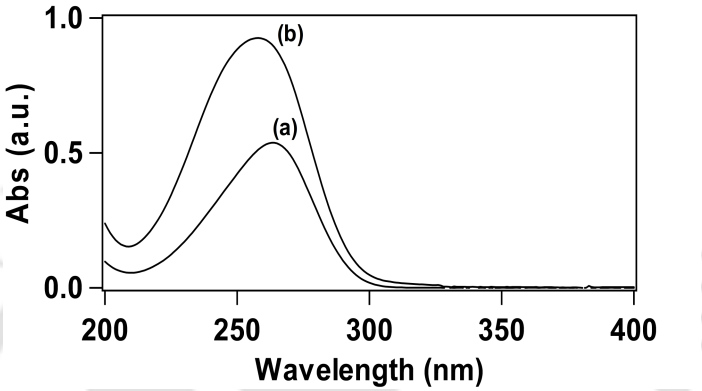


Figure 9.1.1*. Time dependent UV-Visible spectra of ascorbic acid in aqueous acidic solution. (a) Typical absorption spectrum of a dilute solution immediately after preparation. (b)The absorption spectrum recorded a solution of AA recorded after 12 days (original solution diluted to 0.14 mM).*

It is interesting to observe that the fibers were rather smooth (Figure 9.1.2 (b)) and there is no indication that the fibers were formed from smaller particles. In other words, the fibers grew by systematic polymerization rather than agglomeration of nanoscale particles. EDX analysis (Figure 9.1.2 (c)) of the fiber indicated the presence of only organic components confirming that the fibers were made from the degradation products of AA. It was also observed that the fibers were not at all soluble in any common organic solvent as well as in aqueous solution. If the fibers were made of simple oligomers i.e. degradation product of DHA then it should have been soluble in organic solvents or in water. Thus the possibility of a monomer forming the fibers, in the present set of experiments, could be discounted.

Possible use of these fibers for depositions of metallic NPs onto them was pursued subsequently. Pt NPs synthesized separately, without the presence of any additional

TH-777_05612211

stabilizer. Fibers were then taken out of the original medium and transferred to the medium containing NPs dispersions. It was found that in about two days Pt NPs were deposited on the fibers and no precipitation of the metallic NPs at the bottom of the container had occurred. Thus Pt NPs, dispersed in the medium, preferentially deposited on the fibers rather than precipitation in a short time. A typical SEM of the Pt-deposited fibers, shown in Figure 9.1.3, indicates clearly the presence of NPs on the fiber as extra growth and the fibers appeared rough in comparison to the smooth ones that were observed for the fibers generated from AA.

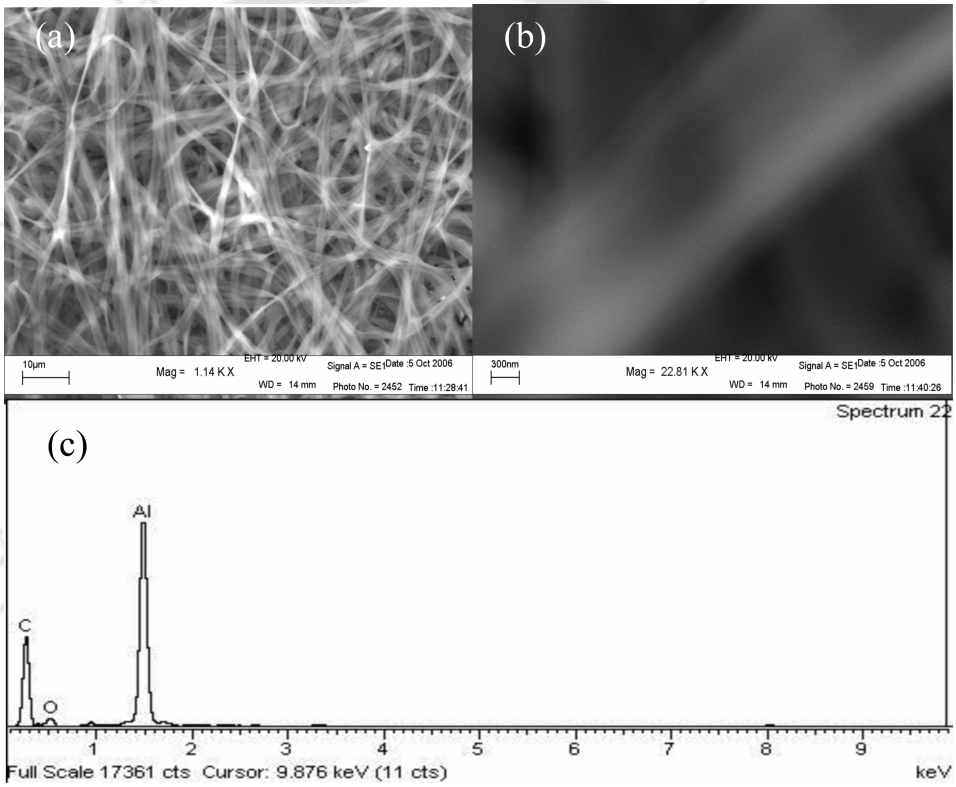


Figure 9.1.2. *Scanning Electron Micrograph of ascorbic acid fiber bundle (a). (b) is an expanded view of (a). (c) EDX of the fibers. The Al peak is due to the sample holder.*

TH-777_05612211

Further, in some parts of the fibers there were significant depositions of the NPs that appeared more like beads in the necklace of the fibers. The presence of the Pt NPs on the fibers was ascertained by EDX, which is shown in Figure 9.1.3 (c).

TH-777_05612211

Further, deposition of Au NPs and Ag NPs on the fibers was pursued using the same method. Here again the depositions of the NPs on the fiber were observed, where the particles deposited could be clearly seen under the electron microscope (Figure 9.1.5A (Refer: Appendix-I) for deposition of Au NPs on ascorbic acid fiber, while Figure 9.1.6B (Refer: Appendix-II) is for the deposition of Ag NPs on the ascorbic acid fiber).

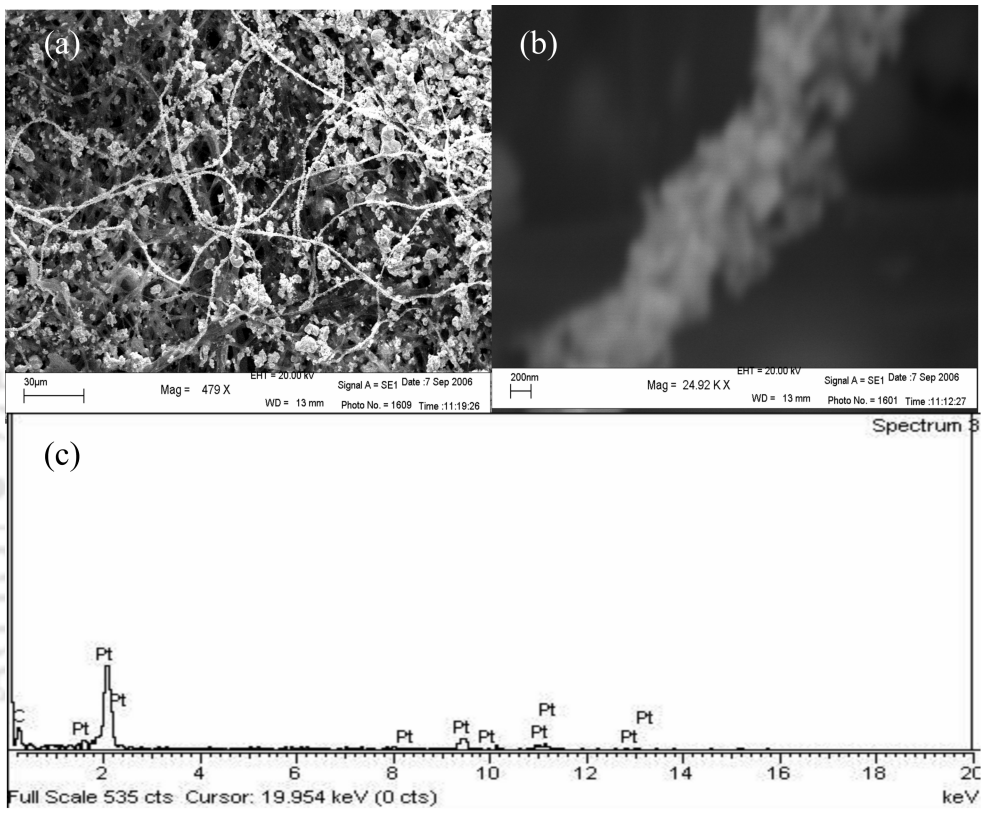
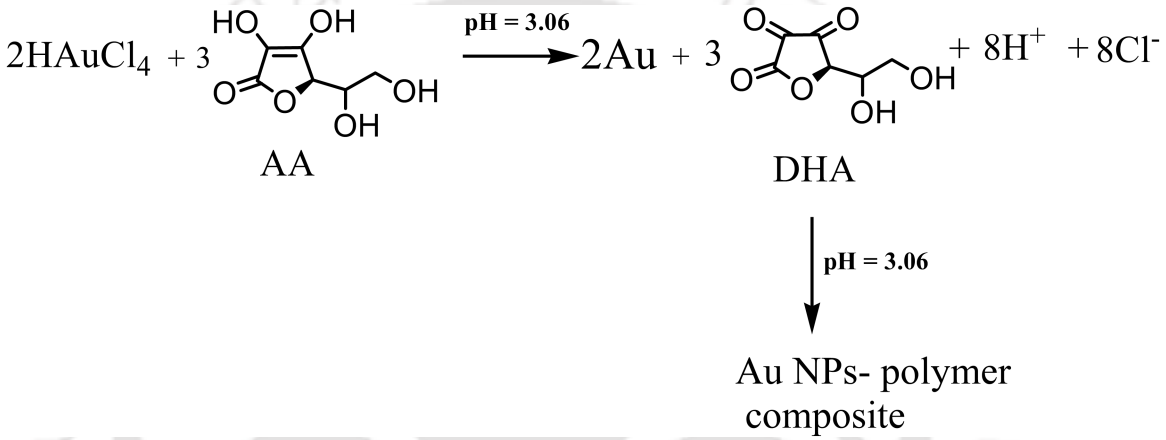


***Figure 9.1.3**. (a) Scanning electron micrograph of Pt NPs deposited on fiber. (b) An expanded view of (a) and (c) EDX spectrum of the fiber.*

While pursuing the deposition of metallic NPs as above, it was observed that the process did not result in uniformly distributed NPs on the fiber and also there were substantial depositions at some places, while there was less deposition of NPs in other parts of the fibers. This is less desirable as the application potential of the composite fiber would be limited. Also, the properties could be due to agglomeration of NPs rather than specially

TH-777_05612211

deposited NPs on the fiber backbone. This gave rise to a need for the development of a method where a more uniform composite fiber could be grown. For example, reduction of metallic salt to NPs followed by growth into a composite fiber would be more appropriate. As AA is a reducing agent, the synthesis of Au NPs by the reduction of $HAuCl_4$ using AA as the only reducing agent was pursued[31]. Au NPs was easily synthesized using the method and the Au NPs produced exhibited characteristic surface plasmon resonance peak at 535 nm (Figure 9.1.4). The possible pathway of the product formation is shown in Scheme 9.1.2.



***Scheme 9.1.2**. A scheme for the generation of Au Nnanoparticles-polymer composites.*

When the as-synthesized Au NPs under acidic condition were left to themselves then formation of assembly of NPs along with AA was observed. Time dependent UV-vis spectra of the medium revealed gradual decrease in intensity of the peak at 535 nm (Figure 9.1.4 (a) and (b)). The fiber formation in the present system was observed in about 6 days similar to those of AA derivative as discussed before. The additional absorbance peak at 292 nm in the figure (Figure 9.1.4 (b)) indicated the presence of other degradation products of AA. Further, Au NPs peak at 535 nm vanished by the 20th day indicating that there was virtually no Au NPs present in the solution and all of them lead to the formation of the composite fiber as there was no visible precipitation of NPs.

TH-777_05612211

TH-777_05612211

SEM and TEM studies of the fibers were pursued further to understand their structure and compositions better. As is clear from the SEM images shown in Figures 9.1.5 (a) and (b), these fibers had typically same dimensions and shapes as those generated from AA. However, the fibers were not as smooth as those of the above. On the other hand, there were distinct particles present in the fibers and the particles were embedded in the fibers in a more uniform manner in comparison to those deposited on the backbone using the other method (discussed earlier).

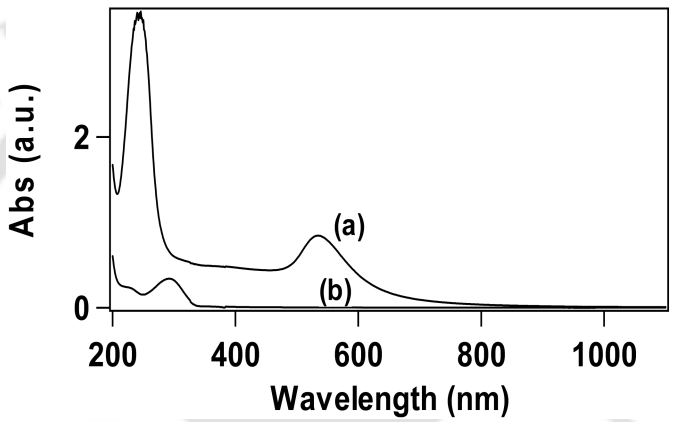


Figure 9.1.4*. The UV-Vis spectra of the formation of Au nanoparticles by ascorbic acid. (a) Spectrum recorded on day 1. (b) Spectrum recorded on day 20.*

X-ray diffraction (XRD) measurements (Figure 8.1.5 (c)) of the fibers revealed peaks at 2θ values of 38.4^{o}, 44.5^{o}, 64.5^{o} and 77.5^{o} corresponding to those of metallic Au[32]. Thus the Au NPs formed in the medium were present in the fibers. The overall appearance of the Au NPs containing fibers appears to be much smoother than those where Pt NPs were deposited after the formation of fibers from AA. Also, there were no special agglomerations of NPs into large-scale particles in the fibers indicating systematic fiber formation from Au NPs stabilized by decomposition products of AA. FTIR investigation of the fibers containing Au NPs indicated the presence of organic materials in addition to Au NPs. The FTIR spectra of AA, the fibers as well as of that of Au NPs – fibers composite are shown in Figure 9.1.6.

TH-777_05612211

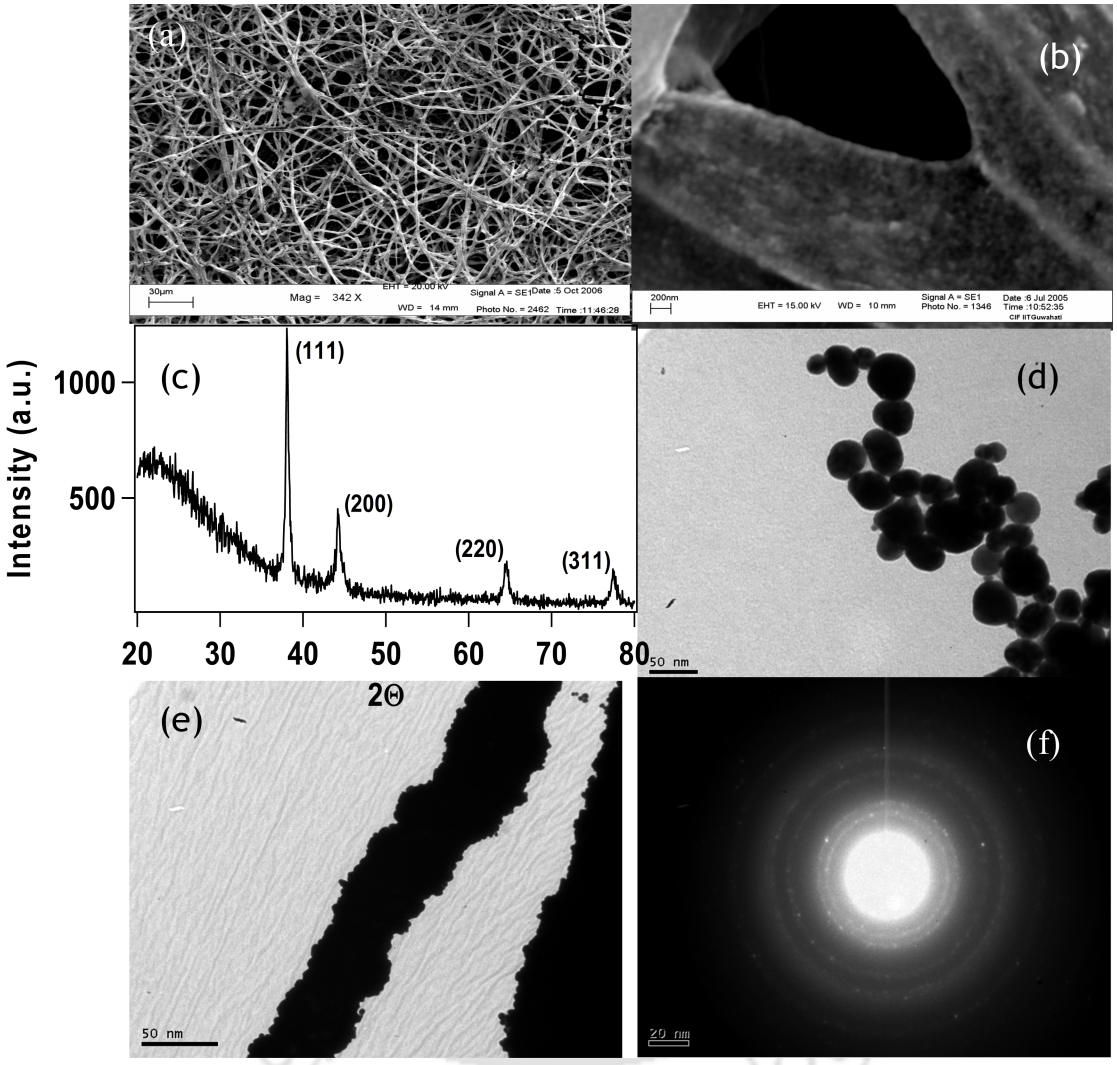


Figure 9.1.5*. (a) Scanning electron micrograph of the composite fiber. (b) An expanded view of the picture in (a). (c) X-ray diffraction results of the composite fibers. The index corresponding to Au peaks are identified. (d) Transmission electron micrograph of a growing composite fiber on day 5 and (e) on day 20. (f) Selected area electron diffraction of a spot in the fiber.*

TH-777_05612211

The spectra of the ordinary fiber and the composite fibers are identical indicating that both the fibers were made of the same organic components. Also interesting to note is the difference between spectrum of AA and that of the fibers. AA spectrum consists of a broad peak in the region of 3500-2700 cm^{-1} indicating the presence of OH stretching (free as well as H-bonded) and also C-H stretching vibrations[24c]. However, the same peak of the fibers consists of a rather sharp peak at 3400cm^{-1} indicating less extensive H-bonding.

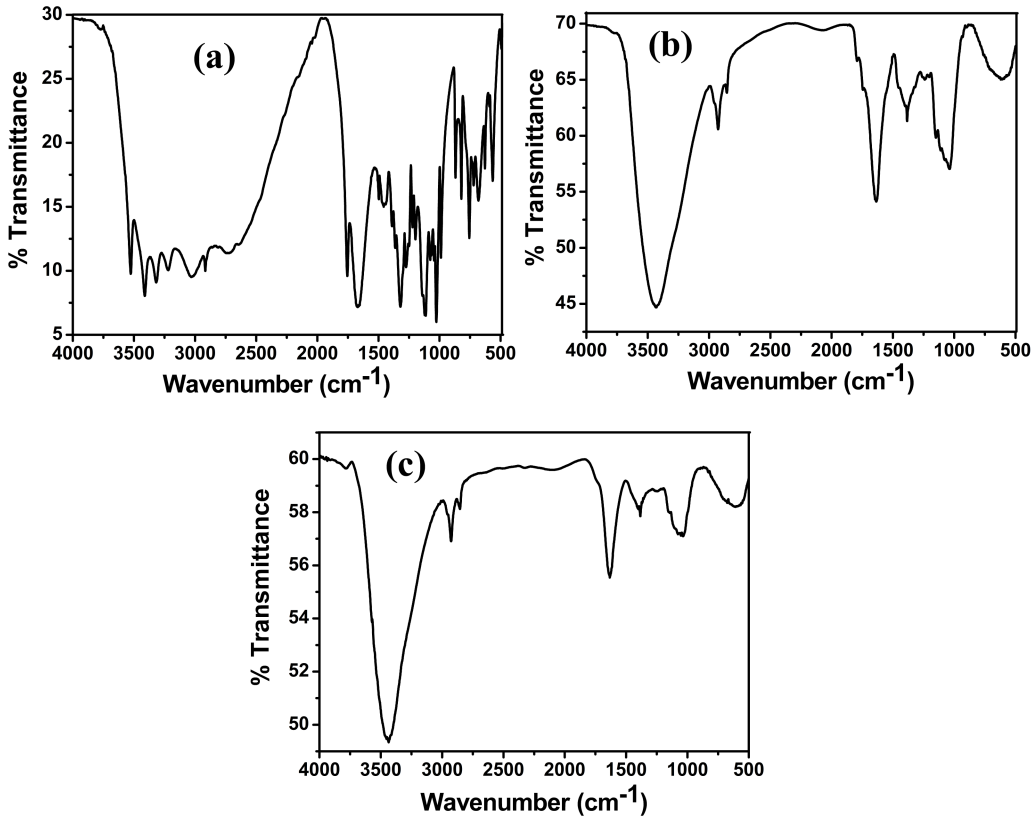


Figure 9.1.6. *Infrared spectrum of (a) Ascorbic acid only, (b) AA-degraded polymer of fiber and (c) Au NPs -AA composite polymer fiber.*

This can be explained by the degradation products of AA i.e. DHA or DKG, where the number of OH groups is reduced. Further, the C-H stretching vibration peak at 2925 cm^{-1} is

TH-777_05612211

also present in the fibers. The presence of a single, rather sharp peak at 1635 cm^{-1} in both the fibers are due to α, β- unsaturated C=O stretching vibration and the absence of a peak at 1751 cm^{-1} in the fibers in comparison to that of AA further suggest that there are no free acid in the fibers. The observations of the above peaks in the fibers vis-à-vis AA, suggest that the fibers are indeed made of polymers of DHA, DKG or other degradation product rather than AA. Further, FTIR spectral observations also suggest that the nature of polymers present in the composite fibers to be the same as those in the pure ones. Time dependent TEM measurements showed assembly formation of particles slowly. In the beginning (fifth day) the particles were agglomerated into smaller fibers of hundreds of nanometers (Figure 9.1.5 (d)) long. These small fibers were made of spherical Au NPs of typical diameters ranging from 20-50 nm. They grew into larger ones in 20 days. TEM micrographs of the large fibers were difficult to observe in terms of identifying individual NPs in the fibers (Figure 9.1.5 (e)). However, the selected area electron diffraction (SAED) patterns shown in Figure 9.1.5 (f) clearly indicate the presence of Au in the fibers. SAED indexes were matched to those of Au.

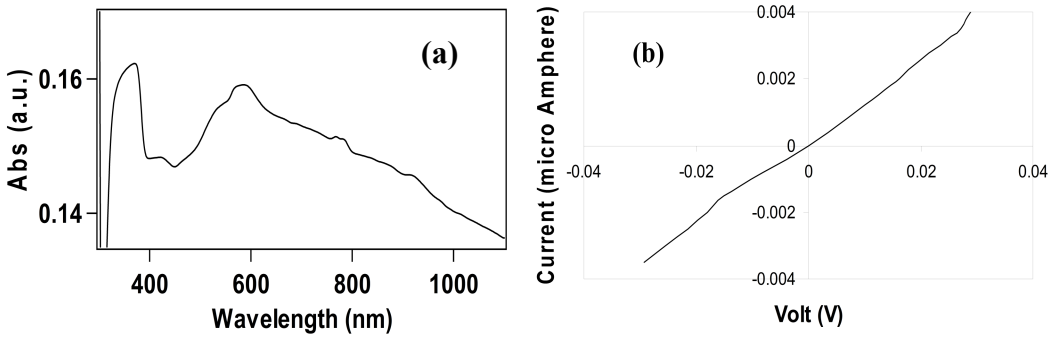


Figure 9.1.7*. (a) Absorbance spectra of Au-AA bush deposited on glass slide. (b) I-V curve of the conductivity of Au-AA composite fiber.*

It was also noticed that by the 20th day the UV-Vis spectrum of the solution had minimum absorption at 535 nm indicating the assimilation of majority of NPs into the formation of

TH-777_05612211

fibrous structures (Figure 9.1.4 (b)). On the other hand the appearance of a peak at 292 nm indicates the formation of products degraded from the AA. Additionally, when the spectrum of the solid fibers isolated from the solution was recorded in the UV-vis spectrophotometer, a broad visible absorption of the fiber with a peak around 583 nm could be observed (Figure 9.1.7 (a)). This means that the NPs present in the solution and stabilized by the degradation products of AA, although might have undergone some sort of agglomeration, retained the NP character even when agglomerated into larger assemblies in the fibers. Alternatively, at least one dimension of the composite fiber must retain the NP character in order to have the absorption spectrum observed as above. Further, the electrical conductivity measurements of the composite fibers were pursued by four-probe method using linear method. The surface resistivity of Au NPs-AA composite fiber was measured to be 2.16 $X10^3$ ohm cm. A typical I-V curve of the conductivity is shown in Figure 9.1.7 (b). As clear from the figure the linear nature of I-V curve indicates that metallic conductivity is present in the composite fiber. This is interesting as the composite fiber exhibit the optical character of NPs and conductivity of the assemblies of metal NPs. Thus we have a rather uniformly grown composite fiber, which is electrically conducting.

Systematic development of three-dimensional assembly of nanoscale materials has been and still is a challenge to scientists. Directed and controlled growth of materials with nanoscale components is still far from being complete. However, understanding of the process and discovery of newer methods would help build the base for advanced materials, whose properties can be tuned by systematic changes at the nanoscale. AA is an important vitamin and the chemistry and biochemistry of AA is well established. In the present work, these important cellular materials have been used in a new way of organizing NPs into three-dimensional fibrous structure, where the electrical conductivity of the fiber provides a basis for future developments of sensors, actuators and other devices.

In the present work, two ways of organizing metal NPs into three-dimensional networks of fibers were discovered. In the first method, the self-degradation products of AA

TH-777_05612211

lead to the formation of fiber bundle with a rather smooth surface profile. However, these surfaces acted as the host for metal NPs when kept in a solution containing the dispersed particles. The preferential depositions of NPs onto the fiber surface in comparison to simple agglomeration in the medium, which is generally followed by precipitation, may be thermodynamically more favorable. The preferential deposition process, even though diffusion limited, is interesting as it provides a basis for organization of NPs onto well-defined surfaces. Still one has to consider the over-depositions at several points of the fiber bundle that may render the method less favored. Alternatively, systematic development of metal NPs stabilized by appropriate ligands that would form chemical bonds with the fiber polymer backbone may serve as a superior way of controlled deposition. When Au NPs are formed by reduction of $HAuCl_4$ and consequent oxidation of AA, the products of oxidation would act as the stabilizers for the generated Au NPs. These stabilized Au NPs surrounded by the organic moieties eventually organizes into three-dimensional fibrous structures, similar to the ones generated from the degradation products of AA. This could be superior to the other method as the separation between NPs are likely to be uniform, which would be roughly that of the twice of the length of the stabilizer. Consequently, the fiber grown from the composite materials would have NPs present in its backbone in addition to its surface. It is important to note that the basic skeletons of the fibers in three dimensions are the same for both kinds of starting materials. This present a new way of organizing particles into three-dimensional materials, where well-defined metal NPs are separated at nearly equal separating distances rendering a more uniform structure with possible superior mechanical, chemical and electrical properties. The electrical conductivity of the fiber indicates association of the metal NPs in the structure, while its value also indicates that bulk metal is not formed. It is interesting to have a fiber where the optical properties of the NPs are somewhat retained and electrical conductivity in the range between insulator and metallic conductor is achieved. This provides a new opportunity for the generation of sensors, actuators, logic gate structures where the Au NPs would act as the primary functional elements in the architecture. Finally, in the presence of $HAuCl_4$, the formation of fibers was faster than those formed from only AA. This is possibly due the formation of

TH-777_05612211

DHA from AA due to oxidation in the presence of $HAuCl_4$ (Scheme 9.1.2) in comparison to self-oxidation of AA (Scheme 9.1.1). This provides an added advantage, as faster formation of fibers would effectively reduce the time required for the fabrication of devices. It may also be mentioned here that even though the formation of complete fiber bundles was allowed in all the cases, for ease of handling the fibers and composites, slow growth of fibers would allow generation of size-selected fibers as the products (fibers) can always be picked up at any time during the evolution of structures allowing more versatile nature of the composite fiber generation. This is substantiated by the smaller fibers formed detected at earlier times in the formation of composite fiber bundles as shown in Figure 9.1.5 (d). The composite fibers are electrically conducting and hence they can provide a new approach in the generation of sensors, where the chemical and biochemical properties of the Au NPs and the electrical conductivity of the fibers can simultaneously be exploited.

9.1.4 Conclusion

In the present chapter, the use of L-ascorbic acid (AA) in assembling metal nanoparticles (NPs) into three-dimensional fibrous structures has been reported. The degradation product of AA led to the formation of fibrous structures, which was used as a template for deposition of metal NPs such as Au, Pt and Ag. In addition, AA has also been used as the reducing agent in generating Au NPs. The spontaneous fiber formation and formation of Au NPs by AA have been coupled to generate fibers made up of composite of Au NPs and the polymer from the degradation products of AA. The composite fiber bundle has been found to be electrically conducting, with surface resistivity on the order of 2.16 X 10^3 ohm cm. Therefore, the present work is expected to provide a new and interesting way of generating and organizing metallic NPs into three-dimensional functional networks useful for future nanotechnology based devices.

TH-777_05612211

TH-777_05612211

9.1.5 Appendix I

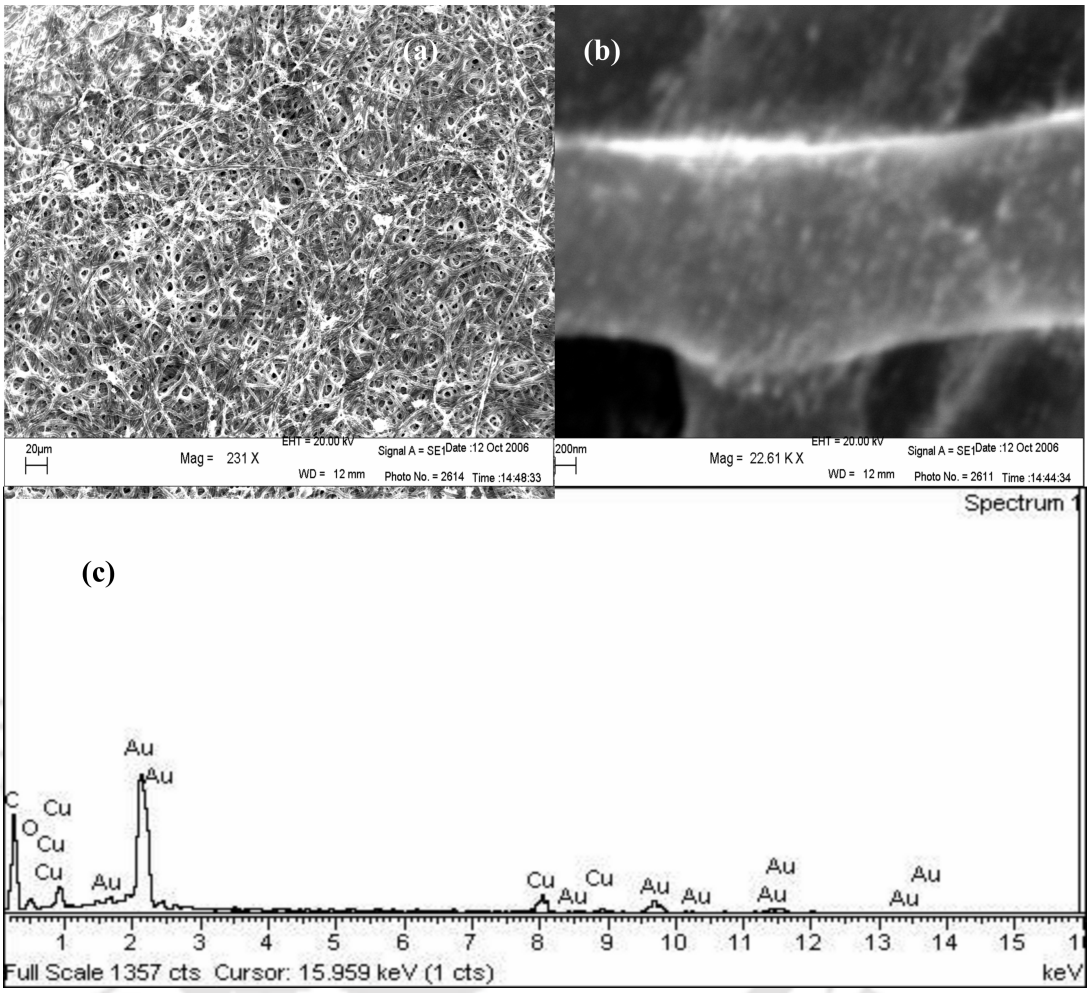


***Figure 9.1.5A**. (a) Scanning electron micrograph of Au NPs deposited on AA-degradation fiber. (b) is an expanded view of (a). (c) is the EDX spectrum of the fiber.*

TH-777_05612211

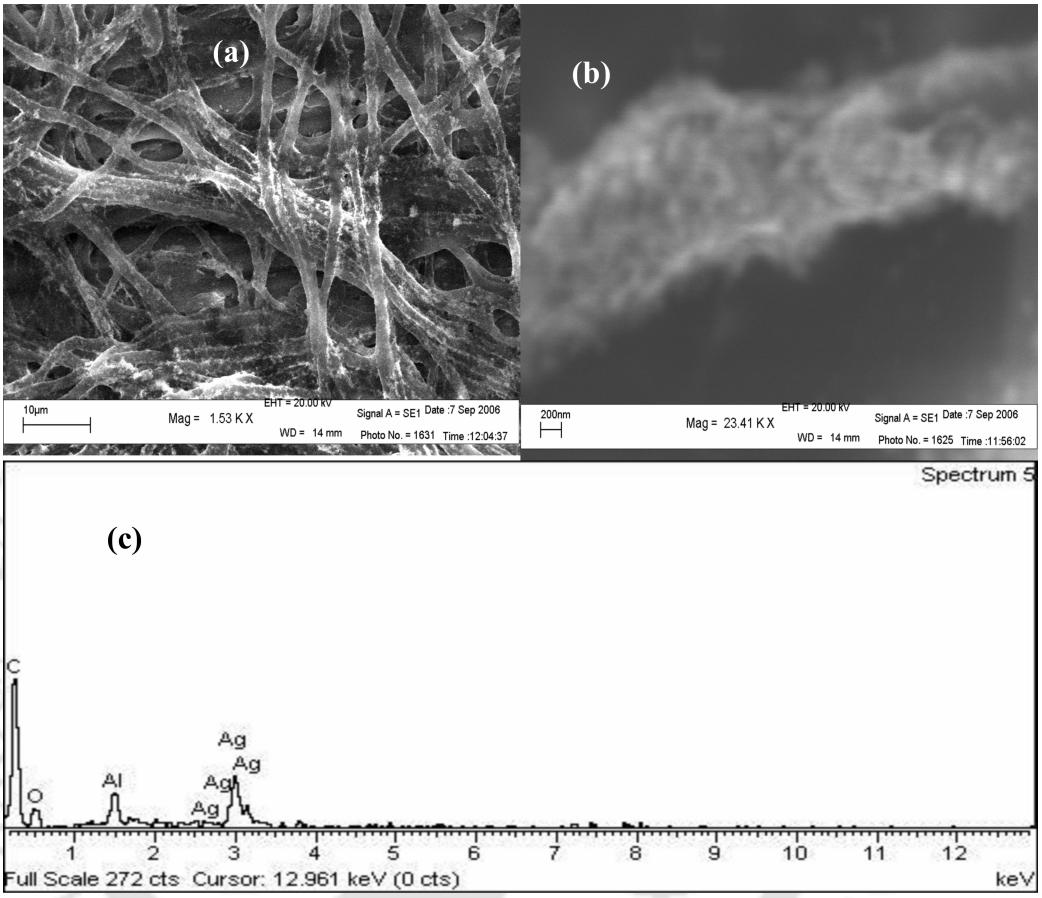


***Figure 9.1.5B**. (a) Scanning electron micrograph of Ag NPs deposited on AA-degradation fiber. (b) is an expanded view of (a). (c) is the EDX spectrum of the fiber.*

TH-777_05612211

9.1.6 References

1. Pan, Z. W.; Dai, Z. R.; Wang, Z. L. *Science* **2001**, *291*, 1947.

2. Tang, Z.; Wang, Y.; Sun, K.; Kotov, N. A. *Adv. Mater*. **2005**, *17*, 358.

3. Tang, Z.; Kotov, N. A.; Giersig, M. *Science* **2002**, *297*, 237.

4. Cao, H.; Xu, Z.; Sang, H.; Sheng, D.; Tie, C. *Adv. Mater*. **2001**, *13*, 121.

5. Edmondson, M. J.; Zhou, W.; Siber, S. A.; Jones, I. P. Gameson, I.; Anderson, P. A.; Edwards, P. P. *Adv. Mater*. **2001**, *13*, 1608.

6. Braun, E.; Eichen, Y.; Sivan, U.; Ben-Yoseph, G. *Nature* **1998**, *391*, 775.

7. (a) Maddanimath, T.; Kumar, A.; Darcy-Gall, J.; Ganesan, P. G.; Vijayamohanan, K.; Ramanath, G. *Chem. Commun*. **2005**, 1435. (b) Bannerjee, A. I.; Yu, L.; Matsui, H. *J. Am. Chem. Soc*. **2005**, *127*, 16002. (c) Gao, X.; Matsui, H. *Adv. Mater*. **2005**, *17*, 2037.

8. Cheng, C.; Gonela, R. K.; Gu, Q.; Haynie, D. T. *Nano Lett*. **2005**, *5*, 175.

9. Huang, Y.; Duan, X.; Wei, Q.; Lieber, C. M. *Science* **2001**, *291*, 630.

10. Sharma, J.; Chhabra, R,; Liu, Y.; Ke, Yonggang.; Hao. Y. *Angew. Chem. Int. Ed*. **2005**, *44*, 1.

11. Jung, H. Y.; Lee, K.; Kim, Y.; Insung, C. S. *Angew. Chem. Int. Ed*. **2006**, *45*, 5960.

12. Lytton-Jean, A. K. R.; Mirkin, C. A. *J. Am. Chem. Soc*. **2005**, *127*, 12754.

13. Tseng, J. R.; Tsai, C.; Ma, L.; Ouyang, J.; Ozkan, S. C.; Yang, Y. *Nature* **2006**, *1*, 72.

14. Caswell, K. K.; Bender, C. M.; Murphy, C. J. *Nano Lett*. **2003**, *3*, 667.

15. Jana, N. R.; Gearheart, L.; Murphy, C. J. *Adv. Mater*. **2001**, *13*, 1389.

16. Sun, Y.; Xia, Y. *Adv. Mater*. **2002**, *14*, 833.

17. Yen, M.; Chiu, C.; Hsia, C.; Chen, F.; Kai, J.; Lee, C. Chiu, H. *Adv. Mater*. **2003**, *15*, 235.

18. Kim, J.; Cha, S.; Shin, K.; Jho, J. Y.; Lee, J. *Adv. Mater*. **2004**, *16*, 459.

TH-777_05612211

19. Chang, Y.; Lye, M. L.; Zeng, H. C. *Langmuir* **2005**, *21*, 3746.

20. Y, J.-P.; Chen, F. J. *Agric. Food Chem*. **1998**, *46*, 5078.

21. Van den Broeck, I.; Ludikhuyze, L.; Weemaes, C.; Van Loey, A.; Hendrickx, M. J. *Agric. Food Chem*. **1998**, *46*, 2001.

22. Prieto, F.; Coles, B. A.; Compton, R. G. *J. Phys. Chem. B* **1998,** *102*, 7442.

23. Y. J.-P.; Chen, F. *Food Chem*. **1999**, *64*, 423.

24. (a) Kimoto, E.; Tanaka, H.; Ohmoto, T.; Choami, M. *Anal. Biochem*. **1993**, *214*, 38. (b) Lohmann, W.; Pagel, D.; Penka, V. *Eur. J. Biochem.* **1984**, *138*, 479. (c) Tajmir-Riahi, A. H. J. *Inorg. Biochem*. **1991**, *42*, 47.

25. Deutsch, C. J. *Anal. Biochem*. **1998,** *255*, 1.

26. Borsook, h.; Davenport, H. W.; Jeffreys, P. E. C.; Warner, C. R. *J. Biol. Chem.* **1937**, *117,* 237.

27. Shin, D. B.; Feather, M. S. *Carbohydr. Res*. **1990**, *208*. 246.

28. Lopez, M. G.; Feather, M. S. *J. Carbohydr. Chem.* **1992**, *11,* 799.

29. Grandhee, S. K.; Monnier, V. M. *J. Biol. Chem*. **1991**, *266*, 11649.

30. Buettner, G. R.; Jurkiewics, B. A. *Free Radical Biol. Med*. **1993**, *14*, 49.

31. Mieszawska, A. J.; Zamborini, F. P. *Chem. Mater*. **2005**, *17*, 3415.

32. Chen, S.; Liu, Y.; Wu, G. *Nanotechnology* **2005**, *16*, 2360.

TH-777_05612211

9.2 Silver Fused Conducting Fiber Formation of Au@Ag Core-shell Nanoparticles Mediated by Ascorbic Acid

9.2.1 Introduction

In the earlier section of this chapter we have reported the formation of composite fibers consisting of metallic NPs and the polymer from degradation products of L-ascorbic acid (AA). There the composite consisted of single metallic NPs embedded in the polymer matrix. In this chapter, a new method of assembling metallic core-shell NPs into millimeter - scale fibrous superstructures is reported. Here also L-ascorbic acid (AA) has been used as the reducing agent in the formation of core-shell particles and also in the transformation of core-shell NPs assembly into fiber bundles. As mentioned before, AA is known to get self-oxidized and degraded into several products one of which is the polymerization in aqueous solution [1-4]. In earlier examples, when AA was treated with $HAuCl_4$ formation of Au NPs was observed, which subsequently resulted into organized fibrous structures with time.[5] On the other hand, when initially grown Au NPs, in the presence of AA, were treated with $AgNO_3$, formation of core-shell NPs, with Ag covering Au, could be observed. Interestingly, it was observed that the presence of silver in the solution helped in the organization of the core-shell NPs into fibrous structures where metallic Ag acted as glue for joining the NPs in the fiber. Furthermore, the fibers made up of only Au NPs showed low electrical conductivity. However, with the increase in the Ag, the conductivity increased to metallic values indicating that Ag was acting as 'glue' to connect the NPs. UV-Vis spectroscopy, electron microscopy, X-ray diffraction and electrical conductivity measurements were pursued with these fibers to characterize them and their properties.

TH-777_05612211

9.2.2 Experimental Section

Materials

Hydrogen tetrachloroaurate ($HAuCl_4$, 17 % Au in HCl purchased from Sigma-Aldrich), silver nitrate ($AgNO_3$ 99.5 % from Merck), L- ascorbic acid (99 %, from Merck) and sodium hydroxide (NaOH, 98 %, from Merck) were used as received without further purification. Milli-Q grade water was used in all the experiments.

General procedure for synthesis of core shell Au@Ag NPs-AA polymer composite

40 μL of 17.26 mM of $HAuCl_4$ was diluted into 10 mL water with the final concentration of $HAuCl_4$ at 0.07 mM and 100 μL of 0.3 M freshly prepared NaOH solution was added followed mixing them by shaking. Measured amount of AA was then added to the solution. The solution immediately turned purple in color indicating the formation of Au NPs. In order to prepare composite particles, various amount of $AgNO_3$ solution was subsequently added to this purple colored solution. The details of the concentrations of $HAuCl_4$, NaOH, AA, $AgNO_3$ used for different samples are given in Table 8.2A. UV-Vis spectra of these solutions were recorded one hour after the preparation of the mixtures. The solutions were then kept at room temperature for 30 days, with occasional visual observation for fiber formation. The fiber formation (either at the bottom of the solution or at the air-water interface) was observed with naked eye typically form the sixth day and they were allowed to grow until the solution became colorless for full formation of fiber assembly. It may be noted that in all the preparations, the concentration of $HAuCl_4$ and NaOH were kept constant (Sample 1 to Sample 13) and the concentration of AA was increased upon increasing the concentration of $AgNO_3$. This was necessary for the formation of Ag NPs as well as the fibers in the medium. The pH of the resultant solution at the end of mixing the reagents was measured and is mention in the table against each mixture.

TH-777_05612211

Analytical Measurements

UV-Visible spectra of the samples were recorded, in the range of 200 to 1100 nm, using a Perkin-Elmer lambda-25 spectrophotometer. All the measurements were carried out under ambient conditions. X-ray diffraction (XRD) pattern of the dried fiber bundle, placed on a microscope glass slide, was recorded using a Bruker D8 Advance XRD machine (Cu α source with wavelength at 1.5406 Å), in thin film mode. Transmission electron microscopy (TEM) of the fiber, placed on carbon coated copper grids at different time of growth, was performed using a JEOL equipment operating at an acceleration voltage at 120 kV or 200 kV (model 2100). Scanning electron micrographs of the fibers placed on Al or Cu stubs were recorded using a LEO scanning electron microscope (model 1430 VP).

Table 9.2A. *Concentration of reagents and corresponding pH of the solutions.*

Sample Name	Con of $HAuCl_4$ (mM)	Con of NaOH (mM)	Con of Ascorbic acid (mM)	Con of $AgNO_3$ (mM)	pH of the solution
Sample: 1	0.07	3	2.0	0.00	6.59
Sample: 2	0.07	3	2.0	0.02	6.54
Sample: 3	0.07	3	2.0	0.04	6.47
Sample: 4	0.07	3	2.4	0.08	5.99
Sample: 5	0.07	3	2.6	0.16	4.82
Sample: 6	0.07	3	2.8	0.20	4.67
Sample: 7	0.07	3	3.6	0.24	4.32
Sample: 8	0.07	3	4.4	0.28	4.09
Sample: 9	0.07	3	5.2	0.32	3.99
Sample: 10	0.07	3	6.0	0.36	3.88
Sample: 11	0.07	3	6.8	0.40	3.79
Sample: 12	0.07	3	7.6	0.44	3.71
Sample: 13	0.07	3	8.0	0.50	3.57

TH-777_05612211

Electrical conductivity measurements

After 30 days of growth, the fiber bundles were picked up from the solution and dried on microscope glass slides under ambient conditions. The total area of the fiber bundle was calculated from the width and thickness of these fibers. The thickness of the fiber was recorded by using atomic force microscope (AFM of VEECO; Model Nanoscope IVa) and the length of the fiber was calculated by measuring the distance between the two electrodes. The resistance of these fibers was recorded with a Keithly constant current source used for applying current and a model 2182-Kit Low-Thermal connector with strain relief was used to measure the voltage.

9.2.3 Results and Discussion

As discussed in the previous section, AA under acidic condition gets oxidized to produce dehydroascorbic (DHA) acid [6]. The oxidation is also possible in the presence of an oxidizing agent such as hydrogen peroxide and some transition metal ions [7]. Further, DHA is known to get transformed into 2, 3-diketo-gulonic acid (DKG), which itself produces a host of products, and among them polymerization has been observed as one of the pathways[3]. However, the most important chemical characteristics of AA (i.e. vitamin C) are its redox properties [8]. AA, being a two-electron reducing agent, can react with metal ions in

TH-777_05612211

solution to reduce them into their zero valent states. The rate of oxidation of AA is dependent on the pH of the medium. For example, it was observed that AA, at low pH, is incapable of reducing Ag^+ ion into Ag[9], while the same reduction can be carried out at a pH typically greater than 9.0. However, the reduction of $HAuCl_4$ to Au can be performed at low as well as high pH values. Interestingly, when Au NPs were present in the medium, the formation of Ag from Ag^+ ions was favored even at lower pH values. We have taken advantage of these behaviors of AA and used the same for the production of core-shell Au@Ag NPs and subsequent assembly of the same into fibrous structures.

An aqueous solution of AA when mixed with $HAuCl_4$ results into purple colored solution. UV-vis spectrum of the solution consisted of a single peak at 533 nm indicating the presence of Au NPs in the medium.[5] Further, as observed before, when the solution was left by itself under ambient conditions, formation of fibers could be observed. These fibers, which appeared as bundles having length of each component fiber of about 100 μm and width of the fiber about 1-4 μm, with Au NPs having characteristic optical properties of the NPs. TEM and SEM analyses of the fibers indicated that small particles of the original sizes were organized into fibers where individual particles could be observed as constituents of the fibers (as observed before). The typical electrical conductivity of the fibers was low and the details of the composite fibers have been discussed earlier.[5] In this section, the primary focus is on the assembly of core-shell NPs.

TH-777_05612211

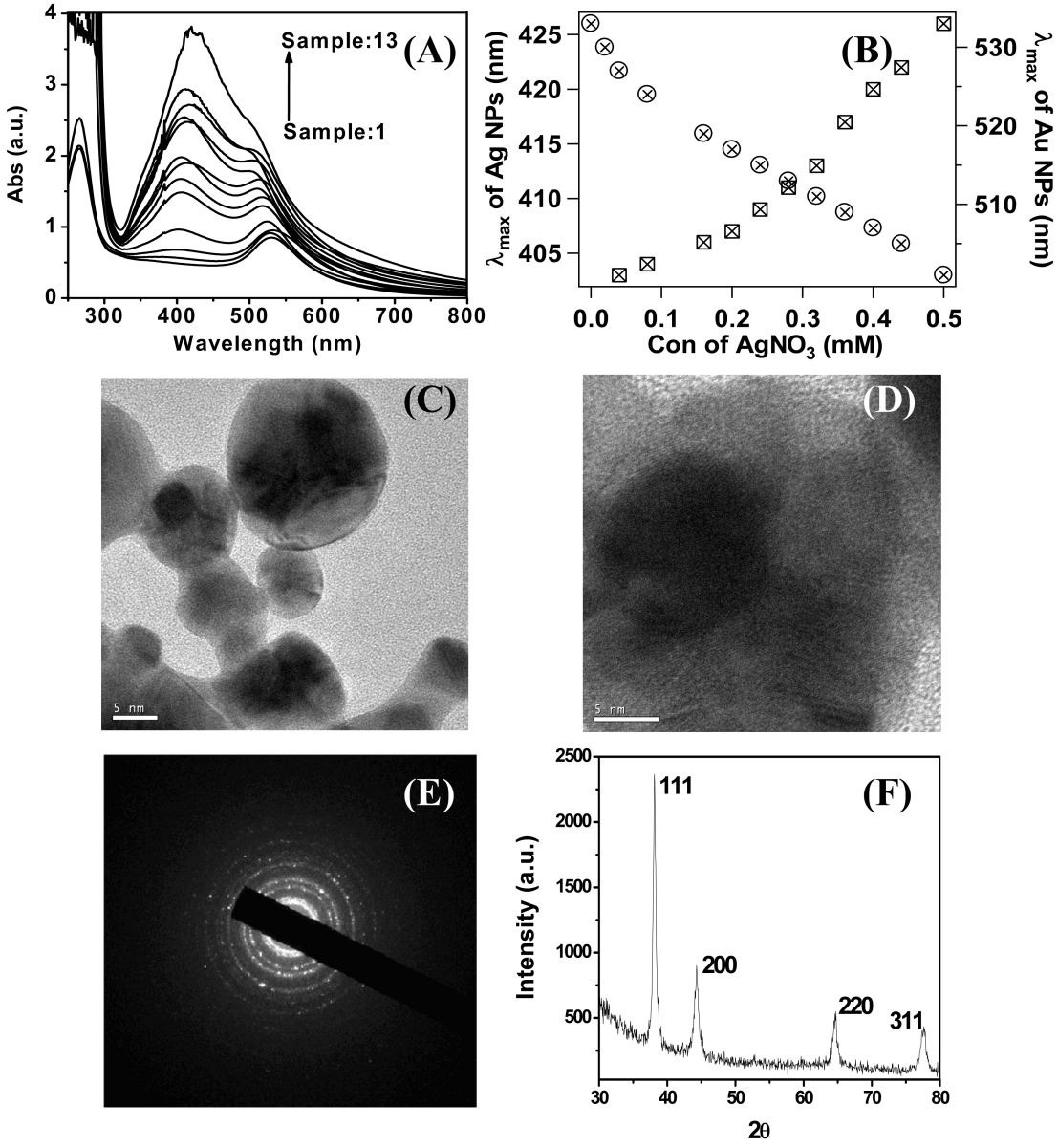


Figure 9.2.1. *(A) The UV-visible spectrum of $AgNO_3$ added Au NP solutions (Samples:1-13 of Table 8.2A). (B) Dependence of the absorption maxima (λ_{max}) of the Ag and Au NPs on the concentration of silver salt added to the Au NP solution. (C) Transmission electron micrograph of the core shell Au@Ag NPs corresponding to sample: 13 (Table 8.2A). (D) High resolution TEM picture of core shell Au@Ag NPs. (E) SAED pattern of particles corresponding to that in (C). (F)*

TH-777_05612211

Based on the formation and organization of Au NPs into fibers, a scheme has been developed for the generation fibers with composite (Ag and Au) NPs whose electrical conductivity could be tuned over a large range of values by changing the reaction conditions, which is primarily the concentrations of $AgNO_3$ and AA in the medium. Firstly Au NPs were synthesized in the medium by reduction of $HAuCl_4$ using AA. This was followed by addition of $AgNO_3$, which initially resulted in the formation of Au@Ag core-shell particles, followed by the formation of fibers. Typical UV-vis spectra of the solution containing Au NPs in AA medium with the addition of various amounts of $AgNO_3$ are shown in Figure 9.2.1 (A). As is clear from the figure, at the lower concentrations of $AgNO_3$, with values ranging from 0.02 mM to 0.50 mM, both the peaks characteristic of Ag NPs (at 383 nm) and Au NPs (occurring at 533 nm) were present in the spectra. This indicates the formation of Ag NPs independently, in addition to the presence of Au NPs. Further addition of $AgNO_3$ led to blue-shift of the peak originally due to Au NPs, while the peak due to Ag NPs continued to increase in intensity. This could possible be due the presence of Ag NPs and Ag coated Au NPs (the peak at 533 nm that blue-shifted upon addition of excess $AgNO_3$). Plots of λ_{max} versus the concentration of $AgNO_3$, shown in Figure 9.2.1 (B), indicate rapid (nearly exponential) decrease in case of Au NP absorption maximum, while the absorption maximum of Ag NPs increases at nearly the same extent.

It has been reported that Au NPs catalyze the growth of Ag NPs in the presence of a reducing agent.[10] Also known is that core-shell NPs could be formed by deposition of Ag on Au.[11] In the present condition, Au NPs in the presence of AA catalyzed the reduction of Ag^+ to Ag, which subsequently grew further on the Au NP seed. UV-vis spectra as a function of concentration of $AgNO_3$ indicates the formation of core-shell structures rather than alloy.[12] TEM images (Figure 9.2.1 (C)) showed the presence of Au@Ag core-shell

TH-777_05612211

NPs in the medium with further growth of Ag NPs on the particles leading to fiber formation. A better view of the core-shell formation is depicted in the high-resolution TEM (HRTEM) picture (Figure 9.2.1 (D)), where the lattice fringes due to Ag grown on Au particles is distinctly different from the dark background due to Au.

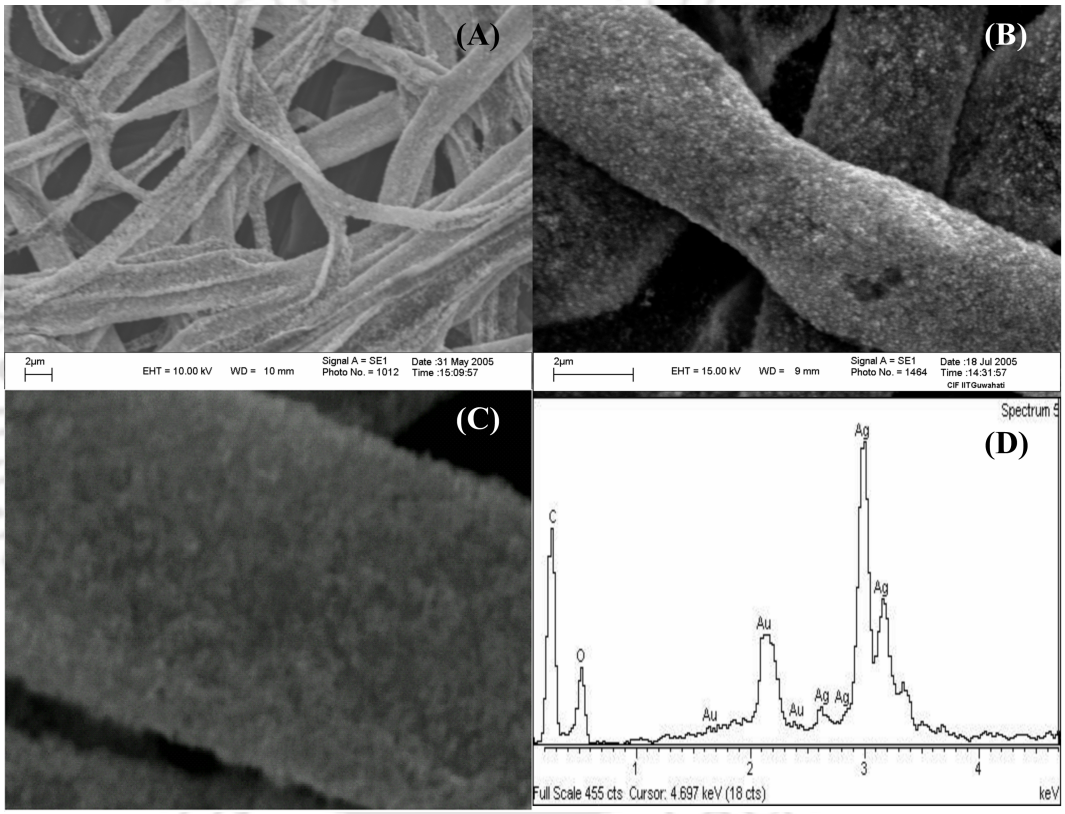


Figure 9.2.2. *(A) Scanning electron micrograph of the core shell NPs composite fiber. (B) and (C) Expanded views of the picture in (A). (D) EDX spectrum of the fiber.*

Also, clear from the figures (Figure 9.2.1 (C) and 9.2.1 (D)) is that in the present reaction conditions core-shell formation rather than alloy formation has taken place, supporting the observations through UV-vis studies. The images suggest that at the beginning, 5-10 nm

TH-777_05612211

diameter core-shell structures were formed in the medium. Selected area electron diffraction (SAED) pattern (Figure 9.2.1 (E)) indicated the presence of agglomerated crystalline particles of Ag and Au. The presence of Ag-Au in the structures was further confirmed by X-ray diffraction (XRD) studies. A typical pattern of a fiber bundle (discussed later) is shown in Figure 9.2.1 (F). The presence of well-defined planes of Ag/ Au occurring at 38.1°, 44.3°, 64.6° and 77.6° corresponding to (111), (200), (220) and (311) lattice planes clearly evidences the presence of Au/Ag in the fibers[13]. Calculation of particle size using Debye-Scherrer[14] formula indicates an average particle size of 16 nm, which is close to the TEM observations for core-shell particles.

When the core-shell NPs present in the solutions were kept for a maximum of 30 days, under ambient conditions, large bundle of fibers settling out of the solution as precipitate or hanging at the air-water interface could be observed. The solution color completely disappeared upon the formation of fiber bundles, and was devoid of characteristic UV-vis spectrum of either Ag or composite NPs. These fibers were further analyzed using SEM, the results of which are shown in Figure 9.2.2. As is clear from Figure 9.2.2 (A), the fibers formed appeared to be intertwined tapes. These tapes seemed to have a structure where each component tape branches out from a head and also several such component tapes meet at a common head. The number of branched tapes as well as tapes meeting at the head was typically four. Each of the component tapes had length of tens of micrometers, with typical width of about 2- 4 μm. Focusing on the fibers indicated the presence of small particles (less than 100 nm) distributed uniformly over the fibers. These are shown in Figures 9.2.2 (B) and (C). EDX spectrum of a spot on the fiber indicated the presence of Au and Ag on the fibers in addition to the presence of carbon. This meanss that the fiber was made of organic components, and was bimetallic in nature consisting of Au and Ag NPs. Further, EDX spectra of the fibers grown with different amount of $AgNO_3$ in the original solution indicated increased amount of Ag present in the fiber with increasing amount present in the original solution. This correlates well with the increased formation of Ag with increasing $AgNO_3$.

TH-777_05612211

Time-dependent growth of the fiber assemblies from a solution containing the above mixture (Au NPs, Au@Ag NPs and organic components from AA) were pursued. About 20 μL portion of the solution at a chosen time of growth was withdrawn and then evaporated on a TEM grid. This was done for the samples from 1st, 5th and the 20th day of growth. The evaporated solutions were then investigated under TEM. The results are shown in Figure 9.2.3. As is clear from Figure 9.2.3 (A), initially core-shell NPs were present in the solution in addition to Ag NPs (attached to them), and the overall particle sizes were about 30 nm or less in diameters.

TH-777_05612211

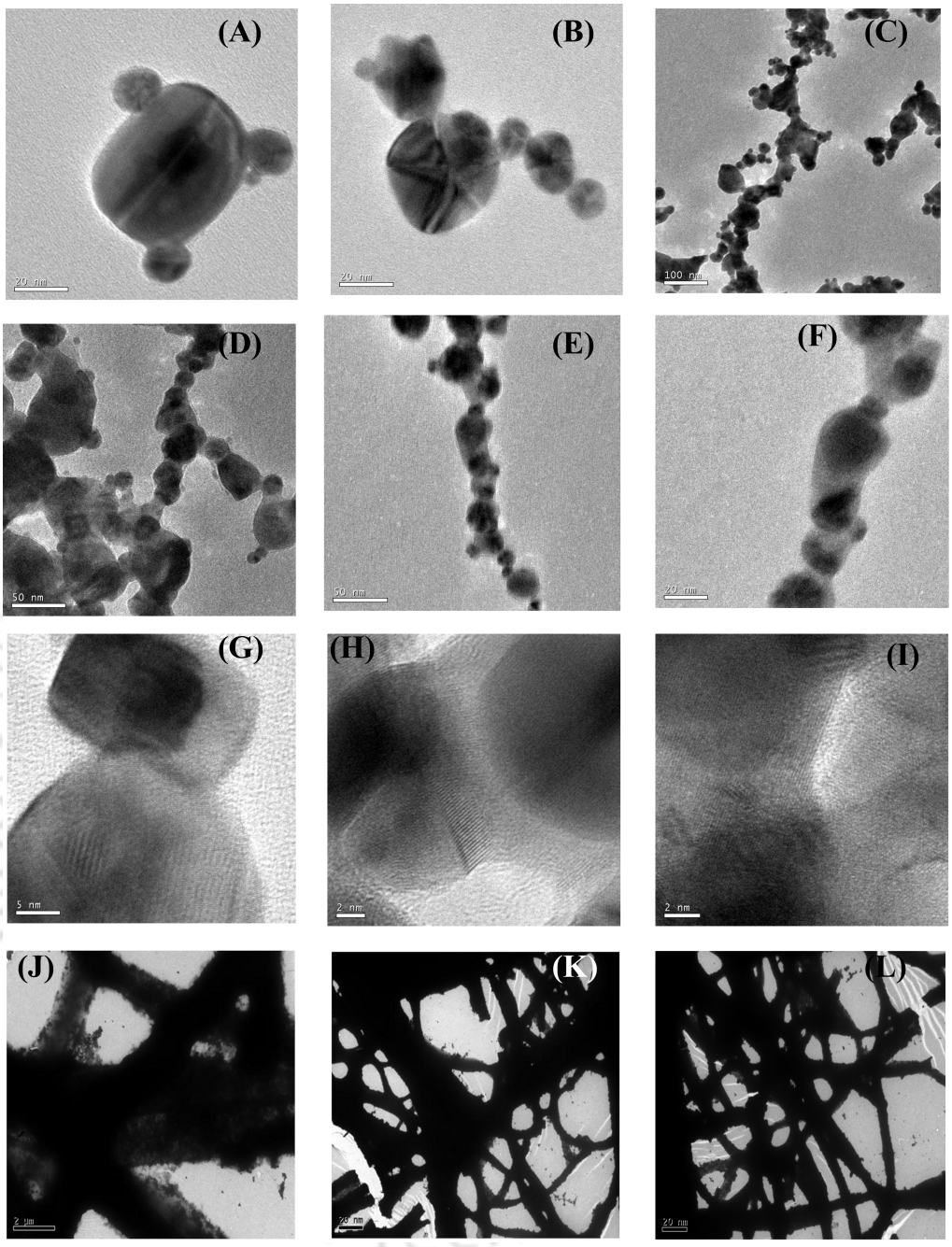


Figure 9.2.3. *(A) and (B) Transmission electron micrographs of core shell Au@Ag NPs on day 1 of sample 13; (C), (D), (E) and (F) that on day 5 of same sample. (G), (H) and (I) are the high resolution TEM pictures obtained from figures (E) and (F). (J), (K) and (L) Transmission electron micrographs of fiber of core shell Au@Ag NPs on day 20.*

TH-777_05612211

Also, the particles tend to grow into a linear chain fashion (Figure 9.2.3 (B)). With time the particles seem to have fused with each other as indicated by the presence of Ag in the intervening region between the two or several NPs. However, as we discussed earlier, upon addition of $AgNO_3$ with increasing the concentration into the seeds of Au NPs solution in the presence of excess reducing agent, deposition of the Ag NPs shell on the surface of the Au NPs occurred and as the thickness of the Ag shell increased the NPs merged together leading to the formation of fibers. The tendency of AA to form fibers upon oxidation followed by polymerization, as observed earlier[5], might act as the template for the growth of fibrous structures. The growth of fibrous structures due to growth of Ag on Au NPs and AA templates is more prominent at higher initial concentrations of AA. This is evident from Figures 9.2.3 (C)-(E), recorded from the sample of the 5^{th} day of growth. The presence of small, dark Au NPs in the linear chains consisting primarily of Ag is event from the figures. Also, better views of the growth of crystalline Ag on the Au NPs are available in the HRTEM pictures shown in Figures 9.2.3 (G)-(I), representing different locations of the fiber. The presence of separate lattice planes of Ag surrounding the dark Au NPs are clearly visible. Also, interesting to note is that the same lattice planes continue to be present not only in the intervening region of the fibers but also above the Au NPs. In other words, continuous growth of same lattice plane on different core-shell structures leads to the formation of linear geometry in the formation of fiber bundles. When the growth continues from different edges of the core-shell structures branched fiber formation could be observed. The observations suggest that when the shell of the Ag NPs continues to grow to form aggregate structures, the particles are fused with the continuation of the most suitable crystallographic faces[15] leading to fibrous structures with linear components. When the concentration of $AgNO_3$ is high and the time of growth long, a large assembly of NPs leads to the formation of micron to millimeters-scale fibers (Figures 9.2.3 (J)-(L)). The assembly appeared to have NPs as the majority component as indicated by the dark image consisting of primarily assemblies of NPs rather than joined by organic materials. Also, the figures indicate the presence of NPs uniformly distributed all over the fibers. It was noticed that in

TH-777_05612211

about 20 days the fiber formation was nearly complete. However, growth could be observed till about 30 days in some cases. As noted before, AA acts as the reducing agent in the formation of Au NPs from $HAuCl_4$. The solution was acidic and it was observed that under acidic condition $AgNO_3$ was not reduced by AA, although the same reduction could be achieved at a pH greater than 9. Thus in the present situation the Au NPs present in the medium possibly acted as catalyst in the reduction of $AgNO_3$ by AA. Firstly, reduction of $AgNO_3$ in the presence of Au NPs could produce Ag NPs and core-shell (Au@Ag) NPs in the medium. The excess Ag^+ ions present in the medium could subsequently be reduced, which in the presence of NPs could act as 'glue' in cementing the NPs into fibers. The TEM micrographs in Figures 9.2.3 (A)-(F) support this speculation as the grey region not only appeared in the core-shell NPs but also was present in the intervening region in the fibers spanning the NPs and appearing to have connected them into forming the fibers. It might also be possible that there is a role of AA in organizing the NPs into fibers as ordinary core-shell (Au@Ag) NPs are not known to spontaneously organize themselves into fibrous structures. The AA themselves or their degradation products could act as the stabilizers, which not only stabilizes the NPs but also help them assemble into fibers.

TH-777_05612211

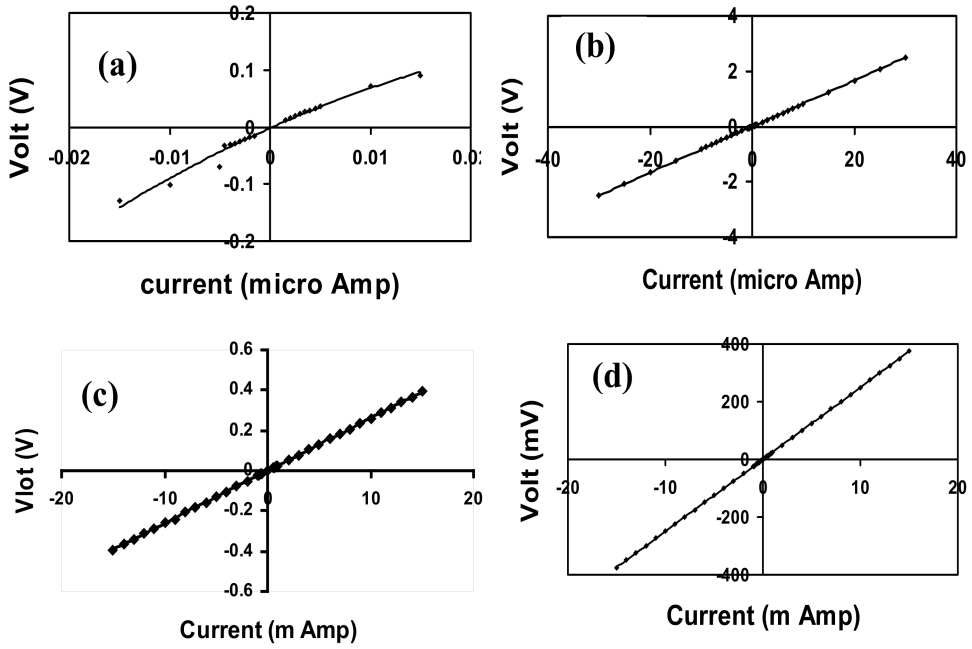


Figure 9.2.4. *I-V curves for the Au and Au@Ag core-shell fiber samples. Fibers obtained from (a) sample 1 (0.0 M $AgNO_3$), (b) Sample: 2 (0.02 mM of AgNO3), (c) sample 3 (0.04 mM of $AgNO_3$)*

TH-777_05612211

It was also noticed that increasing the concentration of $AgNO_3$ increased the rate of formation of the fibers. For example, when 0.08 mM of $AgNO_3$ was added to the preformed Au NPs the fiber formation could be observed to have been completed in 30 days. On the other hand, when the concentration was increased to 0.44 mM then the fiber formation was complete in 20 days.

Further evidence of the role of $AgNO_3$ in the formation of fibers along with the presence of Au NPs came from the electrical conductivity measurements. I-V characteristic and electrical conductivities of fibers so generated under different $AgNO_3$ concentrations were measured at room temperature after being transferred from the medium to a glass slide followed by drying. Figure 9.2.4 shows the I-V curve for (a) sample 1 (Au NPs – fiber composite), (b) Sample 2 (Au-Ag NPs-fiber composite with low $AgNO_3$ concentration), (c) sample 3 (Au-Ag NPs-fiber composite with medium $AgNO_3$ concentration) and (d) sample 4 (Au-Ag NPs-fiber composite with high $AgNO_3$ concentration). The exact concentrations of $AgNO_3$ for the samples are indicated in the captions of Figure 9.2.4. It is interesting to note that the I-V curve of the composite with Au NPs (Figure 8.2.4 (a)) is not a simple straight line. Also, the electrical conductivity of the composite fiber is low. It was observed that when the fibers were made of Au NPs and the organic components, the conductivity was on the order of $4.6 \times 10^{-4}\ \Omega^{-1}cm^{-1}$ and it is far from the metallic conductivity, which is reasonable considering that the NPs are interspersed with organic components in the fiber. However, with the increase in the concentration of $AgNO_3$ the composite fibers exhibit metallic conductivity. This is clear from Figures 9.2.4 (b), (c) and (d), which represent I-V curves of the composite fibers with increasing $AgNO_3$ concentration. It is also noteworthy that the conductivity of the fibers followed Ohm's law when the initial concentration of $AgNO_3$ was $\geq$ 0.04 mM. The conductivity versus concentration of $AgNO_3$ is shown in Figure 9.2.5. One can notice that the conductivity increased with the concentration of $AgNO_3$. The conductivity was low (less than 200 $\Omega^{-1}cm^{-1}$) when the initial concentration

TH-777_05612211

of $AgNO_3$ was less than 0.1 mM. On the other hand conductivity was high (metallic) when the initial concentration of $AgNO_3$ was greater than or equal to 0.1 mM. The increase of conductivity with $AgNO_3$ concentration could be due to the fusion of core shell Au@Ag NPs by Ag and thus increasing the electron flow between two core-shell NPs. When concentration of Ag in the fiber (i.e. the concentration of $AgNO_3$ in the original medium) was low then there would be significant presence of organic components in the fiber, in addition to the presence of sufficient core-shell NPs. Thus it is reasonable that the conductivity would be low. On the other hand, with the increase in concentration of Ag the 'electrical connection' between the NPs is provided by the Ag that is present in the intervening region, and which acts as glue for the formation of fibers from NPs (as was evident from the TEM images). When the presence of Ag is sufficient the electrical continuity is established and the fibers behave like bulk metallic conductor. In absence of sufficient Ag the composite fibers did not exhibit the behavior of a metallic conductor.

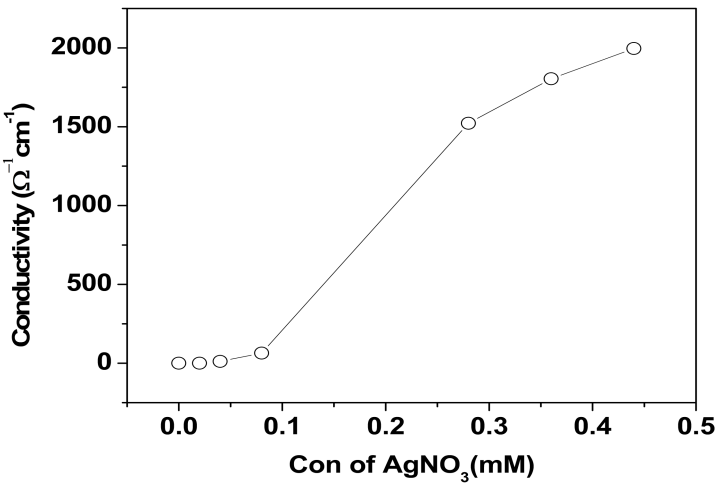


Figure 8.2.5. *Plot of electrical conductivity of the fibers versus concentration of $AgNO_3$*

The origin of the conductivity of these fibers could possibly be accounted for by using the geometric consideration for isotropicaly conductive adhesives (ICA). According to

TH-777_05612211

the model developed by Ruschau et al[16], the contact resistance (R_C) of conductive composites can be written as the sum of constriction resistance and tunneling resistance.

Here,

ρ_i is the intrinsic filler resisitivity.

d is the diameter of the contact spot.

ρ_t is the tunneling resistivity and

α is the contact area.

The constriction resistance is associated with the constriction of electron flow through small area. In the present case, at the small $AgNO_3$ concentrations, the area of contact between two NPs can be small enough to constrict the electron flow across the particles. The tunneling resistance is associated with the tunneling of electron form one particle to other in the presence of insulating film between the two particles. Here the insulating film could be due to organic components present in the fiber. When the concentration of $AgNO_3$ was low (up to 0.1 mM), the contact resistance could have been dominated by both of the above. However, with the increase in concentration of $AgNO_3$ (0.3 mM or more) the contacts between the NPs increase, as the Ag metal that is produced acted as 'glue' to join the NPs into more uniform and continuous wire. The increase in contact dominates the contact resistance and hence normal metallic conductivity is achieved as the length of the wire is sufficient (microns to mm) to behave like metallic conductor. Overall, the conductivity of the fibers is dominated by constriction resistance rather than pure tunneling, as the increase in the concentration of $AgNO_3$ increases the contacts by gluing the NPs. Thus, more NPs are not necessarily produced; rather contacts between NPs are improved by deposition of Ag in the intervening region thereby decreasing the constriction resistance. It is also interesting to note that the increase in the concentration of Ag increases the deposition of the same in the

TH-777_05612211

intervening region between two core-shell NPs rather than produce more NPs (of Ag). In other words, the reduction of $AgNO_3$ to Ag is more favored on the surface of the core-shell NPs rather than in the isolated solution. This deposition (through reduction on the surface) leads to connecting of the core-shell NPs into continuous wire. The presence of organic components might help in templating the deposition into wire rather than other shapes.

9.2.4 Conclusion

Systematic development of three-dimensional assembly of nanoscale materials has been and still remains a challenge. The present method of generating core-shell NPs and their subsequent self organization in the presence of increasing amount of Ag introduces a new approach towards systematic development of three-dimensional structures with nanoscale components. It must also be mentioned here that even though we have allowed the formation of complete fiber bundles in all the cases for ease of handling the fibers and composites, slow growth of fibers would allow generation of size-selected fibers as the products (fibers) could always be picked up at any time during the evolution of structures, allowing more versatile nature of the composite fiber generation. That the composite fibers are electrically conducting introduces a new approach in the generation of sensors, where the chemical and biochemical properties of the Au@Ag NPs and the electrical conductivity of the fibers can simultaneously be exploited. That the backbone of the composite fiber has organic moiety provides additional chemical and mechanical flexibility. The present work is expected to provide a new and interesting way of generating and organizing metallic NPs into three-dimensional functional networks useful for nanotechnology based devices.

9.2.5 References

1. Y. J-P.; Chen, F. *Food Chem*. **1999**, *64*, 423.

TH-777_05612211

2. Kimoto, E.; Tanaka, H.; Ohmoto, T.; and Choami, M. *Anal. Biochem.* **1993**, *214*, 38.

3. Deutsch, C. J. *Anal. Biochem*. **1998**, *255*, 1.

4. Borsook, H.; Davenport, H. W.; Jeffreys, P. E. C.; Warner, C. R. *J. Biol. Chem*. **1937**, *117*, 237.

5. Murugadoss, A.; Pasricha, R.; Chattopadhyay, A. *J. Colloid Interface Sci*. **2007**, *311*, 303.

6. Gou, L.; Murphy, C. *J. Chem. Mater*. **2005**. *17*, 3668.

7. Connett, P. H.; Wetterhahn, K. E. *J. Am. Chem. Soc*. **1986**, *108*, 1842.

8. Grinstead, R. R. *J. Am. Chem. Soc*. **1960**, *82*, 3464.

9. Srnova-Sloufova, I.; Lednicky, F.; Gemperle, A.; Gemperlova, J. *Langmuir* **2000**, *16*, 9928.

10. Kohler, M. J.; Romanus, H.; Hubner, U.; Wagner, J. *J. Nanomater*. **2007**, article ID 98134.

11. (a) Liz-Marsan, L. M. *Langmuir* **2006**, *22*, 32. (b) Mandal, M.; Kundu, S.; Ghosh, S. K.; Jana, P. M; Pal, T. *Current Sci*. **2004**, *86*, 556.

12. (a) Sun, Y.; Wiley, B.; Li, Z-Y.; Xia, Y. *J. Am. Chem. Soc*. **2004**, *126*, 9399. (b) Zhou, M.; Chen, S.; Zhao, S.; Ma, H. *Physica E* **2006**, *33*, 28. (c) Jean-Pierre, A.; Girault, H. H.; Brevet, P. F. *Chem Commun*. **2001**, 829.

13. Chen, D-H.; Chen, C-J. *J. Mater. Chem*. **2002**, *12*, 1557.

14. Devarajan, S.; Bera, P.; Sampath, S. J. Colloid. Interface. Sci. **2005**, *290*, 117.

15. (a) Giersig, M.; Santos-Pastoriza, I.; Liz-Marzan, L. M. *J. Mater. Chem*. **2004**, *14*, 607. (b) Ni, C.; Hassan, P. A.; Kaler, E. W. *Langmuir* **2005**, *21*, 3334. (C) Zhang, D.; Qi, L.; Ma, J.; Cheng, H. *Chem. Mater*. **2001**, *13*, 2753.

16. (a) Ruschau, G. R.; Yoshikawa, S.; Newnham, R. E. *J. App. Phys*. **1992**, *72*, 953 (b) Ye, L.; Lai, Z.; Liu, J.; Tholen, A. *IEEE Transactions on Electronics packing manufacturing* **1999**, *22*, 299. (c) Tholen, A. *Acta Metall*. **1979**, *27*, 1765. (d) Buech, F. *J. App. Phys*. **1973**, *44*, 532. (e) Springett, E. B. *J. App. Phys*. **1973**, *44*, 2925. (f) Kelin, L. D.; Roth, R.; Lim, L. K. A.; Alivisatos, P. A.; Mceuen, L. P. *Nature* **1997**,

TH-777_05612211

389, 699. (g) Berndt, R.; Gimzewski, K. *J. Phys. Rev. B* **1993**, *48*, 4746. (h) Thirstrup, C.; Sakurai, M.; Stokbro, K.; Aono, M. *Phys. Rev. Lett*. **1999**, *82*, 1241.

TH-777_05612211

List of Publications

1. Surface Area Controlled Differential Catalytic Activities of One Dimensional Chain-Like Arrays of Gold Nanoparticles. **A. Murugadoss**, Arun Chattopadhyay. **J. Phys. Chem. C** 2008. 112, 11265.
2. A "Green" Chitosan-Silver Nanoparticle Composite as a Heterogeneous as well as Micro-heterogeneous Catalyst. **A. Murugadoss**, Arun Chattopadhyay. **Nanotechnology** 2008, 19, 015603.
3. Acetanilide Mediated Reversible Assembly and Disassembly of Au Nanoparticles. **A. Murugadoss**, M. Kar, Arun Chattopadhyay, **J. Colloid Interface Sci**. 2008. 324, 230.
4. The antibacterial properties of a novel Chitosan–Ag-nanoparticle composite. S. Pallab, **A. Murugadoss**, P. V. Durga Prasad, S. S. Ghosh, Arun Chattopadhyay. **Inter. J. Food Microbio**. 2008, 124, 142.
5. Tuning photoluminiscence of ZnS Nanoparticles by Silver. **A. Murugadoss**, Arun Chattopadhyay. **Bull. Mater. Sci**. 2008, 31, 533.
6. Ascorbic acid as a Mediator and Template for Assembling Metallic Nanoparticles. **A. Murugadoss**, R. Pasricha, Arun Chattopadhyay. **J. Colloid Interface Sci**. 2007, 311, 303.
7. Stabilizing Agent Specific Synthesis of Multi- branched and Spherical Au Nanoparticles by Reduction of AuCl-4 by Fe2+ ions. **A. Murugadoss**, Arun Chattopadhyay. **J. Nanosci and Nanotechnol**. 2007, 7, 1730.
8. 'Green' Chitosan bound Silver Nanoparticles for Selective C-C bond Formation via in situ Iodination of Phenols. **A. Murugadoss**, Papori Goswami and Arun Chattopadhyay (**Communicated**), 2008.
9. Stabilizer Specific Interaction of Gold Nanoparticles with a Thermosensitive Polymer Hydrogel. **A. Murugadoss**, Aslam Khan, Arun Chattopadhyay (**Communicated**), 2008.

TH-777_05612211

10. Silver Fused Conducting Fiber Formation of Au@Ag Core-shell Nanoparticles Mediated by Ascorbic Acid. **A. Murugadoss**, R. Pasricha, Arun Chattopadhyay. (**Communicated**), 2008.
11. Concentration Dependence and Specificity in the Amino acid induced Assembly of Gold Nanoparticles. **A. Murugadoss**, Arun Chattopadhyay. (**Under preparation**), 2008.
12. Acetanilide as a Precursor for Shape and Size Selective Polyaniline-Au Nanoparticle Composite. **A. Murugadoss**, Arun Chattopadhyay. (**Under preparation**), 2008.

TH-777_05612211